CENTRO DE INVESTIGACIÓN Y DE ESTUDIOS AVANZADOS DEL INSTITUTO POLITÉCNICO NACIONAL

UNIDAD ZACATENCO
DEPARTAMENTO DE INGENIERÍA ELÉCTRICA
SECCIÓN DE BIOELECTRÓNICA

Métodos ópticos y electroquímicos para la detección de contaminantes en alimentos

Tesis que presenta

Diana Bueno Hernández

para obtener el Grado de

Doctor(a) en Ciencias

en la Especialidad de

Ingeniería Eléctrica

Directores(as) de la Tesis:

Dr. Roberto Muñoz Guerrero
Dr. Jean Louis MARTY

Ciudad de México Mayo 2016

CENTER FOR RESEARCH AND ADVANCED STUDIES OF THE NATIONAL POLYTECHNIC INSTITUTE

ZACATENCO
DEPARTMENT OF ELECTRICAL ENGINEERING
BIOELECTRONICS SECTION

Optical and electrochemical sensing methods for the detection of food contaminants

Thesis presents

Diana Bueno Hernández

For the Grade

PhD of Science

in the area of

Electrical Engineering

Directors of the thesis:

Dr. Roberto Muñoz Guerrero
Dr. Jean Louis MARTY

Mexico city May 2016

THÈSE

Pour obtenir le grade de

Docteur

Délivré par

UNIVERSITE DE PERPIGNAN VIA DOMITIA et CENTRO DE INVESTIGACIÓN Y DE ESTUDIOS AVANZADOS DEL INSTITUTO POLITÉCNICO NACIONAL

Préparée au sein de l'école doctorale
Et de l'unité de recherche BAE

Spécialité : **Science d l'Ingénieur**

Présentée par Diana Bueno Hernández

OPTICAL AND ELECTROCHEMICAL SENSING METHODS FOR THE DETECTION OF FOOD CONTAMINANTS

Soutenue le 13 mai 2016 devant le jury composé de

M. Charles GHOMMIDH, Professeur, UMR IATE-Montpellier	Rapporteur
M. Gustavo Adolfo ALONSO SILVERIO, Professeur, UAGro	Rapporteur
M. Jean Louis MARTY, Professeur, BAE-UPVD	Examinateur
M. Roberto MUÑOZ GUERREO, Professeur, CINVESTAV	Examinateur
M. Juan Manuel GUTIÉRREZ SALGADO, Professeur, CINVESTAV	Invité

Dedicated to

My family (Mom, Dad, Sister and Brother)

For their support, time, love and encourage to keep going.
For teaching and reminding me that I must not give up, that the effort, dedication and responsibility lead us to achieve our objectives.

My grandad Lorenzo

For sharing his adventures, experiences, honey, time and for inculcating us the respect and generosity to others.
He is and will always be a great human being.

Acknowledgements

“The highest education is that which does not merely give us information but makes our life in harmony with all existence.”

Rabindranath Tagore

To the Centro de Investigación y Estudios Avanzados del Instituto Politécnico Nacional for the opportunity to belong in a prestigious institution and allowing me to carry out my doctoral studies.

To the Consejo Nacional de Ciencia y Tecnología and the program PCP Mexico- France for the scholarship of my studies in Mexico and France.

To my advisors, Dr. Roberto Muñoz Guerrero and Prof. Jean Louis Marty for giving me their confidence, support, expertise, knowledge and patience to achieve successfully the proposed PhD.

To the external reviewers, Prof. Charles Ghommidh and Dr. Gustavo Adolfo Alonso Silverio; to the members of the jury, Dr. Roberto Muñoz Guerrero, Prof. Jean Louis Marty, Prof. Charles Ghommidh, Dr. Juan Manuel Gutierrez Salgado, Dr. Lorenzo Leija Salas and Dr. Arturo Vera Hernández for your time, corrections and advices to improve the presentation of the thesis.

To M. C. Herlinda Araiza Lizarde for providing the material required, always.

To my fellows in Mexico’s lab: Jose Antonio, Joaquin, Esmeralda, Martín, Leonardo, Sarai and recently Lupita. M. C. Ismael, Araceli, Dr. Gustavo and Dra. Berenice by good time that help us to remove the stress, such as the birthday celebrations.

To my fellows in France's lab: Najwa, Rupesh, Akhtar, Cheng, Nadyn, Wafa, Geoffrey, Laura and Gaëlle. The researchers: Terry, George, Lisse and Carol for their teachings, advices and support me all the time.

To the secretaries: Georgina Villarreal Olmos, Patricia Peña Rivero and Ma. Luisa Nunez Lorán for their support in administrative procedures.

To the workers in the machine shop: Tonatiuh Olmos, Juan Manuel Osorio Velasco, Victor Jimenez Malangón, for all your help in manufacturing the mechanical parts of this work, as well as the recommendations and suggestions to build them. To the manager of the printed circuit boards (PCB) manufacturing area, Silvino Reyes Zárate, for fabricating the PCB used in this thesis.

"The real friendship is like fluorescence, it shines better when everything has darkened."
Rabindranath Tagore

Special thanks to Luis, Anais, Alejandro, Raquel, Lupita, Atul, Amina, Elise and Emilie.
I am grateful for everything, especially for their FRIENDSHIP.

To Israel Rivera, for his time, support, understanding and advice. I am especially grateful for sharing wonderful moments.

To God who has given me a wonderful family and has allowed me to live important and special moments in my life, to meet great friends, but the most important thing, he has taught me that no matter how difficult the road of life may be, I always have to take it and learn from it.

Table of contents

Optical and electrochemical sensing methods for the detection of food contaminants

List of figures

List of tables

Acronyms

AChE: Acetylcholinesterase

ACN: Acetonitrile

ACTh: Acetylthiocholine

AOAC: Association of Official Agricultural Chemists

APD: Avalanche Photodiode

APP: Mobile application

ATChI: Acetylthiocholine iodide

b.w.: body weight

BB: Binding buffer

BEN: Balkan Endemic Nephropathy

BGYF: Bright Greenish Yellow Fluorescence

BL: Bioluminescence

BSA: Bovine Serum Albumin

CCD: Charge Coupled Device

CE: Capillary Electrophoresis

$CHCl_3$: Chloroform

CIA: Chemiluminescent Immunoassay

CIE: Comission Internationale de L'Eclairage

CL: Chemiluminescence

CMOS: Complementary Metal Oxide Semiconductor

CMOS: Complementary Metal Oxide Semiconductor

CMY: Cyan, Magenta, Yellow

DAD: Diode Array Detector

DEA: Diethanolamine

DFT: Discrete Fourier Transform

DM: D. melanogaster

DTNB: 5,5'-dithiobis-2-nitrobenzoic acid

EC: European Commission

EC_{50}: Effective concentration

EDC: *N*-(3-dimethylaminopropyle)-*N*,-ethylecarbodiimide hydrochloride

EE: Electric eel

ELIFA: Enzyme Linked Immune Filtration Assay

ELISA: Enzyme linked immunosorbent assays

EPA: Environmental Protection Agency

EtOH: Ethanol

EU: European Union

FAO/WHO: Food and Agriculture Organization/World Health Organization

FAO: Food and Agriculture Organization of the United Nations

FD: Fluorescence Detector

FFT: Fast Fourier Transform

FIA: Flow Injection Analysis

FP: Fluorescence polarization

FTI: Flow-through immunoassay

GaN: Gallium Nitride

GB: GigaBytes

GC: Gas Chromatography

G-DM: Genetically-modified D. melanogaster

H_2O: Water

HgI_2: Mercury iode

HIS: Hue, Saturation, Intensity

HPLC: High Performance Liquid Chromatography

HRP: Horseradish Peroxidase

HSV: Hue, Saturation, Value

IAC: ImmunoAffinity Column

IARC: International Agency for Research on Cancer

I_F: Forward current

IP: Internet Protocol address (address)

IUPAC: International Union of Pure and Applied Chemistry

JECFA: Joint FAO/WHO expert Committee on Food Additives

JPEG: Joint Photographic Experts Group

KCl: Potassium chloride

KH_2PO4: Potassium phosphate monobasic

Ki: Inhibition constants

KI: Potassium iodide

LC/MS: Liquid Chromatography

LD50: lethal dose 50

LDs: Laser Diodes

LED: Light Emitting Diode

LFT: Lateral flow test

LIB: Lithium-ion battery

LOD: Limit Of Detection

MBs: Magnetic beads

MeCN: Acetonitrile

MeOH: Methanol

$MgCl_2$: Magnesium chloride

MIP: Molecularly Imprinted Polymer

MIT: Molecular imprinted technique

MP: MegaPixel

mSAM: mixed Self Assembled Monolayer

MSPD: Matriz Solid Phase Dispersion

Na_2HPO_4: Sodium hydrogen phosphate

Na_2HPO4: Sodium phosphate dibasic

NaCl: Sodium chloride

$NaHCO_3$: Sodium hydrogen carbonate

NHS: *N*- hydroxysuccinimide

OP: Organophosphate

OTA: Ochratoxin A

OTB: Ochratoxin B

OTC: Ochratoxin C

OTα: Ochratoxin α

OTβ: Ochratoxin β

OWLS: Optical Waveguide Light Mode Spectroscopy

PBS: Phosphate buffer

PD: Photodiodes

PMT: Photo-multiplier tube

PTWI: Provisional Tolerable Weekly Intake

R.S.D: Relative Standard Deviation

R: Resistance

RGB: Red, Green, Blue

SCF: Scientific Committee on Food

SERS: Surface Enhanced Raman Scattering

SIA: Sequential Injection Analysis

SOIC: Small Outline Integrated Circuit

SPCE: Screen Printed Carbon Electrodes

SPE: Solid Phase Extraction

SPME: Solid Phase MicroExtraction

SPR: Surface Plasmon Resonance

TE: Tris-EDTA buffer

TIRF: Total Internal Reflection

TLC: Thin Layer Chromatography

TT: Tris-Tween buffer

UAE: United Arab Emirates

UB LED: Ultra-bright LED

URL: Uniform Resource Locator

USB: Universal Serial Bus

UV/VIS: Ultraviolet/Visible

UV: Ultraviolet

Resumen

Un dispositivo portátil y de bajo costo fue diseñado para cuantificar las concentraciones de OTA en muestras reales. El principio de detección consiste en un emisor ultravioleta a 365 nm y un sensor CMOS, controlado por una interfaz diseñada en LabVIEW o MATLAB, con un tiempo de 20 segundos desde la adquisición de la imagen hasta mostrar al usuario.

Está documentado que la OTA es naturalmente fluorescente, lo que permite al usuario emplear un LED UV para excitar la muestra con lo cual se obtiene un valor de voltaje cuando se emplea un fotodetector o una fotografía de la muestra contaminada OTA, ambos con la finalidad de predecir las concentraciones de la muestra. Para capturar y procesar la imagen, de manera automática, el sistema se basa en las componentes RGB (por sus siglas en ingles) azul, rojo y verde. Para cada concentración de la OTA, se obtienen sus respectivas componentes RGB, las cuales se representan de manera grafica para así cuantificar la micotoxina presente en la muestra. Se obtuvo un comportamiento lineal en el rango de concentraciones corresponde a 2-40 g / L de OTA.

Las Columnas de Inmunoafinidad (IAC) y Columnas de Polímeros de Impresión Molecular (MIP) se utilizaron con muestras de cacao, cerveza y vino. Los resultados obtenidos fueron validados utilizando métodos cromatográficos tales como HPLC y el equipo Fluoroskan. La interfaz desarrollada es fácil de usar, económico y portátil.

Además, se hizo uso de recientes tendencias como emplear el celular para detectar OTA y el desarrollo de una APP. La imagen fluorescente obtenida con la cámara del smartphone fue analizada por una computadora personal y descompuesta en sus componentes RGB, la imagen fue enviada a través del WIFI entre los dispositivos, así mismo se uso el smartphone como fuente de alimentación del circuito eléctrico. Finalmente, una APP para un sistema Android se desarrollo, esta aplicación tiene como funciones la captura y obtención de las componentes RGB de la imagen

El sistema desarrollado fue empleado para cuantificar OTA en muestras reales sin la utilización de columnas de extracción, empleando técnicas colorimétricas o análisis de color.

Abstract

A portable and low cost fluorescence set-up to quantify the concentrations of Ochratoxin A (OTA) in real samples was developed. The detection through the device consist of an ultraviolet light at 365 nm and an photo detector or a CMOS sensor controlled by an executable interface designed in LabVIEW or MATLAB, with a time from acquisition to processing to image display of 20 seconds.

It has been reported that OTA is naturally fluorescent, so it allows the user to get a UV LED to excite the sample, get a value in voltage when a photodetector is employed or a photograph of the OTA under excitation conditions, and process that image in order to predict the concentrations of the sample. To capture and process the image, in an automatically manner, the system was completely based on the Red, Green and Blue (RGB) components. For each concentration of the OTA, the RGB coordinates obtained and plotted to quantify the mycotoxin presented in the sample. The linearity for OTA obtained in the range of concentrations corresponds to 2-40 µg/L.

Immunoaffinity columns (IAC) and molecular imprinted polymer columns (MIP) were used with cocoa, beer and wine samples. The obtained results were cross-validated using chromatographic method such as HPLC and the Fluoroskan equipment. The developed setup is easy to use, economical and portable.

Besides, the use of new tendencies was included such as employ the smartphone to detect OTA and the creation of an APP. Fluorescence image data from the smartphone camera are analyzed by a personal computer and presented in RGB components, where the image is sent to the computer by WIFI and the smartphone is used as a power source too. Finally, an APP for android system was created to capture the image and provides the RGB values.

At the end, the use of image processing to quantify the OTA in real samples without incorporated IAC or MIP columns to extract the mycotoxin from a complex solution, employing colorimetric techniques and color analysis.

MÉTHODES DE DÉTECTION OPTIQUE ET ÉLECTROCHIMIQUES POUR LA DETECTION DE CONTAMINANTS ALIMENTAIRES

Résumé

Un appareil de mesure de la fluorescence, à faible coût et portable a été développé pour quantifier les concentrations d'Ochratoxine A (OTA) dans des échantillons réels. Le système est basé sur l'excitation par une UV-LED à 365 nm et un photo détecteur contrôlé par une interface dans LabVIEW. Aussi, une image capteur, CMOS, contrôlée par une interface conçue dans MATLAB, permet l'acquisition et le traitement de l'image en 20 secondes.

L'OTA est une molécule naturellement fluorescente. Après excitation par une UV-, l'image de la fluorescence émise est captée par une caméra et traitée en vue de la mesure de la concentration de l'OTA. Le système d'analyse a été basé sur les 3 composants rouge, vert et bleu (RGB, selon l'acronyme anglais). Pour chaque concentration d'OTA, les coordonnées (RGB) sont obtenues et représentés graphiquement pour quantifier la mycotoxine présente dans l'échantillon. La gamme est linéaire entre de 2-40 µg / L.

L'extraction de l'OTA est réalisée par des colonnes d'immuno affinité (IAC, selon l'acronyme anglais) et les colonnes à empreinte moléculaire (MIP, selon l'acronyme anglais) pour les échantillons de cacao, de la bière et du vin. Les résultats obtenus ont été validés par la méthode chromatographique (HPLC). L'appareil conçu est facile à utiliser, économique et portable.

En outre, l'utilisation des nouvelles technologies a été inclus tels que l'emploi du smartphone pour détecter l'OTA et la création d'un APP. Des données d'image de fluorescence provenant de la caméra du smartphone et sont analysées par un ordinateur personnel et présentés dans les composantes RGB, où l'image est envoyée à l'ordinateur par WIFI et le téléphone intelligent est utilisé comme source d'énergie trop. Enfin, une APP pour le système Android a été créé pour capturer l'image et fournit les valeurs RGB.

Enfin l'utilisation du traitement de l'image a été utilisée pour quantifier l'OTA dans les échantillons réels sans colonnes IAC ou MIP, employée pour extraire la mycotoxine.

L'analyse a été réalisée par des techniques colorimétriques et d'analyse de la couleur.

CHAPITRE I

INTRODUCTION ET CONTEXTE DE L'ÉTUDE

1. Introduction

Depuis la découverte des aflatoxines dans les années 1960 [1], la communauté scientifique estime qu'elles sont, avec d'autres métabolites secondaires, responsables de la toxicité de certains aliments. Par conséquent la détermination des mycotoxines dans les échantillons alimentaires joue un rôle important dans la protection de la santé animale et humaine.

La plupart des céréales, des graines oléagineuses, les noix et les fruits déshydratés sont sensibles à la formation de mycotoxines. Ces dernières sont produites, pendant la récolte, le transport ou le stockage. L'impact des mycotoxines sur la santé dépend à la fois de la quantité et du type de mycotoxine consommée. La toxicité et ses effets sur l'individu dépend de la présence des autres mycotoxines et d'autres composés alimentaires [2].

Les mycotoxines ont attiré l'attention dans le monde entier parce qu'elles représentent un problème économique majeur en raison des pertes économiques importantes liées à leur impact sur la santé humaine, la productivité animale et le commerce international. Des procédures « qualité » et une législation sur les niveaux de contamination qui sont toxicologiquement acceptables sont nécessaires pour réduire au maximum l'exposition aux mycotoxines; Il est donc indispensable de contrôler les produits destinés à la consommation humaine ou animale.

Les techniques d'analyses les plus utilisées pour la détermination des mycotoxines sont (a) la chromatographie et (b) les techniques ELISA [3]. Les faibles niveaux de concentration des mycotoxines dans les denrées alimentaires, allant du picogramme au microgramme, nécessitent l'application de méthodes de détection très sensibles. Les techniques d'analyse couplées à une détection fluorimétrique, sont les méthodes les plus largement utilisées pour la détermination de mycotoxines [4].

Compte tenu des limites des techniques d'analyse, de leur coût élevé du à l'utilisation d'un appareillage sophistiqué et la nécessité d'un personnel qualifié, il est apparu clairement la nécessité de développer des méthodes d'analyse sensibles, précises, simples et peu coûteuses.

Les biocapteurs sont un outil de dépistage pour une estimation rapide de la

contamination par les mycotoxines dans les produits. Plusieurs systèmes de transduction peuvent être envisagés comme la luminescence ou la fluorescence utilisée dans les industries agro-alimentaire et pharmaceutique. La détection optique est une des techniques les plus anciennes. Ses principaux avantages sont la simplicité des opérations, le faible coût, la faible consommation d'énergie, une grande stabilité et la possibilité de miniaturiser pour les mesures sur le terrain. [3].

1.1 Définition du problème

La pénétration de mycotoxines dans le corps humain (ingestion, inhalation, absorption cutanée) peut provoquer une intoxication aiguë ou chronique dans les systèmes digestifs, cardiovasculaires, respiratoires et excréteurs. Ces dernières années, l'action cancérigène, mutagène, tératogène et immunosuppressive de certaines mycotoxines a été confirmée. Actuellement, plus de 400 mycotoxines sont produites par environ 350 espèces de champignons filamenteux. Cinq classes de mycotoxines sont considérés comme les plus importantes dans l'agriculture et dans l'industrie alimentaire, l'OTA est l'une d'elles[5].

L'Organisation pour l'Alimentation et l'Agriculture des Nations Unies (FAO, pour son sigle en anglais) a estimé que 25% des cultures dans le monde sont contaminés par des mycotoxines et que les pertes de produits alimentaires s'élèvent à un milliard de tonnes par an [6]. L'OTA été trouvée dans la viande, les produits laitiers, la boulangerie et la charcuterie [11,12]. Une dose journalière de 1,21 µg est associée à la néphropathie endémique [7]. La présence dans la sang de l'OTA a été découverte chez les habitants de certaines régions de Croatie [9].

Il existe une relation entre la présence de l'ochratoxine A dans la ration alimentaire et certaines maladies spécifiques. En outre, au Mexique il n'y a pas un règlement spécifique sur les mycotoxines et notamment l'OTA, ce qui justifie pleinement le choix de cette thématique de recherche.

L'information au Mexique concernant les niveaux de contamination par les mycotoxines dans les aliments est limitée par de nombreux facteurs, comme les ressources disponibles pour la recherche, le nombre et l'équipement des laboratoires d'analyse, la pertinence des procédures d'échantillonnage et la sensibilité des méthodes de quantification.

Au Mexique, il n'y a pas de classification, ni de valeurs recommandées concernant la contamination des aliments par l'ochratoxine A.

Il y a seulement trois réglementations concernant seulement les aflatoxines. Sa limite maximale dans le maïs pour la consommation humaine est de 20 pg/Kg et pour la consommation animale de 21 à 300 pg/Kg pour l'aflatoxine B1 [15]. De la même façon, pour les « tortillas » à base de farine de maïs, le niveau maximum est de 12 µg/kg et pour les « tortillas » à base de farine blé la limite est de 20 µg/Kg [16]. Dans le cas du lait ou des produits laitiers, la teneur maximale autorisée pour l'aflatoxine M_1 est de 0,5 µg/L [17]. Il n'y a pas de législation pour les autres mycotoxines alors qu'elles ont été, comme l'ochratoxine A, détectées.

L'apport alimentaire quotidien de l'ochratoxine A est assez difficile à estimer en raison de la fréquence de la présence de mycotoxines dans les produits alimentaires, et de leur 'hétérogénéité. L'apport quotidien d'OTA peut être estimée à partir des valeurs trouvées dans les fluides biologiques (lait maternel, le sang). La présence d'OTA dans des échantillons complexes est un important facteur de risque pour la santé chez les personnes. Ces aspects montrent l'importance d'évaluer la teneur en OTA dans les produits alimentaires. C'est l'objectif de mon travail de thèse est de développer des méthodes rapides et sensibles de dosage de l'OTA.

1.2 Objectifs de la recherche

1.2.1 Général

⇒ L'élaboration d'un système micro fluidique à faible coût et portable pour détecter et analyser l'ochratoxine A dans des échantillons liquides.

1.2.2 En particulier

- Fabrication d'un biocapteur basé sur l'utilisation des aptamères: aptacapteur
- Détection de l'OTA dans des échantillons liquides par détection ampérométrique.
- Mise en œuvre d'un système optique pour la détection de l'OTA.
- Essais expérimentaux avec détection optique.
- Couplage du système optique avec un système fluidique.
- Tests expérimentaux de dosage vde l'OTA avec le système fluidique avec détection optique.
- Détection de l'ochratoxine A dans des échantillons réels.

CHAPITRE II

ETAT DE L'ART

L'ochratoxine A est une mycotoxine produite par le métabolisme secondaire de nombreuses espèces filamenteuses des genres *Aspergillus et Penicillium* [10]. Chez l'homme, l'OTA a été impliqué dans la néphropathie endémique des Balkans [1,13].

2.1 Définition, la structure et le profil toxicologique de l'OTA

La structure chimique de l'OTA est représentée dans la figure 1. La formule empirique de l'ochratoxine A est $C_{20}H_{18}ClNO_6$. Selon l'International Union of Pure and Applied Chemistry (IUPAC) le nom chimique de l'OTA est le *N*-{[(3*R*)-5-chloro-8-hydroxy-3-methyl-1-oxo-3,4-dihydro-1*H*-isochromen-7-yl]carbonyl}-L-phenylalanine [11].

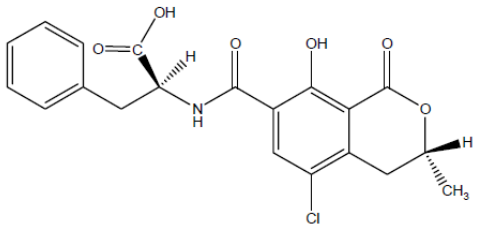

Figure 1 Structure chimique de l'OTA.

L'OTA est une poudre blanche, cristalline qui est très instable en présence de la lumière, mais assez résistante à la chaleur. C'est un acide organique faible[10]. Il possède une fluorescence verte intense sous la lumière UV en milieu acide et de la fluorescence bleue dans des conditions alcalines [12]. Il est très soluble dans des solvants organiques polaires, légèrement soluble dans l'eau et insoluble dans l'éther de pétrole et les hydrocarbures saturés. Elle possède une résistance à l'acidité et aux températures élevées.

Plusieurs études ont été réalisées afin de montrer l'implication de l'OTA dans les maladies avec des effets tels que néphrétique, hépatotoxique, neurotoxique, tératogène et neurotoxique sur plusieurs espèces d'animaux [8, 13].

2.2 Contamination et règlement

Dans le monde, les céréales sont la source la plus importante pour l'alimentation humaine. La figure 2 montre la prévalence des céréales comme la principale source de contamination par l'OTA pour la population européenne.

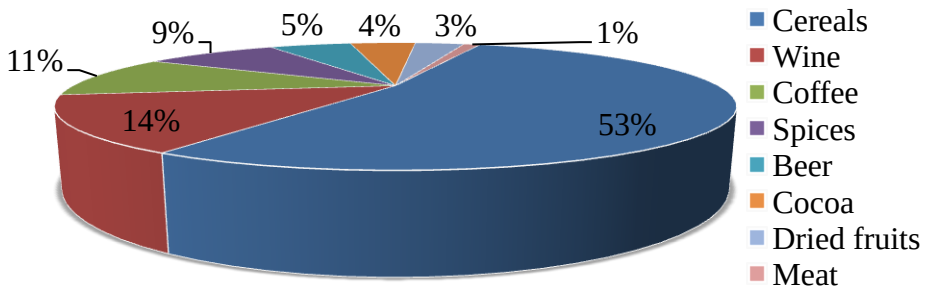

Figure 2 Contribution de chaque produit alimentaire à l'OTA et l'exposition moyenne de la population européenne [14].

Cependant, la contamination par l'OTA de nombreux produits agricoles est bien documentée; cette contamination affecte de nombreux produits tels que les grains de café, les légumineuses, les épices, la viande et les produits laitiers. L'IARC a classé l'ochratoxine A comme cancérogène possible pour les humains (Groupe 2B). Les limites maximales pour l'OTA ont été établies dans les États membres de l'UE (comme le Danemark, la Hongrie, l'Italie et l'Allemagne dans leur législation nationale présenté dans le tableau 1 [3] mais aussi par la Commission européenne.

Tableau 1. Maximum accepté niveaux d'OTA.

Aliments	**Maximum niveau (µg/Kg)**
Céréales, grains de café torréfié et café torréfié moulu	5
Tous les produits dérivés des céréales	3
Les raisins secs et le café soluble (café instantané)	10
Vin (vin mousseux), vin de fruits, vin aromatisé, des boissons aromatisées à base de vin et de jus de raisin, nectar de raisin, les moûts et les produits	2
Aliments pour bébés	0.5
Épices, y compris les épices séchées	15
Réglisse racine	20
Extraits de réglisse	80
Le gluten de blé pas vendu directement au consommateur	8

2.3 Méthodes de détection dans les denrées alimentaires contaminées par l'OTA.

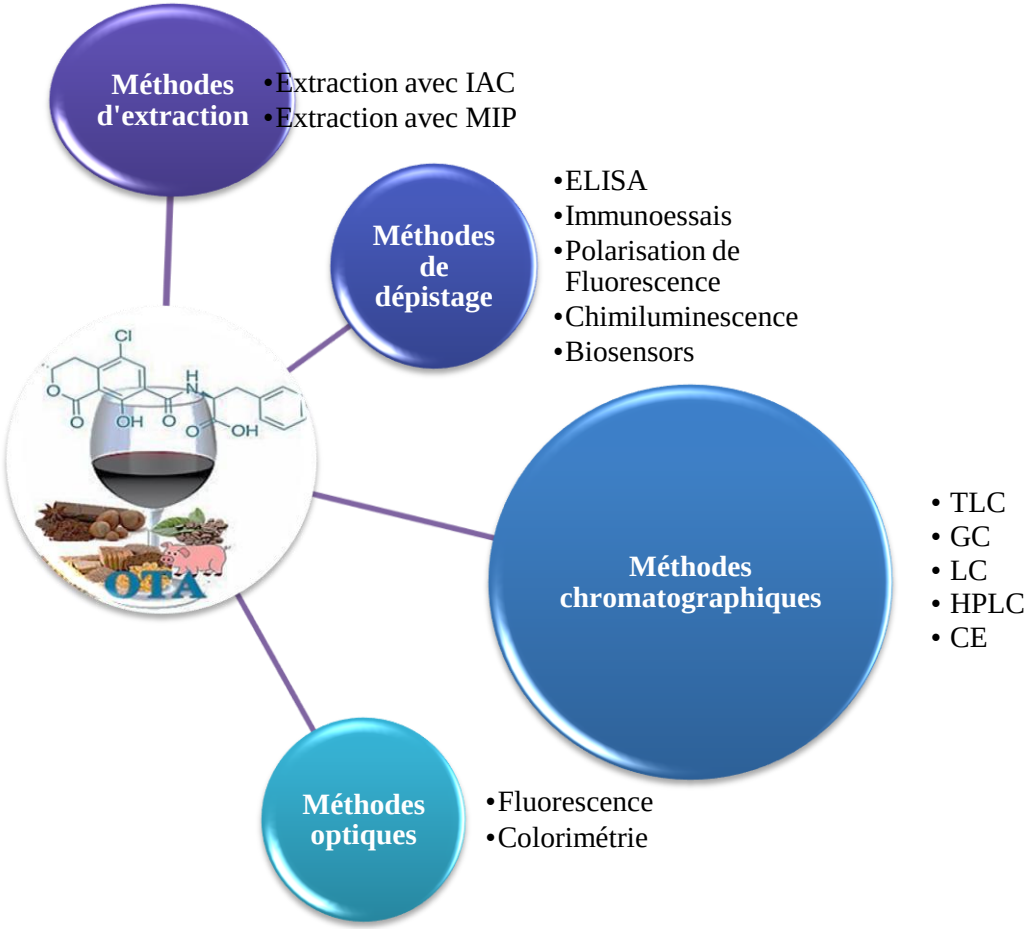

IAC: ImmunoAffinity Column; MIP: Molecularly Imprinted Polymer; ELISA: Enzyme linked immunosorbent assays; TLC: Thin Layer Chromatography; GC: Gas Chromatography; LC/MS: Liquid Chromatography; HPLC: High Performance Liquid Chromatography; CE: Capillary electrophoresis, selon l'acronyme anglais.

Figure 3 Classification des méthodes employées pour détecter ou quantifiée l'OTA dans les aliments.

2.3.1 Biocapteurs

Les biocapteurs apparaissent comme l'une des méthodes prometteuses pour le diagnostic médical mais aussi pour le contrôle des composés alimentaires et la surveillance de l'environnement en raison de leur rapidité, spécificité, facilité de fabrication, faible coût et large champ d'application. Le principe de base d'un biocapteur est de détecter la reconnaissance moléculaire entre un biorécepteur et la cible et de transformer un signal chimique en un autre type de signal à l'aide d'un transducteur optique ou électrique, [15].

2.3.2 La détection optique

Les capteurs optiques sont également appelés "optodes". Ceux-ci sont basés sur l'absorption de lumière entre les réactifs et les produits d'une réaction, ou la mesure de la lumière émise par un processus de luminescence ou fluorescence. Les biocapteurs optiques intègrent la technique optique avec un élément biologique pour identifier les espèces chimiques à doser.

2.3.2.1 La fluorescence de l'OTA

La fluorescence est le phénomène d'émission d'un quantum de lumière par une molécule ou d'un matériau après la première excitation électronique dans un processus d'absorption de lumière. Après excitation, une molécule reste pendant un certain temps dans le soi-disant état excité et son émission de fluorescence peut être observée habituellement avec une énergie plus faible que l'excitation. Hashemi et al. indiquent que la longueur d'onde d'excitation des solutions aqueuses d'OTA est à 330 nm. Dans des conditions alcalines, le maximum d'excitation de l'OTA se produit à 330-380 nm associé à un augmentation du signal d'émission à 453 nm [16].

2.3.2.2 Optoélectronique

Les techniques spectroscopiques optiques ont quatre modules de base: source de lumière, détecteur de lumière, des dispositifs de sélection de longueur d'onde et une unité de traitement du signal, Par conséquent, les principales techniques spectroscopiques sont désignées sous le terme « optoélectronique ». L'utilisation des LED-UV pour induire la fluorescence est largement décrite, Dickens et al ont proposé un réseau de LED-fluorescence à

base de capteur réel compact et portable [17] ou le développement d'un fluorimètre portable pour l'aflatoxine [18] ou un système d'analyse par luminescence [19].

2.3.2.3 Colorimétrie

La colorimétrie est un exemple d'un procédé d'analyse spectroscopique. A la fin du XIXe siècle, la spectroscopie était limitée à l'absorption, l'émission et la diffusion dans le visible, l'ultraviolet et le rayonnement électromagnétique infrarouge. La colorimétrie est utilisée en chimie analytique pour l'identification et la détermination des concentrations de substances qui absorbent la lumière. Il est similaire à spectrophotométrie, mais se distingue par son intérêt à réduire les spectres aux corrélations physiques de perception des couleurs [20].

CHAPITRE III

MÉTHODOLOGIE

La première étape a consisté en l'élaboration d'un aptacapteur électrochimique dans un système de flux automatisé pour la détection en ligne de l'OTA en employant l'analyse immunologique directe et indirecte. Les transducteurs sont des électrodes sérigraphiées en graphite. Le système est formé de trois électrodes: une électrode de travail, une électrode auxiliaire en graphite et une électrode de référence Ag / AgCl comme indiquée sur la figure 4.

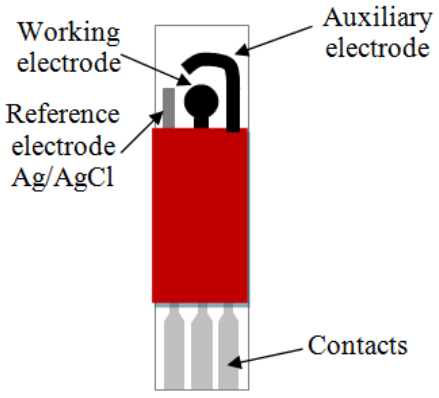

Figure 4 Représentation de l'écran imprimé électrode de carbone.

Préparation de l'OTA biotine: Le groupe carboxylique de l''OTA a été activé avec un mélange EDC / NHS. 400 µL d'une solution à 34 mM d'EDC et NHS ont été ajoutés, goutte à goutte, à 200 µL d'une solution à 2,5 mg/mL d'OTA préparé dans du tampon MES 0,1 M à pH 5,5. Le mélange OTA-NHS-EDC a été agité à température ambiante pendant une heure. Puis 250µL d'une solution à 50 nM de EZ-link-biotine amine PEO3 ont été ajoutés au mélange et agité à température ambiante pendant 24 heures. Le conjugué a été dialysé à 4 °C dans du tampon carbonate puis avec de l'eau distillée.

La modification des groupes carboxyle des billes magnétiques avec un aptamère aminé: 500 nM de l'aptamère 5'-amino-modifiée a été préparée dans un tampon et chauffé à 94 ° C pendant 5 min. Puis on laisse reposer à température ambiante pendant 20 min. Ensuite, l'OTA-aptamère a été immobilisé sur les MBs carboxyle en utilisant le protocole décrit par la société Invitrogen. Après avoir lavé 2 fois avec du tampon MES 25 mM, MBs ont été incubées pendant 30 min avec l'aptamère à température ambiante. Le carbodiimide (EDC) a incubé avec le mélange pendant une nuit à température ambiante sous une légère agitation pour activer le groupe carboxyle des billes magnétiques. Ensuite, les MBs sont lavées avec 1 ml de tampon TT 3 fois (chaque lavage dure 30 min). L'incubation des MBs avec le tampon TT est utilisée pour le lavage et le blocage des groupes carboxyliques qui n'ont pas réagi. Les MBs modifiées ont été mises en suspension dans un tampon TE et stockées à 4 °C. Les MBs de contrôle ont été préparés en suivant le même mode opératoire sans addition d'aptamère.

Modification des billes magnétiques acides avec l'OTA: Après de lavage avec du PBS, 75 µl de MBs ont été incubées avec 100 µl d'OTA (1 mg/ml) et EDC / NHS durant la nuit. La réaction a été stoppée avec de la glycine 30 mM et les résidus non liés ont été éliminés par lavage trois fois avec du PBS. Les MBs modifiées ont été mises en suspension dans 100 µl de PBS et stockées à 4 °C. Avant utilisation dans l'aptacapteur dans le système à flux, les électrodes ont été soumises à un prétraitement électrochimique avec 5 balayages de potentiel entre 1,0 et -1,5 V avec une solution 0,5 M H_2SO_4 en utilisant le potentiostat Autolab PGSTAT 12.

Aptacapteur compétitif direct : Les électrodes ont été bloquées avec du BSA 2% pendant 1 h à température ambiante pour éviter une adsorption non spécifique. L'électrode a été introduite dans une cellule d'écoulement relié à un potentiostat. Une solution de 2 µl de MBs modifiées avec l'aptamère dans du tampon de liaison a été injectée sur la surface de

l'électrode. L'étape de compétition a été réalisée en faisant passer différentes concentrations d'OTA préparées dans une solution tampon ou de l'échantillon réel avec OTA-biotine. Ensuite, une solution d'avidine-ALP a été injectée sur la surface d'électrode pour effectuer la réaction avidine-biotine. Des séquences spéciales ont été utilisées pour injecter et incuber le mélange et l'addition de l'avidine-ALP, le temps d'incubation était de 10 min pour chaque étape. Enfin, une solution de 1-NP dans du tampon DEA à pH 9,5 a été déposée sur l'aptasensor. La génération du signal est fondée sur la déphosphorylation du non électro actif 1-NP par la ALP, suivie par l'oxydation de l'électroactif -1-naphtol- en 1-iminoquinone sur la surface de l'électrode. Le lavage a été effectué en faisant passer automatiquement du PBS-Tween (0,05%) de la solution après chaque étape.

Aptacapteur compétitif indirect: Les sites non spécifiques sur la surface des SPCEs ont été bloqués avec 100 µl de BSA à 2% pendant 1 h à température ambiante. Puis, 4 µL de MBs modifiées avec l'OTA diluées dans le tampon de liaison a été injecté sur la surface de l'électrode. La deuxième étape a consisté à passer de 150 nM d'aptamère biotinylé avec l'OTA libre dans une solution tampon ou dans l'échantillon réel. Par conséquent, l'OTA présente dans les échantillons alimentaires est entré en compétition avec l'OTA immobilisé sur les MBs. Une solution d'avidine-ALP a été ajoutée à l'aptamère biotinylé. La détection électrochimique a été réalisée de la même manière que celle décrite pour l'aptacapteur coécrit précédemment

Détection ampérométrique de l'OTA: La mesure de l'activité de la ALP, l'enzyme qui marque l'OTA ou l'aptamère, a été réalisée par ampérométrie. Les mesures ampérométriques ont été effectuées en utilisant la carte d'acquisition de données (PMD1208FS), qui relie le potentiostat avec un ordinateur pour l'acquisition du signal. Le substrat de la ALP (le NP-1) a été injecté sur l'aptacapteur dans la cellule d'écoulement reliée au potentiostat. Après incubation du substrat pendant 6 minutes, un potentiel de 200 mV a été appliqué. Ce potentiel correspond au potentiel d'oxydation du produit 1-naphtol en 1-iminoquinone. Le signal est proportionnel à l'activité enzymatique de la ALP et par conséquent proportionne à la quantité d'OTA. Dans le cas de l'aptacapteur de type compétitif direct, le signal est proportionnel à la quantité d'OTA et dans le cas de la compétition indirecte le courant est inversement proportionnel à la quantité d'OTA.

Préparation des échantillons de bière: Les échantillons de bière ont été enrichis avec une concentration connue de la solution mère d'OTA. Ensuite, les échantillons enrichis, préalablement refroidis à 4 ° C pendant 30 min pour empêcher la formation de mousse ont été dégazé par sonication pendant 1 h. Le pH de la bière a ensuite été ajusté à 7.4. Enfin, la bière est passée à travers un filtre (0.45 mm). L'analogue déchloré de l'OTA, l'ochratoxine B (OTB) a été utilisé comme analyte non spécifique pour tester la spécificité de l'aptacapteur

Système de flux automatisé: Dans le système d'écoulement, tous les paramètres: tels que le temps d'incubation, l'étape de lavage, le pompage, l'injection et les volumes d'aspiration, l'arrêt de l'écoulement, les mesures des signaux et leur enregistrement sont contrôlés automatiquement par une interface graphique personnalisée développée sous LabVIEW 8.5. Les réactifs ont été délivrés par une pompe seringue bidirectionnelle (XLP Cavro 6000) avec quatre vannes. La vanne 1 (V1) est utilisée pour injecter des billes magnétiques, des aptamères et de l'OTA, le lavage a été effectué par V2 et V3 a été utilisé pour l'injection du substrat d'ALP tandis que les déchets a été éliminé par V4, un schéma est présenté sur la figure 5.

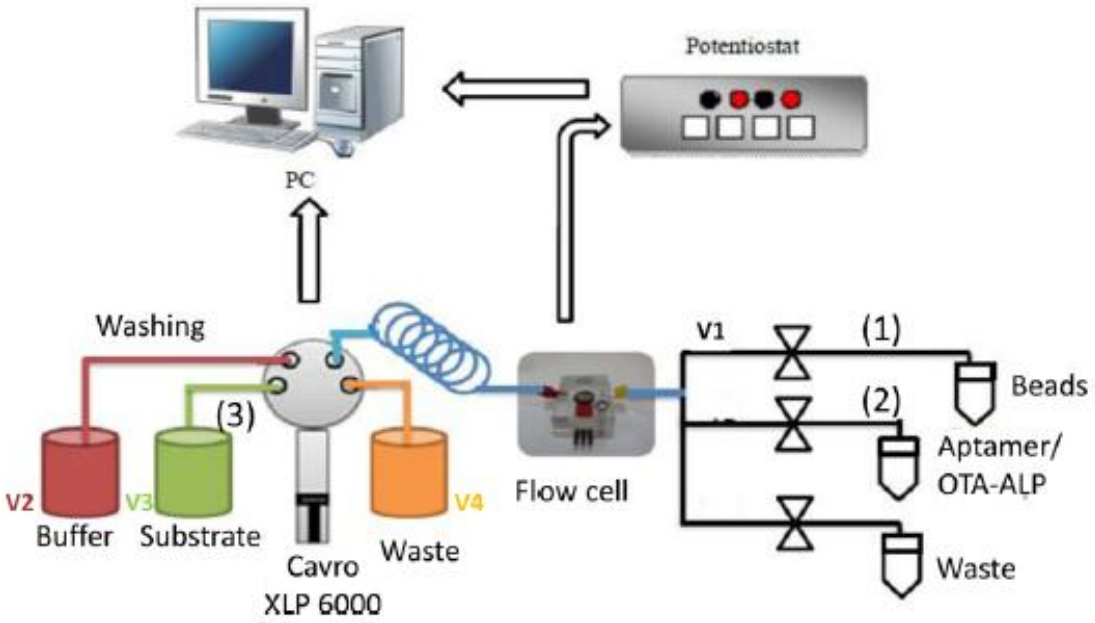

Figure 5 Représentation schématique du système d'écoulement automatisé.

Partie A: Absorbance basée sur l'émetteur et les photos détecteurs

3.1 Photo détecteurs pour détecter les pesticides

Un système analogue constitué d'une LED comme source de lumière et d'un photo détecteur, une carte d'acquisition de données et un ordinateur ont été utilisés pour détecter la thiocoline après l'hydrolyse de l'acétylthiocholine (ACTH) par l'acétylcholinestérase. La mesure de la relation entre la quantité de lumière libérée a été mesurée en utilisant trois enzymes différentes (electric eel, Drosophila melanogaster et D. melanogaster génétiquement modifiée) vis-à-vis de 3 insecticides: paraoxon, carbofurane et malaoxon [21].

3.1.1 Détermination spectrophotométrique de l'activité des enzymes et des constantes d'inhibition

La détermination de l'activité de l'acétylcholinestérase et des paramètres cinétiques d'inhibition a été réalisée en utilisant un spectrophotomètre à barrette de diodes Hewlett Packard 8451.

3.1.2 Détermination de l'activité acétylcholinestérase (AChE).

La détermination de l'activité enzymatique a été réalisée par spectrophotométrie à 412 nm, selon la méthode d'Ellman [22], par la réaction en continu du groupement thiol de la thiocholine avec le DTNB qui donne un composé de couleur jaune. La quantité du composé coloré (thio nitrobenzoate,) est mesurée à 412 nm [23]. L'essai a été effectué comme suit:

- Blanc, 600µL de tampon phosphate, 300 µL de 2,5 mM de DTNB, 100 µL de 10 mM ATChI.
- Réaction enzymatique, 590µL de tampon phosphate, 300 µL de 2.5 mM DTNB, 100 µL de 10 mM ATChI et 10 µL de solution d'enzyme a été ajoutée.

Le DTNB a été préparé dans 0,1 mM de tampon phosphate à pH 7; l'ATChI a été préparé dans du NaCl à 0.9%. Une courbe d'absorbance en fonction du temps a été obtenue, l'activité enzymatique est exprimée en unités de potentiel.

3.1.3 Détermination de la constante d'inhibition (Ki)

Dans ce but, des solutions d'insecticides à différentes concentrations ont été préparées. 100 µL de solution d'enzyme incubée avec les solutions d'insecticides ont été prélevés à des intervalles de temps fixes (1, 3, 5, 7, 10 et 15 minutes) et ajoutés à la cuvette spectrophotométrique contenant 300 µL de 25 mM DTNB, 100 µL de 10 mM ATChI et 500 µL de tampon phosphate, le dosage a été réalisé à 30 °C. La V0 a été déterminée en incubant 100 µL de solution la enzymatique ajoutée 900 µL d'un tampon phosphate, Le processus a été répété trois fois pour les enzymes et les pesticides. Ensuite, l'activité enzymatique en présence de l'insecticide a été enregistrée à partir du temps 1 min et la pente de l'absorbance en fonction du temps a été obtenue. Le taux de réaction est proportionnel à la concentration du produit présent. Cet ensemble de données sera utilisée pour estimer Ki comme une caractérisation cinétique de la réaction enzymatique inhibée. La méthodologie est expliquée dans la figure 6.

3.1.4 Détermination optique des activités enzymatiques et des constantes d'inhibition

L'activité de l'acétylcholinestérase a été déterminée et comparée à celle obtenue avec l'équipement commercial. Dans ce cas, la méthode Ellman a été employée avec une solution enzymatique à $2*10^{-2}$ UA/sec, et la solution a été diluée de 10 à 0,08 mg/ml, pour établir les limites de détection pour le spectrophotomètre développé et commercial. Pour calculer Ki en présence du mélange enzyme-pesticide, la pente a été enregistrée avec la carte d'acquisition s pour chaque concentration d'enzyme et d'insecticide à différents temps d'incubation. Ensuite, la tension obtenue pour chaque concentration d'insecticide et d'enzyme a été normalisée.

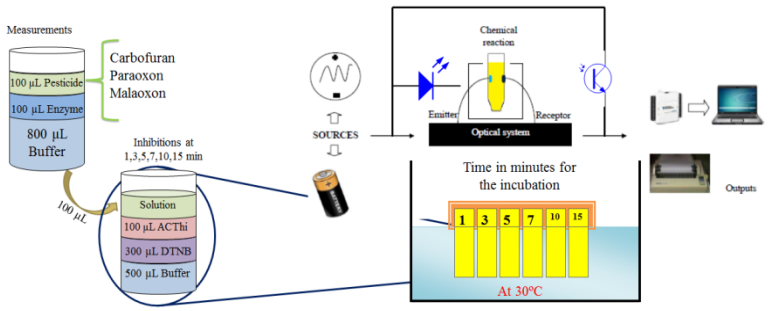

Figure 6 Description du mode d'acquisition des mesures optiques et spectroscopiques.

3.2 LED-UV et photo détecteurs pour détecter OTA

Le photo détecteur est un BPW85B, à base de silicium NPN phototransistor, le circuit utilise une source de 5V. Il a été testé par le biais d'une interface graphique conçue sous LabVIEW 2010 avec une carte d'acquisition. La concentration d'OTA est établie en fonction de la tension générée. Différentes concentrations d'OTA (1000 µg/L, 500 µg/L, 250 µg/L et 125 µg/L) ont été préparées dans le MeOH ainsi qu'un essai témoin sans OTA. 1,5 ml de solution ont été ajouté dans la cuvette puis elle a été insérée dans la chambre. La solution a été excitée par UV-LED à 365 ou 375 nm et différents flux de rayonnement. Le signal a été enregistré par l'interface avec la carte d'acquisition. L'interface a acquis 3 cycles, chaque cycle consistait à détecter la concentration d'OTA de façon continue (plus concentrée à moins concentrée), cela a été répété 2 fois plus pour chaque UV-LED et chaque essai a été répété trois fois.

Partie B: Fluorescence avec capteur CMOS.

3.3 ArduCAM pour détecter la fluorescence

Le dispositif est formé d'un support conçu pour fixer le module de caméra ArduCAM, il se déplace vers le haut et vers le bas pour insérer ou retirer la cuvette dans la chambre. Un trou a été foré dans la chambre à 90 degrés à partir de module de caméra pour l'émetteur. ArduCAM est contrôlé pour Arduino, 3,2 pouces TFT LCD avec écran tactile, construit en prise / TF carte SD. Un 4/1 pouce, 5 mégapixels capteur d'image (MP) CMOS est utilisé conjointement caméra. Un LM317 régulateur de tension a été utilisé comme un limiteur de courant pour protéger l'UV-LED. Il a été alimenté par le port USB de Arduino. Pour stocker l'image dans une carte Micro SD avec le format Joint Photographic Experts Group (JPEG) en 10 secondes environ. Pour traiter l'image, une interface dans MATLAB2011 a été construit, il permet de choisir le processus de l'image, ou pour traiter une image ou toutes l'image contenue dans un dossier. En outre, il est possible de modifier la zone à mesurer et la rotation de l'image.

3.4 CMOS pour détecter la fluorescence

Le module de caméra, Linksprite (LS-Y201-infrarouge) capture des images et les transmet via une interface série TTL avec un capteur 1/4 Omnivision CMOS à partir d'un port série avec communication via UART. Il fonctionne avec une alimentation 5VDC. Une interface utilisateur graphique a été créée en Matlab R2011a. L'utilisateur n'a pas besoin d'installer Matlab depuis l'interface car c'est un fichier exécutable. L'interface est facile à utiliser, pour obtenir les valeurs et sauvegarder toutes les informations permettant automatiquement son utilisation comme un système portable.

3.5 Téléphone mobile pour détecter la fluorescence

Le téléphone mobile se compose d'un appareil photo de 8 mégapixels, la source de la LED est un LM317 régulateur comme courant constant alimenté par la batterie lithium-ion intégrée dans le téléphone. Une interface est développée pour l'imagerie par fluorescence pour détecter la présence de l'OTA dans les échantillons.

3.6 Image de fluorescence

Les photographies capturées par des dispositifs optiques comme les caméras sont considérés comme des images numériques, qui sont une représentation numérique d'une image en deux dimensions. L'image numérique contient un nombre fixe de lignes et de colonnes de pixels. Chaque pixel est défini par trois valeurs pour les composantes rouges, bleues et vertes du réseau de pixels, matrice de M lignes par N colonnes pour chacune des couleurs avec un qui varie de 0 à 255. La position du pixel est décrite par une paire de coordonnées (xi, xj). Dans le modèle de couleur RGB, l'image peut être représentée par la fonction d'intensité: IRGB = (PR, PG, PB). Sur la figure 7, les couleurs rouge, vert et bleu sont représentées par un système de coordonnées cartésiennes tridimensionnel.

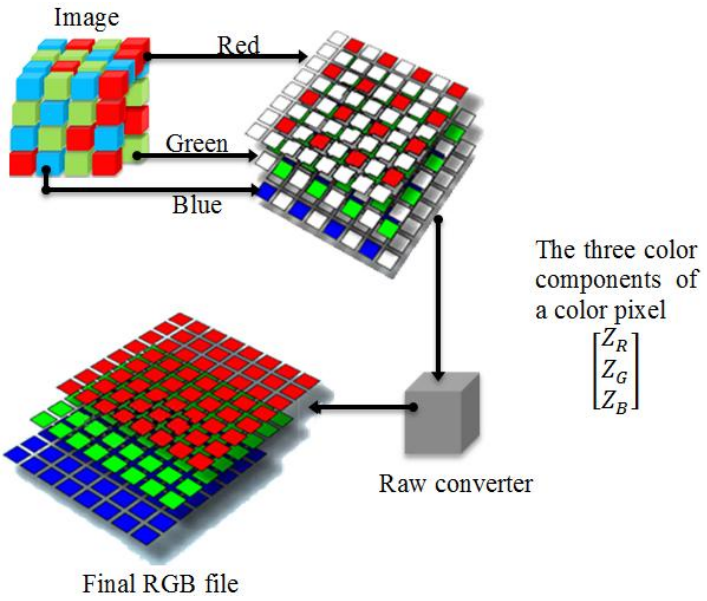

Figure 7 Schéma de la mise en œuvre du modèle de couleur RGB pour traiter les images.

3.7 Fluorescence avec HPLC (selon l'acronyme anglais)

La phase mobile utilisée pour l'HPLC est un mélange acétonitrile/eau / acide acétique (40/59/1) pour les échantillons de vin et de bière. Dans le cas de l'extraction de l'OTA du cacao, la phase mobile est un mélange de 48/51/1. Il a été traité par ultrasons pendant 20 minutes. La détection a été effectuée par détection de fluorescence à 333 et 460 nm comme longueur d'onde d'excitation et d'émission respectivement. Avant l'injection, tous les échantillons ont été filtrés à travers un filtre de 0,2 µm en PTFE. 200 µL de solution d'élution des colonnes et des solutions étalons d'OTA ont été injectées à trois reprises dans l'HPLC. L'OTA est identifié par son temps de rétention constant (5 minutes) pour la bière et le vin, 12 minutes pour l'extraction de cacao et quantifiée en comparant avec la surface du pic des solutions étalons. Au début, l'HPLC a été nettoyée avec la phase mobile à trois reprises et après l'injection des échantillons, le même lavage est réalisé.

3.8 Méthodes d'extraction

3.8.1 Extraction de l'OTA du cacao en utilisant des colonnes MIP

1 Kg de fèves de cacao a été étalé sur une feuille de nylon noir et séchés pendant une nuit. Des solution d'OTA à 20, 10, 5 et 1,5 µg préparées dans 100 mL de tampon contenant

5% d'éthanol ont été pulvérisées lentement sur les fèves de cacao. Les échantillons ont été conservés à la température ambiante pendant une nuit.

3.8.2 Extraction avec des solutions à 1% NaHCO3 dans l'eau

L'OTA a été extrait, en utilisant directement 50 g de grains contaminés, par 200 ml de solution aqueuse à 1% de $NaHCO_3$ dans un agitateur horizontal pendant 30 minutes. Una aliquote de 50 ml a été filtrée en utilisant un filtre en acier de 45 pm. Avant le chargement de la colonne par la solution d'extraction, celle-ci a été équilibrée en utilisant 2 ml d'acétonitrile, puis 2 ml d'eau. Pour le chargement, un échantillon de 20 ml a été passé à travers la colonne en maintenant constante la vitesse d'écoulement (1 goutte/s). La colonne a été lavée pour éliminer les interférences en utilisant 8 ml d'un mélange 60:40 eau et d'acétonitrile. L'échantillon a été élué en utilisant 2 ml de méthanol dans de l'acide acétique à 2%. Les colonnes MIPs ont été pré-conditionnées avec 10 ml de PBS avant le chargement des échantillons. Après passage de l'extrait au travers de la colonne. La colonne MIP a été rincée avec 20 ml de PBS contenant 20 µl de Tween-20. L'OTA a été élué en utilisant 3 ml de méthanol avec rinçage en continu.

3.8.3 Extraction avec l'acétonitrile

Les fèves de cacao contaminés ont été conservés à -80 °C pendant une nuit, puis les fèves ont été broyées. On mélange 50 g de poudre de cacao avec 200 ml d'un acétonitrile / eau (60:40) en présence de 4 g de NaCl et on agite pendant 30 minutes. Le liquide extrait a été filtré à l'aide de un filtre 45 µm puis centrifugé à 5000 rpm pendant 10 minutes. Pour la purification, 25 ml de PBS ont été mélangés avec 48 µl de tween-20 et de 20 ml d'extrait et l'ensemble est centrifugé. En outre, la colonne IAC a été équilibrée avec 10 ml de PBS (pH 7,4). L'échantillon extrait a été chargé goutte à goutte sur la colonne en maintenant le débit 1 goutte/sec. La colonne a été soigneusement rincée avec 20 ml de PBS. L'OTA retenue dans la colonne a été élue en utilisant 3 ml de méthanol avec rinçage en continu.

3.8.4 Extraction de l'OTA à partir du vin et de la bière échantillon

3.8.4.1 Colonnes IAC (selon l'acronyme anglais)

Le vin a été enrichi avec des solutions connues d'OTA (2, 4, 6, 10 µg/l, les échantillons de vin ont été préparés de la manière suivante : 8 ml d'échantillon avec 1 ml de 10% $NaHCO_3$ et concentration 1 ml d'OTA dans le méthanol a été mélangés. L'extrait a été filtré en utilisant un filtre de 45 µm monté sur une seringue stérile. Le processus pour préparer des échantillons de bière est le même que pour le vin, mais la solution de $NaHCO_3$ est à 1%. Dans l'étape de chargement, 10 ml de l'extrait filtré sont passés à travers les colonnes d'IAC deux fois, après qu'elles aient été pré-conditionnées avec 10 mL de tampon PBS. Après, la colonne a été lavée avec 20 ml du tampon PBS contenant 20 µL de Tween 20. Pour la dernière étape, l'OTA a été élué en utilisant 3 ml de méthanol à un débit constant de 1 goutte/sec. Le blanc a été préparé sans OTA.

3.8.4.2 Colonnes MIP (selon l'acronyme anglais)

La colonne a été pré-conditionnée avec 4 ml d'acétonitrile et 4 ml d'eau distillée. Dans l'étape de chargement, 10 ml de l'extrait filtré sont passés à travers la colonne 2 fois. L'étape de lavage est réalisée avec 4 ml HCl 0,1 M avec 3 ml d'acétonitrile. L'élution est réalisée avec 20 µl d'acide acétique dans 2 ml de méthanol. L'éluant est recueilli dans une bouteille ambrée et analysé par HPLC et par le dispositif de fluorescence développée.

3.9 Les systèmes d'écoulement

Le système SIA développé dans cette thèse ont été programmés en utilisant HyperTerminal en raison sa facilité d'utilisation sans exigences spécifiques. De plus il peut être installé très facilement sur un ordinateur portable. L'affichage se fait très facilement il est aisé de de transférer les données entre deux ordinateurs en utilisant les ports série et pour le contrôle du port série de dispositifs ou de systèmes externes tels que des instruments ou des robots scientifiques, entre autres. Pour utiliser HyperTerminal il est nécessaire le sélectionner l'écoulement dans le champ prévu: Bits per second: 9600; Data bits: 8; Parity: None; Stop bits: 1; Flow control: None; Select the Menu Setting. Select "Send line ends with line feed"; Select "Echo typed characters locally"; Enter a line delay of 0; Enter a character delay of 0; Select

“Wrap lines that exceed terminal width”. La pompe est connectée à l'ordinateur à l'aide d'un connecteur série RS232, qui est une norme pour la transmission série de communication des données. Le programme est écrit avec les commandes suivantes pour créer les séquences: I = entrée; O = sortie; suivi du numéro de soupape; A = aspirer; D = drain; suivie par le volume en microlitres; g = à partir d'un cycle; G = fin du cycle, suivi par le nombre total de cycles; S = vitesse; R = exécuter la séquence; M = retard, un maximum de 30 secondes.

3.10 L’evaluation de la performance du dispositif de fluorescence dans des conditions particulières

Le capteur CMOS avec un LED-UV à 365nm à 4mW a été évalué sous trois conditions,

a) Les différents solvants: d'abord, une solution à 20 µg/l d'OTA a été préparée dans le méthanol, l'éthanol, le tampon PBS, l'acétonitrile, l'eau distillée, la phase mobile (48/51/1), l'eau du robinet et de HEPES un tampon (6,507g HEPES (50 mM), 3,504 g de NaCl (120 mM), 186,25 mg KCl (5 mM), 238 mg de MgCl2 (5 mM) dans 500 mL d'eau de distillation à un pH de 7,4). 1 ml de solvant a été préparé sans OTA et ceux-ci ont été considérés comme en blanc, 1 ml des concentrations d'OTA ou blanc ont été insérés dans la cuvette et dans la chambre du système développé.

b) Variation de la concentration en NaCl: Elle a été modifiée dans le tampon HEPES comme suit: 0 mM, 10 mM, 30 mM, 60 mM, 90 mM et 120 mM de NaCl. Ceux-ci ont été considérés comme le blanc et après pour effectuer les mesures une concentration de 20 µg/l d'OTA a été préparé en ce que les solutions et la fluorescence a été mesurée avec le système développé. Une heure plus tard, les mesures ont été répétées pour vérifier s’il y avait les changements avec le temps. Le pH a été ajusté à 7,4 avec du NaOH 3M.

c) Modifications de pH: le tampon HEPES a été préparé dans une gamme de pH de 6 à 8,4, avec une même concentration de 20 µg/l d'OTA. L'intensité de la fluorescence en fonction du pH a été mesurée et les résultats ont été traités.

Partie C: Traitement de l'image

La propriété la plus courante pour mesurer la qualité de tout matériau est son aspect. Les différents paramètres sont la couleur, la forme, la taille et surface. Les mesures de couleur ont également été utilisées en tant que paramètres de qualité et indicateurs de certains constituants du matériau. Plusieurs facteurs qui influencent le rayonnement affectent la couleur exacte qu'une personne perçoit. Ces facteurs sont: la distribution d'énergie spectrale de la lumière, les conditions dans lesquelles la couleur est visualisée, les caractéristiques spectrales de l'objet par rapport à l'absorption, la réflexion et la transmission et la sensibilité de l'œil [204]. La lumière est le stimulus de base de couleurs.

Tout d'abord, l'image fluorescente a été l'image générée par la propre fluorescence de l''OTA excité par la lumière UV, les échantillons ont été préparés avec une concentration connue d''OTA (2, 5, 10 µg/l), les échantillons de vin ont été préparés de la manière suivante. 8 ml d'échantillon avec 1 ml d'une solution à 10% de $NaHCO_3$ dans l'eau et 1 ml d'une solution d'OTA dans le méthanol ont été mélangés. L'extrait a été filtré sur filtre de 45 µm monté sur une seringue stérile. Le processus pour préparer des échantillons de bière est le même pour le vin, mais la solution de $NaHCO_3$ est à 1%. Le blanc a été préparé sans OTA; 1 ml de méthanol a été mélangé avec 8 ml de l'échantillon de vin ou de la bière et 1 ml de $NaHCO_3$.

Les colonnes IAC ou MIP n'ont pas été utilisées; l'image de chaque concentration était directement capturée. Les mêmes échantillons ont été analysés avec le Fluoroskan pour comparer les résultats. En outre, les images peuvent être traitées de différentes façons histogramme gris-échelle; Bleu histogramme ; Rouge, Vert et Bleu (RGB) modèle; Teinte, Saturation et Valeur (HSV) modèle; Teinte, Saturation et Intensité (HSI) modèle; Teinte, Saturation et Luminosité (HSL) modèle; L* a* b* modèle. Tous les programmes ont été réalisés sur Matlab, les programmes lisent tous les fichiers d'image avec un nom, t, le programme réalise ses fonctions et enregistre les données dans un fichier texte, jpg ou fig format conservant le nom du fichier, éventuellement, il est possible d'ajouter un nom supplémentaire pour identifier tous les fichiers et les résultats obtenus.

CHAPITRE IV

RÉSULTATS

Nous avons décrit le premier aptacapteur électrochimique à base de flux automatisé pour la détection en ligne de l'ochratoxine A L'applicabilité de l'aptacapteur à base de flux développé a été validée par la détection de l'OTA dans les échantillons de bière. L'incorporation de l'aptamère dans le dispositif d'écoulement a augmenté la sensibilité du système pour déterminer OTA à faible concentration. Un débit de 0,2 µl/s a été utilisé pour injecter les billes sur la surface de l'électrode.

Aptacapteur compétitif direct: La présence d'OTA dans la solution empêche la liaison de l'OTA immobilisé à l'aptamère, conduisant à une diminution de l'activité de la ALP. La détection électrochimique est effectuée en utilisant une SPCE pour augmenter la sensibilité de la méthode. La génération du signal est fondée sur la déphosphorylation du substrat non-électro-actif 1-naphtyl phosphate, suivie par l'oxydation du produit électro-actif du phosphate de 1-naphtol en 1-iminoquinone sur la surface de l'électrode. Le signal électrochimique généré est mesuré par ampérométrie après application d'un potentiel de travail de 200 mV *vs* Ag / AgCl. La valeur obtenue est inversement proportionnelle à la concentration d'OTA. Une valeur médiane (IC50) de 0,098 µg/l et un LOD de 0,06 µg/l ont été obtenus au cours des essais de compétition directe.

Aptacapteur compétitif indirect: Une étude comparative a été effectuée dans un système d'écoulement automatisé dans lequel la solution d'aptamère marqué est en compétition entre l'OTA immobilisé et l'OTA libre. La détection électrochimique a été réalisée selon une procédure similaire à celle décrite dans le format compétitif direct La limite de détection (0,05 mg / l) correspond 80% de la liaison et IC50 (0,090 mg /l) correspond à 50% de la liaison, il a été calculée à partir de la courbe d'étalonnage présentée dans la figure 8,

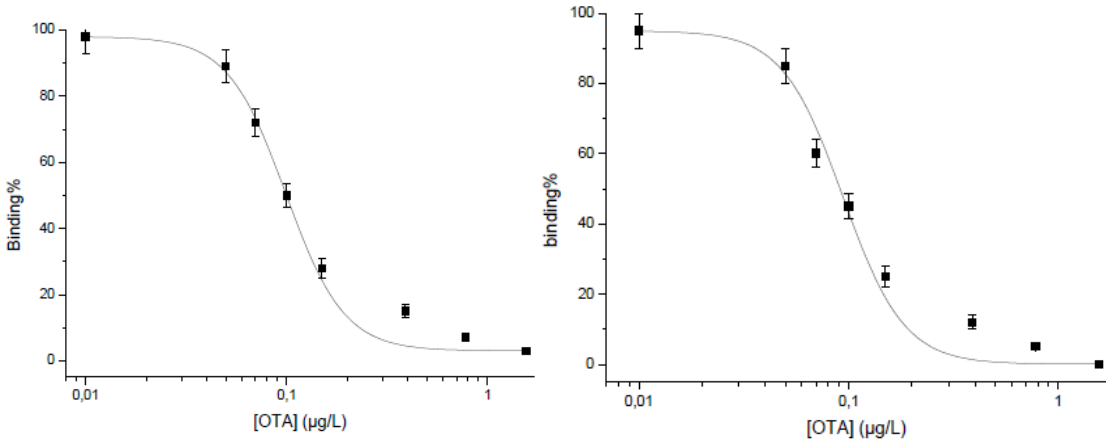

Figure 8 Courbe d'étalonnage pour l'aptasensor dans un essai d'écoulement compétitif direct (à gauche) et pour le dosage compétitif indirect (à droite).

Effet de la matrice et applicabilité de l'aptacapteur basé sur les flux pour la détection de l'OTA dans la bière: Des échantillons de bière exempts d'OTA sont enrichis avec des concentrations connues d'OTA (0.2 et 0.8 µg/l), Les résultats analytiques et les taux de récupération sont montrés dans le tableau 2.

Tableau 2 Les pourcentages de récupération de l'OTA pour le dosage compétitif indirect.

Concentration dopé avec OTA (µg/L)	OTA concentration (µg/L)	R.S.D (%)	R.E (%)	R (%)
0.2	0.21	5	5	105
0.8	0.78	4	5	97.5

Partie A: Absorbance basée sur l'émetteur et les photo détecteurs.

4.1 La détection des pesticides à l'aide d'un phototransistor et d'une diode

Le pourcentage d'inhibition de l'acétylcholinestérase a été déterminé par absorbance. La figure 9 montre les mesures de l'activité enzymatique pour l'EE et le blanc, la stabilité, la reproductibilité et le LOD du système développé. La LOD de l'activité enzymatique pour le système développé est de $6{,}91 \times 10^{-4}$ Absorbance unités / s et pour l'équipement commercial elle est de $2{,}29 \times 10^{-3}$ Absorbance Unités / s. Le système développé est trois fois plus sensible que le système commercial et il a un coût inférieur à celui du spectrophotomètre commercial;

En outre, le système développé est portable grâce à sa petite taille par rapport au produit commercial.

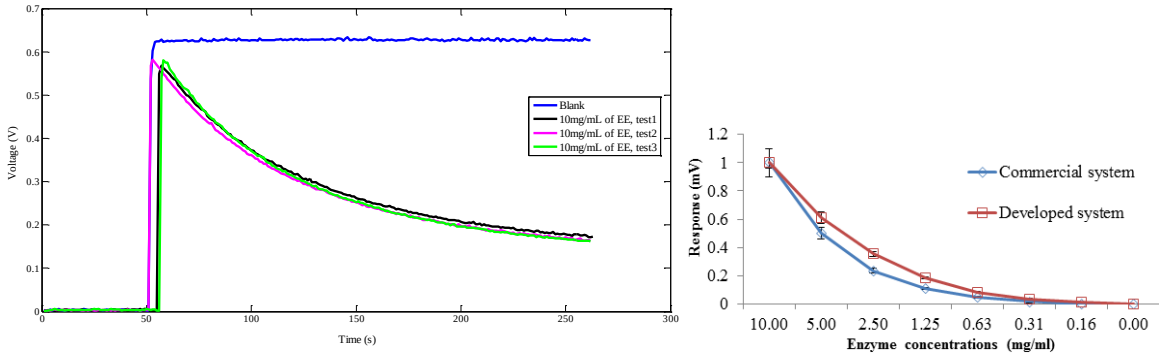

Figure 9 Moyenne et écart type obtenu avec les données vierges et l'enzyme EE, ont montré la stabilité et la reproductibilité du système développé (à gauche) et le LOD obtenu avec l'appareil commercial par rapport au système développé au système mis au point (à droite).

Par exemple, l'inhibition du malaoxon sur l'enzyme d'anguille électrique est représentée dans la figure 10. Les valeurs de la pente sont directement proportionnelles aux concentrations de pesticides et les constantes d'inhibition ont été obtenues en traçant 1 / pente fonction de 1 / [concentration], pour chaque AChE testé. Ensuite, Ki a été calculé à partir de la pente de cette relation [24,25].

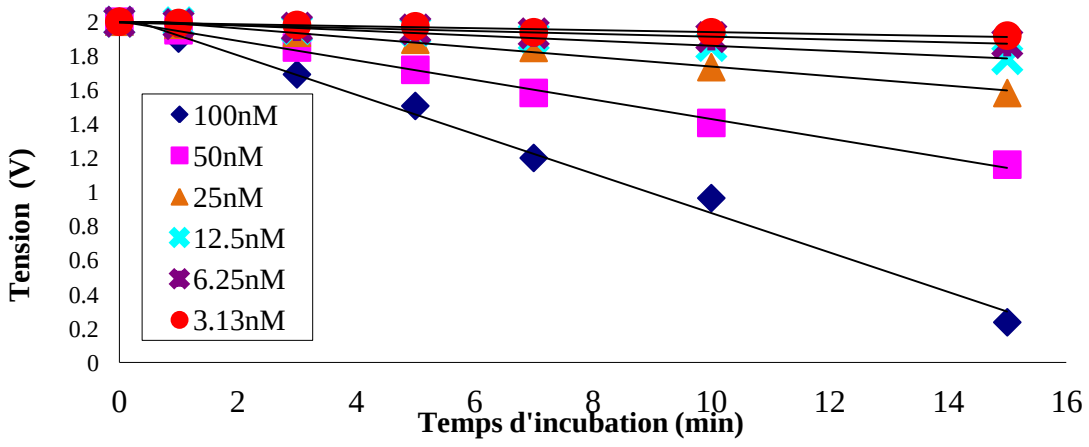

Figure 10 inhibition cinétique de l'acétylcholinestérase de l'anguille électrique par le malaoxon à différentes concentrations obtenues avec le système mis au point.

La LOD du système développé et les LOD obtenues par les méthodes électrochimiques pour l'enzyme et l'insecticide testé sont indiquées dans le tableau 3. Pour le paraoxon et la carbofurane, les LOD sont inférieures avec le système développé par rapport à celles trouvées dans la littérature.

Tableau 3 Limite de détection [nM]

Enzymes	**Carbofurane**		**Malaoxon**		**Paraoxon**	
	LOD	LOD_{Obtenu}	LOD	LOD_{Obtenu}	LOD	LOD_{Obtenu}
EE	38	7.81	----	25	----	156
B131	4.5	6.25	----	0.78	----	31.3
B394	50	31.3	0.1	1.56	10	7.80

4.2 La détection de l'OTA en utilisant un photo détecteur et UV-LED

Quatre UV-LED ont été employés, le blanc et les différentes concentrations ont été acquis à trois reprises, il a utilisé un taux de 1000 données par seconde et le temps d'acquisition était de dix minutes et le processus a été répété trois fois pour chaque UV-LED. Le photo détecteur capte l'absorbance de la lumière UV (intensité de fluorescence) et fournit un rapport de la fluorescence par rapport à la concentration en valeur de tension. Il est possible de voir une relation linéaire comme la figure 11 le montre pour un UV-LED; l'intensité de chaque concentration détectée par le photo détecteur est une tension très faible, en dépit de l'utilisation d'un circuit d'amplification. Ce système n'a pas la possibilité de déterminer des concentrations inférieures à 250 ng / ml.

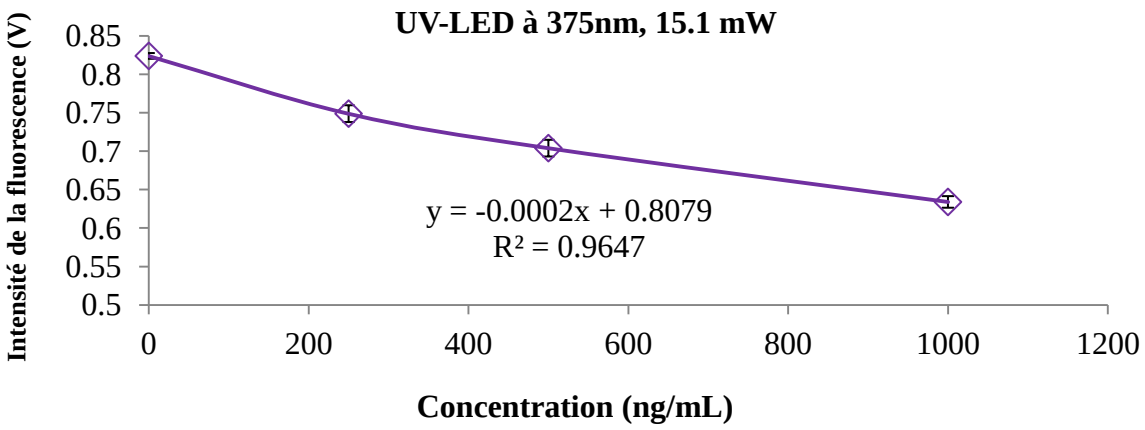

Figure 11 Relation linéaire entre les concentrations en OTA par rapport à l'intensité de la fluorescence détectée par un photo détecteur.

Partie B: Fluorescence avec capteur CMOS.

Cinq UV-LED ont été utilisés pour construire la courbe d'étalonnage, ses principales caractéristiques telles que le code d'identification, le pic de longueur d'onde et le flux de rayonnement émis ont été décrits dans le tableau 4. Les cinq ont chacune un diamètre de 5 mm.

Tableau 4 Caractéristiques des UV-LED.

Code d'identification	Longueurs d'onde (nm)	Radiant flux (mW)
NSHU551A	370-380	12
NSHU551B	360-370	5.4
NSHU591A	370-380	9
NSHU591B	360-370	4
NSPU510CS	370-380	15.1

4.3 Calibration de l'OTA en utilisant ArduCAM

4.3.1 Des échantillons d'OTA préparés dans l'éthanol (EtOH)

Les solutions standards OTA ont été préparées à partir de la solution stockée de l'OTA (1mg/ml). Pour construire cinq points de la courbe d'étalonnage, différentes dilutions de l'OTA ont été préparées à différentes concentrations telles que 40, 20, 10, 5, 2, 1 µg/L. Pour traiter l'image sélectionnée, la zone avec la fluorescence est ciblée et les valeurs RGB et le diagramme sont obtenues. Le tableau 5 résume la gamme linéaire et l'équation ainsi que le coefficient de corrélation R linéaire pour les cinq LED utilisées pour construire les courbes de calibrations.

Tableau 5 Gamme linéaire de LED différente caractérisée.

Longueur d'onde de crête (nm)	**Radiant flux (mW)**	**Plage de linéarité (µg/L)**	**Équation linéaire**	**R^2**
375	9	1-40	5.4821x-4.5179	0.9950
	12	1-40	5.2041x-3.0333	0.9792
	15.1	1-5	33.391x+40.606	0.9160
365	4	2-40	4.1973x-10.901	0.9900
	5.4	10-40	4.2823x+87.73	0.9694

4.3.2 Des échantillons d'OTA préparés dans le méthanol (MeOH)

La même méthodologie que les échantillons dans l'EtOH a été suivie pour analyser les échantillons préparés dans le méthanol, toutes les solutions ont été testées de façon continue. Dans ce cas, l'ArduCAM présente moins de résolution et d'intensité. La qualité de l'image et l'excitation continue avec UV affecté le capteur d'image de ce module.

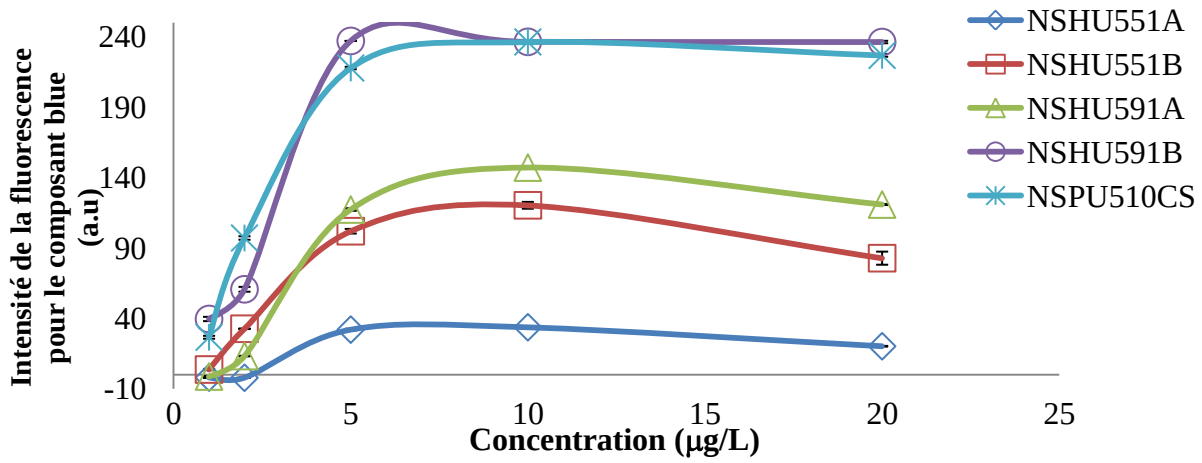

Figure 12 Réponse normalisée des LED UV- pour composante bleue en utilisant MeOH.

4.4 Détection d'OTA en utilisant un capteur CMOS

Différentes concentrations d'OTA (1, 2, 5, 10, 20, 30, 40, 50, 80 µg/L) dans le méthanol ont été préparées et le méthanol a été considéré comme blanc (figure 12), la courbe d'étalonnage est présentée sur la figure 13 et on a utilisé la UV LED avec un pic d'émission à 365 nm avec 4 mW de puissance rayonnante. La meilleure plage linéaire a été obtenue dans la gamme de 5-40 µg/L pour la détection de l'OTA.

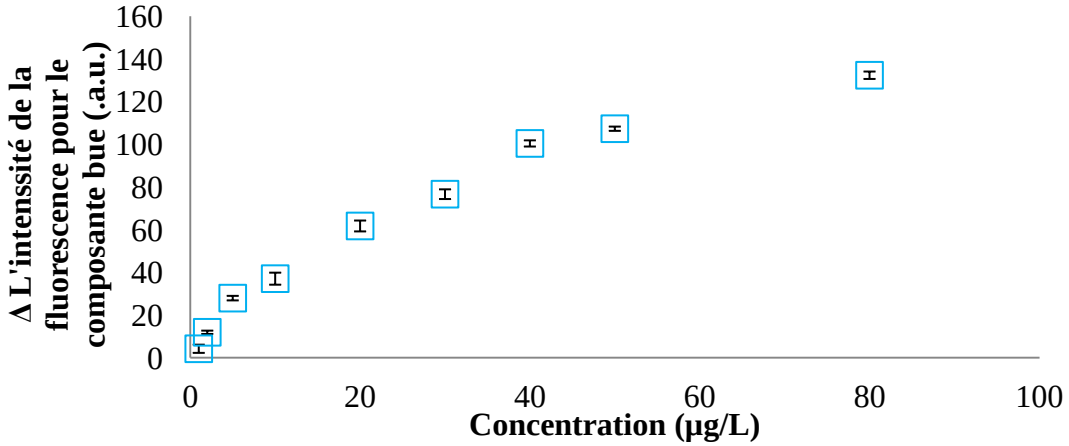

Figure 13 Calibration courbe des concentrations en OTA dans le méthanol en utilisant développé dispositif de fluorescence.

4.4.1 Extraction avec des colonnes IAC pour le vin et la bière

Dans le cas des échantillons réels, un mélange de 800 µl de l'échantillon réel (vin ou bière) et 200 µl de méthanol a été injectée en HPLC pour confirmer que les échantillons réels étaient exempts d'OTA. Par la suite, afin d'éviter l'effet de matrice, un protocole d'extraction

est utilisé en combinaison avec une colonne d'affinité. Le tableau 6 résume la moyenne (n = 3) pour les solutions OTA standard et le pourcentage de récupération de l'OTA en utilisant des colonnes d'immuno affinité pour l'extraction de l'OTA du vin et de la bière. Les échantillons ont été analysés aussi par HPLC. Le blanc, comme attendu, ne présente pas de pic.

Tableau 6 Récupération d'échantillons réels par rapport à des solutions standard d'OTA dans le HPLC.

Concentration (µg/L)	Surface du pic des normes OTA (a.u.)	%RSD	Récupération de l'échantillon de bière (%)	%RSD	Récupération dans échantillon de vin (%)	%RSD
2	5825.1	1.39	95.41	0.80	86.97	0.50
4	13375.0	4.97	79.90	3.54	76.47	1.64
6	20062.5	4.89	97.68	3.32	86.59	4.85
10	30492.3	2.12	91.18	2.36	95.98	7.46

Dans le cas du module de série de l'appareil, le pourcentage de récupération pour l'OTA à l'aide de l'IAC a été calculé en divisant l'intensité de fluorescence des concentrations en OTA des échantillons réels par l'intensité de fluorescence de la concentration de la courbe d'étalonnage et le résultat était multiple par 100 pour obtenir le pourcentage. Pour certaines concentrations, la valeur de l'aire du pic et l'intensité de fluorescence a été interpolée à partir de la courbe d'étalonnage. Les résultats de la récupération de l'aide de colonnes d'immuno affinité pour les échantillons de vin et de bière sont présentés dans le tableau 7. Les recouvrements obtenus sont meilleurs que ceux obtenus par HPLC.

Tableau 7 Récupération d'échantillons réels par rapport au module de série de la caméra.

Concentrations (µg/L)	Récupération de l'échantillon de bière (%)	Récupération dans échantillon de vin (%)
2	107.76	94.38
4	105.23	91.56
6	98.30	85.72
10	109.68	91.82

En outre, l'intensité de fluorescence a une relation linéaire avec la composante bleue pour les échantillons de bière et de vin enrichis en OTA; la relation linéaire est présentée dans les figures 14a et 14b.

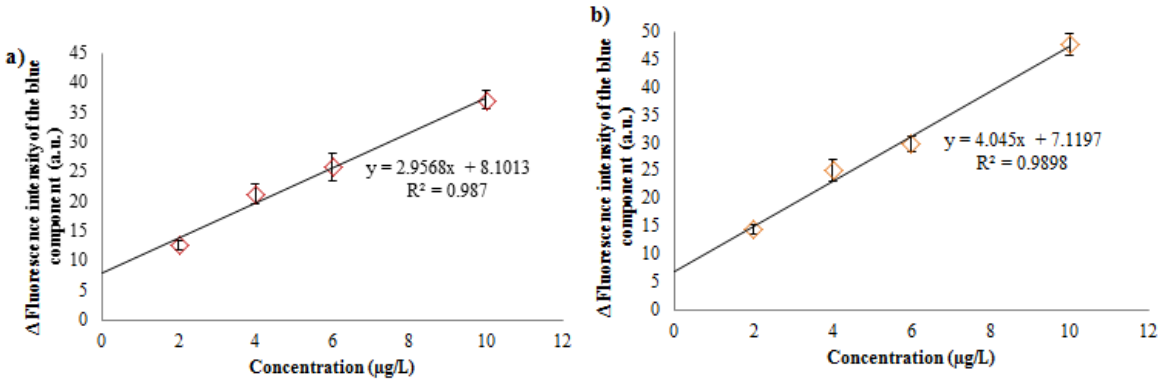

Figure 14 Comportement de la composante bleue pour l'OTA dans les échantillons enrichis de vin (a) et de bière (b) des échantillons dans le module la caméra de port série.

4.4.2 Extraction avec des colonnes MIP pour le vin et la bière

Les résultats de la récupération dans des échantillons de vin et de bière sont présentés respectivement dans les tableaux 8 et 9 pour l'HPLC et le dispositif mis au point. Les taux de récupération pour la bière sont meilleurs que pour le vin. Pour la bière, la récupération est équivalente en utilisant les deux systèmes. Par contre pour le vin, la détection par HPLC donne de meilleurs résultats que notre système.

Tableau 8 Recouvrement des échantillons réels avec HPLC en utilisant des colonnes MIP.

Concentration (µg/L)	Récupération de l'échantillon de bière (%)	%RSD	Récupération dans échantillon de vin (%)	%RSD
2	92.47	2.56	88.35	1.26
4	100.17	1.69	76.01	0.35
6	94.99	0.87	95.33	4.73
10	94.99	3.85	108.05	4.38

Tableau 9 Récupération de l'OTA dans des échantillons réels avec des colonnes MIP en utilisant le dispositif mis au point.

Concentration (µg/L)	Récupération de l'échantillon de bière (%)	%RSD	Récupération dans échantillon de vin (%)	%RSD
2	111.67	3.25	68.60	4.56
4	114.49	3.67	68.75	4.87
6	82.82	2.85	57.88	5.32
10	93.20	3.09	62.00	6.72

Dans ce cas, l'intensité de la fluorescence ne montre pas une relation linéaire avec la composante bleue pour les échantillons de bière et de vin enrichis en OTA, les résultats pour le vin et la bière avec des colonnes MIP sont présentées dans la figure 15a et 15b.

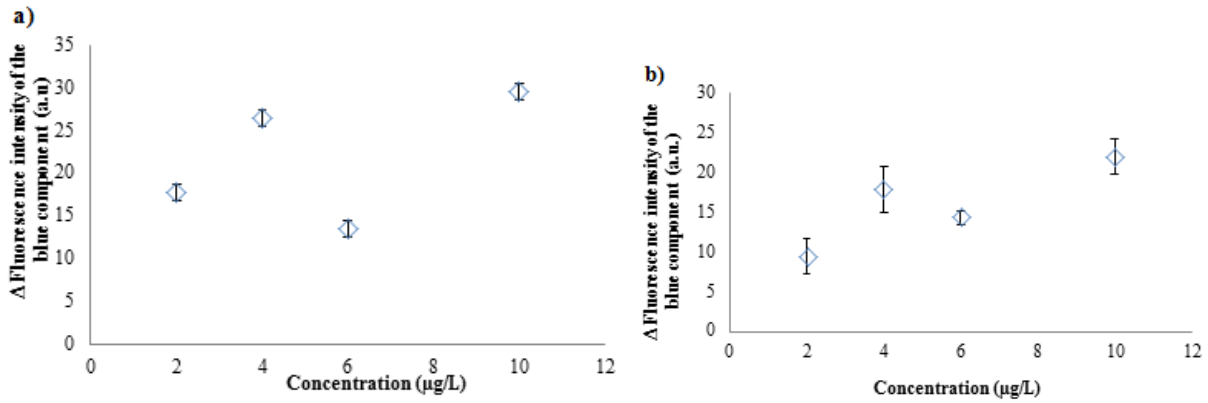

Figure 15 Échantillons de bière (a) et de e vin (b) en utilisant des colonnes MIP dans le module de caméra.

Par ailleurs, le taux récupération pour les échantillons de vin est moins bonne que pour les échantillons de bière. De plus les taux de récupération sont faibles sont faibles, cela est dû à la complexité de l'échantillon de vin et il est possible que l'OTA piégé dans les colonnes de MIP ne puisse pas être élué. La complexité et les impuretés peuvent interférer avec la quantification [211] de l'OTA en utilisant des instruments de fluorescence. Pour confirmer ces résultats, les échantillons ont été testés avec le Fluoroskan, l'affichage des résultats similaires à ceux obtenus avec le CMOS capteur et la réponse est montré dans la figure 16.

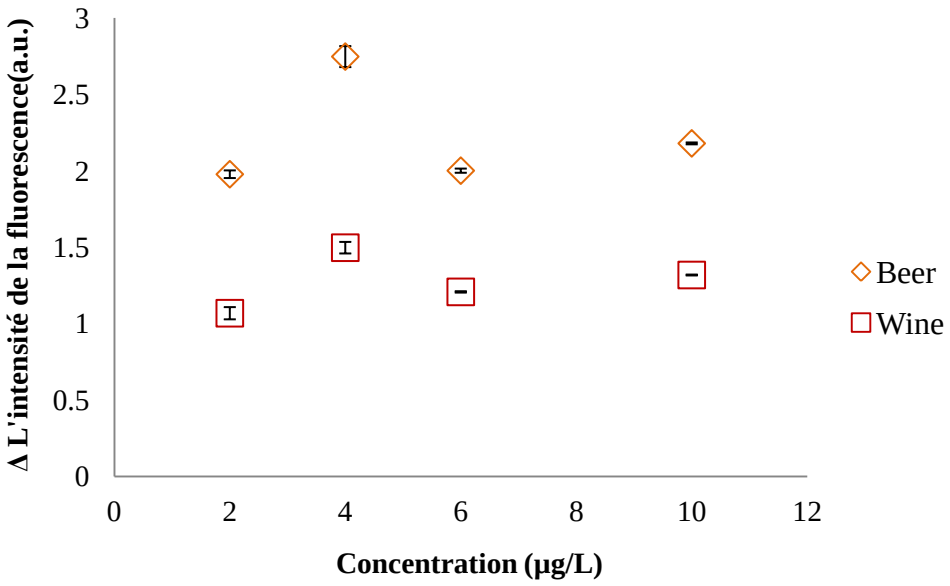

Figure 16 L'intensité de fluorescence obtenue avec l'instrument de fluorescence.

4.4.3 Extraction de l'OTA du cacao avec des colonnes MIP

Les différentes concentrations d'OTA 40, 30, 20, 10, 7,5, 5, 2,5, 1,25 ng/ml sont préparées respectivement dans l'éthanol et analysés en utilisant le dispositif de fluorescence mis au point. Cinq lots différents de fèves de cacao ont été testés par le protocole mis au point, mais aucun d'entre eux ont confirmé la présence d'OTA. Afin d'évaluer la faisabilité de la méthode proposée pour des applications possibles, des expériences ont été effectuées avec des échantillons de cacao artificiellement contaminés aux concentrations de 10, 5 et 2 µg/kg, (en dupliqua). Tout d'abord, les échantillons de cacao brut ont été extraits en utilisant une colonne d'immuno-affinité,. Le RSD a été calculée à 4,05% indiquant la précision et la reproductibilité du système développé. La précision est obtenue en comparant le montant (2, 5 et 10 µg/kg) et la moyenne des valeurs mesurées (1,66 ; 4,23 et 8,75 µg/kg). Les taux de récupération obtenus ont été présentés dans le tableau 10.

Tableau 10 Recouvrements d'OTA à l'aide de deux protocoles différents d'extraction et leur évaluation en utilisant la configuration de fluorescence développé.

OTA dopés [µg/kg]	OTA trouvé [µg/kg]	% Récupération (1% $NaHCO_3$)	%Récupération (Classique)	% RSD
2	1.69	84.5	79.05	3.8
2	1.64	82.0	80.25	3.95
5	4.28	85.6	81.50	4.12
5	4.18	83.6	82.00	3.95
10	8.7	87.0	83.25	4.02
10	8.8	88.0	82.29	4.5

La spécificité de la méthode a été testée en utilisant l'ochratoxine B (OTB). Des échantillons ont été contaminées par de l'OTB Les expériences ont été effectuées en utilisant des concentrations d'OTB de 5 µg/kg et 10 µg/kg en employant un protocole semblable à celui utilisé pour l'OTA. Les échantillons ont été dilués puis élués pour préparer les concentrations 5 et 10 ng / ml et mis en cuvette pour la fluorescence. Après analyse, la valeur de la coordonnée bleu pour l'OTB est très inférieure à celle de l'OTA.. Il ressort de la figure 17 que le système mis au point et les colonnes utilisées sont sélectives pour l'OTA.

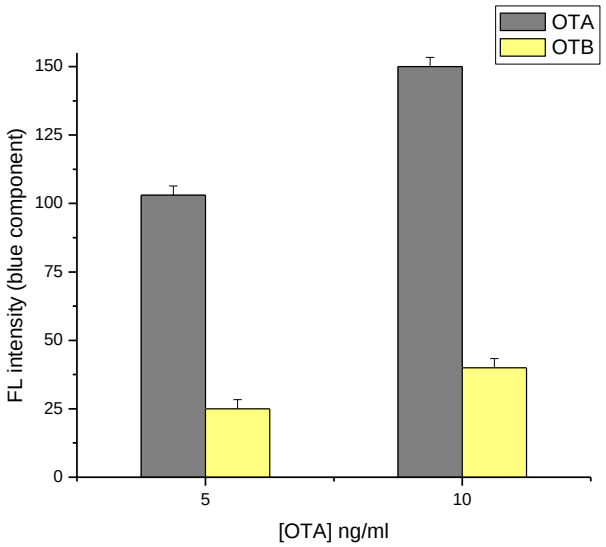

Fig. 17 Spécificité de la méthode développée à une longueur d'onde particulière

4.5 Téléphone mobile comme détecteur d'OTA

Les solutions de concentration différente d'OTA ont été préparées dans le méthanol et numérisés à l'aide de la caméra et du WIFI pour obtenir la courbe d'étalonnage. Les images de fluorescence capturées à différentes concentrations en fonction de la composante bleue de l'intensité de la fluorescence fournie par LED à longueur d'onde maximale de 365 nm ou 375 nm à différents flux de rayonnement. Il est présenté dans la figure 18.

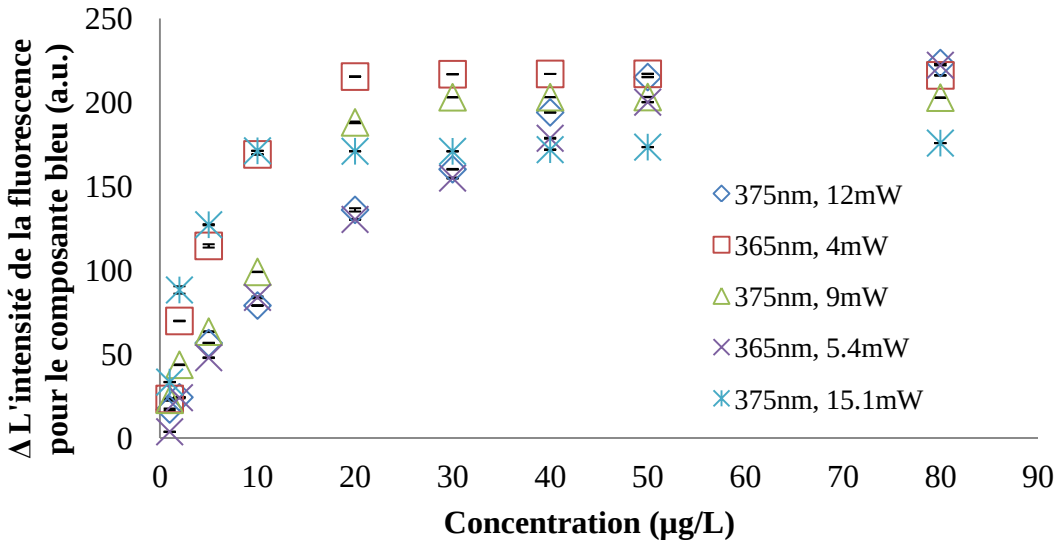

Figure 18 Courbe d'étalonnage pour l'OTA sur la base de la composante bleue de l'intensité de fluorescence.

Une meilleure linéarité a été trouvée dans la gamme 1,25 à 20 µg/L et les résultats concernant le facteur de corrélation (R), et la gamme linéaire basée sur la longueur d'onde de crête et flux de rayonnement sont présentés dans le tableau 11.

Tableau 11 Plage linéaire de LED différente caractérisée.

Longueur d'onde de crête (nm)	Radiant flux (mW)	Plage de linéarité (µg/L)	Linear equation	R^2
375	9	1.25-20	y=8.7746x+13.994	0.98
	12	1.25-20	y=6.4865x+11.123	0.97
	15.1	1.25-5	y=24.867x+12.501	0.90
365	5	1.25-10	y=16.412x+16.297	0.94
	5.4	1.25-10	y=8.5211x+1.285	0.98

Il a été décrit que l'utilisation de NaOH pouvait être un activateur de fluorescence [121]. Pour cette raison, 1 µL NaOH 3M a été ajouté le lendemain après l'élaboration de la courbe d'étalonnage. Les résultats sont présentés dans la figure 19. La LED à 365 nm et 4 mW a été utilisé en raison de sa bonne linéarité et sa gamme linéaire jusqu'à 10 µg/L L'objectif était de savoir s'il était possible d'augmenter la composante bleue de la fluorescence avec un renforçateur de fluorescence.

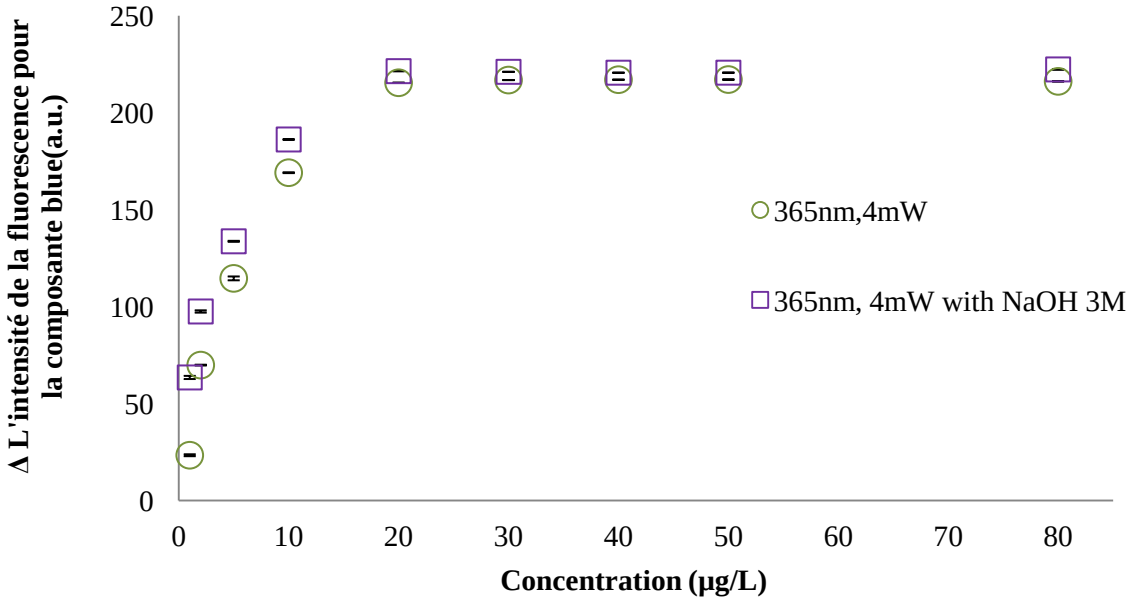

Figure 19 Augmentation de la composante bleue de l'intensité de fluorescence avec un activateur de la fluorescence.

Avec le NaOH comme activateur de fluorescence, il y a une augmentation de la fluorescence pour les faibles concentrations dans la composante bleue de l'intensité de fluorescence, la plus grande augmentation est observée dans la plage linéaire de 1,25 à 10 µg/l. Pour évaluer l'utilisation de la caméra de téléphone mobile, LED-UV et WIFI dans la détection de l'OTA, des tests de détection de l'OTA dans l'échantillon de bière ont été réalisés. Le tableau 12 montre la récupération de la LED à 365 nm avec 4 mW.

Tableau 12 Récupération de la LED à 365 nm.

Concentration (µg/L)	**Surface du pic des normes OTA (a.u.)**	%RSD	**Récupération de l'échantillon de bière (%)**	%RSD
2	5825.1	3.39	89.65	3.80
4	13375.0	4.97	91.97	3.54
6	20062.5	4.89	96.69	3.89
10	30492.3	3.12	79.20	4.03

4.6 Les systèmes d'écoulement

Dans le cas de la colonne aptamère d'immuno-affinité, on a suivi le même mode opératoire décrit par Amina Rhouati et al. [174, 214]. Les solution de filtration, de lavage et d'élution ont été analysées avec l'ArduCAM. Les échantillons obtenus ont été excités par la lumière ultraviolette pour établir une relation entre la composante bleue et la concentration de l'OTA dans les colonnes d'immuno- affinité. La figure 20 montre que le système est adapté à la détection de l'OTA. Les quantités retrouvées dans le percolât, le lavage et l'éluât démontrent que la capacité de fixation de la colonne était insuffisante.

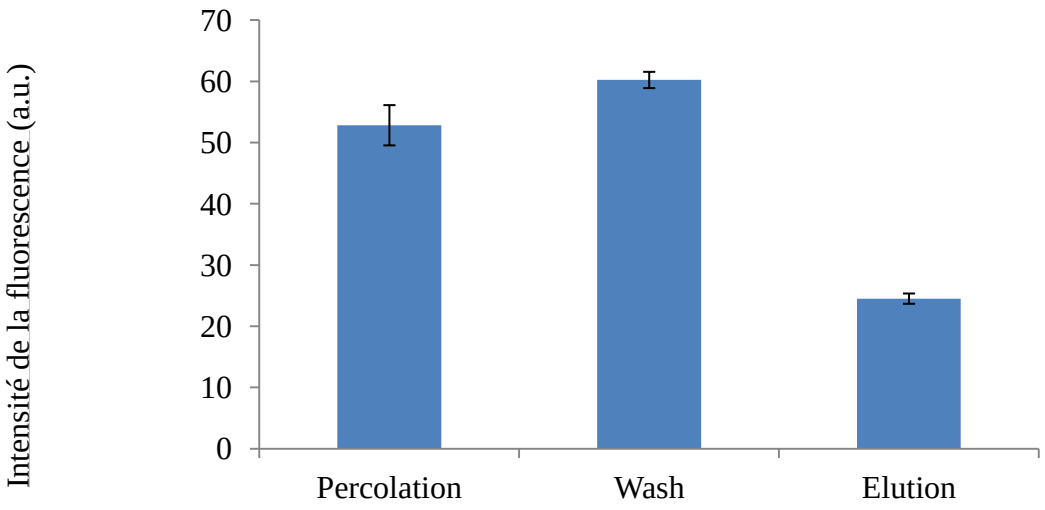

Figure 20 Comparaison des profils d'élution d'OTA 10 µg / L de l'IAC.

4.7 L'évaluation de la performance du dispositif de fluorescence dans des conditions particulières

4.7.1 Effet du solvant sur l'intensité de fluorescence de l'OTA

Les solutions tampon (PBS, HEPES) et les alcools (méthanol, éthanol) montrent les meilleurs résultats avec la plus grande intensité de fluorescence pour l'OTA, l'OTA a montré moins de fluorescence dans l'eau distillée qui est due à la lente décomposition de l'OTA dans l'eau [215]. La fluorescence significativement plus élevée a été observée dans un tampon et du méthanol par rapport à l'acétonitrile [216]. Les résultats obtenus en outre par rapport à la réponse d'intensité de fluorescence enregistrée avec le Fluoroskan. Il a été observé que la appareil développée présente des résultats similaires comme indiqué dans les figures 21 (a) et 21 (b).

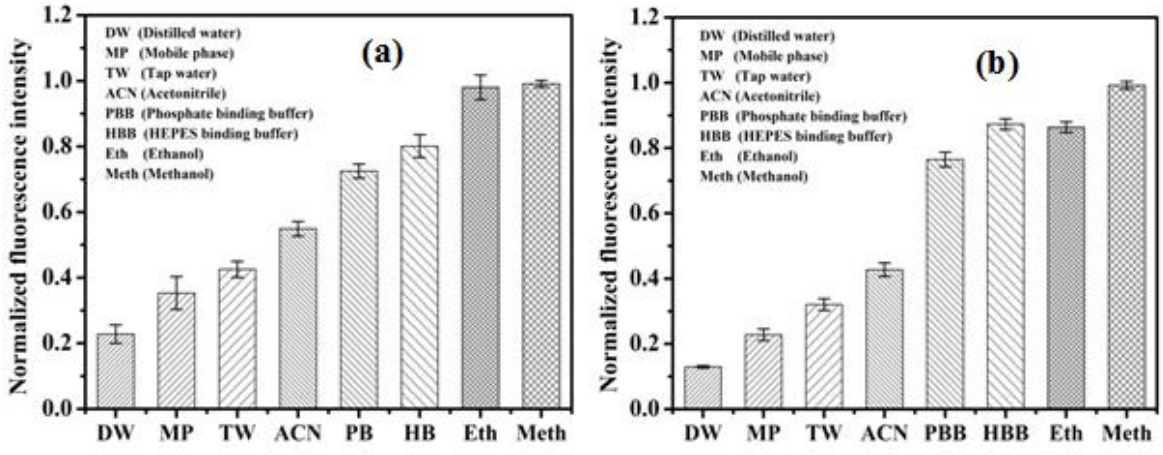

Figure 21 Réponse de l'intensité de fluorescence de 20 µg de L-1 OTA obtenu dans un solvant différent (a) de la plate-forme d'imagerie développée (b) d'un lecteur de microplaques Fluoroskan (n = 3)

4.7.2 Effet de la concentration en sel du tampon et l'intensité de fluorescence de l'OTA

L'effet de la concentration en sel affecte l'émission de fluorescence des fluorophores. Pour étudier le phénomène d'émission de fluorescence de l'OTA, l'effet de la concentration en sel du tampon a été testé. Comme le montre la figure 22, l'intensité d'émission de fluorescence OTA augmente avec l'augmentation de la concentration de sel de Na de 10 à 120 mM [121 ,217]. Ainsi, les résultats suggèrent que la concentration en sel a un effet significatif sur l'émission de fluorescence de l'OTA. En outre, étant donné que, la concentration de sel est

optimisée pour une interaction de liaison optimale de l'OTA, donc d'éviter l'effet de la concentration excessive de sel, des concentrations plus élevées n'ont pas été testées [218].

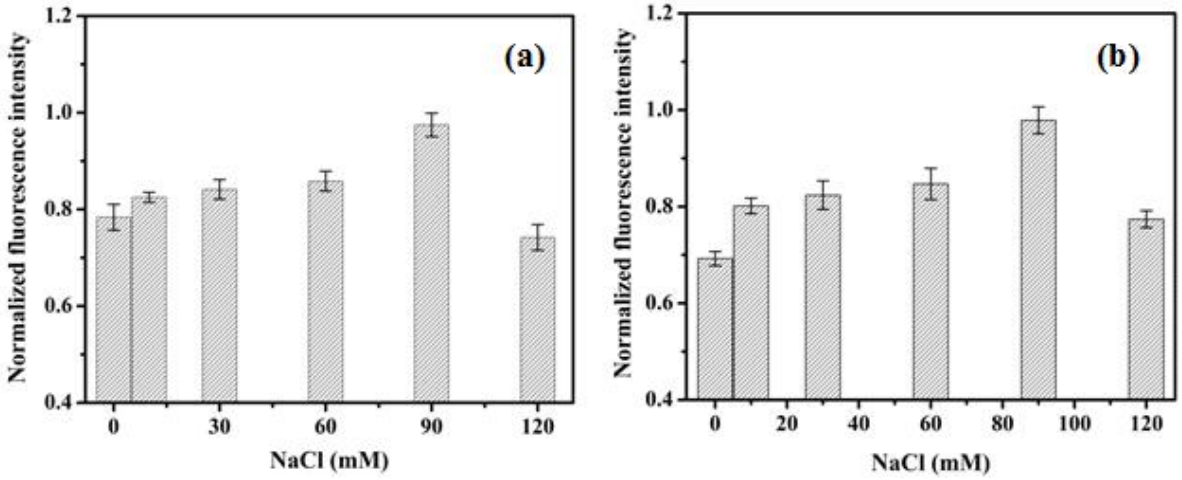

Figure 22 Réponse de l'intensité de fluorescence de 20 µg de L-1 OTA obtenu dans l'HEPES à un pH de 7,2 avec des concentrations différentes de NaCl (a) de la plate-forme d'imagerie développée (b) un lecteur de microplaques Fluoroskan (n = 3)

4.7.3 Effet du pH sur l'intensité de fluorescence de l'OTA

En solution, l'OTA montre un comportement de fluorescence dépendant du pH due à la présence d'entités fonctionnelles acides et basiques dans la structure de l'OTA, ce qui influence fortement par son état de protonation [119]. Il a été observé sur la figure 23 que l'augmentation de l'intensité de la fluorescence avec l'augmentation du pH du tampon HEPES 6,8 à 7,2. Aucune autre augmentation de la fluorescence a été observée avec plus d'augmentation du pH du tampon. L'augmentation de la modification du pH de l'environnement acide à alcalin, ce qui se traduit par l'hydrolyse du cycle lactone anneau provoquant l'ouverture [122, 219]. Ainsi, le résultat obtenu limite l'analyse de l'OTA à pH élevé qui conduira à une analyse négative.

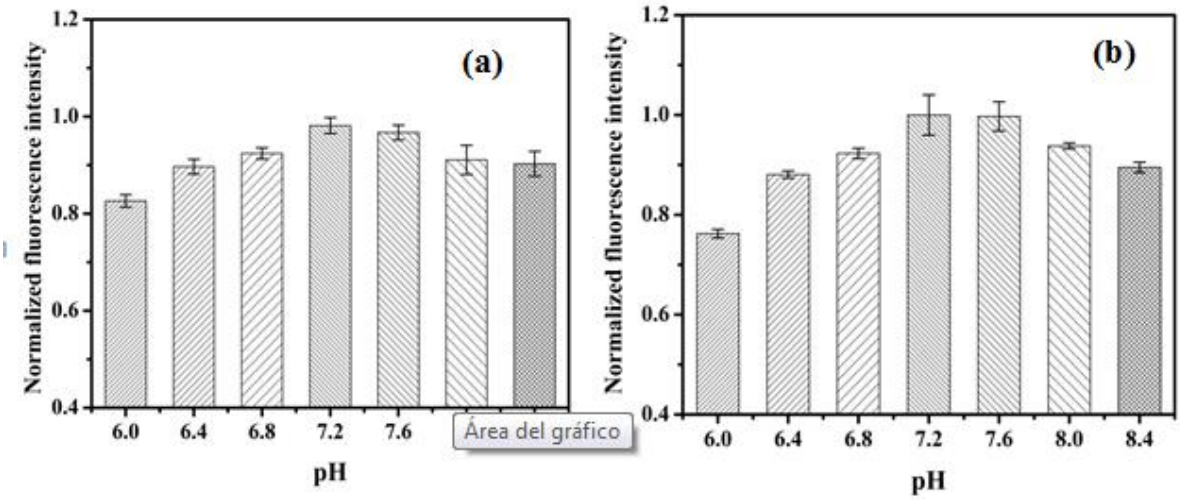

Figure 23 Réponse de l'intensité de fluorescence de 20 µg de L-1 OTA obtenu dans du tampon HEPES à un pH allant de 6 à 8,4 (a) de la plate-forme d'imagerie développée (b) d'un lecteur de microplaques Fluoroskan (n = 4)

Partie C: Traitement de l'image

Dans la figure 24, il est possible de voir que pour le blanc, le spectre est plus large que pour la gamme des concentrations d'OTA et la concentration d'OTA supérieure à un spectre plus faible. Pour la plus grande concentration, il y a un maximum de l'intensité. Avec l'histogramme d'échelle de gris pour les échantillons de vin et de bière, il n'était pas possible de déterminer les concentrations. Il , a toutefois été possible d'identifier les deux échantillons. Pour les échantillons de bière l'histogramme montre un large spectre et dans le cas des échantillons de vin, le spectre présente une pente décroissante.

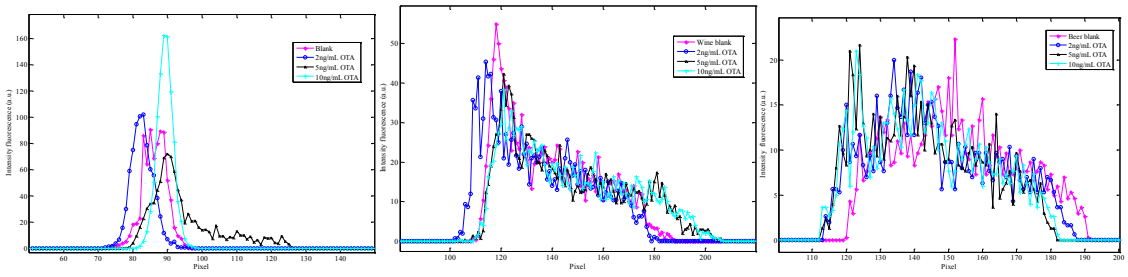

Figure 24 Histogramme en échelle de gris de la courbe d'étalonnage de la courbe d'étalonnage (à gauche), le vin (centre) et la bière (à droite) l'échantillon enrichi en OTA.

Les composants bleus des solutions d'étalonnage et des échantillons réels obtenus à la figure 25 démontrent que dans les conditions de l'expérience, la composante bleu est décalée

vers la droite car l'intensité de la fluorescence de l'OTA est plus faible et cela se traduit par une coloration plus claire. L'histogramme de la composante bleue présente le même comportement que la composante grise de l'histogramme échelle.

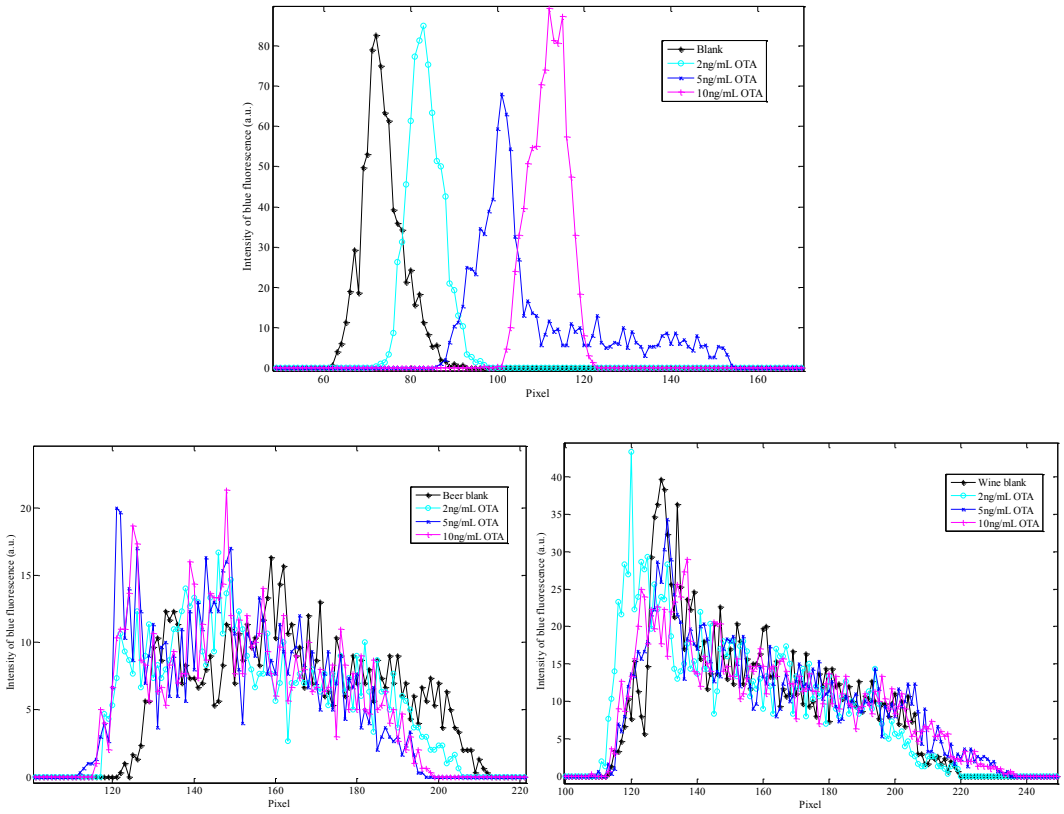

Figure 25 Histogramme de composante bleue de la courbe d'étalonnage (en haut), la bière (à gauche) et le vin (à droite) des échantillons.

La figure 26 représente la composante bleue du modèle RGB. Il existe une relation linéaire pour les concentrations, à l'exception de 10 ng/ml, cette concentration montre que le capteur d'image est saturée pour cette concentration. Il est évident que la saturation par la composante bleue ne permet pas d'évaluer correctement la concentration. Il est peut être possible d'utiliser les autres couleurs.

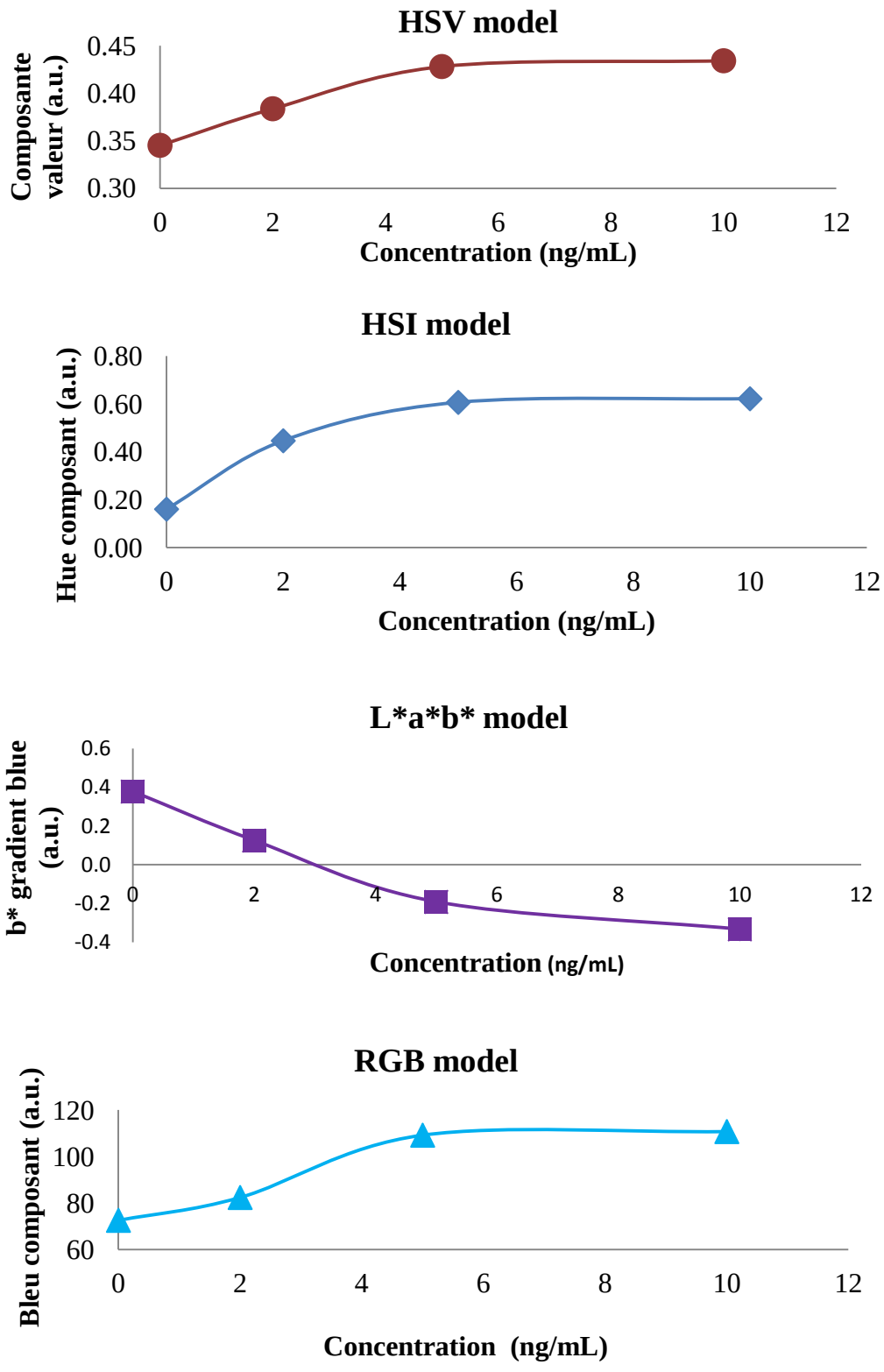

Figure 26 Modèle de couleur de la courbe d'étalonnage qui représente une corrélation linéaire entre les concentrations.

Pour les échantillons de bière enrichis avec l'OTA, le même résultat est obtenue quelle que soit la méthode de traitement utilisée. La détection maximale permise est de 5 ng/ml (Figure 27)

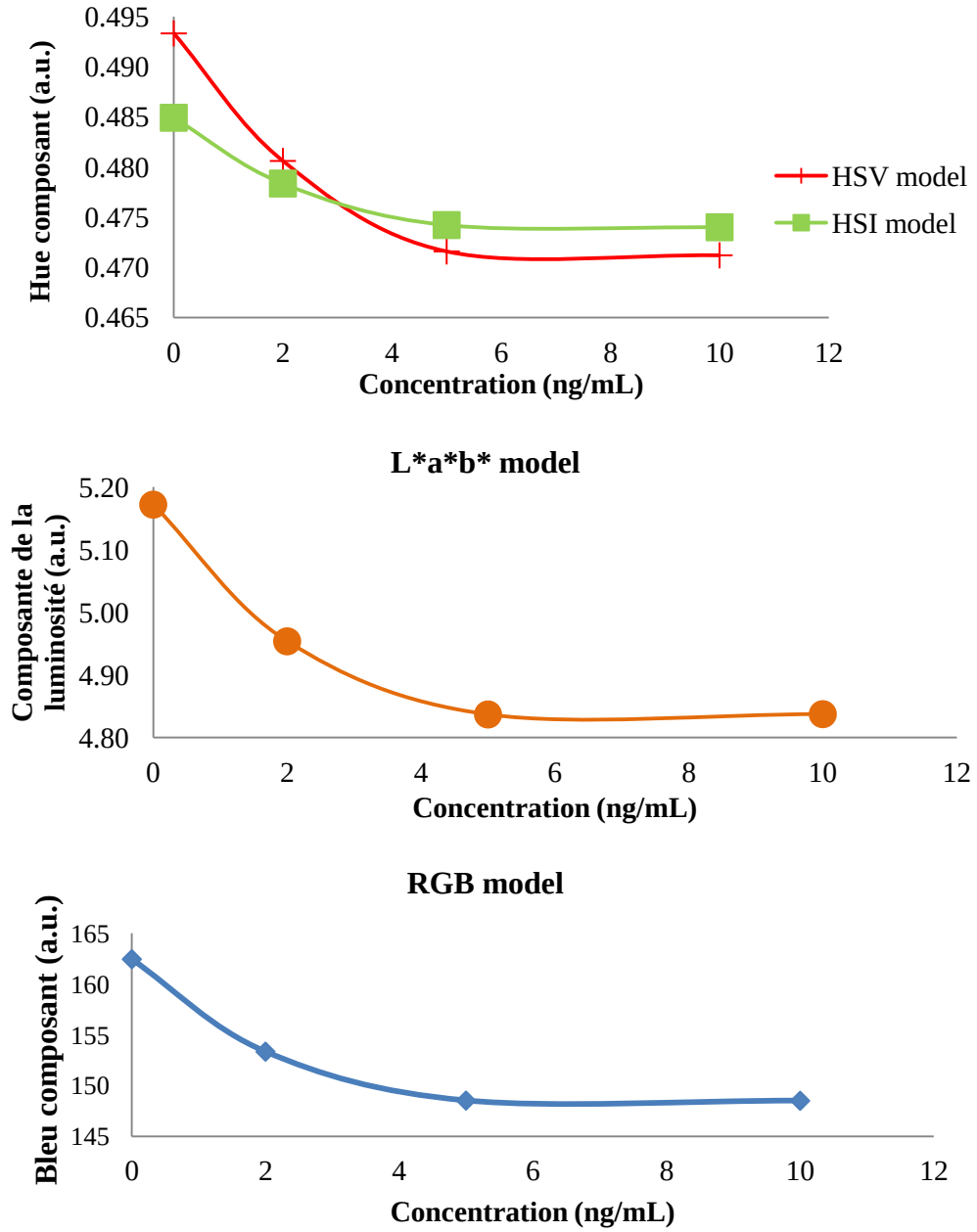

Figure 27 Modèle de couleur des échantillons de bière enrichi avec l'OTA qui présente une corrélation linéaire entre les concentrations.

Les différents modèles employés qui présentent une relation linéaire directe ou indirecte avec des échantillons de vin pour détecter la concentration d'OTA sans utiliser une concentration par colonne d'extraction sont présentés dans la figure 28.

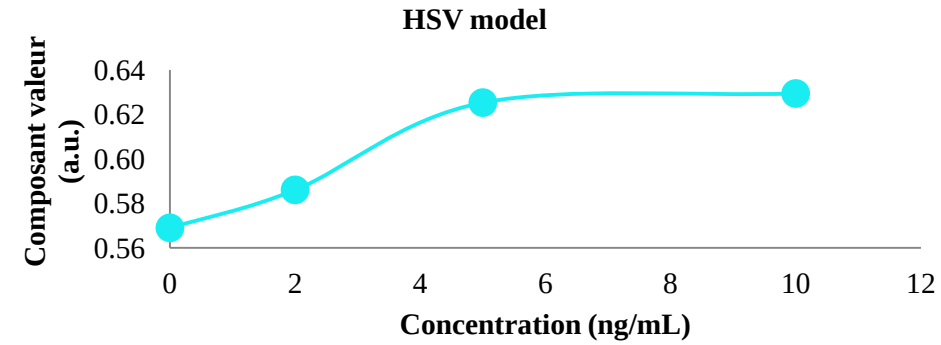

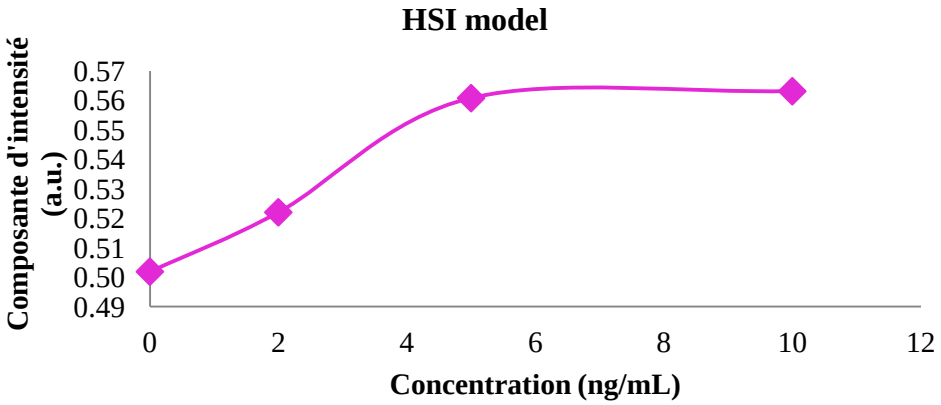

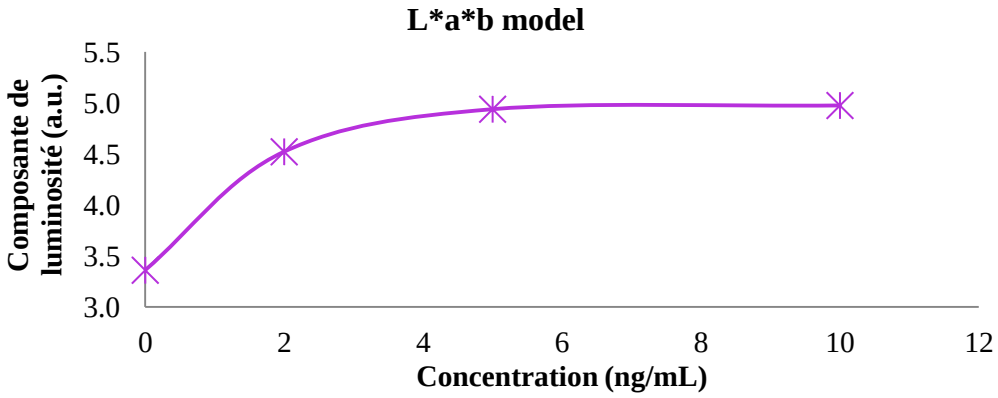

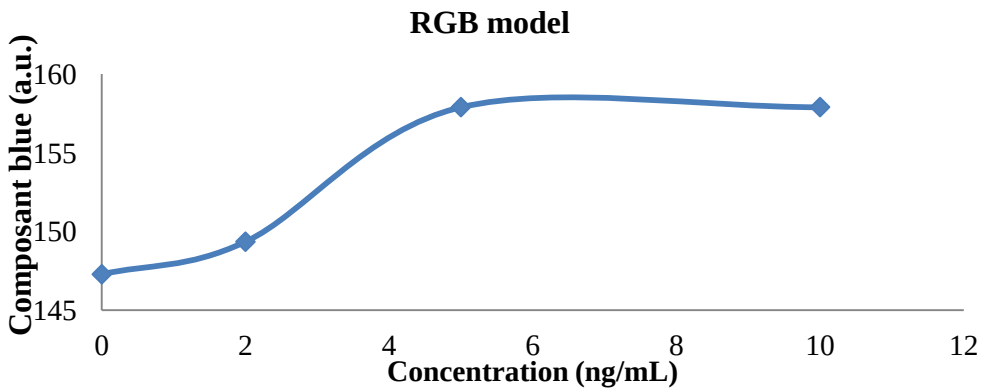

Figure 28 Modèles de couleurs d'échantillons de vin.

Le modèle de couleur des échantillons de bière et de vin sont à soustraire à partir des modèles de couleur de la courbe d'étalonnage pour normaliser les données et trouver des composants à différents parmi les concentrations testées, les résultats sont présentés dans la figure 29 pour les échantillons de bière.

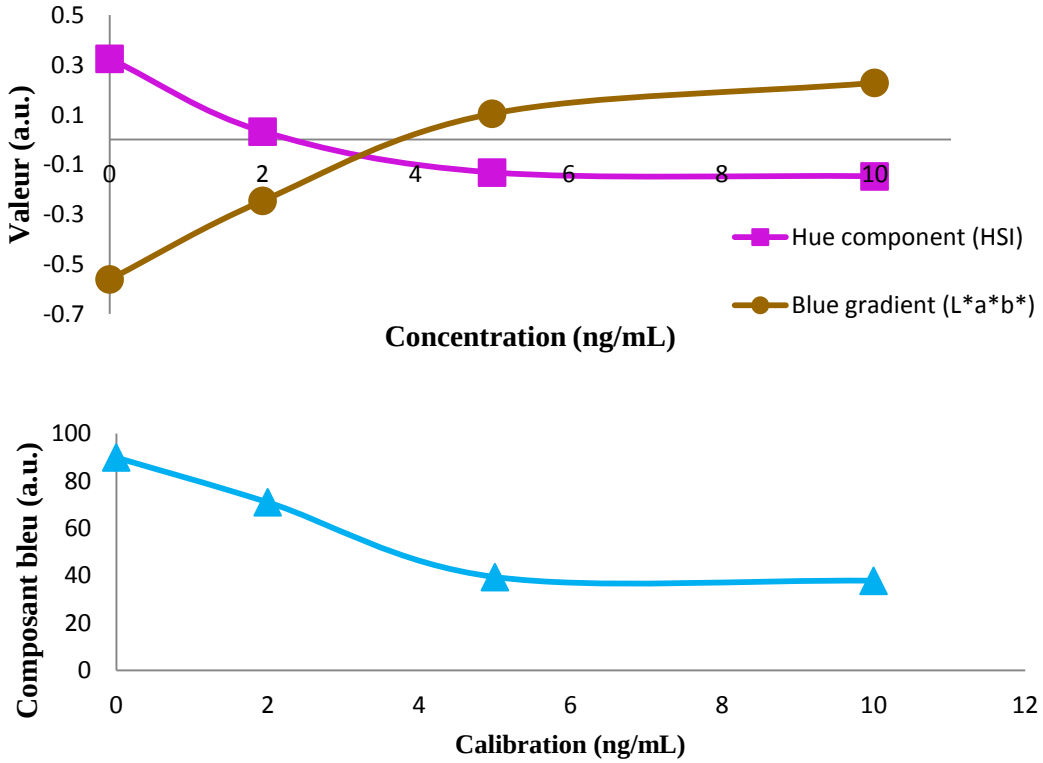

Figure 29 Modèle de couleur avec une relation pour les échantillons de bière, composante Hue de HSI et bleu dégradé de L*a*b* et RGB est exprimé en tant que composant bleu.

Dans le cas du vin, les éléments comparatifs sont dans la figure 30. La composante bleue du modèle RGB est utilisé à nouveau. Cette composante a présenté de bons résultats pour avoir une relation directe de la fluorescence de l'OTA dans le cas des colonnes d'extraction et sans colonnes d'extraction. Ceux-ci confirment qu'il existe une relation directe de la composante bleue et l'intensité de fluorescence fournie par chaque concentration d'OTA.

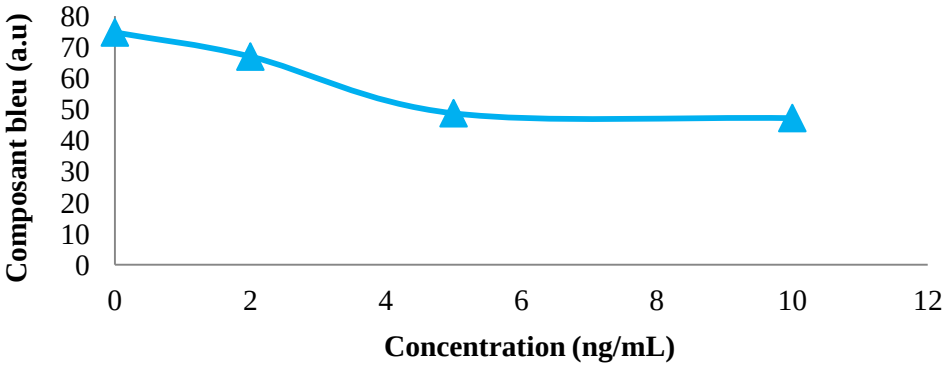

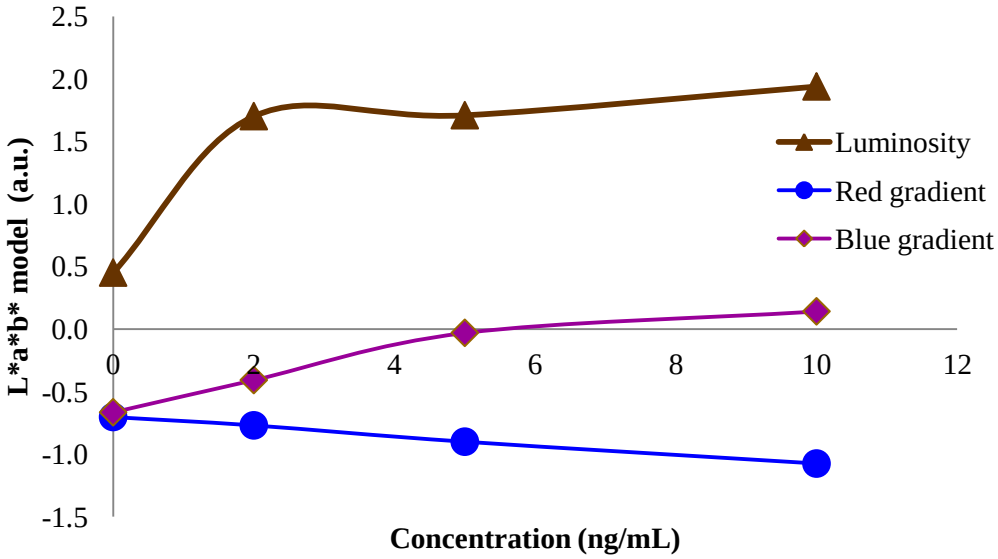

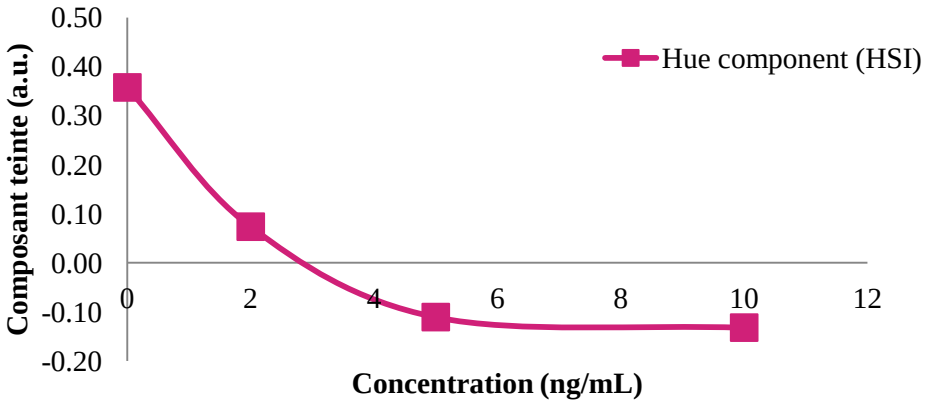

Figure 30 Modèle de couleur avec une relation pour les échantillons de bière, RGB, L*a*b* et HIS, respectivement.

CHAPITRE V

CONCLUSIONS

Aptacapteur électrochimique dans un système de flux automatisé

L'applicabilité de l'aptacapteur dans le système de flux développé a été validée par la détection de l'OTA dans les échantillons de bière; l'incorporation de l'aptamère dans le dispositif a augmenté la sensibilité du système pour détecter de faibles concentrations d'OTA. Cette amélioration a été obtenue grâce à l'automatisation des procédures, de la fabrication de l'aptacapteur à l'étape de détection. En plus d'une réduction du temps d'analyse et une diminution de la complexité du procédé, la simplicité du système automatisée ne requiert pas de personnel qualifié. Il est envisagé de l'étendre à la détection d'autres biomolécules. Pour le test indirect, le LOD obtenu et IC50 étaient inférieurs à ceux obtenus dans l'essai compétitif direct.

Détection des pesticides avec l'utilisation de diodes électroluminescentes

La limite de détection du système optique est trois fois inférieure à celle du système de spectrophotomètre. Nous avons observé une sensibilité élevée de B394-AChE avec les insecticides organophosphorés. Tout le système est basé sur un équipement peu coûteux, est un système optique innovant, efficace et facile à utiliser. Il est possible de l'utiliser pour la

détection « on site » des insecticides. En outre, il permet l'acquisition des données et l'enregistrement avec un ordinateur. Un spectrophotomètre miniature à une longueur d'onde de 412 nm a été produit avec des LEDs et des détecteurs de photo.

Détection de l'OTA avec UV-LED

Le système est facile à utiliser, c'est un système portable Malheureusement . Il n'est pas possible de détecter des concentrations d'OTA inférieures à 250 ng/ml.

Fluorescence avec ArduCAM

L'utilisation d'un capteur CMOS pour détecteur de solutions de fluorescence est possible et permet de déterminer la concentration de ces solutions. Le concept des composants RGB a été employé, compte tenu de la fluorescence naturelle d'OTA. L'utilisation d'ArduCAM n'est pas bonne en l'absence de lumière, l'image est pixélisée et de mauvaise qualité, même si un capteur de 5 MP a été utilisé, l'image est sombre et la cuvette ne se définit pas complètement, produisant une confusion pour sélectionner la bande de fluorescence. L'UV-LED à 375 nm à 9mW présente les meilleurs résultats pour détecter la faible concentration avec une gamme linéaire de 1-40 µg/l d'OTA dans EtOH. Les meilleurs résultats ont été les échantillons préparés dans de l'EtOH, car les échantillons préparés dans du MeOH ont présenté une réduction de la fluorescence, qui peut être attribuée à une diminution de l'efficacité du capteur CMOS du à l'exposition continue au rayonnement UV.

Fluorescence avec CMOS port sérié

Il a démontré une bonne stabilité et la reproductibilité dans des échantillons réels tels que le vin, la bière et le cacao. La relation de composante bleue est directement proportionnelle à l'intensité de fluorescence des concentrations d'OTA avec ce capteur CMOS. Dans le cas du vin et de la bière, le LOD était de 2µg/l comparable à la LOD de l'OTA dans l'HPLC. Un facteur important est l'efficacité de la récupération, de l'OTA. Dans les deux cas, le taux de récupération de l'échantillon IAC se situait entre 70-110% pour la HPLC et le capteur CMOS. Pour le cacao, la méthodologie proposée fournit un LOD à 2 µg/l avec une bonne reproductibilité. Il est un coût très faible par rapport à la HPLC et les résultats entre les deux appareils sont comparables.

Téléphone mobile comme détecteur d'OTA

Les mesures ont été comparées avec un équipement commercial . Le système conçu fournit une LOD à 2 µg/l avec une bonne reproductibilité et stabilité. On a constaté que la fluorescence des échantillons est directement proportionnelle à la concentration d'OTA, mais le flux de rayonnement de la diode électroluminescente est une inversement proportionnelle à la concentration d'OTA. Il est possible d'utiliser un amplificateur de fluorescence pour augmenter la composante intensité de la fluorescence bleue à une meilleure résolution. L'utilisation des nouvelles technologies permet employer l'équipement du laboratoire dans mode simple, économique et portable.

Les systèmes d'écoulement

En raison de l'automatisation des méthodes, il était possible de contrôler le débit, le volume et le temps. Le système permet la réduction de la consommation des réactifs, l'emploi de personnel non qualifié et une diminution de la complexité du procédé. L'utilisation d'HyperTerminal permet la portabilité et il peut être utilisé avec un ordinateur portable avec des exigences minimales.

L'évaluation de la performance du dispositif de fluorescence dans des conditions particulières

L'influence du solvant, le pH et la force ionique sur l'émission de fluorescence de l'OTA permet de voir qu'il y a une intensité de fluorescence maximale dans un tampon et d'un solvant alcoolique, les études de pH ont suggéré que le motif d'émission de fluorescence dépendant de la structure et le tampon avec une concentration en sel plus élevée révèle une fluorescence élevée.

Traitement d'image

Une analyse plus approfondie et d'autres méthodes sont nécessaires pour quantifier la concentration d'OTA sans l'utilisation de colonnes d'extraction. Il existe une relation de composante bleue directement proportionnelle à l'intensité de fluorescence des concentrations d'OTA, Ceci a été démontré avec la méthodologie développée.

OPTICAL AND ELECTROCHEMICAL SENSING METHODS FOR THE DETECTION OF FOOD CONTAMINANTS

CHAPTER I

INTRODUCTION AND BACKGROUND OF THE STUDY

1. Introduction

Ingestion of food contaminated with toxins synthesized by molds, causes various clinical symptoms known by the term "mycotoxicosis" [10]. Mycotoxins, term derived from the Greek, *mikes* and toxin that respectively mean fungi and poison. It has been unambiguously linked to the etiology of several diseases in animals. Those induce powerful and dissimilar biological effects such as carcinogenic (aflatoxins, Ochratoxins, fumonisins), mutagenic (aflatoxins, sterigmatocystin), teratogenic (Ochratoxin), estrogenic (zearalenone), hemorhagic (trichothecenes), immunotoxic (aflatoxins and Ochratoxins), nephrotoxic (Ochratoxins), hepatotoxic (aflatoxins and phomopsins), dermotoxic (trichothecenes) and neurotoxic (ergotoxins, penitrems, lolitrems, and paxilline). The ingestion of the mycotoxins is due to the consumption of plan-based foods and their residues or metabolites in animal products [26].

Since the discovery of aflatoxins in the 1960s [1] with approximately 100,000 turkey poultry deaths in England, was the fundamental event that made the scientific community realize that mold secondary metabolites could be responsible for food and feed safety problems. Several other mycotoxins have been identified when fungi in food were more fully investigated hence due to the determination of mycotoxins in food samples plays an important role in the protection of animal and human health.

Agricultural products are susceptible to contamination from production in the field, during harvest, transport or in storage as shown in figure 1. The impact of mycotoxins on health depends on the amount of the mycotoxin consumed, the toxicity of the compound, acute or chronic effects, the body weight of the individual, the presence of the other mycotoxins and other dietary effects [2]. Hsieh proposed that the evidence that a certain form of cancer or a human disease caused by a mycotoxin is a mycotoxicosis and it requires that all the following five criteria being satisfied [27]:

- Occurrence of the mycotoxin in food.
- Human exposure to the mycotoxin.
- Correlation between exposure and incidence.
- Reproducibility of characteristic symptoms in experimental animals.
- Similar mode of action in humans and animals models.

Nevertheless, the most important evidence that indicate a mycotoxin is involved in the etiology of a human disease is the correlation between the mycotoxin and the incidence of the disease.

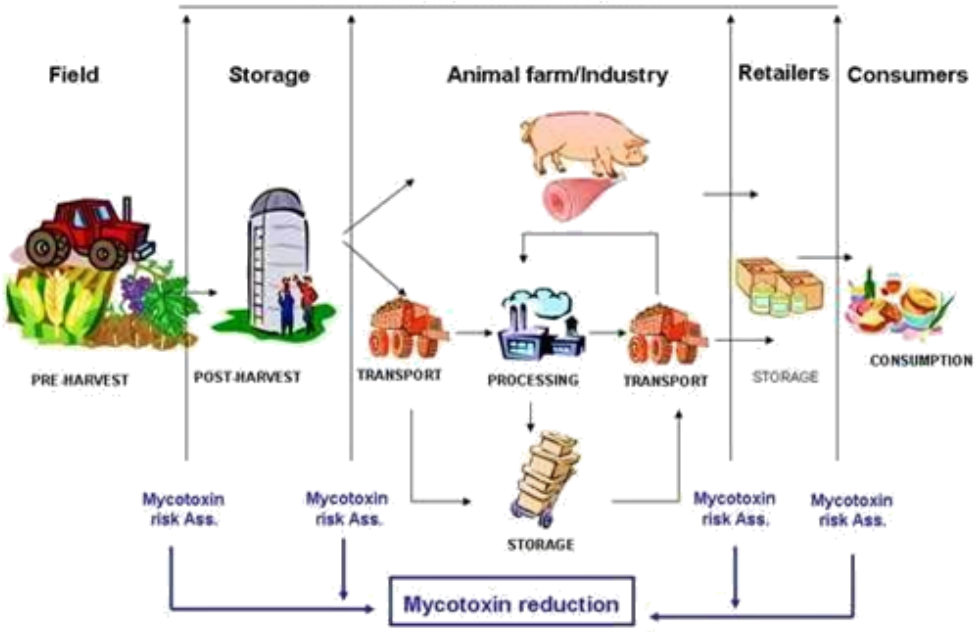

Fig. 1 Scheme of mycotoxins contamination.

Mycotoxins have attracted worldwide attention because these have been recognized as a major economic problem due to the significant economic losses associated with their impact on human health, animal productivity, domestic and international trade. Quality procedures and legislation of levels that are toxicologically acceptable are needed to minimize the exposure to mycotoxins; these actions are carrying out in the agricultural practice, storage of products and control of the products intended for human or animal consumption. The analytical techniques most used for mycotoxin determination are (a) chromatography and (b)

ELISA techniques [3]. The low levels of mycotoxins in foodstuffs, ranging from nanograms to micrograms, require the application of highly sensitive detection methods, analytical techniques coupled to a fluorometric detection, is the most widely used method for mycotoxins' determination [4].

Considering the limitations of the analytical techniques, high cost lack of sensitivity or need to skill technician; there is an urgent need for other accurate, simple and cost-effective techniques. Biosensors could be a screening tool for a rapid estimation of mycotoxin contamination in raw materials. Luminescence assays used in food testing and pharmaceutical industry could be promising rapid and sensitive technique. Optical detection is one of the oldest and most established techniques. Its main advantages are the simplicity of operations, low-cost, low power consumption and high stability [3].

Ochratoxins are the most dangerous mycotoxins found in food and beverages, one of these is Ochratoxin A (OTA), nowadays, OTA is one of the most relevant mycotoxins, with its presence in food and feed products being regulated in many countries [4]. OTA is produced by several species of the genera *Aspergillus* and *Penicillium*, it can occur in cereals, dried fruits, coffee, cocoa, spices, wheat, barley, rice, oats, rye, beans, soy and peas or peanuts.

1.1 Problem definition

Penetration of mycotoxins into the human body (ingestion, inhalation, skin absorption) may cause acute or chronic poisoning in the digestive, cardiovascular, respiratory, excretory systems. In recent years, the carcinogenic, mutagenic, teratogenic and immunosuppressive action of some mycotoxins has been confirmed.

Currently, more than 400 mycotoxins are produced by about 350 species of filamentous fungi. Thus, scientific attention has mainly focused on those that have proven to be carcinogenic and/or toxic in humans and animals. Five classes of mycotoxins are considered the most significant in agriculture and in the food industry, including the OTA [5].

Contamination of forage, cereals and other crops is the main entry of many mycotoxins into food and animal feed [28], being the cause that the contamination of food and feeds with mycotoxins is a world-wide problem. Consequently, the Food and Agriculture Organization of the United Nations (FAO) has estimated that 25% of crops worldwide are contaminated with mycotoxins and that the food losses amount to one billion tonnes per year [6].

Considering that OTA is one of the most relevant mycotoxins , it has also been found in meat, dairy and baked products, especially swine sausages and breads [11,12]. In humans a dietary intake of 1.21 μg per day has been linked to endemic nephropathy [7]. In human blood OTA was first found in inhabitants of endemic regions in Croatia [9]. The concentration range of OTA in human serum is 5–50 ng/mL and OTA has a long serum half-life in various species including humans [29].

Employing the analytical techniques but considering the disadvantages of these and the new techniques as the use of biosensor or the optoelectronics and the carcinogenic potential of the OTA. Besides, there is a relation between dietary intake of Ochratoxin and specific diseases. Additionally, in Mexico there is no a rigorous regulation about the limits of OTA, are the reasons for setting this research topic.

The information in Mexico concerning the incidence and levels of mycotoxin contamination in foods is limited by many factors, including available resources for research, laboratory facilities to carry out the analysis, the adequacy of the procedures sampling and the sensitivity of the quantification methods used. In Mexico, there is no classification of Ochratoxin A recommended values for certain foods.

There are only three regulations, which the maximum limit for aflatoxin in corn for human consumption (20 μg/Kg) and animals (from 21 to 300 μg/Kg) [30]. Likewise dough, tortillas, corn flour nixtamalized, the maximum level is 12 μg/Kg; wheat tortillas and flour is 20 μg/Kg [31]. In the case of milk or dairy products the maximum permitted level of aflatoxin M_1 is 0.5 μg/L [32]. Although, there is no legislation for other mycotoxins detected in foods for humans or animals as Ochratoxin A.

The daily dietary intake of Ochratoxin is quite difficult to estimate due to the frequency of mycotoxin presence in food products and the heterogeneity of food habits, the daily intake of OTA can be estimated based on its values in biological fluids (human milk, blood). The presence of OTA in complex samples is an important health risk factor in the people. These aspects related to the importance of assessing OTA content in food products allowed me to establish the research objectives, which pinpoint what the thesis sets out to achieve.

1.2 Research Objectives

1.2.1 General

⇒ Developing a microfluidic system to detect and analyze Ochratoxin A in liquid samples, low cost and portable.

1.2.2 Particulars

- Making a biosensor based on aptamer. The biosensor can be based on the immobilization of the Ochratoxin A with aptamer.
- Detection of OTA in liquid sample by amperometric detection.
- Implement an optical system to detect OTA.
- Experimental tests with the optical system for OTA in batch.
- Coupling the optical system to the flow system.
- OTA perform experimental trials with the flow system and optical.
- Optical detection of Ochratoxin A in complex liquid samples.

1.3 Thesis structure

This thesis is divided into four chapters and appendices. The first chapter introduces the reader to the problem to be analyzed in this thesis, in addition to the research objective besides of the specific objectives, proposed.

The second chapter contains a review of the state of the art of the OTA, its definition, physical and chemical properties, legislation as well as the methods of detection. Principally, biosensors and optical methods are described and It is emphasized the fluorescence property of the OTA and colorimetric methods.

The third chapter describes the methodology used for the detection of OTA, the aptasensor developed, the use of Light Emitting Diode (LED) and photodetectors to detect OTA, besides to incorporated image sensors. Finally, the optical system and interface developed to quantify OTA.

The fourth chapter shows the results, the analysis thereof, the limits of detection achieved. The calibration curves. Moreover, the recovery percentages with the columns for complex samples (cocoa, wine, beer).

Finally, in chapter five mentioned the conclusions and future prospects of this thesis.

CHAPTER II

REVIEW OF RELATED LITERATURE AND STUDIES

Ochratoxin A is a mycotoxin produced by several species of *Aspergillus* and *Penicillium* fungi that structurally consists of a para-chlorophenolic group containing a dihydroisocoumarin moiety that is amide-linked to L-phenylalanine. OTA is detected worldwide in various foods and feed sources. Studies show that this molecule can have several toxicological effects. In humans, the OTA has been implicated in the etiology of chronic kidney disease: Endemic Nephropathy the Balkans in 1972 [1,13]. It will be mentioned the general aspect of OTA: physic-chemical properties, toxicological profile, contaminated food, legislation, detection methods, recent publications and the new tendencies to detect OTA in real samples.

2.1 Definition

Ochratoxin A is a mycotoxin produced by secondary metabolism of many filamentous species belonging to the genera *Aspergillus* and *Penicillium* [10]. The chemical structure of OTA is shown in figure 2. Structurally, OTA includes a dihydrocoumarin moiety linked to a molecule of l-β-phenylalanine by an amide bond. Several metabolites related to OTA have been identified, such as dechlorinated analog Ochratoxin B (OTB), the isocoumaric nucleus of OTA, Ochratoxin α (OTα), its dechlorinated analog Ochratoxin β (OTβ) and Ochratoxin C (OTC), which is an ethyl ester derivative of OTA.

Among these compounds, the OTA is the most abundant and most toxic. The main sources of OTA in the diet are cereals. However, significant levels of contamination can be identified in grape juice and red wine, coffee, cocoa, tree nuts, spices and dried fruit. Contamination can also spread to pork, based on pig blood and beer products. *Penicillum verrucosum* is the main source of OTA of products stored in temperate climates while *Aspergillus spp*. dominates in countries with warmer climates.

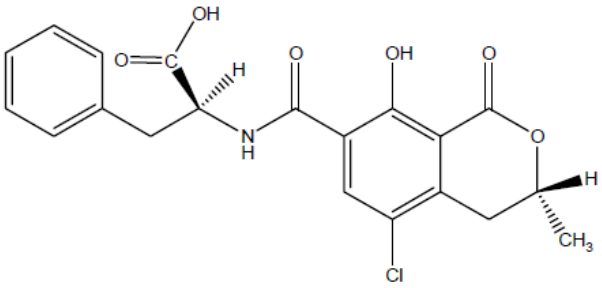

Fig. 2 Chemical structure of OTA.

2.1.1 Structure

Ochratoxin A has been isolated for the first time, from Aspergillus ochraceus in 1965 during laboratory screening for toxigenic fungi. The empirical formula of Ochratoxin A is $C_{20}H_{18}ClNO_6$. Its International Union of Pure and Applied Chemistry (IUPAC) name is: *N*-{[(3*R*)-5-chloro-8-hydroxy-3-methyl-1-oxo-3,4-dihydro-1*H*-isochromen-7-yl]carbonyl}-L-phenylalanine or N-[[(3R)-5-chloro-3,4-dihydro-8-hydroxy-3-methyl-1-oxo-1H-2-benzopyran-7-yl]carbonyl-L-phenylalanine [11]. Other names are (*R*)-*N*- [(5-Chloro- 3,4-dihydro- 8-hydroxy- 3-methyl- 1-oxo- 1H-2-benzopyran-7-yl) -carbonyl]- *L*- phenylalanine or -*N*-[(5-chloro-8-hydroxy-3-methyl-1-oxo-7-isochromanyl)carbonyl]-3-phenylalanine.

Biosynthetically, it is a pentaketide derived from the dihydrocoumarins family coupled to β-phenylalanine. Depending on the substituents R1, R2, R3 and R4 are different Ochratoxins. Various derivatives of Ochratoxin A have been identified, figure 3 presents the general structure common to these different metabolites and Table 1 shows the characteristics composition of each one [10,11].

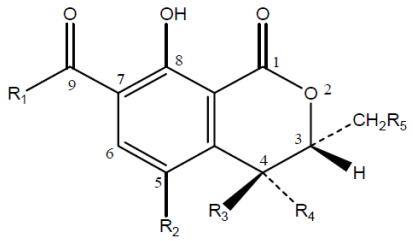

Fig. 3 General structure of Ochratoxin A metabolites.

Table 1 Characteristics composition of OTA derived metabolites.

Name	R1	R2	R3	R4	R5
OTA	Phenylalanine	Cl	H	H	H
OTB	Phenylalanine	H	H	H	H
OTC	Ethyl-ester, Phenylalanine	Cl	H	H	H
OTA Methyl-ester	Methyl-ester, Phenylalanine	Cl	H	H	H
OTB Methyl-ester	Methyl-ester, Phenylalanine	H	H	H	H
OTB Ethyl-ester	Ethyl-ester, Phenylalanine	H	H	H	H
OTα	OH	Cl	Cl	H	H
OTβ	OH	H	H	H	H

2.2 Physical and chemical properties for OTA

OTA is a white, crystalline powder that is very unstable in the presence of light but fairly heat resistant, is a weak organic acid with a pKa value of 7.1 and its molecular weight is 403.8 g/mol [10]. With a crystalline structure varying from colorless to white. OTA possess an intense green fluorescence under UV light in acid medium and blue fluorescence in alkaline conditions [12].

A neutral or acid pH, OTA is soluble in polar organic solvents (alcohols, ketones, chloroform), slightly soluble in water and insoluble in petroleum ethers and saturated hydrocarbons. At alkaline pH, this molecule is soluble in aqueous sodium bicarbonate solution (0.1 M, pH 7.4) and in alkaline solutions.

Its melting point is 90 °C when it is crystallized from benzene and 169 °C when it is crystallized in xylene [33]. The particularity of OTA is its high stability. OTA possesses a resistance to acidity and high temperatures. Thus, once foodstuffs are contaminated, it is very difficult to totally remove this molecule [10,34].

OTA is optically active, its rotational coefficient is $\alpha_D^{21} = -46.8°$. The UV absorption spectrum of OTA varies depending on the pH and polarity of the solvent. OTA has an absorption maximum at 333 nm with a molar extinction coefficient of 5500/mol×cm in methanol. It absorbs at 338 nm with a coefficient of 5600. OTA has an absorption maximum at 378 nm with an extinction coefficient of 14700. Ochratoxin A is also fluorescent; it has an emission maximum at 467 nm in 96% ethanol and 428 nm in absolute ethanol after excitation at 340 nm.

Moreover, after excitation at 365 nm, OTA has green fluorescence in an acidic medium and blue fluorescence in alkaline medium; This property is used for the detection and determination of OTA [10][33]. OTA is relatively stable to temperature; it is however completely degraded by sodium hypochlorite [35]. These properties are used in the laboratory, for the decontamination of equipment.

2.3. Toxicological profile

The toxicological status of OTA has been examined and it was the subject of a complete monograph by the IARC (International Agency for Research on Cancer) in 1993 [36]. Several studies were carried out in order to show the implication of OTA in diseases with effects such as nephrotoxic, hepatotoxic, neurotoxic, teratogenic and immunotoxic on several species of animals [8], and can cause kidney and liver tumors in mice and rats. However, its toxicity varies depending on the sex, the species and the cellular type of the tested animals [13].

The genotoxic status of OTA is still controversial, due to contradictory results obtained in various microbial and mammalian tests. Ochratoxins have been related to human and animal diseases in literature especially since the early 1970s. Most reports indicate that Ochratoxin plagued especially the North Eastern European countries and Africa [37, 38].

2.3.1 Hepatotoxic

In studies with broiler chicks, liver damage was present in concert with nephrotoxicity. Lymphocyte infiltration occurred in the liver along with lymphocytosis in lymphoid organs. Necrotic changes in periportal cells were observed in rats given an LD_{50} (20 mg/kg body weight) dose of Ochratoxin A and apparently prevented fatty degeneration of the liver caused by aflatoxins when the two toxins were given simultaneously to broiler chickens [39].

2.3.2 Nephrotoxicity

Nephropathy is the major toxic effect of OTA. This molecule shows to be potentially nephrotoxic in all non-ruminant mammals, such as dogs, rats, and swine are known to be affected with kidney problems due to Ochratoxin A, affected pigs show signs of pain in the

kidney area, consume excessive amounts of water, appear depressed, urinate almost continuously, and have decreased feed consumption [39].

Epidemiological studies carried out showed that OTA plays an important role in the etiology of porcine nephropathy. This mycotoxin was also associated with human nephropathy and it is suspected to be the cause of the human fatal disease known as Balkan Endemic Nephropathy (BEN), an interstitial chronic disease affecting the south-eastern population of Europe [37]. The toxic activity of Ochratoxin A may relate to one of its structural components, phenylalanine, which likely is involved in inhibition of enzyme reactions where it is known its function [39].

2.3.3 Neurotoxicity

The administration of OTA at gestation period in rats induced malformations in the central nervous system. Soleas *et al.* [40] reported that OTA can be regarded as a possible cause of damage at the cerebral level.

2.3.4 Teratogenicity

OTA is highly toxic for the nervous cells and is a potent teratogen to laboratory animals. It can cross the placenta and accumulate in fetal tissue causing various morphological anomalies. It has been reported to malformations caused by OTA in rats [41- 43] or hamsters [44] and chicken embryos [45].

2.3.5 Immunotoxicity

Toxic effects resulting from very low concentrations of OTA in the ng/ml range affect the immune system. It appears that this system is by far the most sensitive among all other sensitive organs [46]. It has been mentioned that OTA is clearly an immunosuppressive agent [10] [47], presents immunosuppressor effect at low or high doses [10].

2.3.6 Carcinogenesis

OTA has been considered as cause of human carcinogen based on evidence of carcinogenicity in experimental animals. When OTA was administered in the diet, hepatocellular, renal cell tumors, and hyperplastic hepatic nodules were observed in male mice besides, hepatocellular carcinomas and adenomas in female mice [10]. However, no adequate

human studies of the relationship between exposure to OTA and human cancer have been reported.

2.4 Contaminated food

Recent international exposure assessments were performed by the Scientific Committee on Food (SCF), European Commission (EC), the Joint FAO/WHO expert Committee on Food Additives (JECFA) and Food and Agriculture Organization/World Health Organization (FAO/WHO). The SCF estimated that the mean dietary intake ranged from 0.7 to 4.6 ng/kg body weight per day. By combining the average contamination levels with the 95 percentage of food consumption, thus, the consumption of foodstuffs contaminated by OTA represents a major source of exposure to OTA in humans [48]. While dermal contact or inhalation exposures to OTA show minor importance for the general population [49].

Ochratoxin A by *Aspergillus* and *Penicillium* toxins in foodstuffs such as barley, bean, bee pollen, beef, beer, grapes, strawberries, beverage, biscuit, pig blood, bran, barley bran, oat bran, rice bran, wheat bran, bread, buckwheat, butter, cocoa butter, peanut butter, cake, peanut cake, rice cake, cassis, cereal, blue cheese, chicken, chickpea, chocolate, cocoa, cocoa bean, cocoa mass, cocoa nib, coffee, coffee bean, confectionery, currant, date, maize dough, cocoa drink, duck, fig, fish, flakes barley flakes, cornflakes, maize flakes, oat flakes, flour, barley flour, buckwheat flour, cassava flour, lentil flour, maize flour, oat flour, potato flour, rice flour, rye flour, soybean flour, Vetch flour, wheat flour, baby food, infant food, apple, cherry, grape, peach, prune, quince, fruit dried, fruits and nuts, germ, wheat germ, goose, black gram), green gram, durum grits, maize grits, groats, barley groats, wheat groats, gruel, ham, soy, jam, apple juice, black currant juice, carrot juice, fruit juice, grape juice, tomato juice, pig kidney, poultry kidney, lentil, linseed, liquorice, cow liver, duck liver, goose liver, pig liver, turkey liver, maize, malt, barley malt, buckwheat meal, maize meal, oat meal, rye meal, spelt meal, wheat meal, pig meat, poultry meat, medicinal plant, cow milk, human breast milk, infant formula, millet, muesli, chicken muscle, pig muscle, must, noodle, nut, almonds, cashew nuts, coconuts, hazelnuts, peanuts, pistachio nuts, walnuts, oat, olive oil, sesame oil, olive, curry paste, fig paste, pastries, pâté, pea, pork, potato, cocoa, cocoa powder, milk powder, bakery products, cereal products, coconut products, food products, meat products, rye products, wheat products, pudding, crème, grape pulp, pulses, puree, raisin, rice, rolls, rusk, rye, sandwich,

sauce, chili sauce, soy sauce, sausage, pig serum, sesame, snack, sorghum, soybean, spelt, caraway, cardamom, cayenne pepper, chili, coriander, cumin, curcuma, curry, fennel, garlic, ginger, mustard, nutmeg, paprika, pepper, pili-pili, tandoori, turmeric, maize starch, rice starch, wheat starch, sultana, sunflower seed, tea, tomato ketchup, turkey, vegetables, vine fruit (dried), vinegar, red wine, rosé wine, white wine [50]. Tables 2 and 3 give an overview of the current identity of micro fungi *Aspergillus* and *Penicillium* species that produce OTA in foodstuffs [49].

Table 2 *Aspergillus* species as OTA producers in foodstuffs.

Species	Foodstuff
A. ochraceus G. Wilh.	Soya bean, nuts, red pepper, cereals, green coffee beans
A. steynii Frisvad & Samson	Coffee beans
A. westerdijkiae Frisvad & Samson	Coffee beans
A. carbonarius (Bainier) Thom	Grapes, red pepper, coffee beans
A. foetidus Thom & Raper	Grapes
A. lacticoffeatus Frisvad & Samson	Coffee beans
A. niger Tiegh	Grapes, peanuts
A. sclerotioniger Frisvad & Samson	Coffee beans
A. tubingensis Mosseray	Grapes

Table 3 *Penicillium* species as OTA producers in foodstuffs.

Species	Foodstuff
P. verrucosum Dierckx	Cereals
P. nordicum Dragoni & Cantoni	Dry ham, salami

Worldwide, the cereals are the most important source of human food; thus, rice, corn, and millet considered the basic foods of the populations are often contaminated mainly by Ochratoxins. Particularly in the countries with hot and wet climatic conditions, that the growth of toxigenic filamentous fungi is most favored. The figure 4 shows the prevalence of the cereals as the major as being the major source of OTA contamination for European population.

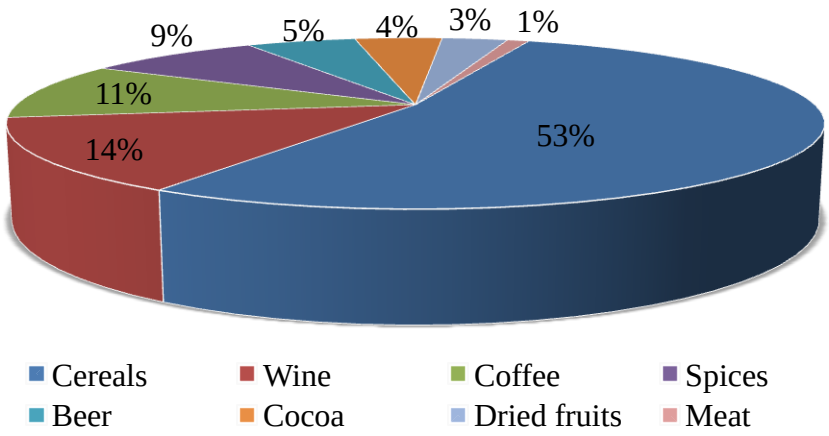

Fig. 4 Contribution of each foodstuff to OTA, average exposure of the European population [14].

Moreover, wine was recently considered as the second source of OTA human consumption, recent works [51-53] highlight the presence of considerable levels of this toxin in wines, musts and grape juices. However, OTA contamination of many other raw agricultural products has been well documented; such contamination occurs in a variety of food and feed, such as coffee beans, pulses, spices, meat and cheese products as is represented in the figure 5. OTA has also been detected in other beverages such as beer [10].

Fig. 5 Prevalence of the OTA in some food and feed stuffs in the world [50][54].

2.5 Regulation and Legislation

The International Agency for Research on Cancer (IARC) [55] classified several mycotoxins as carcinogenic or potentially carcinogenic to humans according to the following groups:

- *Group 1*: The agent is carcinogenic to humans.
- *Group 2A*: Probably carcinogenic agent in humans, there is limited evidence in humans but sufficient animal.
- *Group 2B*: Possibly carcinogenic agent, the evidence in humans is limited and there is no sufficient evidence in experimental animals.
- *Group 3*: The agent is not classified as a human carcinogen, and cannot be included in another group.
- *Group 4*: The agent is probably not carcinogenic to humans; the available evidence from both human and animal studies suggests so.

The IARC has classified Ochratoxin A as a possible human carcinogen (Group 2B) in 1993[56]. In the European Union (EU), the Commission Regulation lays down specific maximum limits for OTA to foodstuffs such as unprocessed cereals, dried vine fruit, coffee, beans, soluble coffee, wine, grape juice, spices, liquorice, and products for infants. The lowest maximum limit in products for infants is established for wine and grape juice at 2.0 µg/kg, while the highest maximum limit is set at 80 µg/kg for liquorice extract for use in foods.

Additional, maximum limits for OTA established in EU Member States such as Denmark, Hungary, Italy, and Germany in their national legislation are presented in the table 4[3] by the European commission.

Table 4 Maximum accepted levels of OTA.

Foodstuffs	Maximum level (µg/Kg)
Unprocessed cereals, roasted coffee beans and ground roasted coffee	5
All products derived from unprocessed cereals and processed cereal products	3
Dried vine fruit and soluble coffee (instant coffee)	10
Wine (sparkling wine), fruit wine, aromatized wine, aromatized wine based drinks and grape juice, grape nectar, grape must and products	2

Processed cereal based foods, baby foods and dietary foods	0.5
Spices, including dried spices, *Piper* spp (fruits, white and black pepper) *Myristica fragrans* (nutmeg), *Zingiber officinale* (ginger), *Curcuma longa* (turmeric), *Capsicum* spp. (dried fruits, chillies, chili powder, cayenne and paprika)	15
Liquorice root	20
Liquorice extract	80
Wheat gluten not sold directly to the consumer	8

Egypt and Bosnia and Herzegovina refer to the Commission Regulation for setting up their national maximum limit for OTA. In Russia, the limit in wheat, barley, rye, oat and rice cereals and cereal products is set at 0.005 mg/kg while the limit for specific products for children is set to 0.5 μg/kg. In China, a limit of 5.0 μg/kg for OTA is set for cereals, milled products from cereals, legumes and pulses.

GCC (Saudi Arabia, United Arab Emirates (UAE), Kuwait, Bahrain, Oman, Yemen and Qatar), Nigeria and Kenya established OTA limit of 5 μg/kg is set for raw wheat, barley and rye. In India, the limit for OTA is 20 μg/Kg. No specific limits for OTA in foodstuffs are set in USA, Canada, Australia and New Zealand, Japan, Mexico and South Africa [57,58]. The table 5 shows the maximum level of OTA in others countries [59].

Table 5 Maximum level of OTA in some foods and feed as currently regulated in different countries.

Commodity	**Level (ng/g)**	**Country**
Raw cereal grain	5	EU
Products derived from cereals	3	EU
	50	Israel
	2	Switzerland
Dried vine fruits	10	EU
Children's food	6	Czech republic
Pork meat and derived products	1	Italy
Pig kidneys	10	Denmark
Coffee	5	Finland
Roasted and instant coffee	4	Italy

Raw coffee beans	20	Greece
Cocoa and derived products	0.5	Italy
Grain for feed	300	Israel
All foods	5	Romania
All foodstuffs	5	Romania
Foodstuffs for poultry	200	Sweden
Foodstuffs for pigs	100	Sweden
Rice, barley, beans, coffee, maize	50	Uruguay

OTA was evaluated by JECFA [60] and established a provisional tolerable weekly intake (PTWI) of 112 ng/kg body weight (b.w.). This value was proposed according to the porcine nephropathies data basis. However, this molecule was re-evaluated and the PTWI was reconfirmed, rounding it to 100 ng/kg b.w. per week [61].

On the other hand, the Scientific Committee on Food (SCF) expressed its opinion on OTA to the vulnerable groups such as infants and children and groups of consumers, who are exposed to higher levels of OTA than the average consumer due to their dietary habits. This committee proposed to reduce the OTA intake as much as possible to levels between 1.2–14 ng/kg b.w. per day [62].

2.6 Pesticides

A pesticide is defined as a substance or mixture intended to prevent, destroy, repel or mitigate any pest including insects, rodents and weeds. Pesticides include not only insecticides, also herbicides, fungicides, disinfectants, and growth regulators. The International Organisms in charge to declare allowed limits into the environment, one of these is the US Environmental Protection Agency (EPA), the European commission which has regulated the lowest allowed limits for priority hazardous substances (0.1 µg/L). The Mexican Norm established the procedures of: manipulation hazardous substances, control and storage of insecticides and allowed limits. The NOM-052-SEMARNAT-1993 has established 30 µg/L as maximum allowed for pesticides. The use of pesticides in spite of advantages in production also implies side-effects for human health and environment. There are many studies about the relationship between exposure of pesticides and cancer, Parkinson and other endocrine

disrupting causes. The main problem is with the widespread use of pesticides, it is difficult not be exposed to them. The pesticides used in this thesis were:

Organophosphate (OP) pesticides are comprised of a phosphate (or thio- or dithiophosphate) moiety and an organic moiety. In most cases, the phosphate moiety is O,O-diakyl substituted. These pesticides are potent acetylcholinesterase inhibitors. They can reversibly and irreversibly bind covalently with the serine residue in the active site of acetylcholinesterase and prevents its natural function in catabolism of neurotransmitters. This action is not unique to insects, can produce the same effects in wildlife and humans. Once human exposure occurs, OP insecticides are usually metabolized to the more reactive oxon form which may bind to cholinesterase or be hydrolyzed to a dialkyl phosphate and a hydroxylated organic moiety specific to the pesticide. As a result of binding to cholinesterase, the organic portion of the molecule is released. The cholinesterase-bound phosphate group may be dismiss by the loss of the O,O-dialkyl groups, or may be hydrolyzed to regenerate the active site of enzyme.

Carbamate insecticides have the same mechanism of toxicity action as the OP insecticides, except their effects are more reversible and less severe. The most popular of these pesticides for residential uses are carbaryl (sevin) and propux (Baygon). Many carbamates such as aldicarb and methomyl are also used in agriculture applications.

However pesticides can persistence not only in the human body, before to be in contact with humans, the ground, lips, water and other matrices can have high toxicity remainders of pesticides. For this, fast and, effective analytical methods (figure 6) of pesticides or OTA detection are needed to avoid the exposure and possible health and environment pollution. The sample preparation is an important step for the determination of trace compounds, thus, there is considerable interest in developing methods for extracting and isolating components from complex environmental matrices [63].

2.7 Methods of detection in foodstuffs contaminated by OTA

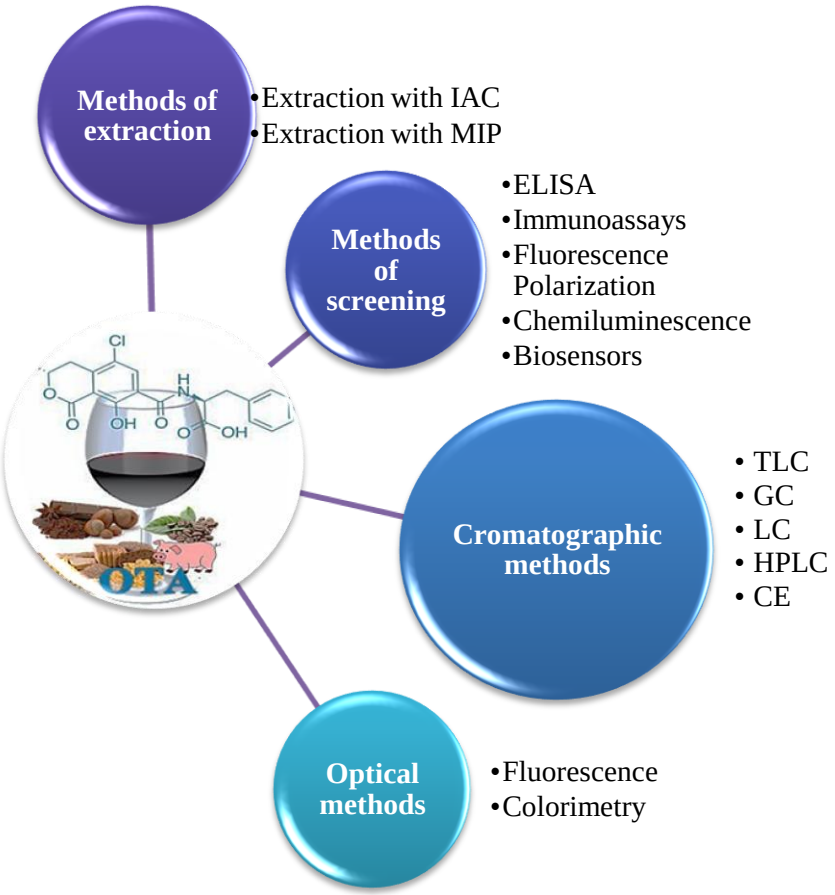

IAC: ImmunoAffinity Column; MIP: Molecularly Imprinted Polymer; ELISA: Enzyme linked immunosorbent assays; TLC: Thin Layer Chromatography; GC: Gas Chromatography; LC/MS: Liquid Chromatography; HPLC: High Performance Liquid Chromatography; CE: Capillary electrophoresis.

Fig. 6 Classification of the methods employed to detect or quantified OTA in food.

The importance of analysis of mycotoxins in food lies in compliance with regulations, such tests requires a high degree of accuracy, precision and reproducibility, therefore the use of quality procedures, certified reference materials are recommended. The analytical techniques most employed in mycotoxin analysis are classified in [64,65]:

1) Methods of extraction
2) Screening methods
3) Chromatography methods

2.7.1 Methods of extraction

Mycotoxins in foods have a patchy distribution; first, the homogenization of the sample is required prior to extraction of the residues, which are in very low concentration matrix. The complexity of food, with significant amounts of proteins, lipids, carbohydrates, water or components of nutrients. If the sample is liquid can be used a solvent immiscible with the sample; when the sample is solid, the organic solvents are used, such as methanol, acetone, ethyl acetate, acetonitrile, dichloromethane, hexane or mix of them. The choice of solvent depends on the polarity of the mycotoxin and nature of the sample. The extraction and cleaning techniques used for the analysis of mycotoxins are [65]:

- Solid Phase Extraction, SPE
- Extraction with Mycosep columns
- Matriz Solid Phase Dispersion, MSPD
- Solid Phase MicroExtraction, SPME
- Ion Exchange Column
- ImmunoAffinity Column, IAC
- Supercritical Fluid Extraction
- Micro-Wave Assisted Extraction
- Accelerated Solvent Extraction
- Molecularly Imprinted Polymer, MIP

This thesis employed immunoaffinity and MIP columns, so will be explained in more detail.

2.7.1.1 ImmunoAffinity columns

Antibody-based immunoaffinity columns clean-up combined with HPLC/fluorescence detection has become very common in mycotoxin analysis of foodstuffs, feedstuffs and biological fluids due to a large number of advantages over other commonly used clean-up procedures. IAC tools are based on the use of anti-mycotoxin antibody into solid support such as agarose gel. Principle of the cleanup is showed in the figure 7 and described below:

(1) Filtered extract is loaded onto the column containing specific antibodies for the mycotoxin of interest.

(2) Antibodies selectively bind the mycotoxin from the crude extract.

(3) Impurities are removed from the column by washing with water or PBS while the toxin is immobilized by antibodies in the column.

(4) Mycotoxin is eluted from the column for its detection by a dedicated fluorometer, HPLC or by other methods. OTA could be eluted with methanol [66].

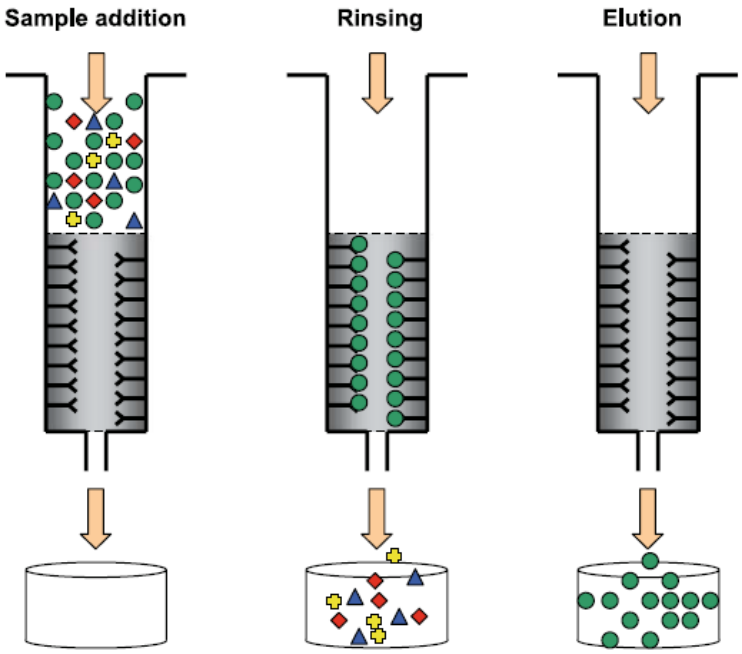

Fig. 7 Principle of immunoaffinity columns (mycotoxin ●, impurities: ◆▲✚) [67].

The methanol solution can be used for HPLC analysis as well. With IAC clean-up, the mycotoxin can be concentrated in the column, thereby increasing the fluorometric assay sensitivity or decrease its limit of detection. However, IACs have a limited loading capacity and the sample clean-up procedures are more complicated compared to others in the rapid

methods for mycotoxins [67]; the advantages and disadvantages of the IAC are presented in the table 6.

Table 6 Advantages and disadvantages of the immunoaffinity columns for mycotoxins analysis [68].

Advantages	Disadvantages
Rapid simple preparation and clean-up procedure	High cost of the columns
Clear extracts from the IAC	Single use
Specificity of the antibody	Analysis of individual mycotoxins
Applicability to complex matrices	
Reduced use of dangerous solvents	
Simultaneous batch processing	
Good performance in terms of precision, accuracy and sensitivity	

Due to the simplicity of clean-up procedures and the good performance of the columns (in particular the high selectivity due to the antibody), IACs are increasingly being used in research and quality control laboratories with several matrices of foodstuffs, beverages and feedstuffs [68].

IACs are commercially available for the clean-up of OTA for example OchrascanR (R-Biopharm Rhone Ltd.). Sample clean-up with antibody-based IAC became increasingly popular for coffee, beer and wine [59,66,69,70] or ham [71]. The effectiveness of an immunoaffinity column coupled with analytical detection has been validated and adopted as official or standard methods by AOAC International or the European Committee for Standardization as AOAC Official Method 991.31 [68,72].

2.7.1.2 Molecularly Imprinted columns

Attempts to replace the bio recognition element of IAC by a less expensive and more stable biomimetic counterpart have been described recently. A molecularly imprinted polymer (MIP) able to recognize Ochratoxin A was prepared [59].

Molecular imprinted technique (MIT) has been investigated to be an efficient and powerful technique for sample clean up and pre-concentration of mycotoxins in applications to different matrices successfully. MIP is a synthetic material with an artificially generated three-dimensional network that is able to bind to a target molecule, specifically.

It has the advantages to be inexpensive, chemically, thermally stable and compatible with all solvents. MIP specifically designed for OTA has already been generated using either OTA or a structural analog as template and successfully applied as SPE sorbent (MIP-SPE) for sample pretreatment. In comparison with IAC, MIP-SPE exhibits reusability, simple operation and longer storage time and is further considered as an alternative to IAC [73]. MIP currently seem to be very promising and cheaper alternative to SPE and IAC sorbents for clean-up and pre-concentration of OTA [59] .

Molecular imprinting is a process where the target molecule (or a derivative thereof) acts as a template around which interacting and cross-linking monomers are arranged and copolymerized to form a cast-like shell, scheme in the figure 8. The use of MIP for Ochratoxin A [74] for extraction and analysis [75] in ginger [73], coffee, grape juice and urine [76] and wine [77] has been documented.

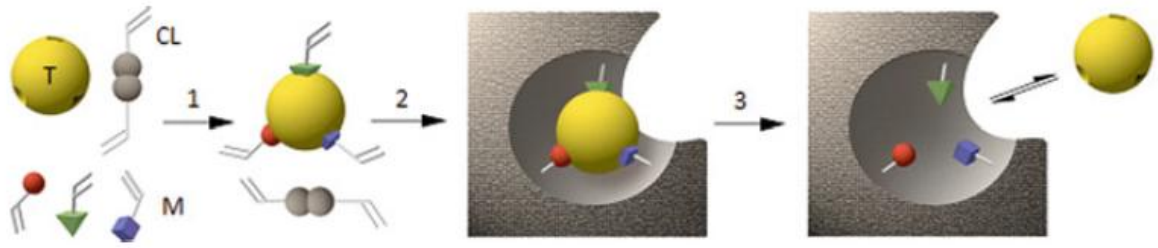

Fig. 8 General principle of molecular imprinting. A molecular template (T) is mixed with functional monomers (M) and a cross-linker (CL) resulting in the formation of a self-assembled complex (1). The polymerization of the resulting system produces a rigid structure bearing imprinted sites (2). Finally removal of the template liberates cavities that can specifically recognize and bind the target molecule (3) [78].

2.7.2 Biosensors

Sensors are devices composed of two elements: the molecule, which selectively reacts with the compound of interest and is in contact with a transducing element converting the change of the physical variable produced by the reaction into a measurable signal. Take it in consideration, biosensors are those using biological molecules as recognition elements: antibodies, enzymes, bacteria, receptors, DNA [79-82].

Biosensor devices are emerging as one of the foremost relevant diagnostic techniques for food, clinical and environmental monitoring due to their rapidity, specificity, ease of mass

fabrication, economics and field applicability. A biosensor can be defined as a quantitative or semi quantitative analytical instrumental technique containing a sensing element of biological origin, which is either integrated within or is in intimate contact with a physicochemical transducer [83].

A chemical sensor is a device that transforms chemical information, ranging from the concentration of a specific sample component to total composition analysis, into an analytically useful signal. Chemical sensors usually contain two basic components connected in series: a chemical (molecular) recognition system (receptor) and a physicochemical transducer. Similarly, biosensors are chemical sensors in which the recognition system uses a biochemical mechanism interfacing the optoelectronic system [84]. That uses specific biochemical reactions such as enzymes, immune-systems, tissues or cells to detect chemical compounds usually by electrical, thermal or optical signals, the structure of a biosensor is in the figure 9 [85].

According to proposed IUPAC definition, "A biosensor is a self-contained integrated device which is capable of providing specific quantitative or semi-quantitative analytical information using a biological recognition element (biochemical receptor) which is in direct spatial contact with a transducer element. A biosensor should be clearly distinguished from a bioanalytical system, which requires additional processing steps, such as reagent addition or a bio-probe which is either disposable after one measurement, i.e. single use, or unable to continuously monitor the analytes concentration [86].

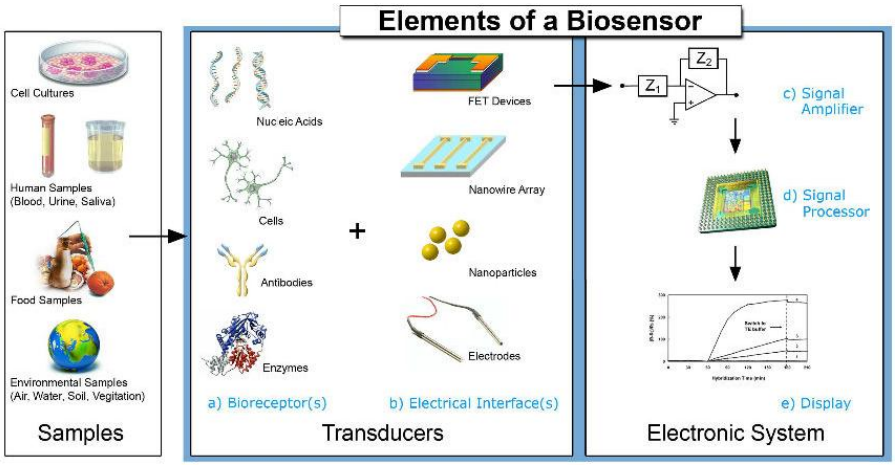

Fig. 9 Structure of a biosensor [87].

The basic principle of a biosensor is to detect the molecular recognition and to transform it into another type of signal using a transducer, due to the two fundamental operating principles of a biosensor is:

(1) Biological recognition system, often called a bioreceptor

(2) Transducer

The main purpose of the recognition system is to provide the sensor with a high degree of selectivity for the analytes to be measured. The interaction of the analytes with the bioreceptor is designed to produce an effect measured by the transducer, which converts the information into a measurable effect [15]. Biosensors can be classified by bioreceptor or transducer type, the figure 10 shows the classification.

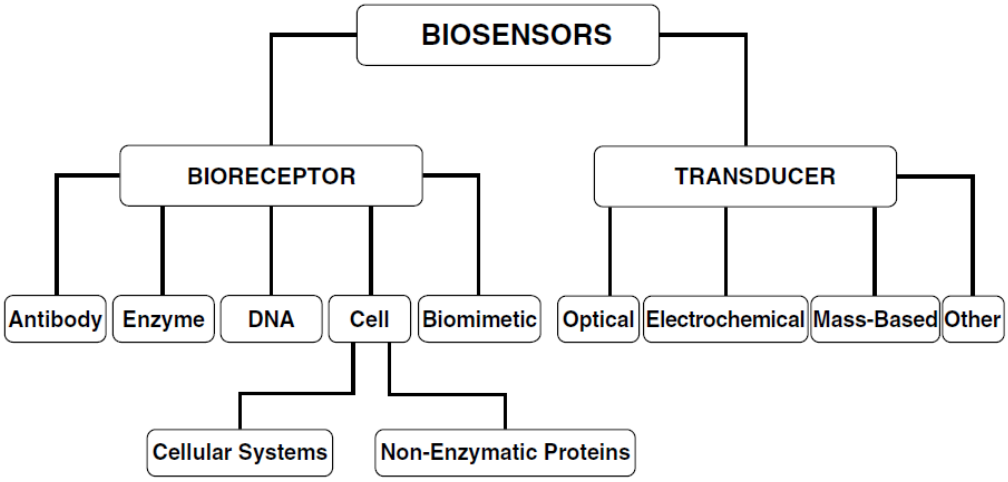

Fig. 10 Biosensor classification schemes.

The principal characteristics requires in a biosensor are [85]:

a. Selectivity: Highly selective for the target analyte and show minimum or no cross reactivity with moieties having similar chemical structure.
b. Sensitivity: Ability to measure in the range of interest for a specific target analyte with minimum additional steps.
c. Linearity: The system should cover the concentration range over which the target analyte is to be measured.
d. Reproducibility: Having same concentrations analyzed several times, they should give same response.

e. Quick response time: The response should be quick enough so that real time monitoring of the target analyte can be done efficiently. The recovery time should be small for reusability of the biosensor system.
f. Stability: The biological element used should be interfaced such that the activity is retained for a long time to make the device marketable and practically useful in the field.

The key component of a biosensor is the transducer that uses a physical change accompanying the reaction. It can be:

- *Electrochemical transducer*. Changes in electrical or electronic output.
  - ⇒ Potentiometric
  - ⇒ Amperometric
  - ⇒ Calorimetric
- *Optical/Optoelectronic transducer*. Light output or light absorbance difference between the reactants and products.
  - ⇒ Light based potentiometric sensors
  - ⇒ Surface Plasmon Resonance
  - ⇒ UV-VIS absorbance
  - ⇒ Luminescence and fluorescence
  - ⇒ Total Internal Reflection (TIRF)
- *Piezoelectric transducer*. Based on mass of the reactants or products.
  - ⇒ Quartz Crystal Microbalance
  - ⇒ Surface Acoustic Wave Sensor
- *Thermal sensor transducer*
  - ⇒ Isothermal Titration Calorimetry
  - ⇒ Heat sensitive change in polymer film color

The advantages and disadvantages of biosensors are: cheap, fast, portable, very suitable for routine screening of samples, but they suffer from the selectivity and reproducibility problems and the results should be therefore confirmed with the conventional method [79].

2.7.3 Chromatography methods

The term conventional method usually refers to a chromatographic separation coupled to a suitable detection system. It has two purposes, principally:

1. To confirm samples that have been determined to contain mycotoxins based on rapid screening tests.
2. To more accurately quantitative the amount of toxin present.

Reference methods for OTA detection generally involve a chromatographic technique such as thin-layer chromatography (TLC), gas chromatography (GC), high-performance liquid chromatography (HPLC), liquid chromatography with mass spectrometry (LC-MS) or tandem mass spectrometry (LC-MS/MS) to further separate mycotoxins from extract impurities. Quantitative methods for the determination of mycotoxins in food or feed implicate the use of HPLC or GC in combination with detectors, such as fluorescence detection with pre- or post-column derivatization step, ultraviolet (UV) detection or MS.

2.7.3.1 High performance liquid chromatography

HPLC coupled with UV, a diode array detector (DAD) or a fluorescence detector (FD) is the most widely used technique for the identification of mycotoxins in food by its characteristics such us accuracy, repeatability, reproducibility and have reasonably low levels of detection. Compounds eluted from the column pass through a detector of some sort (usually fluorescence or ultraviolet depending on the physical and chemical attributes of the analyte of interest) and the detector helps to quantify the specific compounds in the original sample injected onto the column. It is sometimes necessary or an advantage, to use pre-column or post-column derivatization to assist sensitive detection of the mycotoxin. For many mycotoxins, the time for analysis following injection onto the column is less than 20 minutes.

These methods have been adopted as official or standard methods by the AOAC International or the European Standardization Committee. In particular, methods for Ochratoxin A in barley (2000.03), Ochratoxin A in roasted coffee (2000.09), Ochratoxin A in wine and beer (2001.01) and Ochratoxin A in green coffee (2004.10). Additionally, HPLC/immunoaffinity column methods have been validated for the measurement of Ochratoxin A in cocoa powder. HPLC-FD is highly sensitive, selective and repeatable, so

specific labeling reagents have been developed and are commercially available for the derivatization of non-fluorescent mycotoxins to form fluorescent derivatives [3].

The presence of OTA in wine has been determined using clean up with commercially available IA columns and separation with RP-HPLC C-18 column, the sensitive FD method allowed estimation of OTA in 0.01 ng/mL concentration. The researchers employed direct injection of the grape must sample in a HPLC–FD system without prior clean-up procedure, the LOD and LOQ were 0.22 and 0.77 µg/L, respectively [56].

OTA contamination in dried figs was studied using HPLC–FD extraction with methanol and orthophosphoric acid following clean up by an IAC. The LOD for OTA was 0.12 g/Kg. The mean concentration of OTA determined using HPLC was 0.39 ng/mL of plasma. The combination of HPLC method with clean-up step by IAC was used for the detection of OTA in green and roasted coffee beans as well as in the coffee brew. HPLC based OTA detection in dry-cured meat products has been described that comprised no clean-up step [56]. The main advantage is its identification power and possibility to perform determination of multiple analytes from different chemical groups in the same run. The advantages and disadvantages of the most common methods to detect OTA are showed in the table 7.

Table 7 Common methods to detect OTA.

Method	Advantages	Disadvantages
ELISA	Simple sample preparation, Inexpensive equipment High sensitivity Simultaneous analysis of multiples samples Suitable for screening Limited use of organic solvents Visual assessment	Cross-reactivity with related mycotoxins Matrix interference problems Possible false positives / negative results Confirmatory LC analysis required Critical quantification near regulatory limits Semi-quantitative
LFT/FTI	Rapid No clean up No expensive equipment Easy to use No specific training required	Semi-quantitative Cross-reactivity with related mycotoxin Validation required for additional matrices
FPIA	Simple and fast (5-10min) No clean up required Validated for DON in wheat	Inconsistent with ELISA or HPLC analysis Poor sensitivity Cross reactivity with related mycotoxins

Biosensor	Rapid No clean up procedure	Extract clean-up needed to improve sensitivity Cross-reactivity with related mycotoxins No labeling detection
TLC	Simple, expensive, rapid Can be used for screening Simultaneous analyses of multiple mycotoxins	Poor precision and precision Adequate separation may require two dimension analysis Quantitative only when used with a densitometer
GC	Simultaneous analyses of multiple mycotoxins Good sensitivity Option of auto sample Provides confirmation (MS detector)	Expensive Specialist expertise required Derivatization required Matrix interference problems Non-linear calibration curve Drifting response Carry-over effects from previous samples Variation in reproducibility and repeatability
HPLC	Good sensitivity, selectivity, repeatability, option of auto sample Short analysis times Official methods available	Expensive Specialist expertise required May be derivatization is required
LC	Simultaneous analysis of multiple mycotoxins Good sensitivity Provides confirmation No derivatization required	Very expensive Specialist expertise requested Sensitivity relies on ionization technique Matrix assisted calibration curve
CE	Rapid, Limited organic solvent use, Good resolution of analytes from interfering substances and sensitivity	Expensive equipment Alternative to HPLC Clean-up may be required
Spectroscopy	Rapid Non-destructive measure No extraction or clean up	Expensive equipment Calibration model must be validated Poor sensitivity

2.8 Optical detection

Optical detection offers the largest number of possible subcategories due to optical biosensors can be used with many different types of spectroscopies (e.g., absorption, fluorescence, phosphorescence, Raman, surface-enhanced Raman scattering (SERS), refraction, dispersion spectrometry) to measure different spectra-chemical properties of target species such as [15]:

- Amplitude is the most commonly measured parameter of the electromagnetic spectrum because it can generally be correlated with the concentration of the analyte of interest.

- The energy of the electromagnetic radiation measured can provide information about changes just as molecular vibrations (i.e., Raman or infrared absorption spectroscopies) or the formation of new energy levels.
- Polarization of emitted light is usually random when emitted from a free molecule in solution; however, when a molecule becomes bound to a fixed surface, the emitted light often remains polarized.
- The decay time of a specific emission signal (i.e., fluorescence or phosphorescence) can also be used to gain information about molecular interactions because these decay times are highly dependent upon the excited state of the molecules and their local molecular environment.
- The phase of the emitted radiation, when electromagnetic radiation interacts with a surface, the speed or phase of that radiation is altered, based on the refractive index of the medium (analyte). When the medium changes via binding of an analyte, the refractive index may change, thus changing the phase of the impinging radiation.

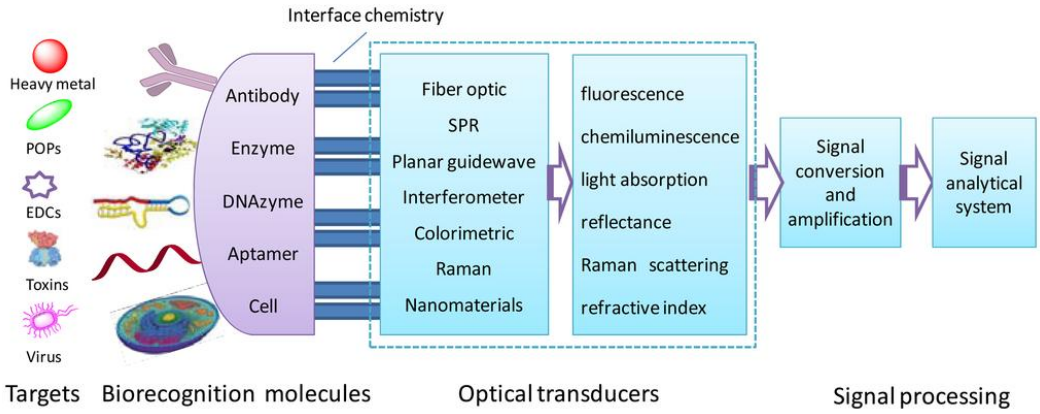

Fig. 11 Schematic of an optical biosensor [88].

Optical biosensors are also known as “optodes”, a scheme is showed in the figure 11, because of their resemblance with electrodes. These include determining changes in light absorption between the reactants and products of a reaction, or measuring the light output by a luminescent process. Optical biosensors integrate optical technique with a biological element to identify chemical or biological species. Several research papers to monitor pesticides, vitamins, carcinogens and toxins based on chemiluminescence and fluorescence has been

published [85]. The advantages and disadvantages of the optical sensors are mentioned in the table 8. A classification of the optical sensors, considering different aspects is presented in the figure 12 [89].

Table 8. Advantages and disadvantages of optical sensors.

Advantages	Disadvantages
No require a reference signal	Interference with the light
Allowing analyses to remote detection	Photo-decomposition of the material employed
An optic fiber is able to transmit several information besides to analyses different analytes at the same time	A limit number of reversible reactions
Allowing miniaturization, flexibility of the fiber optic	Narrow intervals of application
No destroy the analyte	The accessories are not standardized, optimized or commercials
Replaceable components	

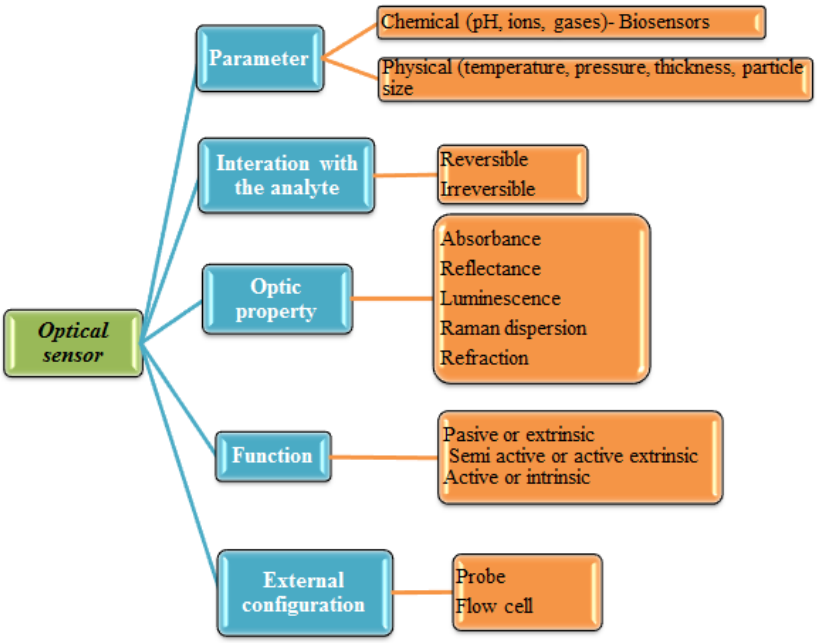

Fig. 12 General classification of an optical sensor.

In order to keep time of analysis low and costs at a minimum, new analytical technologies are incorporated such as the use of biosensors or optical techniques [90] to detect or quantified OTA. Yuan et al developed a rapid and highly sensitive surface plasmon resonance (SPR) assay of OTA using Au nanoparticles for signal enhancement on a mixed

self-assembled monolayer (mSAM) surface. The LODs obtained for OTA in oats and corn were 0.3 and 0.5 ng/g, respectively, while in wine and other beverages, LODs ranged from 0.058 to 0.4 ng/mL [91].

Ngundi et al reported the development of a rapid and highly sensitive array biosensor for the detection and quantitation of Ochratoxin A. The array biosensor utilizes a competitive immunoassay format; this competition is quantified by measuring the formation of the fluorescent immune-complex on the waveguide surface. The fluorescent signal is inversely proportional to the concentration of OTA in the sample. The limit of detection for OTA in several cereals ranged from 3.8 to 100 ng/g, while in coffee and wine the LOD were 7 and 38 ng/g, respectively [92].

In the past years, several immune-sensor protocols were developed based on the optical waveguide light mode spectroscopy OWLS technique, this technique has been applied to the detection of Aflatoxin and Ochratoxin in both competitive and indirect immunoassays. The sensitive detection range of the competitive detection method was between 0.5 and 10 ng/mL in both cases. After the establishment of the indirect method, barley and wheat flour samples were measured, and the results were in good correlation by those measured by ELISA. Regression coefficient between the two methods for Ochratoxin and Aflatoxin was determined as 0.96 and 0.89, respectively [93].

Array biosensors have been developed using competitive-based immunoassays for the simultaneous detection of multiple mycotoxins, including Ochratoxin A, on a single waveguide surface by imaging the fluorescent pattern onto a CCD (charge coupled device) camera [94]. Immunoassays with colorimetric and fluorometric detection display favorable detection limits and were developed for most of the main groups of mycotoxins, such as OTA [95]. The first dipstick assay was developed by Schneider *et al* for the detection of FB_1 in corn based foods and was reported to have a visual limit of detection of 40–60 ng [96]. De Saeger *et al.* [97] presented limits of detection for Ochratoxin A and T-2 toxin in wheat, rye and corn.

The use of fiber optic allows the remote detection and quantification of several analytes, it has been used since the 70s for the monitoring by optic manner diverse environmental contaminants and this technique requires a radiation source of high intensity and steering capability. The chemical sensors with optic fiber are named Fiber Optical Chemical Sensors (FOCS). Fiber-optic biosensors (FOBS) are optical fiber derived devices

that use optical field to measure biological species such as cells, proteins, and DNA. Due to their efficiency, accuracy, low cost and convenience, FOBS are promising alternatives to traditional immunological methods for biomolecule measurements [98].

Over the past decades or so, the incorporation of optical techniques in the development of chemical sensors and biosensors [99] have been investigated resulting in novel and in the develop of devices with great promise for many areas of applications like the detection and quantification of OTA. Just as the use of fiber optic to detect OTA [100].

Wang et al employed the bioluminescent assay system for evaluating the toxicity of OTA. When OTA concentration fell into the range of 0.1–1.0 μg/L, bioluminescence inhibition followed a linear pattern with a good correlation coefficient (R^2 = 0.944). The calculated recovery percentages fell into the range of 81–102% within the spiking range of 20–200 μg/Kg. This system provided a screening method for the measurement of toxic OTA by monitoring the changes in luminescence [101].

Optical detection is usually based on the measurement of luminescent, fluorescent, colorimetric or other optical signals produced by the interaction of microorganisms with the analytes and correlates the observed optical signal with the concentration of target compounds [102].

2.8.1 Fluorescence of OTA

Fluorescence is one of the most sensitive spectroscopic techniques, its sensitivity makes it uniquely suited for the detection of very low concentrations of bio-analyte. Traditionally, It has been the technique of choice for optical detection of trace level analyte. Fluorescence detection is also suitable for time or phase resolved measurements, yielding additional information from the system of interest [15].

The term Luminescence comes from a Latin root (lumen=light) [103]. It defined as the emission of optical radiation resulting from non-thermal excitation of the energy levels of atoms, molecules, polymers and crystals. Luminescent materials can be classified into several broad groups [104]:

i. Aromatic molecules
ii. Inorganic crystals
iii. Noble gases

iv. Simple inorganic molecules
v. Inorganic ions
vi. Biological molecules
vii. Aliphatic molecules

Depending upon the mechanism it follows, there are different types of luminescence, one of them is the photoluminescence, which is the emission of photon from a material when a photon is absorbed by the material and it is formally divided into two categories, depending on the nature of the excited state, fluorescence and phosphorescence. These techniques involve the optical detection and spectral analysis of light emitted by a substance undergoing a transition from an excited electronic state to a lower electronic state [15]. For a long time the distinction between fluorescence and phosphorescence was based on the duration of emission of light that disappears simultaneously with the end of the excitation: fluorescence, whereas in phosphorescence, the emitted light persists after the end of excitation[103].

Phosphorescence is emission of light from triplet-excited states, in which the electron in the excited orbital has the same spin orientation as the ground-state electron. Transitions to the ground state are forbidden and the emission rates are slow (10^3 to 10^0 s^{-1}), so that phosphorescence lifetimes are typically milliseconds to seconds. The phosphorescence substances glow for several minutes while the excited phosphors slowly return to the ground state. Phosphorescence is usually not seen in fluid solutions at room temperature [105].

Fluorescence is the phenomenon of the emission of a light quantum by a molecule or material after initial electronic excitation in a light-absorption process. After excitation, a molecule resides for some time in the so-called excited state and its fluorescence emission can be observed usually with a lower energy (longer wavelength) than the excitation. The time range of fluorescence emission is 10^{-8} to 10^{-11} s. The latter includes the emission of species excited in the course of chemical reactions (chemiluminescence), biochemical reactions (bioluminescence) or upon oxidation/reduction at an electrode (electro-chemiluminescence) [106]. Also, refers to cold light emission by electron transfer in the single state when molecules are excited by photons. Considered as spontaneous emission of radiation (luminescence) from an excited molecular entity with the formation of a molecular entity of the same spin multiplicity by the IUPAC.

In the figure 13, S_0, S_1, S_2 and T_1 represent ground, first, second singlet excited and triplet states of a luminescent material, respectively. Upon absorption of light by the material, it is excited to higher energy states, S_1 or S_2. If S_1 jumps to S_0, directly the type of photoluminescence is fluorescence. On the other hand, if S_1 jump to S_0 through the triple state, T_1, then it is phosphorescence.

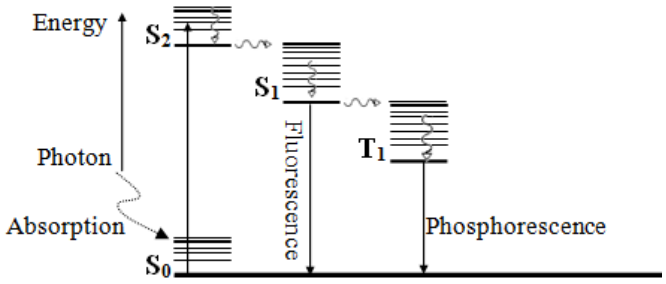

Fig. 13 Jablonski diagram showing fluorescence and phosphorescence.

In order to utilize a fluorescence technique for the analysis of OTA in food and feed stuff, the photo physics of OTA need to be mentioned, specially the influence of pH. Il'ichev et al [107] mentioned that at pH 11, OTA exists in solution as a dianion (deprotonated phenol groups), which has an absorption band that peaks at 380 nm. At pH 6.5, OTA is a monoanion (protonated phenol groups) and dianion. The absorption band of OTA decreases with time and new spectral appears. At pH 6.1 and 10.1, absorption bands centered at ~ 350 and 390nm appear with increased photolysis time. On the other hand, at pH 8 with increasing irradiation time, only a small blue shift is observed in absorption spectra.

Frenette et al, [108] showed a structure–activity relationship for the fluorescence of OTA. Indicated that the protonated phenolic species of OTA absorbs at 332 nm in water at pH<5. The emission spectrum of the protonated phenol peaks at ~460-480 nm and exhibits no overlap with the absorption spectra at 332 nm. They summarized their results for OTA in the table 9. They concluded that the use of excitation (340nm) and emission (465nm) maximum, optimized for OTA might be not suitable for detection of certain OTA metabolites.

Table 9 Photo physical data for OTA.

Data	$CHCl_3$	MeCN	MeOH	H_2O
Absorption λmax (nm)	332	330	330	344/379
Emission λmax (nm)	471	469	469	447
Quantum yield	0.30	0.34	0.26	0.39/0.49
Stokes shift (cm^{-1})	8889	8981	8981	6698

*$CHCl_3$: Chloroform; MeCN:Acetonitrile; MeOH: Methanol; H_2O:Water

Hashemi et al indicate that fluorescence spectra obtained exciting OTA solutions at 330 nm exhibit broad peaks at 460 nm with a shoulder at lower wavelengths, that practically overlap and that are attributable to neutral and monoanionic and dianionic forms, respectively. Specifically the fluorescence spectra for both dianionic and monoanionic species show same peaks at around 450 nm attributed to toxin enol form. Under alkaline conditions, a shift of the excitation maximum of OTA occurs from 330 to 380 nm associated with an increased emission signal at 453 nm. In all methods using fluorescence for determination of OTA, sensitivity can be greatly improved by using alkaline conditions [16]. The table 10 shows their results obtained for determination of fluorescence sensitivity of OTA in four solvents at two excitation-emission maxima. Besides, they proposed the addition of NaOH to methanol and The OTA solutions will change to the dianion form that has more intense spectrum.

Table 10 Fluorescence sensitivity of OTA in different media.

Solvent	λ_{ex}(max)	λ_{em}(max)	Fluorescence sensitivity (count/nM)
Water (pH 7)	336 385	456 446	2.8 0.6
Water (pH 11)	385 336	446 464	5.3 2.5
Methanol	376	432	5.6
Methanol (basic)	376	432	6.8
Acetonitrile	340 374	420 432	2.9 2.8
Chloroform	344 374	410 428	2.4 2.2

Steinbrück et al, obtained that at pH<4.5, the longest wavelength absorption maximum is located at λ_{abs} (max) = 333 nm. At pH>4.5 a second maximum starts to evolve at λ_{abs} (max) = 380 nm. At high pH only the latter absorption maximum in found. At pH<1 the fluorescence maximum is located at λ_{em} (max) = 470 nm and is blue-shifted with increasing pH λ_{ex} (max) = 440nm. Finally, suggests to use two-wavelength excitation/detection scheme with the two λ_{ex}/ λ_{em} pairs 330nm/>470 nm and 380 nm/ 440 nm [109].

It is widely known that the UV absorption spectrum of OTA varies depending on the pH and polarity of the solvent as show the table 11[10].The UV or visible radiation is absorbed by a molecule when the frequency of the light is at the correct energy to cause the electrons of the molecule to rearrange (or become excited) to another, higher energy, state of the system [110].

Table 11 Spectral characteristics of Ochratoxin A.

Spectral	**Solvent**	**Characteristics**
UV-VIS	Ethanol	λmax = 213 nm
		λmax = 333 nm
Fluorescence	Ethanol 96%	λmax = 467 nm
	Ethanol-Absorbance	λmax = 428 nm

Fluorescent methods have been extensively developed for analytical purposes due to their specificity and sensitivity, this phenomenon is presented when the electronic excitation of molecule occurs as the results of the absorption of near ultraviolet or visible light. Methods based on fluorescence are the most common for the study and determination of mycotoxins (OTA) [16]. Frequently, using chromatography methods [56,111-116], nowadays, the detection of OTA based the development of biosensor is widely researched.

Nuo et al developed an aptamer based on fluorescence assay for Ochratoxin A, it was established based on the aptamer recognition and fluorescent probe technology. Under the optimal conditions, the linear range for the OTA concentration detection is 2.0×10^{-8} to 1.0×10^{-5} g/L with a detection limit of 1×10^{-8} g/L. The RSD is 2.6% for eleven parallel measurements of 1×10^{-6} g/L OTA [117].

Because ssDNA aptamer has the ability to form a double-strand structure with its complementary sequence, a simple and rapid aptamer-based label-free approach for highly sensitive and selective fluorescence detection of OTA was developed by using ultra-sensitive double-strand DNA specific dyes PicoGreen. The results showed that as low as 1 ng/mL of OTA could be detected with a dynamic range of more than 5 orders of magnitude which satisfies the requirements for OTA maximum residue limit in various food regulated by European Commission [118].

2.8.2 Optoelectronics

These are the application of electronics devices as source, detection and control light to produce low-cost instruments for measurement in medicine, biotechnology or environmental monitoring. Considering that any optical device that utilizes spectroscopic techniques contains four basic modules: light source, light detector, wavelength selection devices and a signal processing unit, therefore the main spectroscopic techniques can be used with optoelectronics. Recent developments in semiconductor technology and especially in optoelectronics enable very low-cost read out devices, which can detect changes in a very small volume [119].

The most widely used light source was a glow lamp due to its range continuous emission spectrum (UV to IR), but its low power efficiency, low mechanical stability and it is complicate to use it. Another choice is a laser, a bulky and expensive device, which requires laboratory conditions for operation and is inefficient in power utilization. The development of optoelectronics has resulted in the appearance of several economical types of semiconductor light sources such as LEDs [89], laser diodes (LDs). Currently available LEDs cover the entire visible, a part of IR and UV spectrum.

Photodiodes (PD) are the preferred detectors for low cost devices, can operate at high light levels without degradation, depending on the semiconductor material, their spectral response varies from 180 to 2600 nm and their output signal is usually small so it requires additional amplifier. Diode arrays and CCDs are used in spectroscopy. An avalanche photodiode (APD) is quite similar to a normal photodiode and they can tolerate intense illumination, their sensitivity is comparable with some photomultiplier tube (PMT). A PMT is the last option for photodetector where its sensitivity, speed and minimum noise are the

primary requirement for the system but the drawbacks of the PMT include the need for a high-voltage power and its expensive cost.

Some applications of the optoelectronics device are mentioned below. Absorbance measurements or photometric transducers for molecular absorption spectroscopy based on LEDs have been reported [120- 124] as well as LEDs as light sources in devices to provide a small portable sensor for the measurement or detection of different compounds [125] such as metals, cations, anions [126] or aromatic hydrocarbons [127].

There are different use of LED along with fluorescence applications [128- 130] beside the use of UV-LEDs as source such as Belz et al that evaluated the optical performance of these LEDs in UV light delivery system. They showed that UV 365nm LEDs could be coupled into plastic optical fibers for light delivery. Finally, concluded that for specific applications, deuterium and visible light sources and the high quality spectrometer could be replaced by UV or visible LEDs of similar performance in a wavelength range defined [131].

An inexpensive and portable pulsed LED source with variable repetition rate up to 10 MHz suitable for time-resolved fluorescence sensing in medical, environmental and industrial applications was developed by O'Hagan et al the pulses are presented for three LEDs with peak emissions at 525, 560 and 590 nm. The measurement performance is evaluated by the fluorescence lifetime and anisotropy decay of rhodamine 6G in diverse solvents [132].

The use of LEDs to induce fluorescence is widely researches such as Dickens et al that described a compact and portable LED-array based fluorescence sensor for real time monitoring [17] or the development of portable fluorometer for the screening of aflatoxin [18] or for time-resolved luminescence analysis [19].

A flow-through optical absorption detector for HPLC was constructed using a novel deep-UV light-emitting diode as radiation source with a peak emission wavelength of 255 nm. For measuring the transmitted intensity a special UV-sensitive photodiode was employed [133] and for the detection of some mycotoxin, D. Caputo *et al* demonstrated the suitability of amorphous silicon (a-Si:H) photodiodes in detecting Ochratoxin A [134].

The work of Novo et al demonstrated an integrated analytical system that conjugates an indirect competitive enzyme-linked immunosorbent assay strategy developed in PDMS microfluidics with integrated micro fabricated hydrogenated amorphous silicon photodiodes for chemiluminescence detection. A limit of detection of 0.85 ng/mL was obtained for OTA

detection in a PBS solution and for red wine extracts a limit of detection of OTA was 28 ng/mL [135].

2.8.3 Colorimetry

At the beginning, the most quantitative chemical use analytical method but due to the drawbacks other methods are necessary such as colorimetry. One example of an early colorimetric analysis is Nessler's method for ammonia, which was first proposed in 1856. Nessler found that adding an alkaline solution of HgI_2 and KI to a dilute solution of ammonia produced a yellow to reddish brown colloid with the color determined by the concentration of ammonia [136].

Colorimetry, in which a sample absorbs visible light, is one example of a spectroscopic method of analysis. At the end of the nineteenth century, spectroscopy was limited to the absorption, emission, and scattering of visible, ultraviolet and infrared electromagnetic radiation. Colorimetry is used in the color science, photography, printing and graphic communications industries and chemistry, also.

Colorimetry is also a form of analytical chemistry that is used for the identification and determination of concentrations of substances that absorb light. It is similar to spectrophotometry, but is distinguished by its interest in reducing spectra to the physical correlates of color perception [20].

Although, the analytical methods are available for detecting, measuring and/or monitoring with low limits of detection. Its limitations have allowed to emerge new technologies as the developed of optical devices for field measurements that involve the use of LED in ultraviolet or visible spectrum and the use of complementary metal–oxide semiconductor (CMOS) or charge coupled device (CCD) image sensors.

A CMOS image sensor has an imaging area, which consists of an array of pixels, vertical and horizontal access circuitry, readout circuitry, as the figure 14 presents. The imaging area is a two-dimensional array of pixels; each pixel contains a photodetector and some transistors and access circuitry is used to access a pixel and read the signal value in the pixel [137].

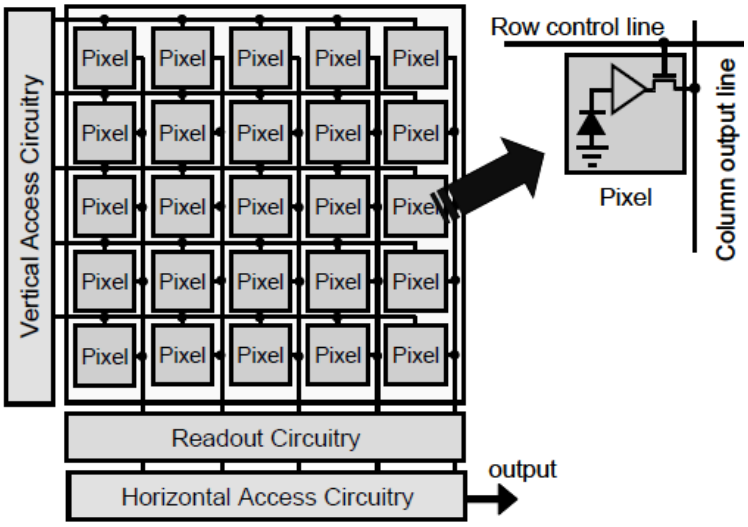

Fig. 14 Architecture of a CMOS image sensor.

CCD is an array of microscopic square-shaped light-sensitive regions arranged in a checkerboard pattern. Tiny light-sensitive squares, usually called pixels (for picture elements) are formed directly in slab silicon. These pixels are so small that they cannot be seen simply by examining the surface of the CCD by eye. These are small, linear in their response to light, stable and low power devices [138].

Evaluating the fluorescence in a pixel image of the sample, the pixels provide information of the light emitted by the sample; these values allow qualitative and quantitative measures. There are different models to work with the information yielded by the pixels, these are: RGB (Red, Green, Blue), HSV (Hue, Saturation, Value), HIS (Hue, Saturation, Intensity), CIELab or CIExyY [139]. One of the most common is RGB color model due to it provides independent values of color channels, is an important index for color expression due to specific and precise value.

Nowadays, there are growing interests to employ the RGB model combined with image sensor or cameras to established a relation with the concentration of analytes, in a colorimetric detection or for its quantification, some examples are the colorimetric sensor array or test strip to semi quantify as NH_3, Hg^{2+}, $Ag^{+,}$ and Cu^{2+} ions [140- 142] also organic [143- 145] and inorganics compounds [146], opiates [147] proteins, glucose, blood cells in urine [148] and amines in water [149].

RGB model is used for field applications as the detection and quantification of sweeteners or sugars [150, 151], toxic industrial chemicals [152] or toxic gases [153] and to

detect the presence of explosives in water, water vapor, air [154] and soil [155] or together other models as Lab [156], besides it can used together an optical sensor array for chemical sensing [157].

Other methods considered as colorimetric is the use of image, for example UV photography to identified aflatoxins such as Yabe et al described at work about aflatoxin monitored in agar medium by UV photography like screening method [158]. The aflatoxin-producing strains appeared as gray or black colonies in the UV photographs, whereas the aflatoxin non-producing strains appeared as white colonies [159].

Other application presented by Hara et al, whom developed a method based on UV detection of aflatoxin diffused into an agar medium. Blue fluorescence in agar surrounding a colony is strongly indicative of aflatoxin-producing capability. However, they made extraction by $CHCl_3$ and identification by TLC for positive identification of aflatoxin [160].

On the other hand, it is important consider the influence of light of the wavelength on growth and biosynthesis of OTA, this work is presented by Schmidt et al, where they highlight that the light of 590 to 530 nm had more a positive than a negative influence on growth or Ochratoxin A biosynthesis compared to the control (dark incubation). The light effect on growth and Ochratoxin A biosynthesis was dependent on the growth medium. The light intensity strongly influences how the fungus reacts. Depending on the intensity and the resistance of the species a complete cessation of growth and/or inhibition of Ochratoxin A biosynthesis could be achieved [161].

The tendency is the use of UV-LED as inductor of fluorescence and image analysis as in the case of Mustafic et al, whom used it to detect sting bug damage in cotton bolls due to damage of cotton bolls can be observed under blue LED-induced fluorescence. Finally they proof of principle that LED-induced fluorescence combined with image analysis can provide an indicator to estimate the levels of stink bug infestation [162].

A non-invasive detection of aflatoxins (AF) using fluorescence and multispectral imaging was developed by Kalkan et al [174] in figs, these were individually investigated to measure their fluorescence level, surface mould concentration and AF levels and noted a strong correlation between mould concentration and bright greenish yellow fluorescence (BGYF)-AF and BGYF-surface. In addition to a pairwise correlation, a machine-vision and machine-learning approach to detect the AF-contaminated figs using their multispectral

images under UV light was proposed. The figs were classified in two different approaches considering their surface mould and AF level with error rates of 9.38% and 11.98%, respectively.

CHAPTER III

METHODOLOGY OF THE STUDY

In this chapter, the proposed solution for this thesis will be explained. The chapter III is divided into three sections: **Section A** corresponds to the use of emitter and photodiodes to try to detect OTA. **Section B** describes the use of CMOS sensors used in cameras for the detection and quantification of OTA through its RGB components. Eventually **section C** refers to image processing for real samples contaminated with OTA, which have not been used with extraction columns.

The first project consisted to detect OTA in food matrices; the objective of the work was the development of an automated flow-based electrochemical aptasensor for on-line detection of OTA employing direct and indirect competitive strategies. Then reagents, solutions and methodology described as follow [4, 163]:

First, the SPCE system or screen-printed carbon electrodes consisted of three electrodes: a working and an auxiliary electrode in graphite and Ag/AgCl as a reference electrode represented in the figure 15. The working electrode was a 4-mm diameter disk, the auxiliary electrode was a 16 mm × 1.5 mm curved line and the Ag/AgCl pseudo-reference electrode was a 5 mm × 1.5 mm straight line.

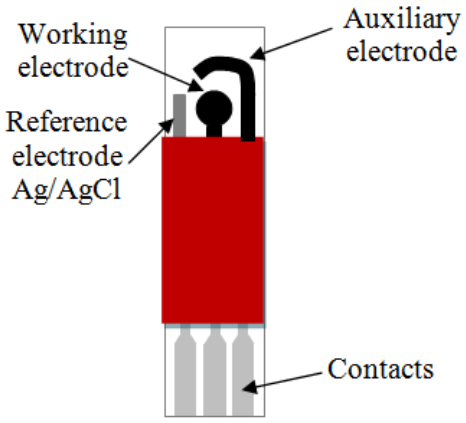

Fig. 15 Representation of the screen-printed carbon electrode.

The fabrication of the electrode comprises to overlay various layers on a solid support in transparent PVC using a DEK 248 screen-printing machine. The printing is carried out by passing the paste with the support of a scraper through the size of the mesh determined by a sieve synthetic (polyester) or metal (stainless steel). The paste deposited uniformly on the surface placed on the movable table of the screen-printing machine.

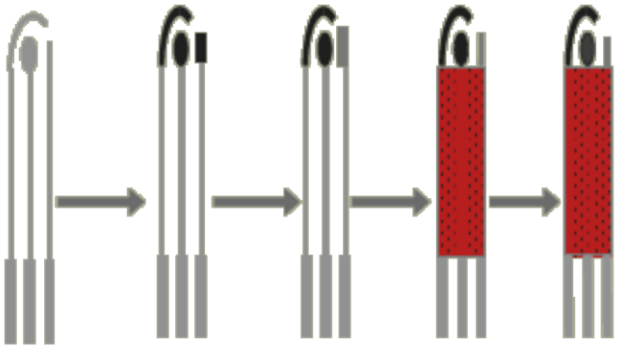

Fig. 16 Stages of the fabrication of SPCE.

The different stages of production are presented in the figure 16, between every stage, the electrodes were dry to 60 ºC during 30 minutes and the stages are described as follow:

1) Apply a layer of silver conductive.

2) Apply a layer of carbon, which cover the superior part of the electrodes and allow the adhesion of the next layers.

3) Apply the Ag/AgCl paste over the site of the reference electrode.

4) Apply an insulating layer between the electrodes and the contacts.

5) Finally, apply on the working electrode a paste of graphite with a mediator.

The reagents employed were:

- 5'-amino-modified DNA oligonucleotide with a C6 spacer arm (sequence 5'-GAT-CGG-GTG-TGG-GTG-GCG-TAA-AGG-GAGCAT-CGG-ACA-3')
- Ochratoxin A from Aspergillus ochraceus
- Phosphate buffer (PBS) was prepared with 8g de NaCl, 0.2g de KH_2PO_4, 1.13 g de Na_2HPO_4 and 0.2g KCl in one liter of distilled water.
- Binding buffer (BB) required PBS 1x and 1Mm $MgCl_2$
- MES buffer 25mM employed 2-(N-morpholino)ethanesulfonic acid

- Tris-Tween buffer (TT)
- Tris-EDTA buffer (TE)
- Bovine Serum Albumin (BSA)
- Diethanolamine (DEA)
- 1-naphthyl phosphate (1-NP)
- *N*- hydroxysuccinimide (NHS)
- *N*-(3-dimethylaminopropyle)-*N*,-ethylecarbodiimide hydrochloride (EDC)
- EZ-link amine-PEO3-biotin
- Alkaline phosphatase avidin (avidin–ALP) conjugate
- Ochratoxin B (OTB) derived from A. ochraceus
- Magnetic beads (MBs) coated with carboxylic or amine group and single magnet position adapted for 1.5 mL micro tubes.

Preparation of biotinylated OTA

The carboxylic group of OTA was activated with EDC/NHS as follow: 400 µL of a solution 34 mM EDC and NHS were added drop by drop to 200 µL of a solution 2.5 mg/mL OTA prepared in 0.1 M MES buffer at pH 5.5. OTA-NHS-EDC mixture was stirred one hour at room temperature. After, 250 µL of 50 nM of EZ-link amine-PEO3-biotin were added to the mixture and was stirred 24 hours at room temperature. The conjugate was dialyzed at 4 ºC consecutively in carbonate buffer and distilled water.

Modification of carboxylic magnetic beads with amino aptamer

The magnetic beads are considered as a support of the immobilization of the biosensor, in this case of the aptamer, 500 nM of the 5'amino-modified aptamer was prepared in binding buffer was heated at 94 ºC for 5 min and allowed to stand at room temperature for 20 min. Then, the OTA-aptamer was immobilized on carboxyl MBs using Invitrogen protocol. Briefly, after washing 2 times with 25 mM MES buffer, MBs were incubated for 30 min with the aptamer at room temperature.

Then, carbodiimide EDC was incubated with the mixture overnight at room temperature under mild agitation to activate carboxyl group of the magnetic beads. Afterwards, the MBs were washed with 1 mL of TT buffer 3 times (each round incubated for

30 min); the incubation of MBs with TT buffer was used for washing and blocking the non-reacted carboxylic groups. The modified MBs were suspended in TE buffer and stored at 4 ºC. Control MBs were prepared following the same procedure without addition of aptamer solution.

Modification of amine magnetic beads with OTA

After washed with PBS, 75 µl of MBs was incubated with 100 µl of OTA (1 mg/mL) and EDC/NHS overnight. The reaction was stopped with glycine 30 mM and the non-bound residues were washed three times with PBS. The modified MBs were suspended in 100 µL of PBS and stored at 4 ºC.

Prior to use in flow-based aptasensor, SPCEs were subjected to electrochemical pretreatment by five cyclic potential scans between 1.0 and −1.5 V in 0.5 M H_2SO_4 in Auto lab PGSTAT12 potentiostat.

Flow-based direct competitive aptasensor

The SPCEs were blocked with BSA 2% for 1 h at room temperature to prevent non-specific adsorption. The electrode was introduced into a flow cell connected to the potentiostat. A solution of 2 µL of aptamer modified MBs diluted in binding buffer was injected onto the electrode surface.

The competition step was performed by passing different concentrations of OTA prepared in buffer solution or real sample with OTA–biotin. Afterwards, a solution of avidin–ALP was passed over the SPCE surface to perform avidin–biotin reaction. Special sequences were used to inject and incubate the competition mixture and avidin–ALP, the incubation time was 10 min for each step.

Finally, 1-NP solution prepared in DEA buffer at pH 9.5 was passed onto the aptasensor. The signal generation was based on the dephosphorylation of non-electroactive 1-NP by ALP, followed by the oxidation of electroactive 1-naphtol to 1-iminoquinone on the electrode surface. Washing was performed by passing a PBS-tween (0.05%) solution automatically after each step.

Flow-based indirect competitive aptasensor

First, the non-specific sites on the SPCE surface were blocked with 100 µL of BSA 2% for 1 h at room temperature. Then 4 µL of OTA modified MBs diluted in binding buffer was injected onto the SPCE surface. The second step consisted of passing 150 nM of biotinylated aptamer with free OTA in buffer solution or real sample. Therefore, OTA present in food samples competed with the immobilized OTA on the MBs. After, a solution of avidin–ALP was bound to the biotinylated aptamer. The electrochemical detection was carried out in the similar way as described for the flow-based direct competitive aptasensor.

Amperometric detection of OTA

The measurement of the activity of ALP, the enzyme that labeled the OTA or the aptamer was carried out by amperometry; the amperometric measurements were performed using the data acquisition card (PMD1208FS), which connected the potentiostat Polarostat type PRGE, Tacussel electronique with the computer for the acquisition of the signal.

The substrate ALP (1-NP) was injected on the aptasensor in the flow cell connected to the potentiostat. After incubation of the substrate for 6 minutes, a potential of 200 mV was applied. This potential corresponds to the oxidation potential of the product 1-naphthol 1-iminoquinone.

The signal obtained is proportional to the enzymatic activity of ALP. It is therefore proportional to the amount of OTA in the case of the direct competitive aptasensor and inversely proportional to the amount of OTA in the case of indirect competitive assay.

Preparation of beer samples

The beer samples were spiked with the known concentration of stock solution of OTA. Then, the spiked samples, previously cooled at 4 ºC for 30 min to prevent rapid foam formation were degassed by sonication for 1 h. The pH of beer was then adjusted to 7.4. Finally, the spiked beer was passed through a filter (0.45 mm). The dechlorinated analog of OTA, Ochratoxin B (OTB) was used as non-specific analyte to test the specificity of the flow-based aptasensor.

Automated flow system

The automated flow system employed in this work consisted of a custom flow cell, which was made of polymethyl methacrylate. The flow cell contained a chamber used to hold the SPCE into the flow system. The flow system was provided with a bidirectional syringe pump. The flow system comprised a 200 µL holding coil between syringe pump and flow chamber to prevent the contamination within the flow cell. The inlet and outlet for carrying solutions were bent downward at the entrance of the flow chamber to facilitate a better flow of reagents over the SPCE surface.

A flow through-cell with 4 mm diameter magnet on the central chamber was used to immobilize the MBs over the electrode surface. In the flow system, all the parameters such as incubation time, washing step, pumping, injection and suction volumes, stopping the flow, signal measurements and saving the obtained signals, were automatically controlled by a graphical custom interface developed in LabVIEW 8.5.

The reagents were provided through control of a bidirectional syringe pump (Cavro XLP6000) with four valves. The valve 1 (V1) was used to inject magnetic beads, aptamer and OTA, washing was performed through V2 and V3 was used for the injection of the substrate of ALP while waste was discarded by V4.

It is noteworthy that all the system was automatically programmed. Perform each stage with preloaded automated sequences. Besides this, the program allowed the modification of different parameters such as speeds, incubation times and volumes aspirated or injected and valves through which the process took place, a schematic diagram is presented in the figure 17.

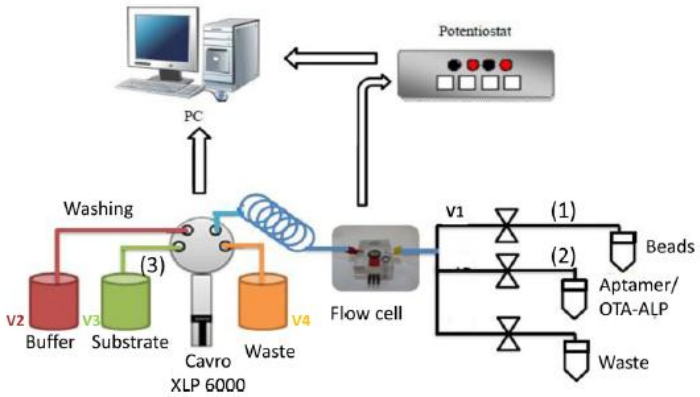

Fig. 17 Schematic diagram of the automated flow system.

PART A

Absorbance based on LED and photodetectors

The light intensity (the number of photons observed per unit time) can be measured by sensitive devices with excellent accuracy. The light coming from a source may be either be transmitted through or reflected back from the sample. The output signal can be further amplified using conventional electronic circuitry without adding significant noise. These are an option for application where less precise measurements are required. Silicon photodiode are also less expensive, more rugged than photomultiplier tubes for example and more useful for portable instrumentation.

There are four basic operational principles for biosensors using optical technology: absorption and reflection spectroscopy, chemiluminescence, fluorescence and phosphorescence. In absorption spectroscopy, the Lambert-Beer Law is used to characterize the intensity of transmitted light (I) through a uniform medium as function of the incident light (I_0) when the optical properties are affected by the chemical concentration (C). The intensity is given by: $I = I_0 e^{-\epsilon C \Delta x}$

Where ϵ is the extinction coefficient and Δx is the thickness of the medium. The optical density of the medium, defined as $O.D. = In\left(\frac{I_0}{I}\right)$ can change as the concentration of different chemical species in the medium. A spectrum of light will be absorbed in some range of wavelengths, which would be distinct for each chemical species [164]. The table 12 summarized some works about the use of photodiodes or LEDs as detectors and LEDs as emitters.

Table 12 Examples of applications of LEDs or photodetectors.

Detection	**LOD**	**Emitter**	**Detector**	**Reference**
Aflatoxin	<25 ppt	UV-LED at 365nm	P25232 PMT	[18]
Tetracycline	0.025 ppb	Xenon lamp	R928 Hamamatsu PMT (photomultiplier tube)	[19]
OTA in PBS	0.85 ng/mL	UV light	Thin film hydrogenated amorphous silicon photodiode	[135]
Quinine	----------	LED	Blue and red LED	[165]
Fluorescein	5nM	Blue LED	H5748 Hamamatsu PMT	[166]
Poison and microbial contamination	----------	UV-LED at 365nm	Red LED	[167]
pH	----------	Orange LED	LED	[168]

The photodiodes generate a small electrical current, generally linear with respect to the intensity of light; it is the photovoltaic mode operation. The photoconductive mode, in which a voltage is applied through a diode inversely connected in series with a resistor. While this mode offers a much faster response to light that, the photovoltaic mode is less sensitive.

In a phototransistor, the amount of light registered as a signal modulated on the basis greater current flowing between the collector and emitter, amplifying a very small signal. Phototransistors capture a greater amount of light and must be used according to the proper polarity [169].

3.1 Photodetectors to detect pesticide

Accordingly, a proposed system consists of a LED as a source of light and a photo detector, a data acquisition board and a computer, it was used to detect the thiocoline after the hydrolysis of substrates acetylthiocholine (ACTh) by acetyl-cholinesterase. Measuring the relation between the amount of light transmitted through and absorbed by the enzymatic reaction in three different enzymes (Electric Eel, *Drosophila melanogaster* and Genetically-modified *D. melanogaster*) toward paraoxon, carbofuran and malaoxon pesticides [21].

3.1.1 Reagents and materials

AChE (EC 3.1.1.7, type V-S, 1000 U/mg) from electrical eel (EE) was purchased from Sigma-Aldrich (Switzerland) and *Drosophila melanogaster* AChE mutants, B131 and B394, were provided by PBS (Toulouse, France). Acetylthiocholine iodide (ATChI), 5,5'-dithiobis-2-nitrobenzoic acid (DTNB) and crystallized chicken Albumin were supplied by Sigma-Aldrich (Switzerland). Stock solutions of enzymes and DTNB were prepared in 0.1M phosphate buffer (Na_2HPO_4/KH_2PO_4 in one liter of distilled water, Sigma-Aldrich, Switzerland) at pH 7. ATChI solution was prepared daily in a 0.9% NaCl (Sigma-Aldrich, Switzerland) solution. Paraoxon, Malaoxon and Carbofuran were purchased from Dr. Ehrenstorfer (Augsburg, Germany). Pesticide stock solutions were prepared in acetonitrile (Carlo Erba Reagenti, Italy) and working pesticide solutions were prepared daily in 0.1 M phosphate buffer by dilution from the stock solution. All the reagents were kept in a freezer at 4 ºC.

Spectrophotometric cuvettes were purchased from Ratiolab (Germany). Spectrophotometric measurements were performed using the Hewlett-Packard diode array model 8452A spectrophotometer. Electronic components, LEDs and photo detectors were supplied by Farnell element14 and Mouser electronics (France). Optical measurements were performed with the developed system and an acquisition card was used in the combination to LabVIEW.

3.1.2 Optical design

The develop system comprises three stages:

- Source: the power supply of the developed system consists of battery with a potential divider to obtain 5VDC to 450mA, it is stable and with minimum current variations.
- Optical detection: the emitter is a blue GaN (gallium nitride) LED, its size is 5mm in a wavelength range 400 to 450nm; the photo detector (wavelength range 400 to 1100nm) of 5mm, consist of NPN silicon phototransistor molded in dark blue epoxy packages; both are through-hole. The electronic circuitry used for conditioning the signal from the LED is a stage of amplification non-inverting that operated with a low power dual operational amplifier and high gain, design to operate with a single power supply, in package SOIC to reduce space.
- Interface and data acquisition: the interface used in the developed system facility the acquisition of the data generated by the changes in the voltage of the photo detector, allows a first analysis of the data and save them. It is easy to use. A graphical user interface was made in Lab VIEW 8.5 and an acquisition card was used.

The circuit was designed in an electrolytic plate with dimensions of 30x60 mm, it permitted to reduce the noise in the signal and avoid interference's sources to the signal. The components decreased the noise in the signal for that reason was no necessary to filter it. The cell was made of black poly methyl methacrylate material, with a chamber to insert the cuvette; the plastic cuvette is for photometric measurements even in the UV range and applicable wavelength range 220 to 900 nm with outer dimensions 12.5x12.5x45 mm, two holes were drilled into black poly methyl methacrylate cell, within a distance of 13.5 mm at 180°, to put the emitter and detector.

3.1.3 Basic principle

When a semiconductor junction is exposed to light, the photons generate hole–electron pairs. These charges diffuse across the junction, they produce photocurrent keeping a relation with the voltage at the output of the operational amplifier and the voltage is recorded. In the developed system: the light strikes the sample in the cuvette, where the reaction between the enzymatic reaction product (thiocholine) and DTNB (5,5'-Dithiobis-2-Nitrobenzoic acid) produce a yellow color, the intensity of this color is measured by the photo detector in units of voltage which is correlated to units of absorbance by the developed system (figure 18). The intensity of the color is proportional to the total enzyme activity but when the enzyme is partially inhibited (by a pesticide), the intensity of the color is also modified. Therefore, this behavior brings the opportunity to correlate the intensity of the color and the pesticide concentrations.

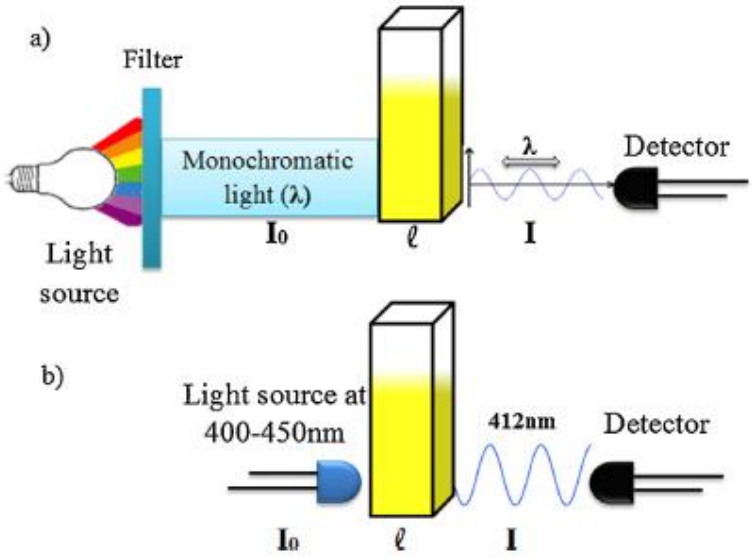

Fig. 18 (a) Schematic of the basic spectrophotometric principle. (b) Schematic of the spectrophotometric principle used in the developed system.

3.1.4 Methodology

3.1.4.1 Spectrophotometric determination of enzyme activities and inhibition constants

The determination of AChE activity and kinetic parameters of inhibition were performed by spectrophotometric measurements with the Hewlett Packard diode array model 8451A spectrophotometer.

3.1.4.2 Determination of acetylcholinesterase activity (AChE).

The determination of enzymatic activity was measured spectrophotometrically by monitoring at 412 nm, according to the Ellman method [22], the appearance of thio nitro benzoate that results from the reaction of DTNB with thiocholine, the product of the enzymatic hydrolysis of acetylthiocholine substrate, according to the following chemical reaction:

$$\text{Acetylthicholine} \xrightarrow{\text{AChE}} \text{thicholine} + CH_3COOH$$

$$\downarrow DTNB$$

$$\text{thiocholine} - \text{thionitrobenzoate disulfide} + \text{thiobenzoate(yellow color)}$$

The principle of the Ellman method is accomplished by the continuous reaction of the thiol with 5:5-dithiobis.2.nitrobenzoate ion (I)[5] to produce the yellow anion of the 5-thio-2-nitro-benzoic acid (II). The rate of colored compound (thionitrobenzoate, yellow color) is measured at 412 nm [23]. The assay was performed as follows:

- Blank, 600µL of phosphate buffer, 300 µL of 2.5 mM DTNB, 100 µL of 10 mM ATChI.
- Enzyme solution, 590µL of phosphate buffer, 300 µL of 2.5 mM DTNB, 100 µL of 10 mM ATChI and 10 µL of enzyme solution was added.

An absorbance versus time curve was obtained, its slope recorded and then enzymatic activity, expressed in voltages units.

3.1.4.3 Determination of inhibition constants (*Ki*)

The procedure used for the determination of inhibition constants was described by Nunes et al [24]. It was adapted from the methodology developed by Segel [25]. The enzymes

were incubated for different time with diverse pesticide concentrations and the pesticide-enzyme activity was determined according to the Ellman method. The mechanism of AChE inhibition by organophosphorus compounds was described by Istamboulie et al [170].

Assays for the determination of inhibition constants, solutions of paraoxon, carbofuran and malaoxon were prepared a different concentrations: 100 µL from enzyme-pesticide solution were taken at fixed time intervals (1, 3, 5, 7, 10 and 15 minutes) and added to the spectrophotometric cuvette containing 300 µL of 25 mM DTNB, 100 µL of 10 mM ATChI and 500 µL of phosphate buffer, the assay was incubated at 30°C in a temperature controlled. Parallel assays, the control was carried out. It consisted of 100 µL of enzymatic solution added 900 µL of phosphate buffer, it was considered as V_0. The process was repeated three times for the enzymes and pesticides.

Then the enzyme-pesticide activity was recorded and the slope of the plot absorbance versus time was obtained. The rate of a reaction is proportional to the concentration of product present. Therefore, it is represented in figure 19(a) [171, 172]. Considering that, the most important and insightful of enzyme kinetic behavior is the original velocity versus concentration, represented as a linear relation. At increasing concentrations of inhibitor [P], the transformed velocity versus [Concentration] for no inhibited and inhibited reactions display the classical pattern of uncompetitive inhibition, diagnosed as parallel plot on this linear plot for reactions inhibited by increasing levels of [P]. This data set would be used to estimate *Ki* as a kinetic characterization of the inhibited enzyme reaction.

3.1.4.4 Optical determination of enzyme activities and inhibition constants

For the determination of AChE activities and inhibition constants were carried out with the developed system, assays were same as described in the section 3.1.4.1, spectrophotometric determination of enzyme activities and inhibition constants.

First, the acetylcholinesterase activity was determined and compared with the commercial equipment. In this case, the Ellman method was prepared for the blank, enzymatic mother solution to $2*10^{-2}$ AU/sec, and the mother solution was diluted of 10 to 0.08 mg/ml of enzyme solution, to establish the limits of detection for the developed and commercial spectrophotometer. To calculate *Ki* in the presence of enzyme–pesticide solution, the slope and the signal was recorded with the acquisition card (NI USB6009) and processed on time for

each enzyme and pesticide concentration at different incubation time. Then, the voltage obtained for each concentration of pesticides and enzymes was normalized with the aid of the follow equation 1.

$$\text{Absorbance} = \log\left(\frac{100 * V_{Obtained}}{V_{[P]_0}}\right) \quad \text{.....eq. 1}$$

Where, $V_{Obtained}$ corresponds to the voltage obtained for each measurement, $V_{[P]0}$ is the value of the voltage for the initial concentration for the three enzymes and pesticides and P indicates the pesticide concentration. The data were normalized and the time versus voltage was plotted in the Figure 19a. The reaction constant *Ki* was calculated by linear regression as the inverse of the slope versus the inverse of the Concentration, as shown in the figure 19(b) [170] [171]. The figure 20 summarize the methodology employed for optical and spectroscopy measurements.

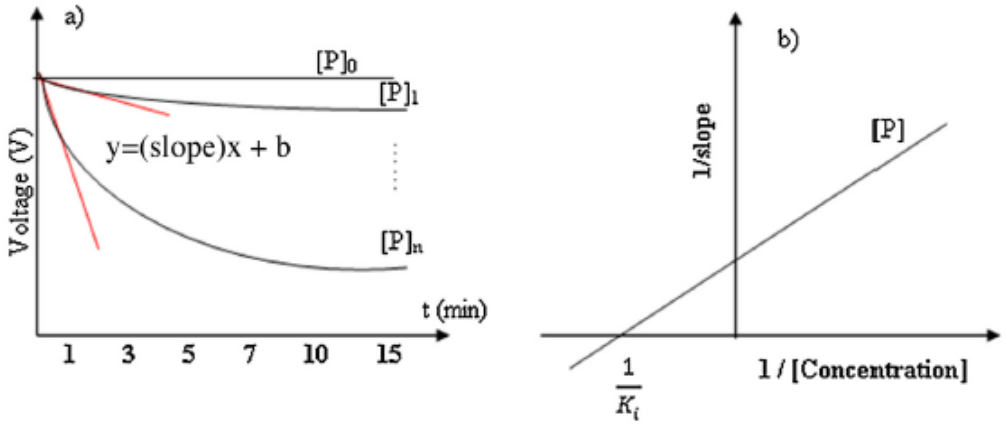

Fig. 19 (a) Changes in pesticide concentration as a function of time. (b) The double reciprocal of [Pesticide] to determine the K_i.

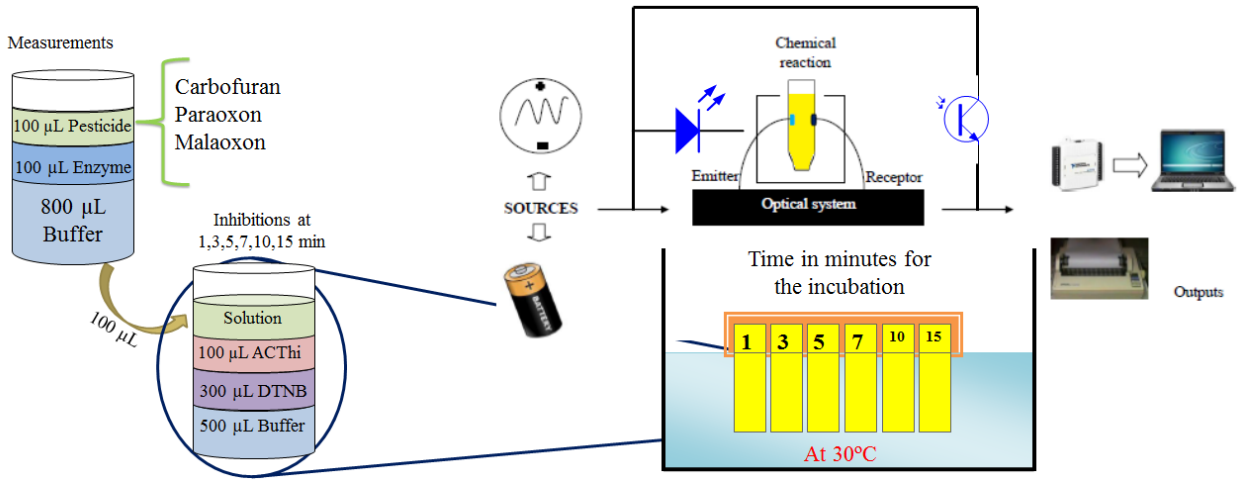

Fig. 20 Description of the optical and spectroscopy measurements.

3.2 UV-LED and photodetectors to detect OTA

Some of the most important characteristics of the photodetectors are their low cost, excellent linearity, good quality, its small size and provides portability, for these reasons, different photodiodes and phototransistors were used to detect OTA excited with UV such as UV absorbance detector [133] for OTA, considering the applications of LED as detector of fluorescence [129] [173] or emitter of UV light, besides to design fluorometric devices [174].

In finding the best photodetector for detecting OTA using ultraviolet light, datasheets supplied by manufacturers and testing with selected photodiodes they were considered, principally that it work in the wavelength range > 400 nm. First selection of the photodetector was based on the datasheets. Subsequently, it was decided to move to the experimentation using the photodetectors without additional electronics. One of the criteria to be followed in the laboratory tests was to evaluate the response of the photodetector excited with UV light. The UV-LED was placed 1 cm from the photodetector, the first test allowed to dispose of photodetectors whose outputs were unchanged respect to UV light or immediately these were saturated at high luminosity.

Finally, the selected photodetector was BPW85B, which is a silicon NPN phototransistor with high radiant sensitivity in clear, T-1 plastic package. It is sensitive to visible and near infrared radiation. It has high photosensitivity and high radiant sensitivity. The photodetector was connected as the figure 21 shows. The emitter was used with a constant current source, subsequently detailed.

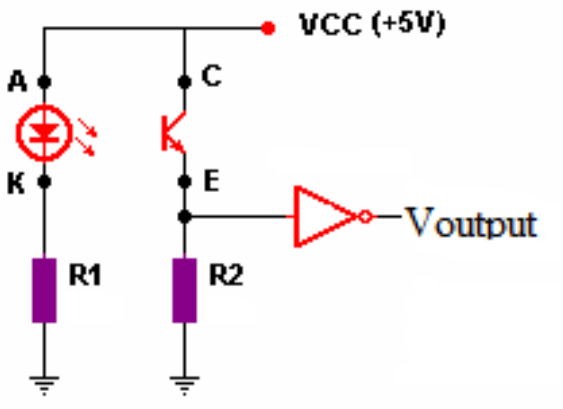

Fig. 21 Basic circuit for the photodetector.

The circuit used a source of 5V and the value of the resistance of 250 Ω provides a current of 20mA. It was tested through a graphical interface designed in LabVIEW 2010 with NI USB6009 as acquisition card. Where the concentration of OTA was established in relation of the voltage generated and this value was acquired by the interface presented in the figure 22. The interface save the data as text file to process later.

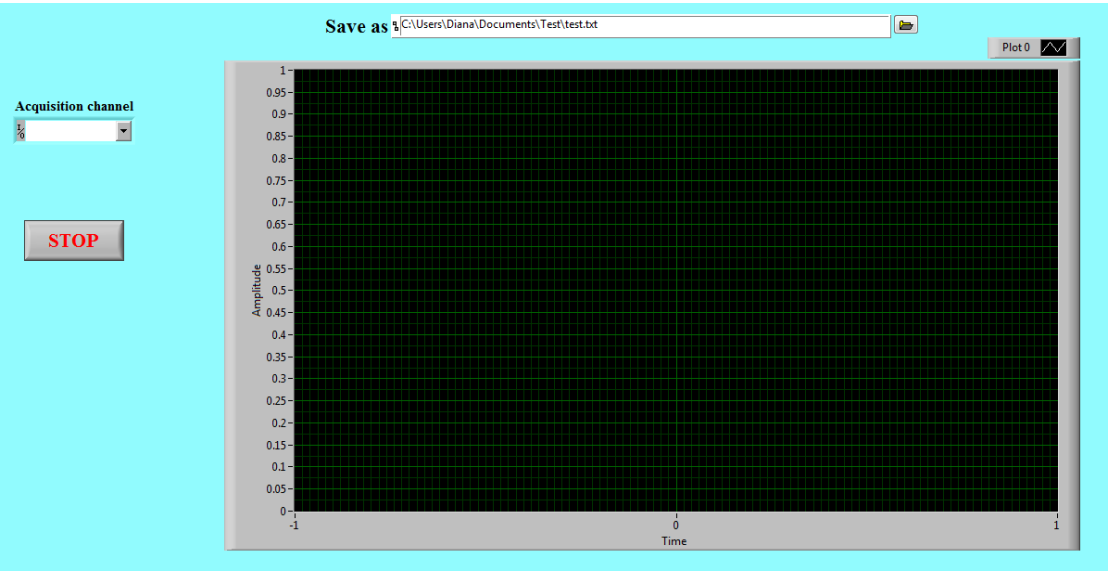

Fig. 22 Interface to evaluate the photodetector.

The methodology was that at different concentrations of OTA (1000 µg/L, 500 µg/L, 250 µg/L and 125 µg/L) were prepared in MeOH and it was the blank. 1.5mL was added in

the cuvette and it was inserted in the chamber, which was built in the 3D printer. The solution was excited with UV-LEDs at 365 or 375 nm and different radiant flux. The signal was acquired with the acquisition card, the interface acquired 3 cycles, each cycle consisted to detect the concentration of OTA in continuous way (more concentrated to less concentrated), this was repeated 2 times more for every UV-LED and all was repeated three times. Five UV-LED were tested, the characteristics of the UV-LEDs employed will be described in the Chapter IV.

PART B

Fluorescence with CMOS sensor

Due to the use of LEDs and photo detectors was no possible to decrease the limit of detection of OTA, other optical method was proposed. Considering the nature fluoresce of OTA, a fluorescence set-up for screening of OTA based on RGB components was developed to detect the OTA in real samples.

An external source of light is required to initiate fluorescence, which occurs in the material excited by the light source, the fluorescent response is assumed to occurred with excitation and the emitted light is also assumed to obey the Lambert-Beer-Law [164].

Fluorescence detection involves (1) an excitation light source (2) a fluorophore (3) wavelength filters and (4) detector that registers emission photons and produces a recordable output, generally an electrical signal [175]. In our case, the developed device is composed of the same elements, these are:

(1) An excitation light source that is specified for the excitation wavelength of OTA, needless the wavelength filters. One of the advantages of fluorescence methods is that, its selectivity can be further enhanced by narrowing the slit width of the emission monochromatic so that only emitted light within a narrow spectral range is measured besides its greater range of linearity [176].

(2) The fluorophore is the own fluorescence of OTA when it is excited by ultraviolet light.

(3) The detector is the camera module controlled by the application software designed.

Considering that a major disadvantage of fluorescence is its fluctuations in pH and temperature, however the pH effect can be eliminated by avoiding the uses of aqueous solvents and normal room temperature fluctuation do not affect the fluorescent intensities [177]. For that reason, the spiked solutions of OTA were prepared in methanol and the real samples were adjusted to pH 7 to maintain the stability in the results. The experiments were done at room temperature. All the solutions were kept in amber bottle to protect them of the light and were store at -18 °C, the methodology for the experiments performed, it described below.

Besides, the position of the camera module and UV-LED was considered due to the usual samples encountered in analytical fluorimetry are liquid solution in non-fluorescent cuvettes, these are viewed using one of the three geometries show in figure 23 [178].

(i) Front-surface viewing of concentrated solutions, where irradiation and viewing occur through the same cuvette face (reflection measurements).

(ii) Right-angle viewing of dilute solutions, where the sample is irradiated and viewed in mutually perpendicular directions through different cuvette faces.

(iii) In-line viewing (absorption measurements), where the fluorescence emission in integrated over the entire width of the cuvette.

The right-angle geometry has the advantage of minimizing stray light and background fluorescence, and is therefore the preferred arrangement in analytical fluorimetry, for that reason was the position selected for this thesis.

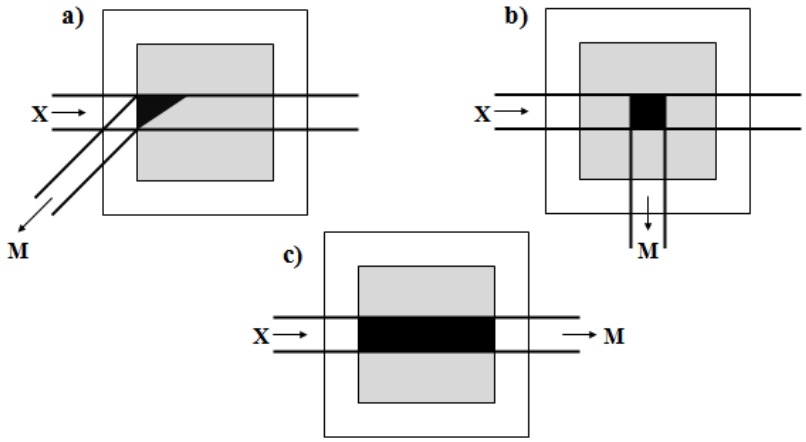

Fig. 23 Viewing geometries in analytical fluorimetry. a) Front-surface; b) Right-angle; c) In-line viewing; X: excitation beam; M: emitted light collected.

3.3 Material and software

Ultraviolet emitter to 360-370 nm from NICHIA Corporation was supplied by Power light systems (Germany). Electronic components were supplied by Farnell Element14 and Mouser Electronics (France). Arduino ® UNO board, a serial port color camera module Link Sprit ® (LS-Y201-Infrared) with CMOS sensor and TTL interface, and iPod connector male style were supplied by Spark fun (Spain). ArduCAM ® and OV5642 sensor were supplied by UCTRONICS (China). An acquisition card from National Instruments NI-USB-6009 together with LabVIEW 2010 ® and the last software employed is MATLAB R2011a®.

3.4 ArduCAM as fluorescence set-up

Design: The device consists of a bracket designed to allocate the ArduCAM camera module, it moves up and down to insert or remove the cuvette into the dark chamber. The

material employed to build the device was black poly methyl methacrylate due to its advantages of impact resistance, hardness, low cost, no electric conductivity as well as its chemical resistance to a vast majority of substances, including acids and alkali solutions such as ammonia, sulfuric acid and aliphatic hydrocarbons (hexane, octane and naphtha). The material is black in color to prevent the transmission of light. The chamber made up of the same material where the cuvette will be inserting.

The plastic cuvette was used for photometric measurements even in the UV range with applicable wavelengths that range from 220 to 900 nm. The cuvette's outer dimensions are 12.5 × 12.5 × 45 mm. One hole was drilled into black chamber at 90 grades from serial port camera module for the emitter. A support, which was especially designed to place the camera module, holds it without moving and it could be attached to the main bracket keeping the cuvette static. The assembly allows the camera module cover the cuvette, avoiding external interferences. The developed system was illustrated in figure 24.

Sensing module: ArduCAM series camera shield is a universal camera control board for Arduino; it was used with ArduCAM Rev.C+. Its features comprises 3.2 inch TFT LCD with touch screen, build in SD/TF card socket, support JPEG compression mode. It can be used with open source code library. ArduCAM's IO ports are 5V/3.3V tolerant.

A 1/4-inch 5 megapixel (MP) CMOS image sensor was used together the module camera with an active array size of 2592 x 1944. Its output formats are for 8 bits, 8-bit compression data and 8/10-bit raw RGB data. Including a lens of 1/4″, allowing a pixel size of 1.4 µm x 1.4 µm and an image area of 3673.6 µm x 2738.4 µm. The concentration of the OTA stock solution was determined by exciting with UV-LED [16] [109].

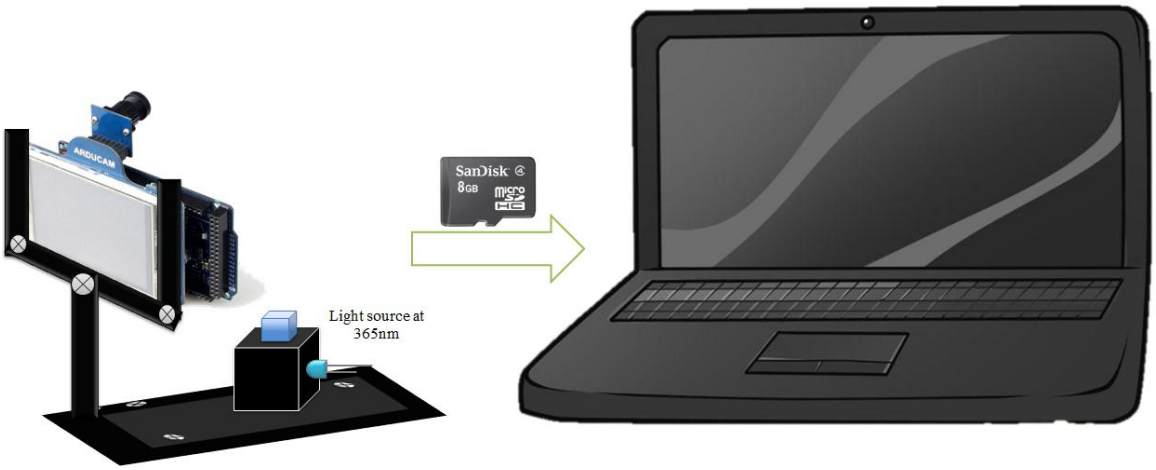

Fig. 24 Schematic of the optical system developed with ArduCAM.

Constant current source: A constant current source produces a constant value of current regardless of source voltage or load resistance was designed. This circuit was used as a current limiter to protect the UV-LED. The design involves a voltage regulator LM317, it was used as constant current source with a single resistance and the resistor range is 0.8Ω< R<120 Ω.

The formula is Iout = 1.25V / R. The resistance (R) of 56 Ω employed produces and current output of 22.3mA, which is in the range of forward current (I_F) of 25mA for every UV-LED. The circuit used is showed in the figure 25, was powered through the USB port of Arduino UNO which provides between 5-4.5V, this variation not affect the light intensity due to the constant current source, designed and placed in an electrolytic plate with dimensions of 30 × 20 mm.

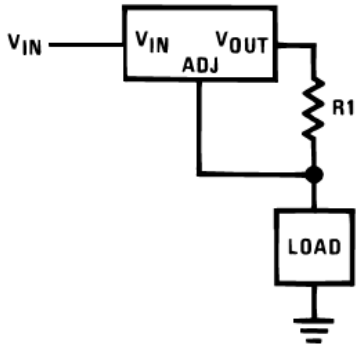

Fig. 25 Setting the regulator LM317 as current regulator.

Software: ArduCAM allows using different image sensor, in this thesis the Omnivision OV5642 5MP sensor was used, it provides both preview and JPEG capture. It is necessary to set the sensor to BMP preview output mode, switch to JPEG mode when shutter button is pressed, this process will capture and buffer the image to store the image in a Micro SD card with JPEG format in approximately 10 seconds.

To process the image, an interface in MATLAB R2011a was built. Previously, the image was saved in a Micro SD card, so the interface permits to choose the process of the image, one image or to process at the same the time all the image contained in a folder. Besides, it is possible to modify the area to be cut off and the rotation, in case that the image is incorrectly angle. The interface consists of three buttons and their functions are listed below, an image of the interface working is present in the figure 26.

1) *OK*. By clicking this button an image can be selected of an specific folder and it is cut off by the area selected and rotate as the angle indicate. Besides the software show the area cropped and obtains its RGB values stores the image with jpeg format and the mean of the RGB components in a text file; keeping original image name and adding tags to identify the results.

2) *Reset*. To cancel the execution, to clean the value and write new values or to take the option Multiple Images.

3) *Exit*. Close the window.

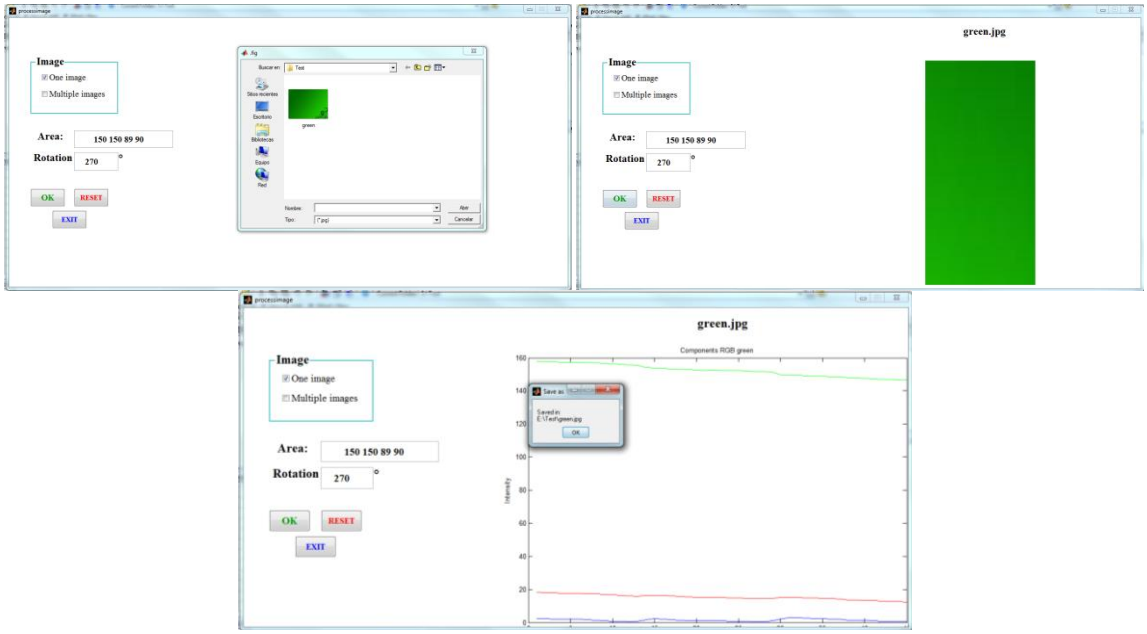

Fig. 26 Interface designed to process the image employing ArduCAM.

3.5 CMOS sensor in serial port camera module for detect OTA

Design: The device uses the same bracket employed in the ArduCAM set-up, this is other advantage of the bracket designed. Only, the base designed to puts on the camera module changes respect of the dimensions of the module utilized. The schematic of developed system was illustrated in figure 27.

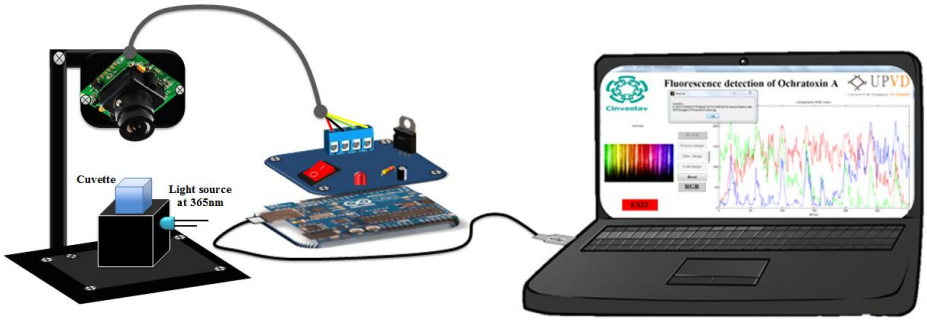

Fig. 27 Sensing module connected to the final device and its control with the computer.

Sensing module: The serial port camera module, Link Sprit (LS-Y201-Infrared), can capture high-resolution pictures and transmit them over a serial TTL interface. It captures and produces Joint Photographic Experts Group (JPEG) images with a 1/4 Omnivision CMOS sensor from a serial port with communication via UART. It works with a 5VDC power supply and has a low current consumption of 80 to 100mA. Its dimensions are 45.6 × 30 × 28 mm. The ultraviolet emitter produces high power light with a specific emission peak was used to detect the presence Of OTA. The circuit designed for control of the camera module and the UV-LED was placed in an electrolytic plate with dimensions of 60 × 20 mm.

Software: A graphical user interface was created in MATLAB R2011a. The interface consists of seven buttons and their functions are listed below:

1) *Blank*. By clicking this button, an image is captured and the name “blank” is assigned to the file automatically. The file is saved in a special folder in order to compare with future concentrations of OTA.

2) *Processing*. It performs a selection of the blue strip area that shows the fluorescence for an image or a folder with many images, obtains its RGB values stores the image with jpeg format and the mean of the RGB components in a text file; keeping original image name and adding tags to identify the results.

3) *Take the image*. This button controls the serial port camera module, captures and produces JPEG images from serial port in communication with the Arduino board, stores the image in text and jpeg formats with a name given by the user and in a folder selected by him. The communication protocol consists in reading the JPEG file in data packages of 8 bytes, starting with the address 0000 and reading that chunk many times until FFD9 is read, which indicates the end of the JPEG file.

The Arduino board keeps the hexadecimal information and transmits it to MATLAB to order the information received in a matrix of eight columns by n rows until FF D9 is read. MATLAB changes the hexadecimal values to decimal values and rebuild the image in order to be stored by the user. The total time consumed from acquisition to processing to image display is 20 seconds with a 38400 baud rate of serial port through the USB interface of Arduino board to the personal computer. The processing between Arduino board and MATLAB is in the figure 28.

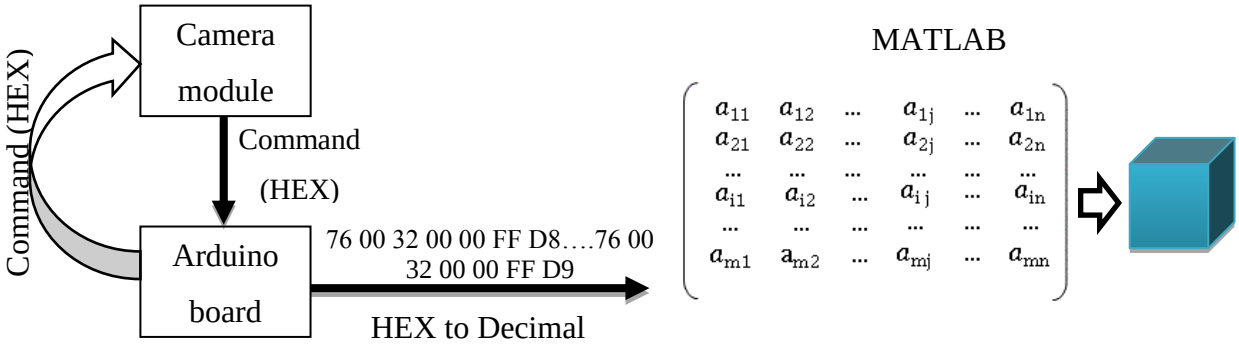

Fig. 28 Communication protocol between Arduino board and MATLAB.

4) *Load*. By clicking this button, the user can "Load" an image that was previously taken. It could be used for any image not limited to the fluorescence images.

5) *RGB*. After clicking it, the RGB values will be obtained automatically and the information will be saved, conserving the original file name of image and adding tags to identify the results. The file path where the results were saved will be shown to the user. This is for any sort of image previously loaded into the software with the button "Load".

6) *Reset*. In case of error, the button Reset cancels the execution and removes the text or image displayed.

7) *Exit*. It exits the application software at point of time during the measurement.

Finally the user does not need to install MATLAB since the interface is an executable file, hence the user should install the executable file generate in its computer. The interface is easy to use, to obtain the values and to save all information (text file, images, figures, names of files) automatically allowing its use as a portable system. When a button is pressed, the other buttons are disabled to prevent user's mistakes and errors in the analysis.

3.6 Smartphone as detector of OTA

Optical characteristics: The smartphone consist of a camera of 8 megapixels, 3264x2448 pixels, with $f/2.4$ aperture of a lens, it has five-element lens, a hybrid IR filter. In addition, it has image stabilization, rapid capture (the first picture in 1.1 seconds and the following pictures in 0.5 seconds).

Also, It was used an ultraviolet emitters to detect the concentration of the OTA. The source of the LED is a regulator LM317 as constant current powered by the lithium-ion battery integrated in the smartphone. The smartphone was used as power supply of the system, the lithium-ion battery (LIB) integrated in the smartphone was connected to a Step-up DC-DC (direct current) converter due to the LIB provides 3.3 V and the source of the LED requires 5 V.

Through a USB wire built in the laboratory to meet the necessary requirements, a dock 30-pin male connector was designed to use the iPhone 4S as a power source at one end of the wire, the other end was connected to a USB port on the electrical circuit, besides an inductor or 22 µH was employed, finally the output voltage of the converter was connected to the source of the LED, the final voltage is 5V at 200 mA. The circuit was designed in an electrolytic plate with dimensions of 60 × 40 mm (see figure 29).

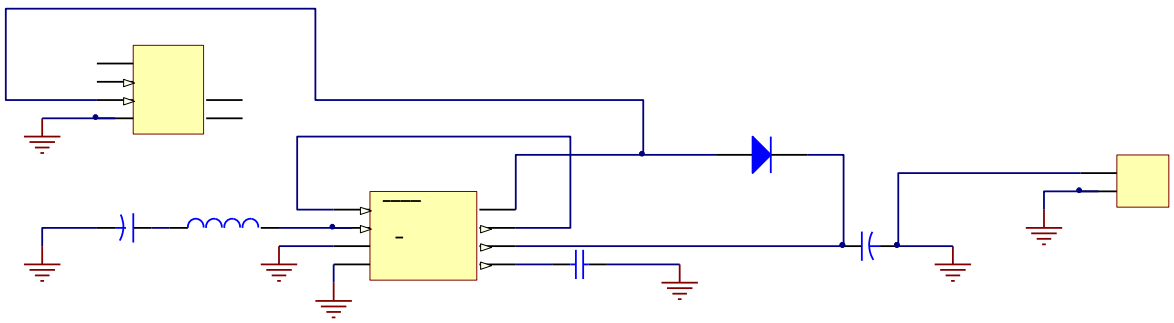

Fig. 29 Electrical circuit to use the smartphone as source of 5 V.

Fig. 30 Fluorescence analyzer developed based on smartphone camera

Software: An interface was developed for fluorescence imaging to detect the presence of OTA in samples. The fluorescence from the UV excited sample passes through a lens to the smartphone camera. The interface illustrated in the figure 30-31 is user friendly and easy to use for even new users and allows:

1) To obtain the image, it is necessary to use the Internet Protocol address (IP address) of the smartphone camera, IP address is a numerical label assigned to each device participating in a network that uses the Internet Protocol for exchange information or communication between the devices connected to it. The IP is used as interface identification and location addressing.

2) In this work, the IP address was obtained with a free application installed in the smartphone. Afterwards, the smartphone send the image to the personal computer by wireless, denoting the IP address as an URL (Uniform Resource Locator) in the interface, therefore it is possible to use any kind of smartphone or camera knowing the IP address of the device, as the figure 34 shows.

3) With the fluorescence image obtained from the smartphone, automatically, the interface decomposed the image is its red, green and blue coordinates (RGB components) plotting its blue component over the others and displaying the RGB diagram for each solution tested.

The designed interface allows the camera to capture the image, save it and then visualize the RGB components; the information's related to the RGB is saved automatically in

the personal computer. The information saved is the image, the RGB values and diagram, with the name given by the user. It possible to use as a portable system due to the interface was made as executable software hence it is not necessary install MATLAB, only the interface created.

Fig. 31 Interface designed for the fluorescence analyzer based on smartphone camera.

3.7 Fluorescence image

An ultraviolet light source is coupled with a light-excluding compartment. The fluorescence from the UV excited sample passes through a lens to a camera module controlled by the computer. Fluorescence image data from the camera module is analyzed by application software in the computer. Images with two dimensions such as photograph captured by optical devices like cameras are considered digital images, which are a numeric representation of a two-dimensional image. The digital image contains a fixed number of rows and columns of pixels. Each pixel is specified by three values for the red, blue and green components of pixel array. M by N by 3 arrays of unit8, which values range are 0 to 255. The position of the pixel is described by a pair of coordinates (x_i,x_j). In the RGB color model, the image can be represented by the intensity function: $I_{RGB}=(P_R,P_G,P_B)$.

Where $P_R(x,y)$ is the intensity of the pixel (x,y) in the red channel, $P_G(x,y)$ for the green channel and the last channel is the blue component expressed as $P_B(x,y)$. For the interface in MATLAB, it was considered that the indexed image is an M-by-N array of integers. The color map is a three-column array of values in the range [0,1]. Each row of the color map is a three-

element RGB triplet that specifies the red, green and blue components of a single color obtained from the color map. In the figure 32, red, green and blue colors are represented by a three dimensional Cartesian coordinate system.

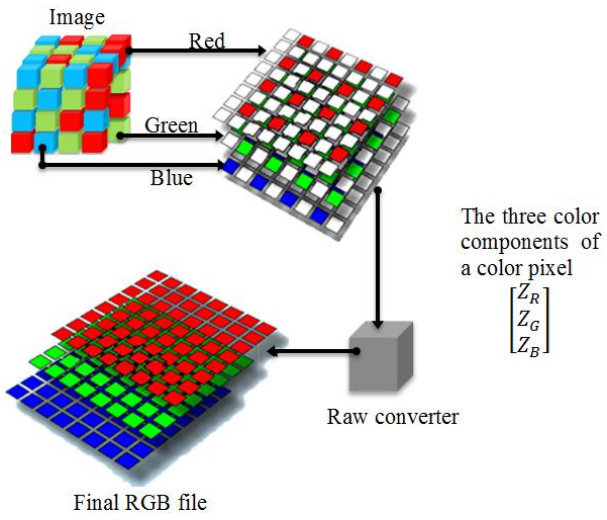

Fig. 32 Schematic of the implementation of RGB color model to process images.

Applying the concept of RGB color model, the interface consists of obtain all the image components and built the RGB diagram for the stock solutions and real samples. In our study, we worked with blue component since the OTA is intensely exhibits fluorescence in ultraviolet light [36][16][109][179]. When the solution is excited with ultraviolet light, the solution contaminated with OTA showed a blue strip for the presence of the mycotoxin and a dark strip for solutions such as buffer or methanol (blank samples) without OTA.

3.8 Fluorescence with HPLC

The mobile phase used for HPLC was a mixture of acetonitrile/water/acetic acid (40/59/1) for wine and beer samples. In the case of cocoa extraction, the mobile phase was 48/51/1. The mobile phase was sonicated for 20 minutes to remove the bubbles. The detection was done by fluorescence detection at 333 and 460nm as excitation and emission wavelengths, respectively.

Different sample injection was assayed; before injection, all samples were filtered through a 0.2 PTFE. A 200 µL of eluted solution of the columns and standard solutions of OTA were injected in the HPLC alternatively, three times.

OTA was identified by constant retention time (5 minutes) for beer and wine, 12 minutes for cocoa extraction and quantified by comparing with peak area of standards solutions. At the beginning, the HPLC was cleaned with the mobile phase three times and after the injection of the samples, again.

3.9 Methods of extraction

3.9.1 Reagents and materials

All reagents and chemicals were obtained from Sigma Aldrich (France), these were: Acetic acid, Acetonitrile HPLC-grade, Ethyl-acetate, Methanol, Ethanol 98% and 100%, Tween 20, sodium chloride NaCl, KCl, sodium phosphate dibasic Na_2HPO_4, potassium phosphate monobasic KH_2PO_4 and $NaHCO_3$.

Ochratoxin A was purchased from Trilogy (France) and Ochratoxin B (OTB), derived from (*A. ochraceus*), was purchased from Santa Cruz Biotechnology, Germany. The standard solutions were stored at 4°C and OTA solutions were kept frozen (-18 °C). Commercial ImmunoAffinity Columns (IAC) Ochrapreps were purchased from R-Biopharm (Saint-Didier au Mont D'Or, France) were store at 2-8 °C, Molecularly Imprinted Polymers based Solid Phase Extraction (AFFINIMIP SPE) Ochratoxin A from POLYINTELL (Val de Reuil, France) were kept at room temperature.

Wine and beer samples were obtained from local supermarket (Perpignan, France) and were stored at 4 °C. Cocoa beans were provided by our industrial partners M/s CEMOI based at Perpignan, France. A syringe filter, PTFE, 25 mm diameter, 0.2µm (Scientific Strategies, USA) and syringe filter at 0.45 µm, sterile and reliable filtration (Sartorius Stedim Biotech, France). The solutions were prepared in deionized Milli-Q water (Millipore, Bedford, MA, USA) for cocoa extraction.

3.9.2 Equipment and instruments

HPLC equipment consisted of an L-7110 LaChrom Hitachi pump (Merck, Germany) and an L-2485 Elite LaChrom Hitachi fluorescence detector (VWR, France). The HPLC Luna 2.6 mmC18 100A, 250 x 4.60 mm column was obtained from Phenomenex (USA).

A fluorescence instrument consisted of a Fluoroskan Ascent FL 2.6 (Thermo Scientific-Finland) equipped with Ascent software version 2.6. All the chemicals were weighed using a PB1501 scale balance (Metter, Toledo, USA) with a precision of ±0.1g.

3.9.3 Extraction of OTA from cocoa using MIP columns

1 Kg of cocoa beans were spread on a black nylon sheet and kept under the fume hood. A 100 Ml of 20, 10, 5 and 1.5 µg OTA solution was prepared in 5% ethanol and slowly sprayed over the cocoa beans. The samples were kept at room temperature for overnight.

3.9.3.1 Extraction based on 1% $NaHCO_3$ in water

OTA was extracted by directly using 50 g contaminated beans with 200 mL aqueous 1% $NaHCO_3$ in a horizontal shaker for 30 min. A 50 mL aliquot was filtered using 45µm steel filter (Fischer scientific). Before loading, the MIP column was equilibrated using 2 mL acetonitrile and then 2 mL of water.

For loading, a 20 mL sample was passed through the column by keeping the flow rate constant (1 drop/sec). The column was washed to remove the interferences using 8 mL 60:40 water and acetonitrile. The sample was eluted using 2 mL methanol in 2% acetic acid. The MIP columns were pre-conditioned with 10 mL PBS before sample loading. A total 20 mL of the filtered extract was taken and passed through the column, keeping the flow rate constant (1 drop/sec).

After the extract had passed through the column, the IAC was rinsed with 20 mL PBS containing 20 µL tween-20. OTA was eluted using 3 mL methanol with continuous back flushing. It was carried out to increase the time the solvent is in contact with the antibody gel ensuring the complete elution of toxin from the column. The collected sample was diluted and directly taken for fluorescence detection.

3.9.3.2 Extraction based on acetonitrile: water mixture (2%NaCl), classical method

Contaminated cocoa beans were kept at -80°C for overnight and then beans were ground using mixer. 50 g of ground cocoa powder was mixed with 200 mL of acetonitrile/water (60:40) in the presence of 4g NaCl and shaken for 30 min. The extracted liquid was filtered using 45 µm filter unit and then centrifuged at 5000 rpm for 10 min. For

purification, 25 mL of PBS was mixed with 48µL of tween-20 and 20 mL of extracted and centrifuged cocoa sample.

Further, the IAC was equilibrated with 10 mL PBS (pH 7.4). The extracted sample was loaded drop wise onto the column by keeping the flow rate 1 drop/sec. The column was thoroughly rinsed with 20 mL of PBS. The OTA retained in the column was eluted using 3 mL methanol with continuous back flushing. The final step was kept similar as method described in the section 3.9.3.1.

3.9.4 Extraction of OTA from wine and beer sample

The wine employed in the analysis has the next characteristics, it was a wine rosé, Bonne Nouvelle, France with alcohol less than 0.5% in a total volume of 750 mL. The beer was a Mosel bier pur malta with a volume of 33 cL, manufactured and packaged in German spiked with OTA. The alcohol content corresponds to 0.5 %. The schema of the extraction in columns in represented in the figure 33.

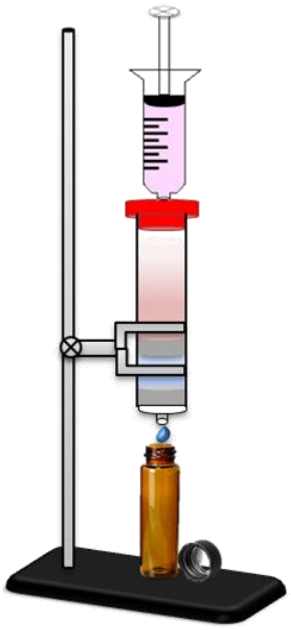

Fig. 33 Drawing the extraction using IAC or MIP.

3.9.4.1 IAC columns

A known concentration of OTA (2, 4, 6, 10 µg/L) was spiked in the wine. First, the wine samples were prepared as follow 8 mL of sample along with 1 mL of 10% $NaHCO_3$ and

1 mL concentration of OTA in methanol were mixed. The extract was filtered using 45 µm sterile syringe filter. The process to prepare beer samples is the same to the wine, but it was used 1 mL of 1% $NaHCO_3$.

In the loading step, 10 mL of the filtered extract was passed through the IAC two times, which was pre-conditioned with 10 mL PBS buffer. After the extract has passed through the IAC, it was washed with 20 mL PBS buffer containing 20 µL of Tween 20. For the last step, OTA was eluted using 3 mL methanol with continuous back flushing at a constant flow rate of 1 drop/sec.

It was carried out to increase the time of solvent in contact with the antibody gel ensuring the complete elution of OTA from the column. The elution was collected in amber bottle to protect of the light and it was analyzed by HPLC and fluorescence device developed with CMOS sensor. The blank was prepared without OTA; 1 mL of methanol was mixed with 8 ml of the wine sample and 1 ml of $NaHCO_3$; it was passed through the IAC in the same process described in this section.

3.9.4.2 MIP columns

The process of the real sample preparation was mentioned in the section 3.9.4.2.The column was pre-conditioned with 4 mL of acetonitrile and 4 mL of distilled water. In the loading step, 10 mL of the filtered extract was passed through the column two times. The washing step consisted of 4 mL 0.1M HCl along to 3 mL of acetonitrile. Finally, the elution carried out passed through the column 20 µL acetic acid in 2 mL Methanol. The elution was collected in amber bottle also and analyzed by the HPLC and the fluorescence device developed with the CMOS sensor.

3.10 Flow systems

Sequential-injection analysis (SIA) is an approach to sample handling that enables the automation of chemistry procedures in a rapid, precise and efficient manner. SIA was developed by Ruzicka and Marshall in response to an industry initiated requirement for a more robust automated chemistry technique than traditional flow injection analysis (FIA) [180].

SIA is widely applied for the determination of several species in a variety of matrices employing a computer-controlled multiposition valve and pump operated synchronously. The

ports of the multiposition valve are connected to a sample and a reagent. The order in which sample and reagent zones are stacked depends on the chemistry being used; additional zones of reagent or diluents may also be aspirated.

The major advantage of SIA is its ability to perform numerous complex chemistries coupled with various modes of detection without re-configuration of the flow manifold. In addition SIA requires very low sample and reagent volumes leading to minimal effluent [181]. The scheme of the sequential injection system is shown in the figure 34. Teflon® tubing was used at the pump to transport the solutions.

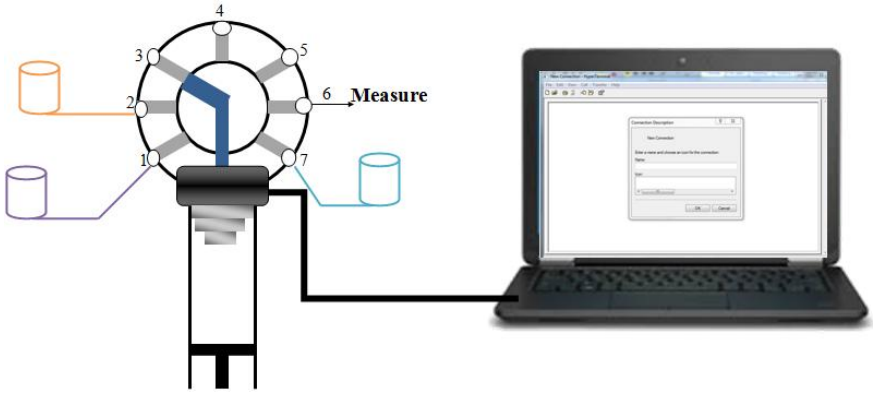

Fig. 34 Representation of a SIA system.

The SIA system developed in this thesis was programmed using HyperTerminal due to it is easy to use, free and no need specific requirements, so it can be installed in a portable computer. HyperTerminal or HyperTerm is a communication program that was included free with Windows 95 until Windows 7. Principally, it is handy for sending data to serial displays, data transfer also between two computers using the serial ports and serial-port control of external devices or systems such as scientific instruments, robots, among other.

To use HyperTerminal is necessary double click or press enter key to execute hyperterm.exe in Windows 7. Then, the dialog box the HyperTerminal will open, it will ask to introduce the connection name and choose the icon corresponding the connection need it. After clicking "OK", HyperTerminal will ask you to dial a telephone number, if you want just enter it and click "OK" but not click on "Cancel".

Choosing Menu File, once you have clicked in the "Properties", choose Connect using: Direct to <communication port> (usually COM1, COM2), COM properties dialog box appear after click OK, the select the flowing in the field provided:

Bits per second: 9600

Data bits: 8

Parity: None

Stop bits: 1

Flow control: None

Select the Menu Setting

Enter the follow options:

Select “Send line ends with line feed”

Select “Echo typed characters locally”

Enter a line delay of 0

Enter a character delay of 0

Select “Wrap lines that exceed terminal width”

Finally, Click OK to close the ASCII Setup dialog box, then click OK to close the properties dialog box, power on the pump and initialize it, loading the program to execute. The pump is connected to the computer using a RS232 serial connector, which is a standard for serial communication transmission of data. The program is written in block notes following the next commands for created the sequences:

/1ZR= initialize the pump

I = input; O = output; both followed by the valve number

A = aspire; D = drain; both followed by the volume in microliters

g = starting of a cycle; G = end of cycle, followed by the total number of cycles

S= speed

R= execute the sequence

M=delay, maximum 30 seconds.

Transfer Menu in HyperTerminal has five options, Send File, Receive file, Capture text, Send Text File and Capture to Printer. The option Sending File allows to select your file with the sequence that you want to execute and select the protocol that will be used to execute the pump and the sequence in automatic way.

3.10.1 Flow system for Aptamer columns

The reagents were provided through control of a bidirectional pump Cavro XLP 6000 Modular Syringe pump (Tecan, Switzerland) fitted with a 2 mL syringe and six valves. The number of valve for the injection of the solution and the speed used will indicated in parenthesis, the first position is for the number of valve and the next position follow by S designated the speed of injection, due to it is more important the speed of injection than the speed used to fill the syringe.

The first step before each extraction was the conditioning of the aptamer column with 5 mL of the selection buffer (20 mM Trizma hydrochloride, 140 mM NaCl, 5 mM KCl and 1 mM MgCl2, pH=7.4, 4 ºC), was injected by the valve 1 (1, S16). The extraction procedure consisted of the percolation at 4 ºC of 500 mL of the selection buffer containing variable amounts of OTA injected trough the valve 2 (2, S22), followed by washing with 500 mL of the selection buffer at 4 ºC. Then, the OTA was eluted with 500 mL of a methanol: acetic acid solution (98: 2, v/v) at room temperature, this was injected by the valve 3 (3, S18). The elution was analyzed by HPLC and fluorescence device developed. The syringe speeds that were used S14 = 0.1333 mL/s, S16 = 0.0666 mL/s, S18 = 0.0316 mL/s, S22 = 0.0250 mL/s.

Between every step, air was injected through the valve 5. The output and waste were located in the valve 6. The sequence wrote was:

1/1S14I1A6400S16I6D6400G5S16I5A3200I6D3200S22I2A3200I6D3200S16I5A3200I6D32
00M30000M30000M30000M30000M30000M30000M30000M30000M30000M30000S14I1A
3200S16I6D3200S16I5A3200I6D3200M30000M30000M30000M30000M30000M30000M30
000M30000M30000M30000S18I3A3200I6D3200S16I5A6400I6D6400M30000M30000M30
000M30000M30000M30000M30000M30000M30000M30000S14I1A6400S16I6D6400G5R

3.11 Evaluation of the fluorescence device performance under specific conditions

The CMOS sensor in serial port camera module for detect OTA described in the section 3.5 with the UV-LED at 365 nm to 4mW of radiant flux, was used as fluorescence device and was evaluated under three conditions, these were:

a) Different solvents

First, 20 μg/L of OTA was prepared in methanol, ethanol, PBS buffer, acetonitrile, distilled water, mobile phase (48/51/1), tap water and HEPES buffer (6.507g HEPES (50mM), 3.504 g NaCl (120mM),186.25 mg KCl (5mM), 238 mg $MgCl_2$ (5mM) in 500 mL of distiller water at pH 7.4). 1 mL of the solvents were prepared without OTA and these were considered as blank, 1 mL of the concentrations of OTA or blanks were inserted in the cuvette and in the chamber of the developed system.

b) Variation of the NaCl concentration

It was modified in the HEPES buffer as follow: 0mM, 10 mM, 30mM, 60 mM, 90 mM and 120 mM of NaCl. These were considered the blank and after to make the measurements a concentration of 20 μg/L of OTA was prepared in that solutions and the fluorescence was measured with the developed system. One hour later, the measurements were repeated to see the changes in the sample with OTA respect the time. The pH was adjusted to 7.4 with NaOH 3M.

c) Changes respect to the pH

HEPES buffer in a range of pH was prepared, the range was 6 to 8.4, it was considered as the blank and a concentration of 20 μg/L of OTA was prepared with the different pH. The intensity of fluorescence was measured and the results were processed.

The ultraviolet led excited the sample and the serial port camera module captures the image when the interface designed was executed. With the option multiples images, its RGB values, the image with jpeg format and the mean of the RGB components in a text file were obtained automatically and the results were saved. All the measurements were made by triplicate; the results were compared with Fluoroskan Ascent FL 2.6.

3.12 APP designed

The new tendencies in technology can also be applied to the research, allowing portability, measurements “in-situ”, colorimetric test, reduction in analysis time and the samples are no destroyed. Besides, these can be compared with the analytical methods.

An example of which is the use of smartphone and tablet [182] to detect, quantified or evaluate compounds [183], biochemical detection [184] or for medical applications [185,186].

In this thesis, a very simple mobile application (app) was designed to run on mobile devices such as smartphone and tablet computers. It was used to detect the OTA presented in a sample, it is important to mention that this is the first version of the app.

The app was created for android system with the support of the computer systems engineer Leonardo M. Delgadillo De la torre, Masters Student in the Laboratory 11, CINVESTAV-Zacatenco. The software Xamarin Studio is a development environment that uses C# language for creating mobile applications. The test device was a LG E410g smartphone with Android version 4.1.2, camera of 2 MP and QVGA 320x240 for resolution.

The app was integrated with five buttons and their functions are described as follow, the principal screen of the app designed is presented in the figure 35:

1) *Take the image*. This button takes a picture of the image, display it in the viewing area and show the RGB values. Besides, it saves the image in a folder named components RGB_img that is created in the pictures directory as componentesRGB_txt file. The time to take the image and extract the RGB value is about one minute due to the complexity of the program loaded in the smartphone. All information is stored in the internal memory of the smartphone, which is of 1.74 gigabytes (GB).

2) Search. Look up the image previously takes it, downloads it or saves it in the folder componentesRGB_img to show in the viewing area and its RGB values.

3*) E-mail.* Send the image of the viewing area and the RGB values through a synchronized device to a g-mail account that is used to store the information. The account by default is cinvestav.rgb@gmail.com. When the E-mail button is pressed, provides a list of others options to save the files generated by the app.

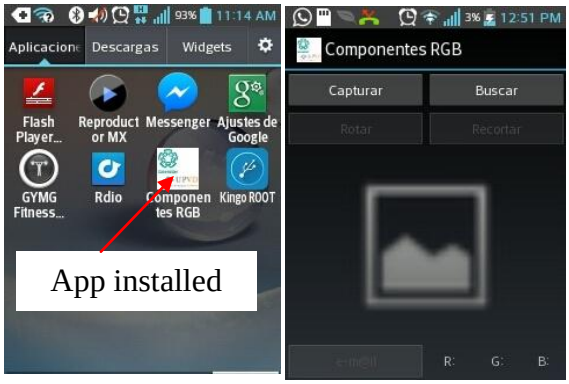

Fig. 35 Principal screen of the app in the smartphone.

PART C

Image processing

Optical biosensor can benefit from advances in digital processing of the images or other types of signal processing techniques. Digital image processing is growing well beyond traditional “photographic” imaging. Chemical imaging takes advantage of a number of spectroscopic techniques. These techniques provide the needed information about the molecular composition, structure and dynamics. Continued advances in chemistry require more powerful techniques to visualize and manipulate matter or to manage the vast quantities of data resulting from imaging, efficiently. The imaging techniques described are divided into three main categories, these are [187]:

- Optical imaging
- Proximal probe
- Processing analysis and computation

Digital imaging includes recording, storing, manipulating and displaying the image. A digital image can be considered as a discrete representation of data possessing both spatial (layout) and intensity (color) information. In addition, it is made up from a great number of pixels; each pixel has a specific numeric tonal value. The contrast is determined by the number of tonal values and the resolution is determined by the number of pixels. There are at least two methods of acquiring a digital image, such as:

✓ Traditional photographs, transparencies or negatives can be scanned

✓ Cameras, which can directly record digital images.

In the case of chemical image processing, a digital camera uses a CCD or CMOS sensor to record the image, the image capture process is almost instantaneous, the sensors are exposed at the same time, the number of pixels is fixed hence the image captured has a fixed resolution. Digital image processing and manipulation refers to the analysis and possible alteration of the original source image. Processing can be performed by computer programs [188].

The most common property to measure quality of any material is its appearance includes color, shape, size and surface conditions. Color measurements have also been used as quality parameters and indicator of constituents [188].

Color has importance in many different disciplines such as in biology, color vision and colorization of plants and animals; in psychology, color vision; in medicine, eye diseases and

human vision; in art, color as an emotional experience; in physics, the signal carrying the color information and light matter interaction; in chemistry, the molecular structure and causes of color; in technology, different color measuring and display systems.

The new technological development in illumination, camera and display technology requires new way of managing colors. The light-emitting diodes (LED) are coming into illumination and displays rapidly. There, the color radiation spectrum is so peaky that managing it requires a more accurate color representation than RGB. There exist also digital cameras and displays, where colors are represented by four or six colors hence this technology requires new ways to express and compute color values [189].

Among the properties widely used for analytical evaluation of materials, color is unique in several aspects. Color is an appearance property attributed to the spectral distribution of light and is related to the illuminant the object to which the color is attributed, and the eye of the observer. Several factors that influence the radiation affect the exact color that an individual perceives. Those factors are: spectral energy distribution of light showed in the figure 36, conditions under which the color is viewed, spectral characteristics of the object with respect to absorption, reflection, transmission and sensitivity of the eye [188]. Light is the basic stimulus of colors.

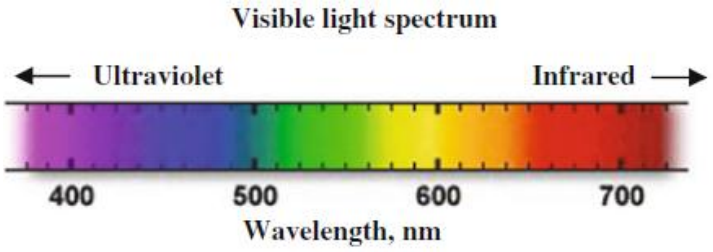

Fig. 36 Color spectra of light in visible range of wavelength.

The following material properties, lighting of the scene and interaction of matter with light affect the total appearance of the object:

(i) Material properties

Optical properties (spectral, reflectance, transmittance)

Physical form (shape, size, surface texture)

Temporal aspects (movement, gesture, rhythm)

(ii) Lighting of the scene:

Illumination type

Spectral and intensity properties; directions and distributions

Color-rendering properties

(iii) Interaction of light with matter

Whereof, the image processing for the fluorescence image is not an objective of the thesis work, image-processing methods were employed to try to identify the OTA without extraction method. First, the fluorescent image was the image generated by own fluorescence of OTA excited with UV light, the samples were spiked with a known concentration of OTA (2, 5, 10 µg/L), the wine samples were prepared as follow 8 mL of sample along with 1 mL of 10% $NaHCO_3$ and 1 mL concentration of OTA in methanol were mixed. The extract was filtered using 45 µm sterile syringe filter. The process to prepare beer samples is the same to the wine, but it was used 1 mL of 1% $NaHCO_3$. The blank was prepared without OTA; 1 mL of methanol was mixed with 8 ml of the wine or beer sample and 1 ml of $NaHCO_3$.

After, non IAC or MIP columns were employed; the image of every concentration was capture directly. The same samples were analyzed with the Fluoroskan to compare the results. In addition, the images were processing follow different technique or model color to image processing. Considered as a mathematical entity, an image is a spatially organized set of numbers with each pixel location addressed as $I(u,v)$.

Grey-scale or binary images are 2D arrays that assign one numerical value to each pixel, which is representative of the intensity at that point. 2D images use a single-channel color space that is either limited to a 2-bit (binary) or intensity (grey-scale) color space. By contrast, true-color images are 3D arrays that assign three numerical values to each pixel, each value corresponding to the red, green and blue component [190]. The image processing was realized with MATLAB R2011a, employing commands and toolbox, also. Described as follow:

The first technique employed was to get the histogram; the histogram is a distribution that describes the frequency of the intensity value (pixels), the spatial domain, which it is based on the direct manipulation of pixels in the image. The histogram of a monochrome

image presents the relative frequency of occurrence of the various levels of the image. This technique modifies an image so that the histogram of the resulting image is uniform.

The histogram for an image in gray scale *I(u,v)* with intensities in the interval [0,K-1] has the histogram H with K different value, a common image in gray scale of 8 bits is $H=2^8=256$. Every value is defined as h(i)=a, the number of pixels of I with the value of the intensity I for $0 \leq i \leq K$. Finally, a vector one-dimensional h with a length of K is obtained and plotted. An image histogram is a plot of the relative frequency of occurrence of each of the permitted pixel values in the image against the values themselves [139, 190].

The cumulative histogram *H(i)* consisted of a variation of the histogram, is defined as $H(i) = \sum_{j=0}^{i} h(j)$ for $0 \leq i \leq K$, where the value of H(i) is the sum of the inferior values of the value specific given by (i) of the histogram h(j) with values j=0,…,1. It is a monotonous and increasing function, with a maximum value $H(K-1) = \sum_{j=0}^{K-1} h(j) = MxN$.

To improve the contrast of color images is a slightly more complex issue than for grey-scale intensity images. In this case, the application of histogram is the same that the histogram for gray scale, but the histogram is calculated for every channel (R, G, B), separately. Visual inspection of an image histogram can reveal the basic contrast that is present in the image and any potential differences in the color distribution of the image foreground and background scene components.

Even though the RGB model is simple, is one of methods most associated to the changes of the color, RGB images are 3D arrays that are considered as three different 2D planes, one corresponding to each of the red (R), green (G) and blue (B) color channels. The colors present in a real image are nearly always a blend of color components from all three channels. If we consider that all the colors represented with their RGB, then the RGB color space is essentially a 3D color space (cube) with axes R, G and B.

Each axis has the same range 0-1, showed in the figure 37. The color black occupies the origin of the cube (position 0,0,0), corresponding to the absence of all three colors; white occupies the opposite corner (position 1,1,1), indicating the maximum amount of all three colors. The RGB color space based upon the portion of the electromagnetic spectrum visible to humans was described previously.

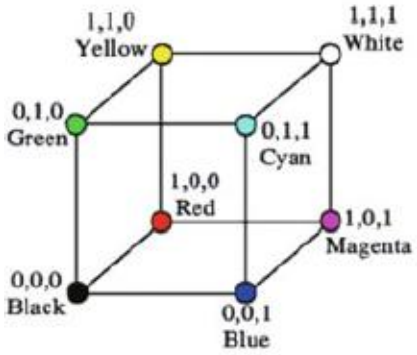

Fig. 37 RGB color space used in representing the color images.

The use a simplified RGB color model that is optimized and standardized towards graphical displays, however, the principal problem with RGB is that it is perceptually nonlinear; it means that moving in a given direction in the RGB color cube does not necessarily produce a color that is perceptually consistent with the change in each of the channels. RGB space is inherently difficult for humans because, it is not related to the natural way we perceive colors. As an alternative, we may use perceptual color representations such as HSV.

Perceptual color space is an alternative way of representing true color images as the human perception and understanding of color besides of the RGB representation. The changes of the Hue, Saturation and Value (HSV) color space follow a perceptually acceptable color gradient. From an image analysis perspective, it allows the separation of color from lighting to a greater degree. A RGB image can be transformed into an HSV color space representation as shown in figure 38.

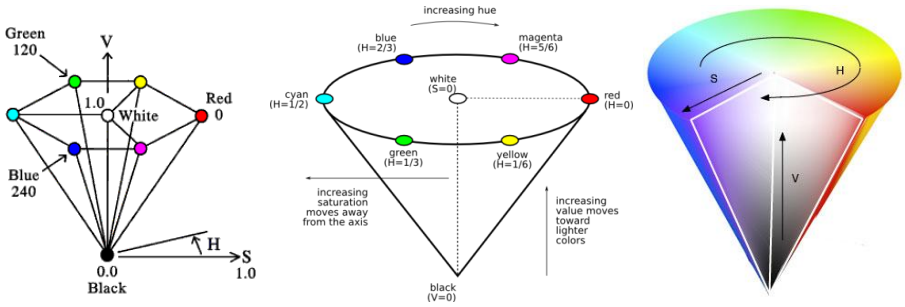

Fig. 38 HSV color space used in representing the color images.

Each of these three parameters can be interpreted as follows:

- H (hue) is the dominant wavelength of the color (red, blue, green).
- S (saturation) is the purity of color (in the sense of the amount of white light mixed with it).
- V (value) is the brightness of the color (also known as luminance).

In the MATLAB HSV implementation each of H, S and V are bounded within the range 0-1 by examining the individual color channels of images in the HSV space, the image objects are more consistently contained in the resulting hue field than in the channels of the RGB representation, despite the presence of varying lighting conditions over the scene. As a result, HSV space is commonly used for color based image segmentation using a technique known as color slicing.

A portion of the hue color is isolated as the color range of interest, allowing objects within that color range to be identified within the image. This ease of color selection in HSV color space also results in its widespread use as the preferred method of color selection in computer graphical interfaces and as a method of adding false color to images. For the conversion of RGB to HSV, is considered the follow equations:

$$Vmax = maximum(R, G, B) \quad \text{.....eq. 2}$$

$$Vmin = minimum(R, G, B) \quad \text{.....eq. 3}$$

$$V = Vmax - Vmin \quad \text{.....eq. 4}$$

$$S = \begin{cases} \frac{V}{Vmax} & if\ Vmax > 0 \\ 0 & V = 0 \end{cases} \quad \text{.....eq. 5}$$

$$R' = \frac{Vmax - R}{V} \quad \text{.....eq. 6}$$

$$G' = \frac{Vmax - G}{V} \quad \text{.....eq. 7}$$

$$B' = \frac{Vmax - B}{V} \quad \text{.....eq. 8}$$

$$H' = \begin{cases} B' - G' & if\ R = Vmax \\ R' - B' + 2 & if\ G = Vmax \\ G' - R' + 4 & if\ B = Vmax \end{cases} \quad \text{.....eq. 9}$$

$$H = \frac{1}{6} * \begin{cases} (H' + 6) & if\ H' < 0 \\ H' & otherwise \end{cases} \quad \text{.....eq. 10}$$

The HSI and HSL spaces are useful for image processing because they separate the color information in ways that correspond to the human visual system's response and the axes correspond to many physical characteristics of specimens. CIE and HSI are used in many color management systems, spectrophotometry and colorimetry.

In HLS space, a maximum value for lightness (L) means that the color is white, regardless of the current values of the hue (H) and saturation (S) components. [188]. The equations to transform a RGB model to HSL model, considering that H is obtained as in the HSV model, are:

$Cmax = maximum(R, G, B)$ .....eq. 11

$Cmin = minimum(R, G, B)$ .....eq. 12

$L = \frac{Cmax+Cmin}{2}$ .....eq. 13

$$S = \begin{cases} 0 & if\ L = 0 \\ 0.5 * \frac{Cmax-Cmin}{L} & if\ 0 \leq L \leq 0.5 \\ 0.5 * \frac{Cmax-Cmin}{1-L} & if\ 0.5 < L < 1 \\ 0 & if\ L = 1 \end{cases}$$ .....eq. 14

Therefore, perceptual features, such as perceived luminance (intensity), saturation and hue correlate well with the human perception of color. However, a color model in which these color attributes form the basis of the space is necessary. Models based on lightness, hue and saturation are considered better suited for human interaction. The analysis of the user-oriented color spaces involves HSI model (Hue, Saturation and Intensity). This model used primarily in computer graphics to specify colors using notion of tints, shades and tones.

However, the HSI model is derived from the RGB color space by coordinate transformations. In a computer centered image processing system, it is necessary to transform the color coordinates to RGB for display and vice versa for color manipulation within the selected space [191]. The color model is represented in the figure 39.

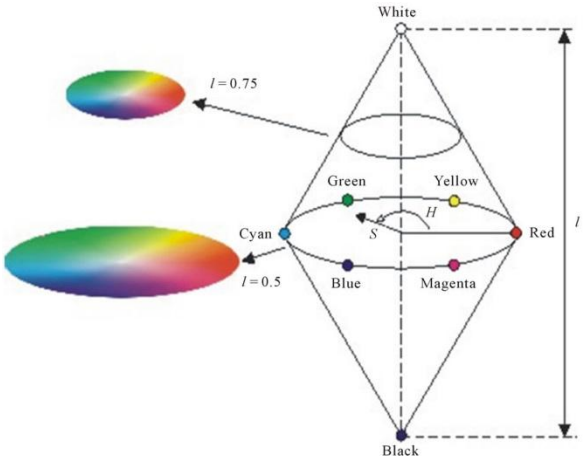

Fig. 39 HSI color space used in representing the color images.

The saturation (S) is proportional to radial distance, and the hue *(H)* is a function of the angle in the polar coordinate system. The intensity (I) is the distance along the axis perpendicular to the polar coordinate plane. The dominant factor in selecting a particular HSI model is the definition of the lightness, which determines the constant-lightness surfaces and thus, the shape of the color solid that represents the model.

The hue is measured by the angle around the vertical axis and has a range of values between 0 and 360 degrees beginning with red at 0°. It gives a measure of the spectral composition of a color. The saturation is a ratio that ranges from 0 to 1 on the surface of the cone. This component refers to the proportion of pure light of the dominant wavelength and indicates how far a color is from a gray of equal brightness. The intensity also ranges between 0 and 1, it is a measure of the relative brightness. At the top and bottom of the cone, where I = 0 and 1 respectively, Hand S are undefined and meaningless. At any point along the I axis the Saturation component is zero and the Hue is undefined. This singularity occurs whenever R = G = B [191].

The CMY and YC_bC_r are color models used in the standardized images for television, in the case of the YC_bC_r model, the chromatics components C_b and C_r are obtained as the difference between the luminance and the color plane R and B. The equations employed for the calculation of this color model are:

$$Y(x,y) = w_R(x,y) + (1 - w_B - w_R)G(x,y) + w_B B(x,y) \quad \text{.....eq. 15}$$

$C_b = \frac{0.5}{1-w_B}(B(x,y) - Y(x,y))$ .....eq. 16

$C_r = \frac{0.5}{1-w_R}(R(x,y) - Y(x,y))$ .....eq. 17

In the case of the CMY model is necessary three basic color such as cyan (C), magenta (M) and yellow (Y).When C=M=Y=0, the white color is obtained while if C=M=Y=1, the color obtained is black. The color cyan involves the red color, the magenta to the green color and finally, the blue color is associated to the cyan. This model is defined as [139]:

$C(x,y) = 1 - R(x,y)$ .....eq. 18

$M(x,y) = 1 - G(x,y)$ .....eq. 19

$Y(x,y) = 1 - B(x,y)$ .....eq. 20

All color models mentioned previously are associated with physical measures of the device used to display the information. To generate color regardless of the device used, it is necessary a color model that does not consider the representation; these models are called colorimetric or calibrated.

In 1920, the *Comission Internationale de L'Eclairage* (CIE) defined a system of describing the color of an object based on three primary stimuli: red (700 nm), green (540 nm) and blue (430 nm), all the colors appear as different combinations of these. The amounts of red, green and blue needed to form any given color are called the tristimulus values, X,Y and Z, respectively. A color is represented by a set of chromaticity coordinates or trichromatic coefficients, x, y and z as defined below:

$x = \frac{X}{X+Y+Z}\ ; y = \frac{Y}{X+Y+Z}\ ;\ z = \frac{Z}{X+Y+Z}$ .....eq. 21

It is clear that x+y+z=1, the value x, y give the form of the diagram CIE, every visible color of the CIE diagram showed in the figure 40. Can be represented by Yxy where Y represents the luminance component of the XYZ system. Inasmuch a constant value of Y, it is possible to extract a horizontal plane of the CIE diagram. The points (x, y) along the border of the CIE surface are the spectral colors having the maximum value of saturation, besides

different wavelength. With this, the position of each color can be calculated in relation to any primary color.

The exception is named connecting line which lies between 380 nm and 780nm, it is out of primary colors. The value of the purple color can be obtained through the obverse of colors in the opposite side. In the halfway through the CIE diagram increases the color saturation up to be a white point of the model, which is reached when x = y = 1/3 or X = Y = Z= 1.

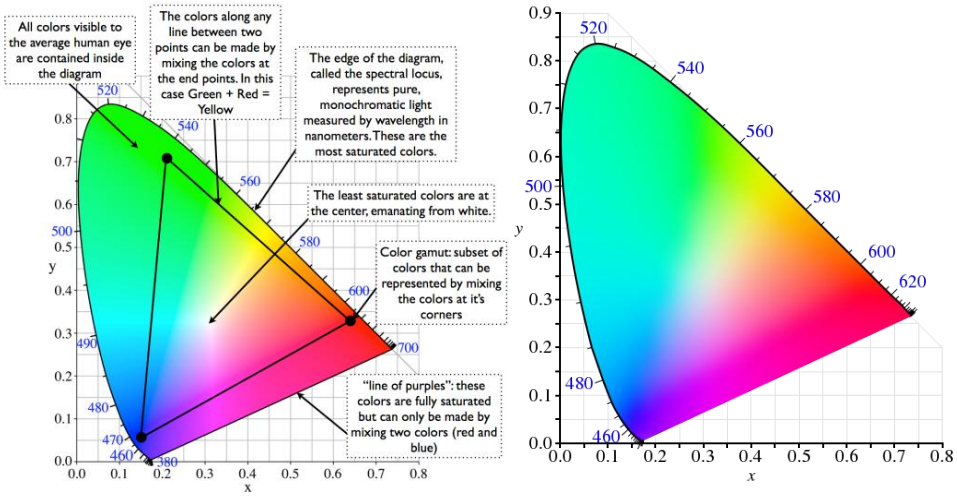

Fig. 40 Chromaticity diagram (CIE).

The model L*a*b is defined by three variables, L* represents brightness and the hue components a* and b*. The value of a* defines the distance along the red-green axis, while the b* represents the distance along the blue-yellow axis in the diagram CIE XYZ. The three components that define the space are relatives to a white point C_{ref} = (X_{ref}, Y_{ref}, Z_{ref}), where a nonlinear correlation is used. The following is a brief description in computing the CIE Lab values from the reflectance value of and object. To take the tristimulus values X,Y,Z, considerer:

$$L* = 116\left(\frac{Y}{Y_n}\right)^{1/3} - 16 \quad \text{.....eq. 22}$$

$$a* = 500\left[\left(\frac{X}{X_n}\right)^{\frac{1}{3}} - \left(\frac{Y}{Y_n}\right)^{\frac{1}{3}}\right] \quad \text{.....eq. 23}$$

$$b* = 200\left[\left(\frac{Y}{Y_n}\right)^{\frac{1}{3}} - \left(\frac{Z}{Z_n}\right)^{\frac{1}{3}}\right] \quad \text{.....eq. 24}$$

Where Y/Yn, X/Xn and Z/Zn >0.008856.

X, Y and Z are tristimulus values of the object measured.

X_n, Y_n and Z_n are the tristimulus values of a reference white object.

L* is the visual lightness coordinate.

a* is the chromatic coordinate ranged approximately from red to green.

b* is the chromatic coordinate ranged approximately from yellow to blue.

The command of MATLAB, graycoprops, calculates the statistics specified in properties from the gray-level co-occurrence for the image define as a m-by-n-by-p array of valid gray-level co-occurrence matrices. This command normalizes the gray-level co-occurrence matrix so that the sum of its elements is equal to 1. Each element (r,c) in the normalized matrix is the joint probability occurrence of pixel pairs with a defined spatial relationship having gray level values r and c in the image. The command uses the normalized matrix to calculate properties presented in the table 13 [192].

Table 13 Properties of gray-level co-occurrence matrix with MATLAB.

Property	**Description**	**Equation**
Contrast	Returns a measure of the intensity contrast between a pixel and its neighbor over the whole image. Contrast is 0 for a constant image.	$\sum_{i,j} \lvert i-j \rvert^2 \, p(i,j)$
Correlation	Returns a measure of how correlated a pixel is to its neighbor over the whole image. Correlation is 1 or -1 for a perfectly positively or negatively correlated image. Correlation is NaN for a constant image.	$\sum_{i,j} \frac{(i-\mu i)(j-\mu j)p(i,j)}{\sigma_i \sigma_j}$
Energy	Returns the sum of squared elements in the matrix. Energy is 1 for a constant image.	$\sum_{i,j} p(i,j)^2$
Homogeneity	Returns a value that measures the closeness of the distribution of elements in the matrix to the diagonal. Homogeneity is 1 for a diagonal matrix.	$\sum_{i,j} \frac{p(i,j)}{1+\lvert i-j \rvert}$

The correlation between the images was obtained returns the correlation coefficient r between image A and image B, where A and B are matrices or vectors of the same size. r is a scalar double. The command corr2 from MATLAB computes the correlation coefficient using $rm \frac{\sum_m \sum_n (A_{mn}-\bar{A})(B_{mn}-\bar{B})}{\sqrt{(\sum_m \sum_n (A_{mn}-\bar{A})^2)(\sum_m \sum_n (B_{mn}-\bar{B})^2)}}$ where where $\bar{A}$ = mean2(A), and $\bar{B}$ = mean2(B). The

correlation was calculated the histogram of gray scale and for the blue component of every image with each one of the rest of the images.

Finally, the discrete Fourier transform (DFT) of X using a fast Fourier transform (FFT) algorithm, the general results from representation theory show that the filter functions implement a transform which has many properties in common with the well-known discrete Fourier transform. As is the case for the Fourier transform where the DFT can be computed efficiently by using the FFT, it can be shown here that the basic color filter operations can be optimized by computing intermediate results.

The Fourier Transform is an important image-processing tool, which is used to decompose an image into its sine and cosine components. The input image is the spatial domain equivalent and the output represents the image in the Fourier or frequency domain. In the Fourier domain image, each point represents a particular frequency contained in the spatial domain image. The Fourier Transform is used in a wide range of applications, such as image analysis, image filtering, image reconstruction and image compression.

The DFT is the sampled Fourier Transform and therefore does not contain all frequencies forming an image, but only a set of samples that is large enough to describe the spatial domain image. The number of frequencies corresponds to the number of pixels in the spatial domain image, the image in the spatial and Fourier domains are of the same size. For a square image of size N×N, the two-dimensional DFT is given:

$$F(k,l) = \sum_{i=0}^{N-1} \sum_{j=0}^{N-1} f(i,j) e^{-t2\pi\left(\frac{ki}{N}+\frac{tj}{N}\right)} \quad \text{.....eq. 25}$$

where *f(a,b)* is the image in the spatial domain and the exponential term is the basis function corresponding to each point *F(k,l)* in the Fourier space. The equation can be interpreted as the value of each point *F(k,l)* is obtained by multiplying the spatial image with the corresponding base function and summing the result.

The basic functions are sine and cosine waves with increasing frequencies, *F(0,0)* represents the DC component of the image that corresponds to the average brightness and *F(N-1,N-1)* represents the highest frequency. The Fourier image can be re-transformed to the spatial domain. The inverse Fourier transform is given by:

$$f(a,b) = \frac{1}{N^2}\sum_{k=0}^{N-1}\sum_{k=0}^{N-1} F(k,l)e^{-t2\pi\left(\frac{ka}{N}+\frac{lb}{N}\right)}$$ .....eq. 26

To obtain the result, a double sum has to be calculated for each image point. However, because the Fourier Transform is separable, it can be written as:

$$F(k,l) = \frac{1}{N}\sum_{b=0}^{N-1} P(k,b)e^{-t2\pi\left(\frac{lb}{N}\right)}$$, where $$P(k,b) = \frac{1}{N}\sum_{a=0}^{N-1} P(k,b)e^{-t2\pi\left(\frac{ka}{N}\right)}$$ .....eq. 27

With these formulas, the spatial domain image is transformed into an intermediate image using *N* one-dimensional Fourier Transforms. This intermediate image is then transformed into the final image, again using *N* one-dimensional Fourier transforms. The two-dimensional Fourier transform in terms of a series of *2N* one-dimensional transforms decreases the number of required calculations; the ordinary one-dimensional DFT has N^2 complexity. This can be reduced to $N\log_2 N$ by the Fast Fourier Transform (FFT) to compute the one-dimensional DFTs. There are various forms of the FFT but the restriction is the size of the input image that may be transformed, often to $N=2^n$ where *n* is an integer.

The Fourier Transform produces a complex number valued output image that can be displayed with two images, either with the real and imaginary part or with magnitude and phase. The Fourier domain image has a greater range than the image in the spatial domain and its values are usually calculated and stored in float values.

The mean in X-axis of the image in gray scale was obtained and the results were processed and analyzed. A smoothing spatial filter was used due to there is pixels where exist an abrupt change in the intensity of every plane.

All the programs were made on MATLAB, the programs read all the image files with the name respective, the program realizes its functions and save the data in text file, jpg or fig format conserving the name of the file, eventually, add an extra name to identify all the files and the results obtained.

CHAPTER IV

PRESENTATION, ANALYSIS AND INTERPRETATION OF DATA

In the case of development of an automated flow-based electrochemical aptasensor for on-line detection of Ochratoxin A, it was described the first automated flow-based electrochemical aptasensor. The applicability of the developed flow-based aptasensor was validated by detecting OTA in beer samples. The results demonstrate the improvement in the analytical performance of the method under batch condition. The incorporation of the aptamer into flow device has increased the sensitivity of the system to determine OTA at low concentration.

Before using the automated flow system for on-line detection of OTA, it was important to optimize the parameters that may affect the efficiency and the sensitivity of the flow-based aptasensor. The flow rate was the main instrumental variable; changes in carrier flow rate would improve the analytical performances like linear range, sample throughput and sensitivity.

A too high flow rate would damage or displace the functionalized MBs causing fluctuation in the current signal, while a lower flow rate could increase the reaction time leading to a signal tailing. The optimal parameters for the aptasensor in the flow system are for the injection rate of the beads, 0.20 µL/s. In the case of the flows stopped, 10 minutes is enough. To the substrate injection rate corresponds to 1.6 µL/s and washing flow, 0.83 µL/s.

A very high injection speed prevents that magnetic beads can be immobilized in the magnetic carrier attached to the flow cell, whereupon, the signal and the reproducibility of the aptasensor decreased. Hence, a flow rate of 0.2 µL/s was used to inject the beads on the electrode surface.

Direct competitive flow-based assay

The direct assay was based on the immobilization of aptamer modified magnetic beads on SPCE surface. Then, biotinylated and free OTA were allowed to compete to bind with the immobilized aptamer. Avidin–ALP conjugate was used to perform electrochemical detection. Under the optimized instrumental conditions, the electrochemical response of the aptasensor

was dependent on the formation of aptamer–OTA complex on the electrode surface, and the enzymatic activity was inversely proportional to OTA concentration in the sample, the figure 41 explained this process.

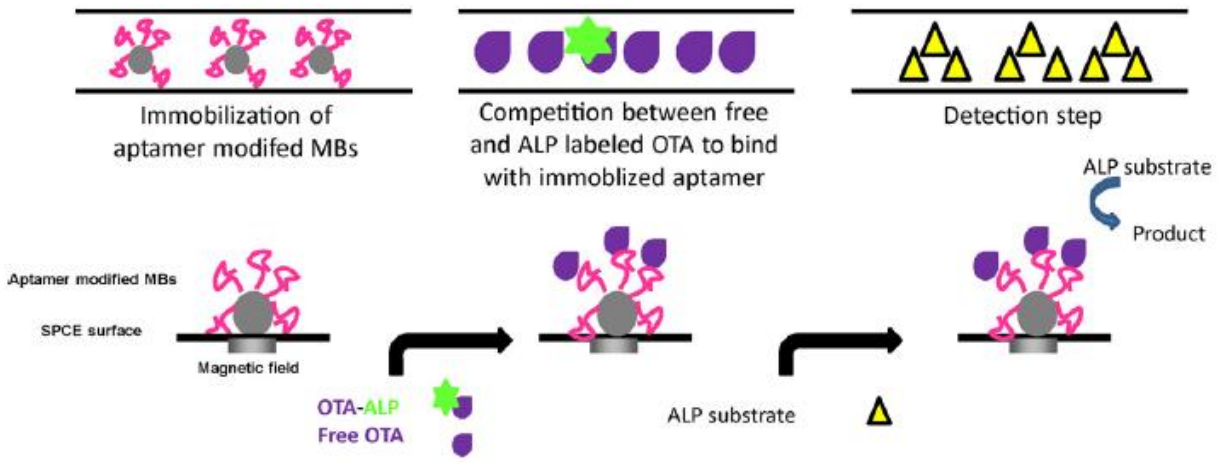

Fig. 41 Schematic representation of the principle for the automated flow system-based electrochemical aptasensor direct competition format.

To obtain optimal modified MBs concentration, experiments with aptamer modified MBs ranging from 1 µL to 3 µL were performed, the optimized volume found was 2 µL. Although high volume of modified beads could increase the signal value by increasing the immobilized aptamer concentration but decrease the sensitivity of the system by increasing background signal, while a lower volume could affect the linear range of the assay.

The dilution of OTA–biotine and avidin–ALP conjugates showed that a high concentration of both reagents could increase the signal intensity but decrease the specificity and sensitivity of the aptasensor. Best working dilutions were 1/30 for OTA-biotine and 1/12500 for avidin-ALP.

Although the amplitude is proportional to the concentration of the labeled OTA, high concentration may influence the specificity and sensitivity of the aptasensor. Due to non-specific adsorption of the OTA and/or ALP on the surface of the carbon electrode thus increasing the background noise.

In order to decrease analysis time, the generally used period of 30 and 45 min for aptamer-based assay was compared to a shorter period of 10 min during competition and avidin–ALP incubation steps but no significant difference in signal was observed. Therefore,

an optimal incubation time of 10 min was selected in both cases for the experiments. The decreased analysis time could be contributed to decreased diffusion distance and increase reactive surface in the flow system.

Therefore, electrochemical flow-based competition assays were performed using different concentrations of free OTA. The presence of OTA in solution prevented binding of the immobilized OTA to the aptamer, leading to a decrease of the ALP activity. The electrochemical detection was carried out using SPCEs to increase the sensitivity of the method.

The generation of the signal was based on the dephosphorylation of the non-electro-active substrate 1-naphtyl phosphate by ALP, followed by the oxidation of the electro-active product 1-naphtol phosphate to 1-iminoquinone on the electrode surface. The generated electrochemical signal was measured by amperometry after applying a working potential of 200 mV vs Ag/AgCl. The obtained enzymatic response was inversely proportional to the OTA concentration. The binding percentages were calculated and the calibration curve plotted in the figure 42.

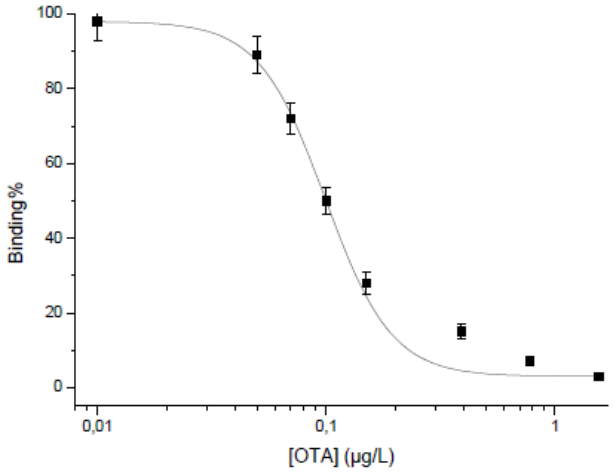

Fig. 42 Calibration curve for the aptasensor in direct flow-competition assay.

Higher binding percentages were obtained with decreasing OTA concentration. Due to the percentage error (5%), the limit of detection (LOD) was defined as the toxin concentration corresponds to the 80% of aptamer binding depending upon the maximum value of standard deviation. The calibration curve was fitted by the sigmoidal logistic four parameter-equation

$y = y0 + \left(\frac{a}{1} + \left(\frac{x}{x0}\right)^{b}\right)$, where a and y0 are the maximum and minimum values, respectively, b is the slope of inflection point, and x0 is the x value at the inflection point. A midpoint value (IC50) of 0.098 µg/L and a LOD of 0.06 µg/L were obtained during competition assays.

Indirect competitive flow-based assay

The indirect assay was based on the immobilization of OTA modified magnetic beads on SPCE surface. Then, the immobilized OTA on SPCE and free OTA in solution competed for the biotinylated aptamer in the solution. Afterwards, avidin–ALP conjugate was used to perform electrochemical detection, the process is in the figure 43.

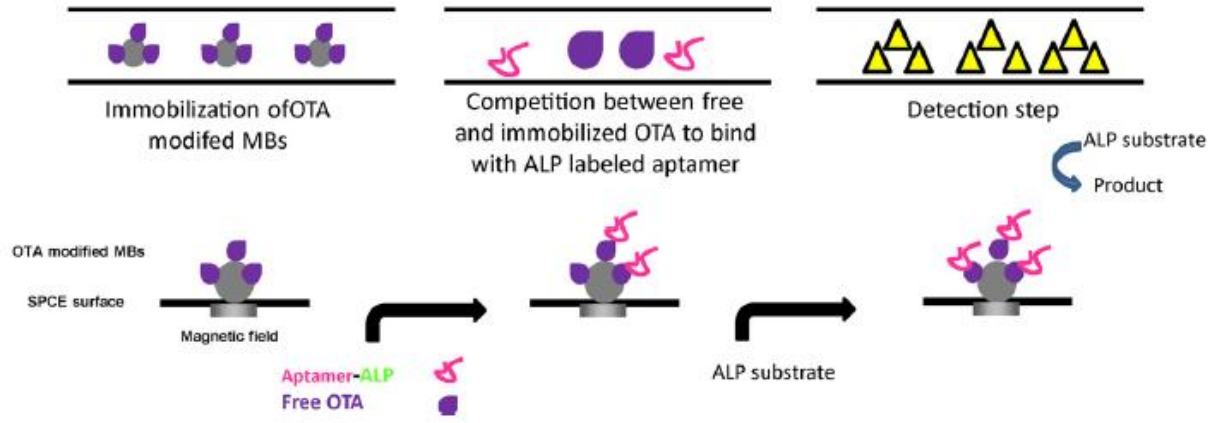

Fig. 43 Scheme of the principle for the automated flow system based indirect competition format.

Firstly, the quantity of OTA modified MBs was optimized by using different volumes of modified MBs. A high quantity of OTA modified MBs could increase the signal intensity, but decrease the sensitivity of the method by occupying most of aptamer's recognition sites and a low quantity of OTA on the electrode surface could decrease the sensitivity by reducing the linear range.

Therefore, an optimized working volume of 4 µL was selected. The current response was higher by increasing the aptamer concentration, but a decrease in LOD was observed. An optimized concentration of 150 nM was selected for electrochemical detection and an optimal incubation time of 10 min was found suitable for the experiments .

An indirect competitive assay was performed in a flow automated system, immobilized and free OTA in solution competed for labeled aptamer in solution (see figure 44).

Electrochemical detection was performed according to a similar procedure described in direct competitive format. A percentage error of 5% was found for the indirect competitive aptasensor. The LOD (0.05 µg/L) corresponding to 80% of binding, and IC50 (0.090 µg/L) corresponding to 50% of binding were calculated from the calibration curve presented in the figure 48, fitted by the sigmoidal logistic four parameter-equation.

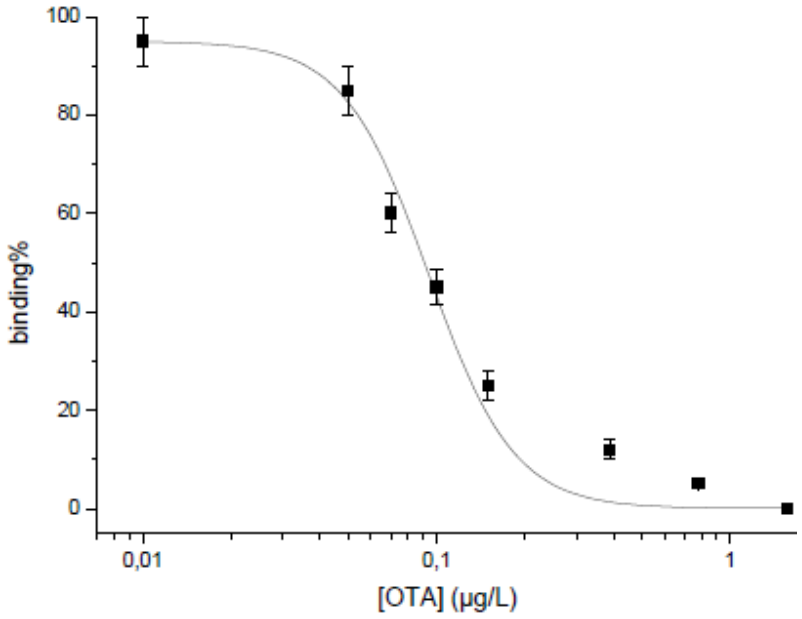

Fig. 44 Calibration curve for the aptasensor indirect flow-competition assay.

Reproducibility and specificity of the flow-based aptasensor

To investigate the reproducibility of the developed electrochemical aptasensor, three electrodes prepared under the same conditions used to detect the same concentration of OTA (0.5 µg/L). The coefficient of variation of inter assay peak current was 5%, showing the good precision and reproducibility of the proposed automated aptasensor.

To confirm that current signal was based on the specific interaction between aptamer and OTA and was not caused by non-specific adsorption of OTA, the aptasensor was incubated with a sample of 0.5 µg/L of OTB as non-specific analyte. No significant difference in binding percentage was observed before and after incubation with OTB. These results confirmed that decrease in the binding percentage observed with OTA were virtually due to specific OTA and aptamer complex formation.

Effect of matrix and applicability of the flow-based aptasensor in beer

To evaluate the feasibility of the proposed method for possible applications, the flow-based aptasensor was used for determining OTA in beer sample. Firstly, the beer sample was analyzed by HPLC–FLD and the chromatograms revealed the absence of OTA in beer. Then, OTA-free beer samples were spiked with two different known concentrations of OTA (0.2 and 0.8 µg/L).

The relative standard deviation (R.S.D) indicated the precision and the reproducibility of the flow-based aptasensor. The accuracy (R.E%) was obtained by comparing the spiked (0.2 and 0.8 µg/L) and the measured values (0.21 and 0.78 µg/L). The analytical results and the obtained recoveries percentages (R) are in the table 14.

Table 14 Recovery percentages with spiked OTA for indirect competition assay.

Concentration spiked OTA (µg/L)	**Found OTA concentration (µg/L)**	**R.S.D (%)**	**R.E (%)**	**R (%)**
0.2	0.21	5	5	105
0.8	0.78	4	5	97.5

The spiked values were consistent with the obtained concentrations of OTA. The developed flow-based method could therefore be applied in a rapid and simple detection of OTA in real samples.

PART A

Absorbance based on LEDs and photodetectors

Before to start the experiments and to choose the photodetector or the CMOS image sensor, the spectrum of different emitters were evaluated with an UV-VIS spectrophotometer (Ocean Optics USB2000, Dunedin, FL, USA). The results are in the figure 45.

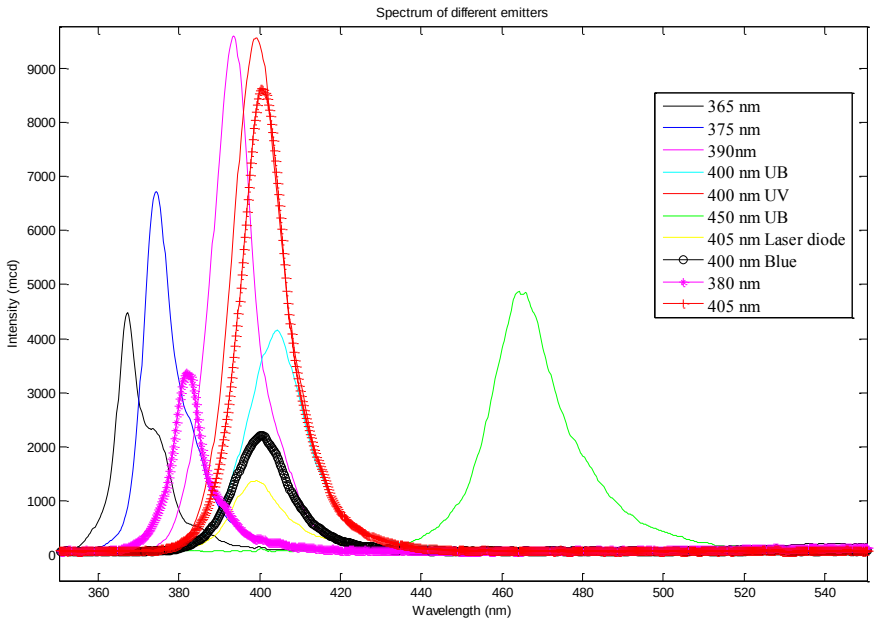

Fig. 45 Spectrum of different emitter.

The word UB indicated that the LED evaluated is an ultra-bright LED. The LEDs at 365,375,390,400 UB, 400 UV, 450 UB were acquired from AG company (Mexico), The LED at 400 nm correspond to the blue color. From RS, the diode laser at 405 nm was obtained. Two more LEDs were evaluated, one of 5 mm (405 nm) and one of 3 mm (380 nm) both from Newark company.

Analyzing the data, the LED at 390 nm and the UV-LED at 400 nm provides the maximum intensity, as well as the LED at 405 nm. The less intensity is provides by the laser diode at 405 nm. Follow by blue LED at 400 nm, LED at 380nm, UB- LED at 400 nm and the LED at 365 nm.

The UB-LED at 400 nm in cyan color shows displacement to right side, but the great displacement is present in the UB LED at 450 nm due to the peak wavelength is at 470 nm, approximately.

4.1 Detection of pesticides using a phototransistor and a LED

The optical spectroscopy is an analytical method, which involves the measurements of light quantity with the properties of matter. Considering that, any optical device utilizes a light source, wavelength selection device, a detector and signal process. In this work, our source of light is a specific wavelength device, for this reason three commercial LEDs were characterized (Newark element14, Mouser electronics, AG Electronica) the wavelength range was 400 to 450 nm and 450 to 500nm. The spectrum of the emitters is in the figure 46. A spectrophotometer (Ocean Optics USB2000, Dunedin, FL, USA) was used to measure the LED emission spectra.

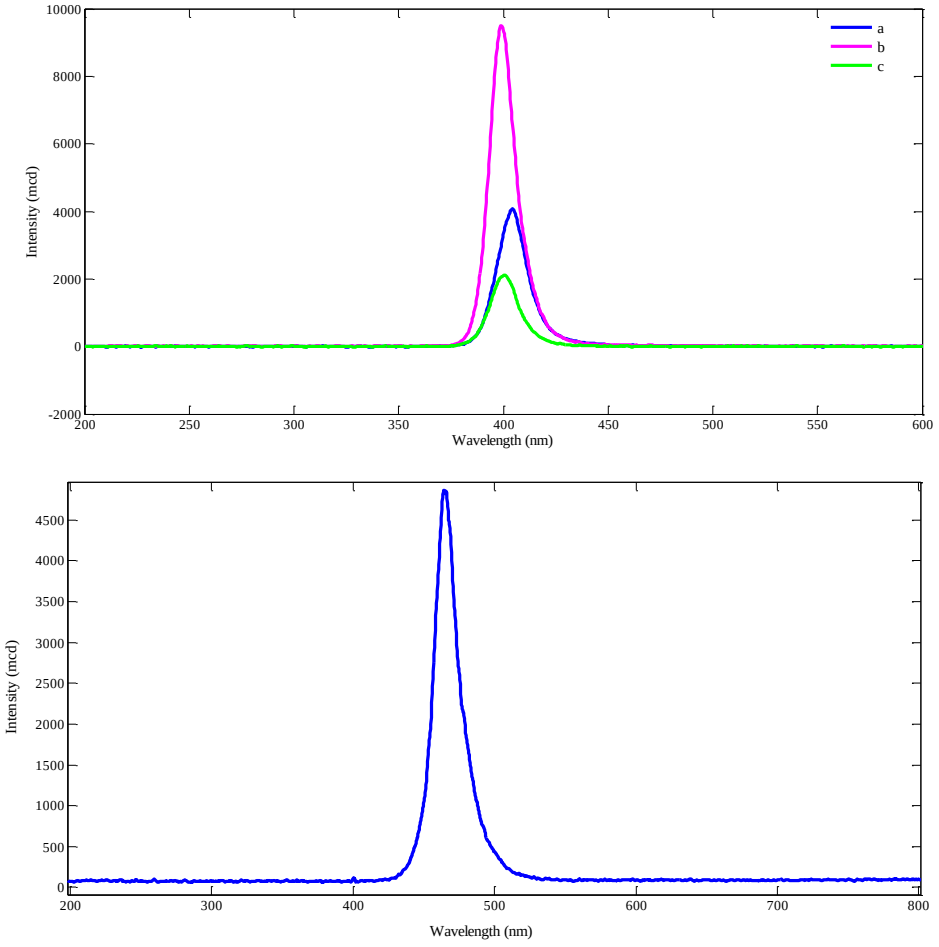

Fig. 46 (a) Emission spectrum of three LEDs ((a)–(c)) to wavelength range 400 to 450 nm. (b) Emission spectrum of an LED to wavelength range 450 to 500 nm.

Acetylcholinesterase inhibition percentage was determined by absorbance variation measurements. The figure 47 shows the measurements of enzyme activity for EE (electric eel) and the blank, besides the stability and reproducibility of the developed system.

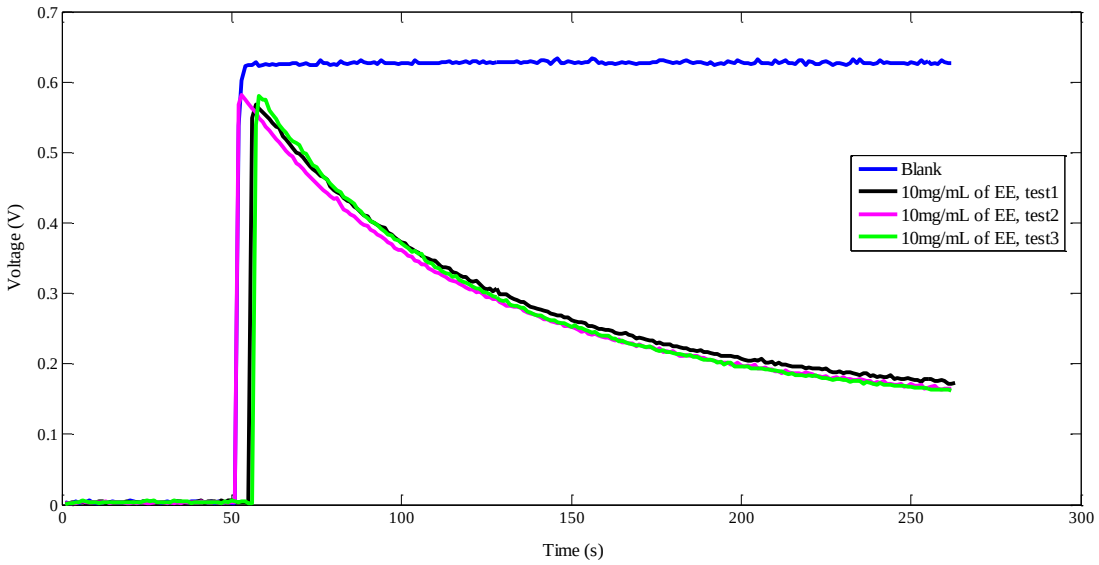

Fig. 47 Stability and reproducibility of the system for the blank data and the EE enzyme.

The developed system showed stability and reproducibility in the samples tested. The limit of detection (LOD) for the enzymatic activity between the developed system and the commercial spectrophotometer is in the figure 48. The LOD of the enzymatic activity for the developed system was 6.91×10^{-4} Absorbance Units/s and for the commercial equipment was 2.29×10^{-3} Absorbance Units/s.

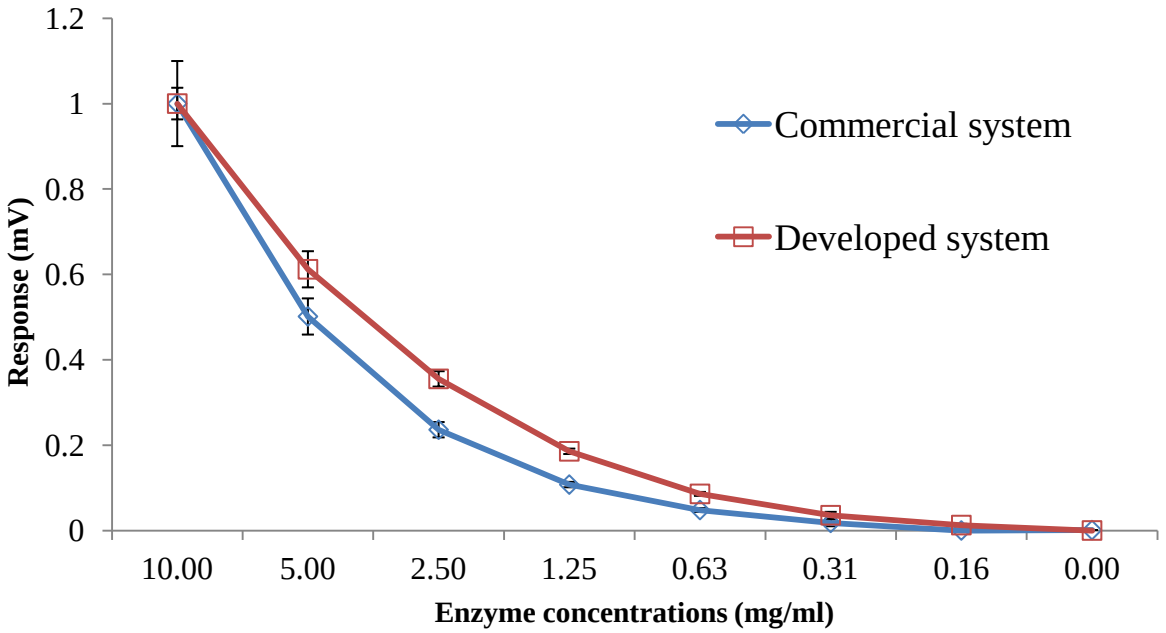

Fig. 48 Comparison of the LOD for the spectrophotometer and developed optical system to low concentrations.

Later, the inhibition curves obtained with optical system for the enzymes (EE, *D. melanogaster* (DM) and genetically-modified *D. melanogaster* (G-DM) were evaluated to calculate their inhibition constants. To estimate the *Ki*, a spectrophotometric plot of residual activity versus incubation time was performed for each pesticide and enzyme, the method employed in the determination of inhibition constants was previously described, an example is malaoxon pesticide, it was assayed for the electric eel presented in the figure 49, each plot was linear and values for the reaction rate were obtained from the linear correlation slope [24,25].

In the absence of inhibitor, the activity remained almost unchanged. The slope values were directly proportional of the pesticide concentrations, and the inhibition constants were obtained by plotting 1/slope versus 1/[Concentration], for each AChE tested. Then, *Ki* was calculated from slope of this relation.

The inhibition effect of paraoxon, malaoxon and carbofuran toward EE, B131 and B394 is shown in the figure 50. The LOD with the spectrophotometer and the developed system are comparable, considering the drawbacks of the commercial system. The advantages of the developed system are its sensitivity, stability and reproducibility; the proposed system is more sensible to low concentrations than the spectrophotometer.

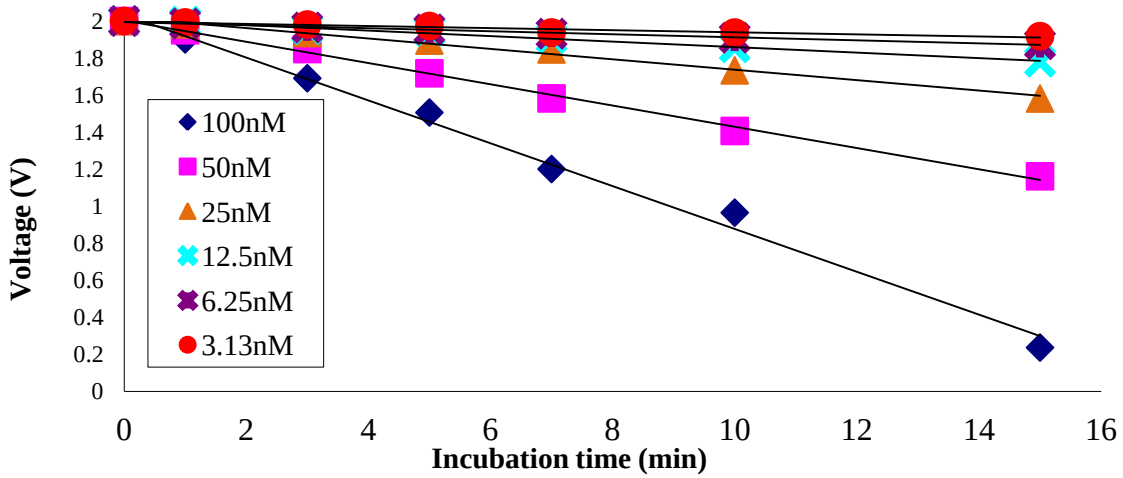

Fig. 49 Kinetic inhibition of electric eel against malaoxon pesticide in different concentrations obtained with the developed system.

The developed system shows more linearity for carbofuran, mainly for the B394 (r = 0.9994), B131 (r = 0.9282) and EE (r = 0.9057). Malaoxon has a lineal relation in the case of EE (r = 0.9950) and B131(r = 0.9604). In the case of paraoxon, its linearity is better for B131(r = 0.9964) and EE (r = 0.9810); the B394 presented more instability during the experiments than the other enzymes.

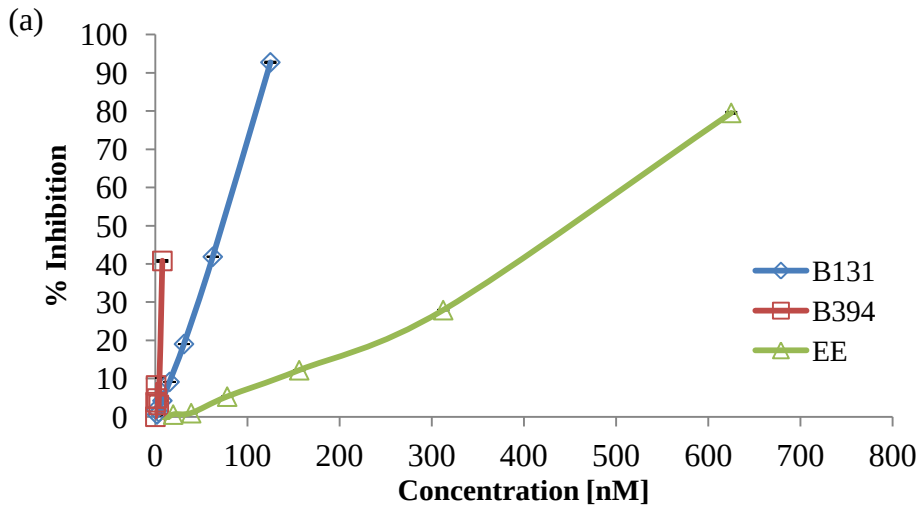

(b)

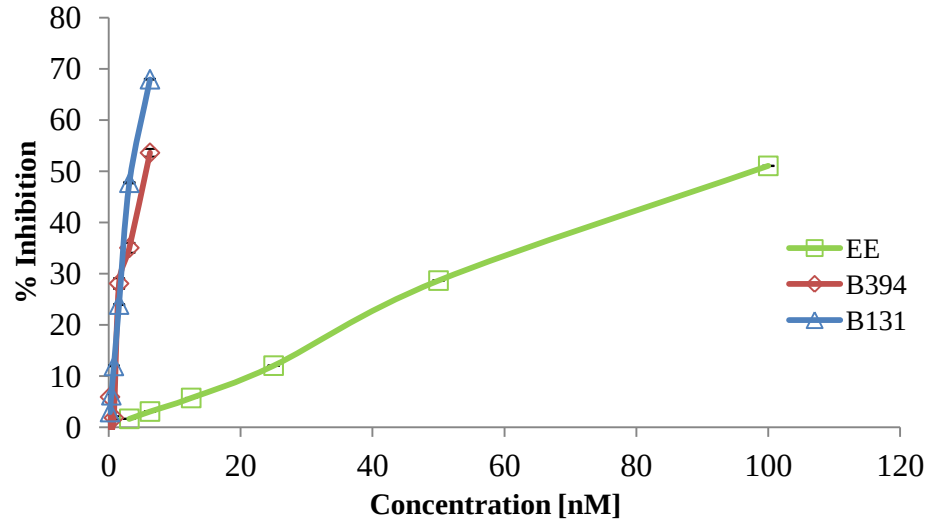

(c)

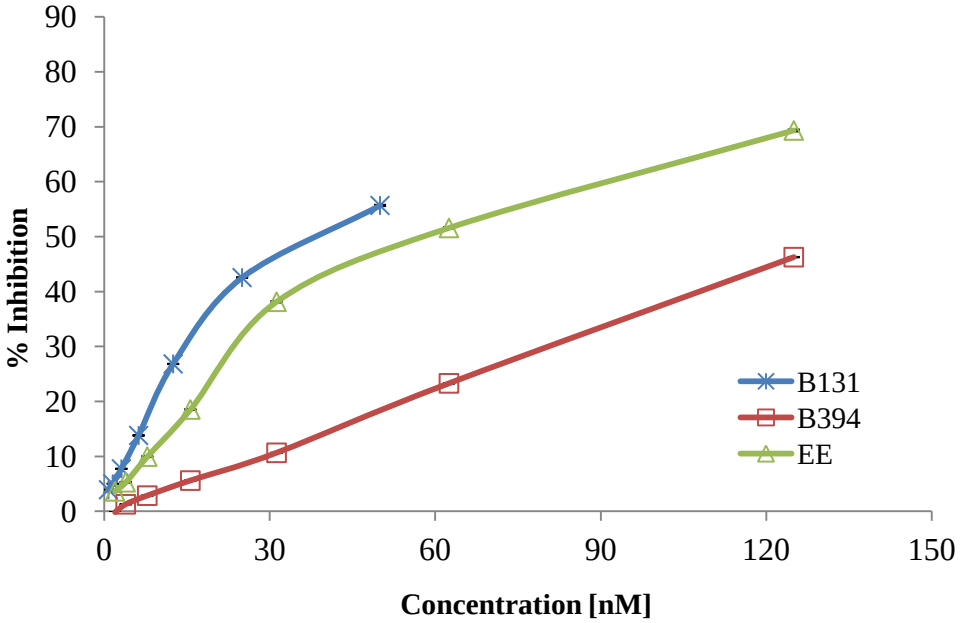

Fig. 50 Inhibition curves of AChE biosensor by the pesticides: (a) paraoxon, (b) malaoxon and (c) carbofuran after incubation for 10 min for each enzyme used.

The values of *Ki* for carbamate and organophosphate pesticides reported [193] are comparable with the *Ki* obtained with the developed system. As expected from the values of inhibition rate constants, which are summarized in the table 15, the inhibitory effect of carbofuran on the Genetically-modified D. melanogaster (B394) was weaker than the electric eel and the D. melanogaster wild-type (B131). In the other hand, it was observed a high sensitivity of B394-AChE toward the two organophosphate pesticides.

Table 15 Ki for pesticides						
Enzymes	**Carbofuran**		**Malaoxon**		**Paraoxon**	
	K_i	$K_{i\text{Obtained}}$	K_i	$K_{i\text{Obtained}}$	$K_{i]}$	$K_{i\text{Obtained}}$
EE	4	3.3	2.98	1.25	1.6	13
B131	6	3.3	---	33.3	---	1.1
B394	1.3	1.4	---	2.5	---	13

The LOD of the developed system and the electro-chemical method is reported in the table 16. In the case of the developed system, the lowest LODs were obtained for the carbofuran with B394. In the case of carbofuran with EE and B131, the system works in the same range of concentration detected by specialized systems. For the maloxon, the LOD values were lower than the results found in previous works. With the paraoxon, the developed system detected the lowest LOD for EE and this is the lowest value for the three enzymes and pesticides. The results were obtained with a system that is easy-to-use, cheap and portable. These results are comparable with robust and specialized equipment.

Table 16 Limit of detection [nM]						
Enzymes	**Carbofuran**		**Malaoxon**		**Paraoxon**	
	LOD	LOD_{Obtained}	LOD	LOD_{Obtained}	LOD	LOD_{Obtained}
EE	38	7.81	----	25	----	156
B131	4.5	6.25	----	0.78	----	31.3
B394	50	31.3	0.1	1.56	10	7.80

To demonstrate the viability of the developed system, it was utilized to detect pesticides in real samples, like river water. Samples were prepared with water from the lake of Villeneuve de la Raho (France). The samples were previously analyzed and spiked with carbofuran, malaoxon and paraoxon. The values obtained with the developed system in buffer were comparable with the values in real samples; the comparison yield is showed in table 17. The values in the limit of detection in real samples were similar to the samples worked in the laboratory for the commercial spectrophotometer and the developed system. In the real

samples, the inhibitory effect was not observed, hence it was no required to filter or pre-treat the sample, the samples were doped with known concentrations of pesticides.

Table 17. Limit of detection obtained in spiked samples,

Enzymes	Developed system in buffer [nM]			Developed system in spike samples[nM]			Comparison yields %		
	Carbofuran	Malaoxon	Paraoxon	Carbofuran	Malaoxon	Paraoxon	Carbofuran	Malaoxon	Paraoxon
EE	7.81	25	156	7.7	24.5	154	98.59	98.00	98.72
B131	6.25	0.78	31.3	6	0.77	31	96.00	98.72	99.04
B394	31.3	1.56	7.8	31	1.5	7.6	99.04	96.15	97.44

4.2 Detection of OTA using a photodetector and UV-LED

Four UV-LED were employed, it used a rate of 1000 samples per second and the time of acquisition was ten minutes. This process was repeated three times for each UV-LED, the mean and standard deviation for the UV-LED is in the table 18. Each concentration was excited with an UV-LED and the photodetector was positioned to 180 ° from the emitter. In this case, the photodetector captures the absorbance of the UV light (intensity of fluorescence) through to the samples and provides a relation with the fluorescence of the concentration in voltage value. The same principle described in the section 3.1.3 is used, except that in this case the emitter is a UV-LED.

The relation between the concentration and the intensity of fluorescence by UV-LED is in the figure 51. There is a linear relation; the problem is that the intensity of each concentration detected with the photodetector is a very small value, in spite of use amplification circuit, the voltage increase but the values between the concentrations are so close. This system does not have the potential to identify concentrations less than 250 ng/mL.

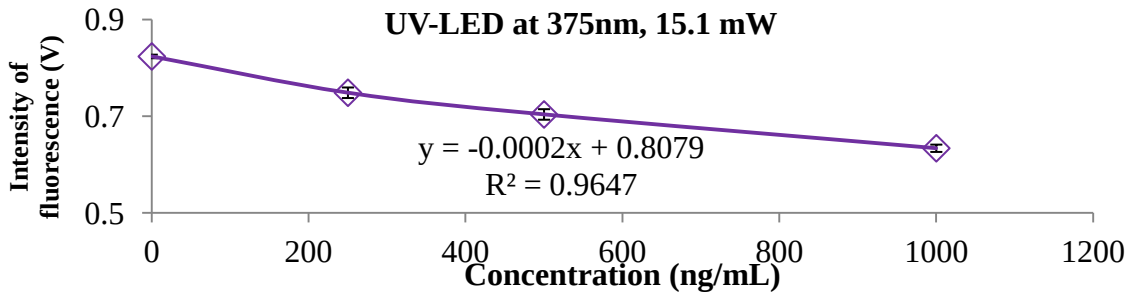

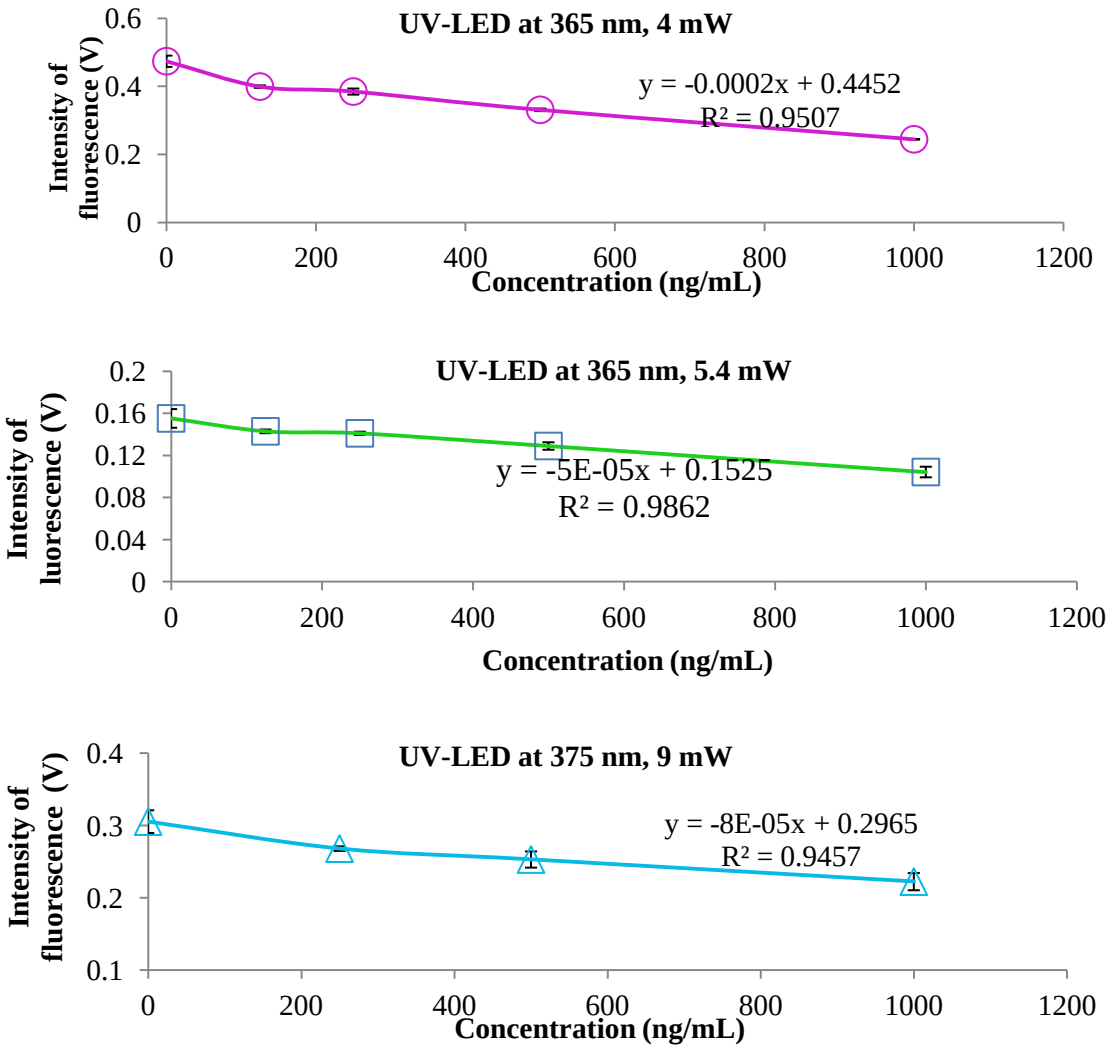

Fig. 51 Lineal relation between the concentrations of OTA versus the intensity of fluorescence detect by a photodetector.

Table 18 Absorbance of each OTA concentration for the UV-LED.

Detector		**Absorbance (V)**				
Λ (nm)	**Radiant flux (mW)**	**Blank**	**1000 ng/mL**	**500 ng/mL**	**250 ng/mL**	**125 ng/mL**
375	15.1	0.8239 ±0.0037	0.6339 ±0.0075	0.7039 ±0.0108	0.7488 ±0.0109	0.7456 ±0.0121
	12	0.1155 ±0.0060	0.0925 ±0.0024	0.1019 ±0.0003	0.1087 ±0.0001	0.1012 ±0.0002
	9	0.3053 ±0.0157	0.2224 ±0.0118	0.2530 ±0.0111	0.2680 ±0.0031	0.2650 ±0.0015
365	5.4	0.1551 ±0.0088	0.1042 ±0.0050	0.1290 ±0.0035	0.1409 ±0.0016	0.1428 ±0.0018
	4	0.4735 ±0.0166	0.2441 ±0.0004	0.3308 ±0.0037	0.3844 ±0.0089	0.3990 ±0.0035

The UV LED at 375nm, 12mW was discarded due to the standard deviation to the voltages obtained for the concentration was ± 0.009; the behavior is in the figure 52. Although the value of the voltage of each concentration can be considered, as there is no variation in the light detect by the photodetector. It must not be omitted, due to a small variation was observed because despite being a very small variation, this was shown repeatability in each of the tests (nine in total), these showed repeatability and reproducibility and values were within the range of the standard deviation as the figure 53 presents, it shows a cycle, where all the concentrations and the blank were repeated three times.

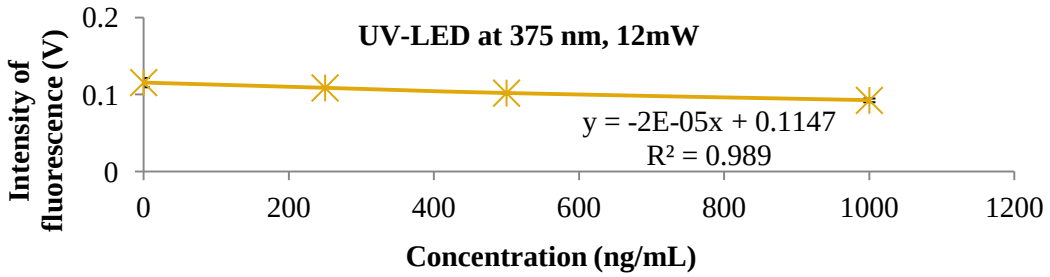

Fig. 52 UV-LED discarded due to the variation was considered without changes.

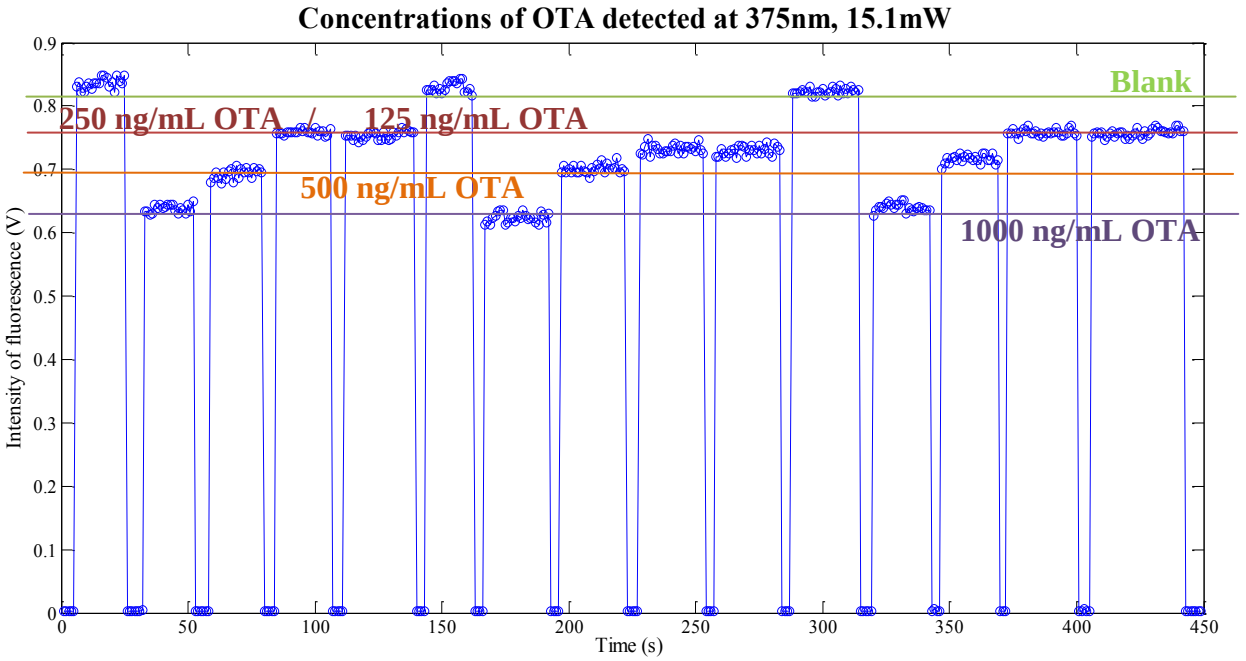

Fig. 53 Concentration of OTA versus the intensity of fluorescence in voltage value.

PART B

Fluorescence with CMOS sensor

Before to start the experiments and to choose the CMOS image sensor, the excitation spectrum of 1 mg/mL of OTA at different wavelength were evaluated in the UV-VIS spectrophotometer USB2000, the results are presented in the figure 54. Where is possible to see the response of the OTA at different wavelength. The maximum excitation is at 330 nm, followed by 365 nm.

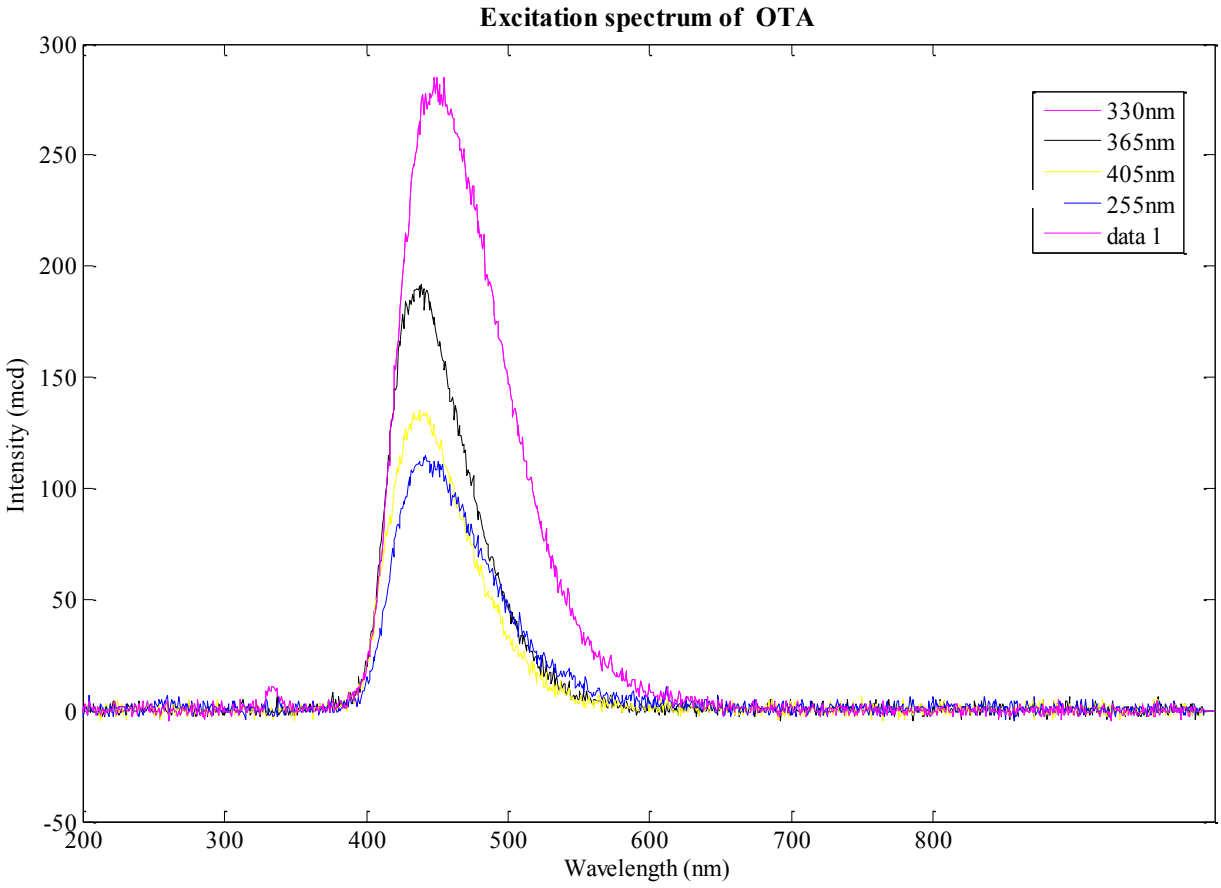

Fig. 54 Representation of the excitation spectrum of OTA excited at different wavelength.

Five UV-LEDs were used to build the calibration curve, these will be mentioned as follow together its principal characteristics such as the code of identification, the wavelength peak and the radiant flux described in the table 19. At the wavelength range of 360-380 nm, 30 nm more than the standard wavelength employed in the HPLC to quantify OTA. A UV-LED at 330 nm cost 120 euro plus taxes and shipment. The five led were through hole and 5 mm was its size.

Table 19 Characteristics of the UV-LEDs.

Identification code	Wavelength range (nm)	Radiant flux (mW)
NSHU551A	370-380	12
NSHU551B	360-370	5.4
NSHU591A	370-380	9
NSHU591B	360-370	4
NSPU510CS	370-380	15.1

4.3 Calibration of OTA using ArduCAM fluorescence set up

4.3.1 Samples of OTA prepared in Ethanol (EtOH)

OTA standard solutions were prepared from the stored stock solution of OTA (1 mg/mL). To construct five points of calibration curve, various OTA dilutions were prepared at different concentrations such as 40, 20, 10, 5, 2, 1 µg/L. Each of the OTA sample was in a cuvette and the fluorescence imaging was performed to find out the RGB components distribution in the sample. The calibration curve built based on the RGB values obtained process the image. To process the image is selected the area with the fluorescence as the figure 55 and 56 represent and obtain the RGB values and diagram.

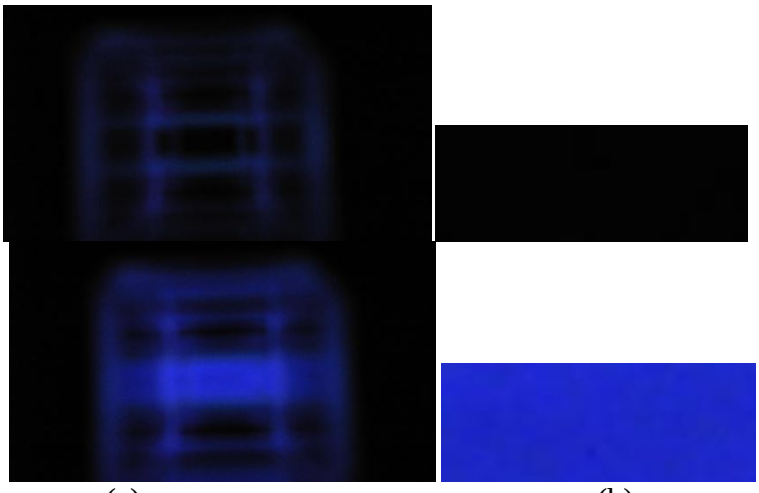

(a) (b)

Fig. 55 The top image corresponds to 1 ml of EtOH. The concentration of 40 µg/L of OTA in EtOH presented in the bottom image. (a) Image provides by the ArduCAM; (b) The area selected with the presence of fluorescence provided and saved by the GUI.

The figures 57 to 61 show the behavior of the OTA concentrations excited at specific wavelength and radiant flux emitted by the UV-LED. In the figure 57, with the UV-LED NSHU551A is possible to see the images capture with the ArduCAM respect to each concentration and the process to acquire and display the image in the ArduCAM is no good in the absence of light, the image is pixilated and poor quality even though a sensor of 5 MP was used. Besides, the image is very dark and the cuvette is not defined completely, producing confusion to select the fluorescence strip.

It is no possible to identify (figure 57) the low concentrations in spite of the good coefficient of linear correlation $R^2 = 0.9792$ and the equation of the linear fit is y=5.2041x-3.0333. Despite all the disadvantages, its three components were plotted and it is perceivable that the blue component protrudes con respect to the red and green component. The mean standard deviation corresponds to ±1.16, been the biggest for the high concentrations (20 and 40 µg/L) ±3.61 and ±1.62, respectively.

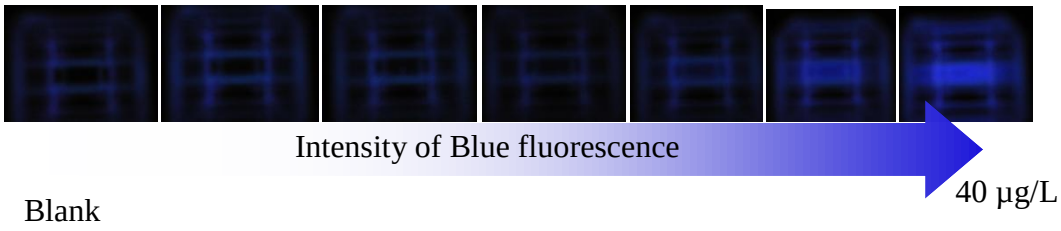

Fig. 56 Increase of the fluorescence depends of the concentration of OTA in the sample.

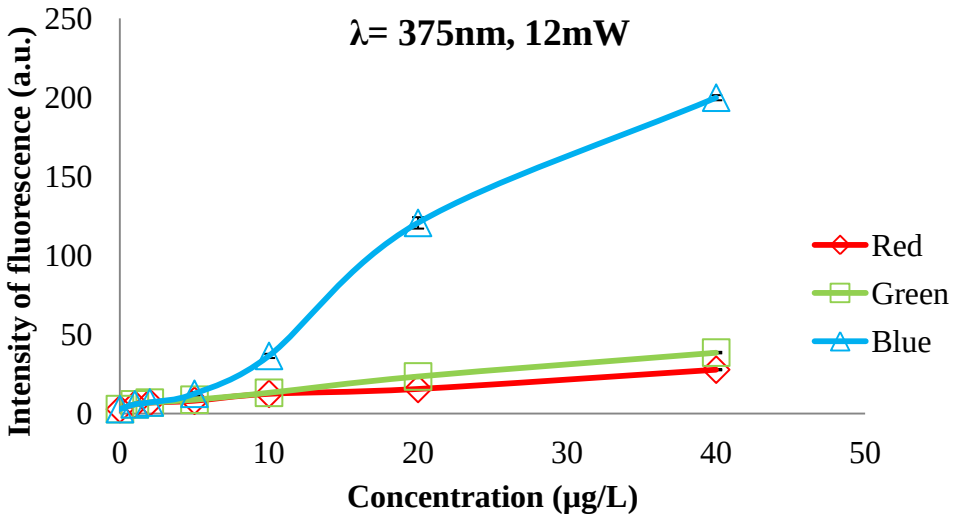

Fig. 57 Calibration curve with the NSHU551A UV-LED.

Employing the UV-LED at 365 nm with a radiant flux of 5.4 mW, its linear range was improved in the range concentrations of 10-40 µg/L gave a R^2=0.9694, due to this wavelength peak is close to the wavelength range employed in the HPLC, the radiant flux is not enough to identify the low concentrations, the results are presented in the figure 58, one objective of this thesis work. The standard deviation for the concentrations is ±0.09, ±0.15,±1.08,±1.38,±3.06,±2.57 and ± 0.02, respectively, considering the blank.

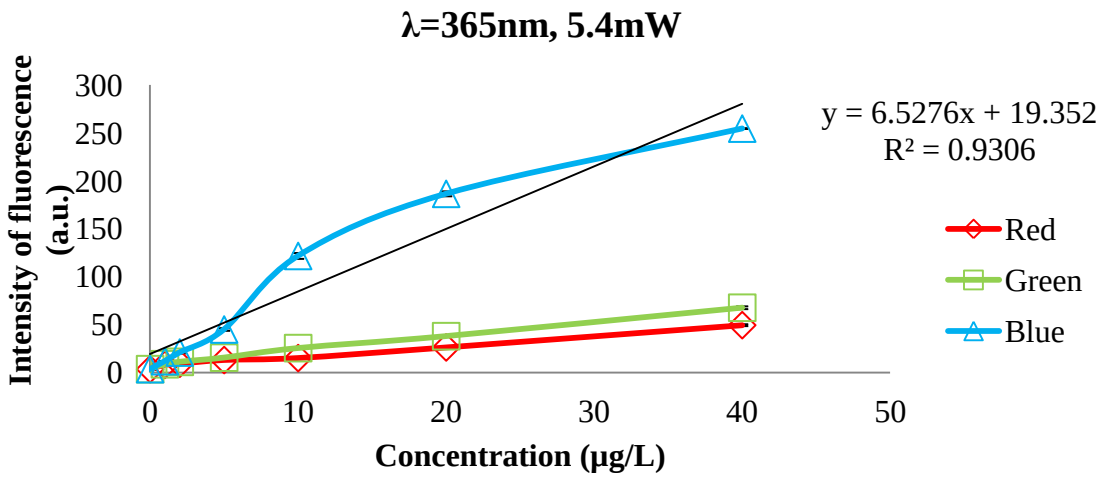

Fig. 58 Calibration curve with the NSHU551B UV-LED.

In the figure 59, the LED at 375nm to 9mW present the best results to detect the low concentration with a linear range of 2-40 µg/L of OTA with a R^2=0.995 and the lineal fit is y=5.4821x-4.5179. Even though is 45 nm more than the 330 nm used in the HPLC, but other wavelengths are used as in the section 2.2 or 2.8.1 was mentioned [10,33,108, 16, 109]. Hence, this wavelength for us experimental shows the best results to detect low concentration of OTA using the ArduCAM fluorescence set-up.

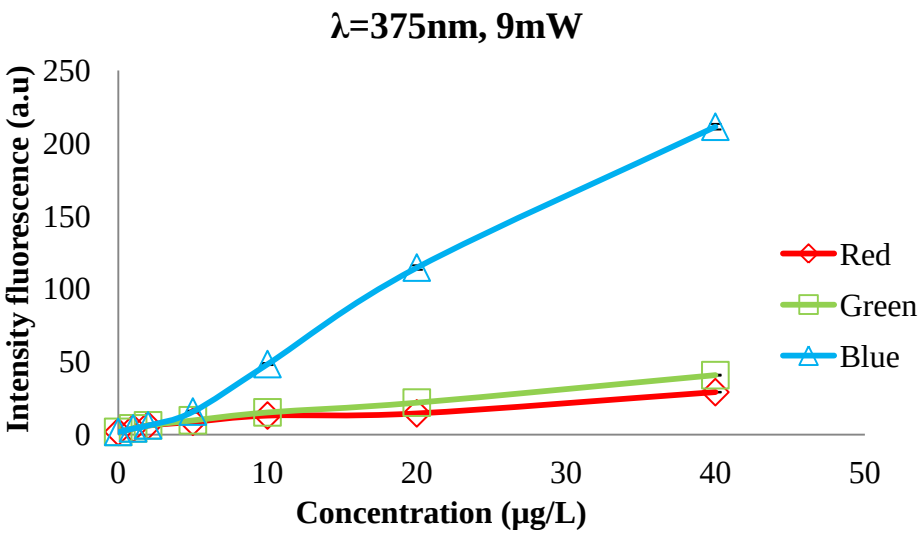

Fig. 59 Calibration curve with the NSHU591A UV-LED.

The LED named NSHU591B at 365 nm and 4 mW of radiant flux shows good linear correlation in the figure 60 for concentrations 2 to 40 µg/L of OTA but the values are so close that it is difficult to quantify this concentrations with an error of ±0.16, ±0.10 and ±1.13 for 2,5 µg/L, respectively.

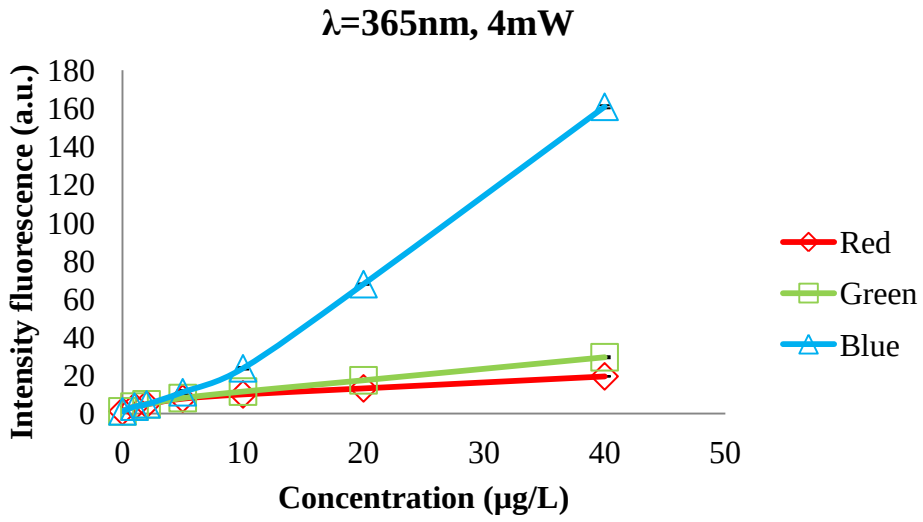

Fig. 60 Calibration curve with the NSHU591B UV-LED.

The UV LED NSPU510CS presents the biggest radiant flux (15.1mW), the intensity of the UV-LED is so high that the intensity saturated the image sensor of the ArduCAM in the highest concentrations, the value do not present changes for concentrations greater than 10 µg/L in the blue component. Nevertheless, the green component shows a lineal correlation that corresponds when OTA in acid medium due to OTA shows green fluorescence. This is because the intensity of the LED is so high that the color emitted by LED (green color) produces an acid medium in the OTA solution as the figure 61 demonstrates.

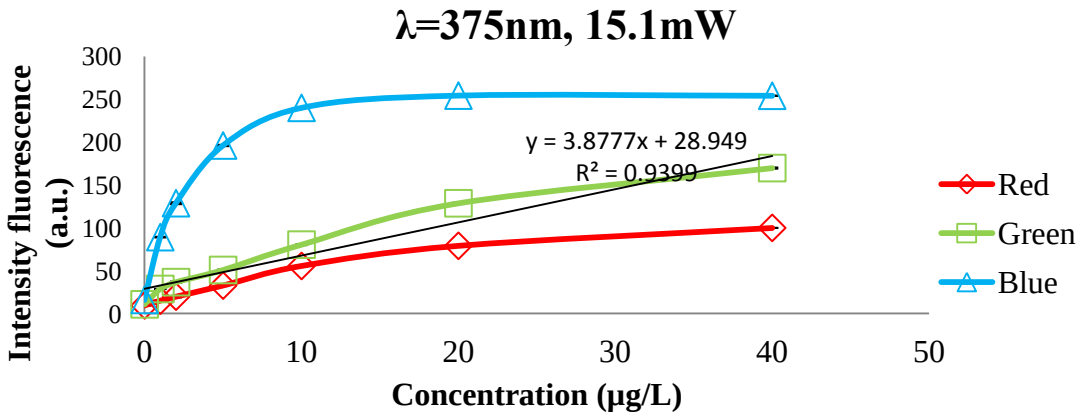

Fig. 61 Calibration curve with the NSPU510CS UV-LED.

The table 20 summarized the linear range and equation as well as the coefficient correlation lineal for the five LEDs used to build the calibrations curves.

Table 20 Linear range of different LED characterized.

Peak wavelength (nm)	Radiant flux (mW)	Linear range (µg/L)	Linear equation	R^2
375	9	2-40	5.4821x-4.5179	0.9950
	12	2-40	5.2041x-3.0333	0.9792
	15.1	1-5	33.391x+40.606	0.9160
365	4	2-40	4.1973x-10.901	0.9900
	5.4	10-40	4.2823x+87.73	0.9694

4.3.2 Samples of OTA prepared in Methanol (MeOH)

The same methodology as the samples in EtOH was follow for analyze the samples prepared in Methanol, all the solutions were tested in a continuous way. In this case, the

ArduCAM presents less resolution and intensity for these samples. Its means that the image sensor reduces its quality with the long-term use. There is no linear range for the concentrations 2-20 µg/L or correlation between the concentrations of OTA and the blue fluorescence, only, the blue fluorescence is greater than the red or green components as the figure 62 and 63 present.

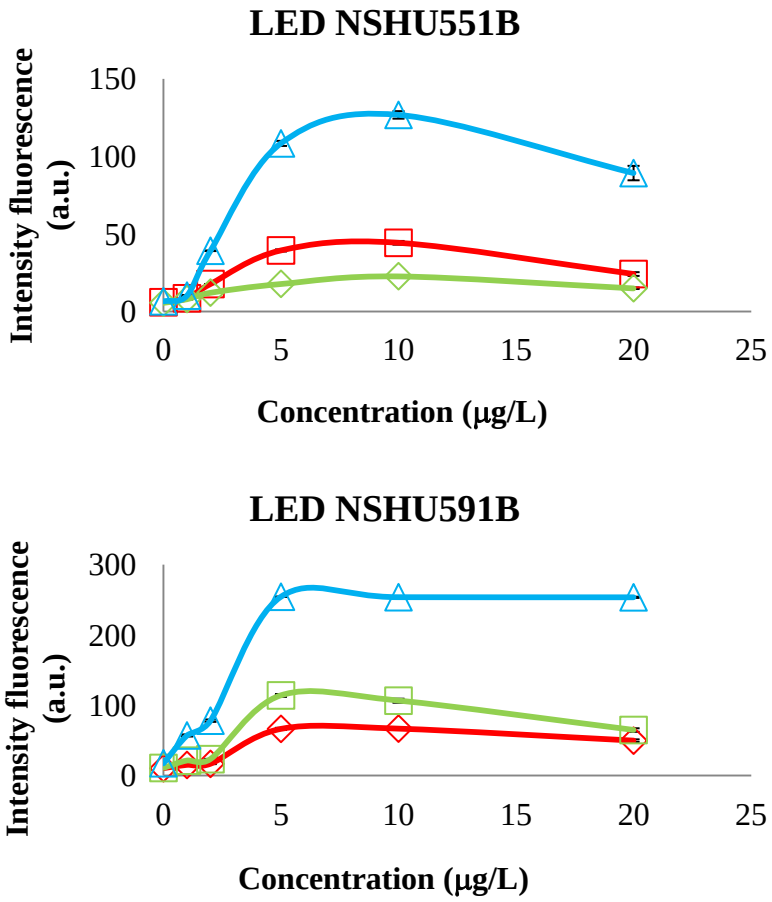

Fig. 62 UV- LEDs at 365 nm. blue Δ refers to the blue component; green □ is related with the green component. Finally, the red compontent was represented as ◊.

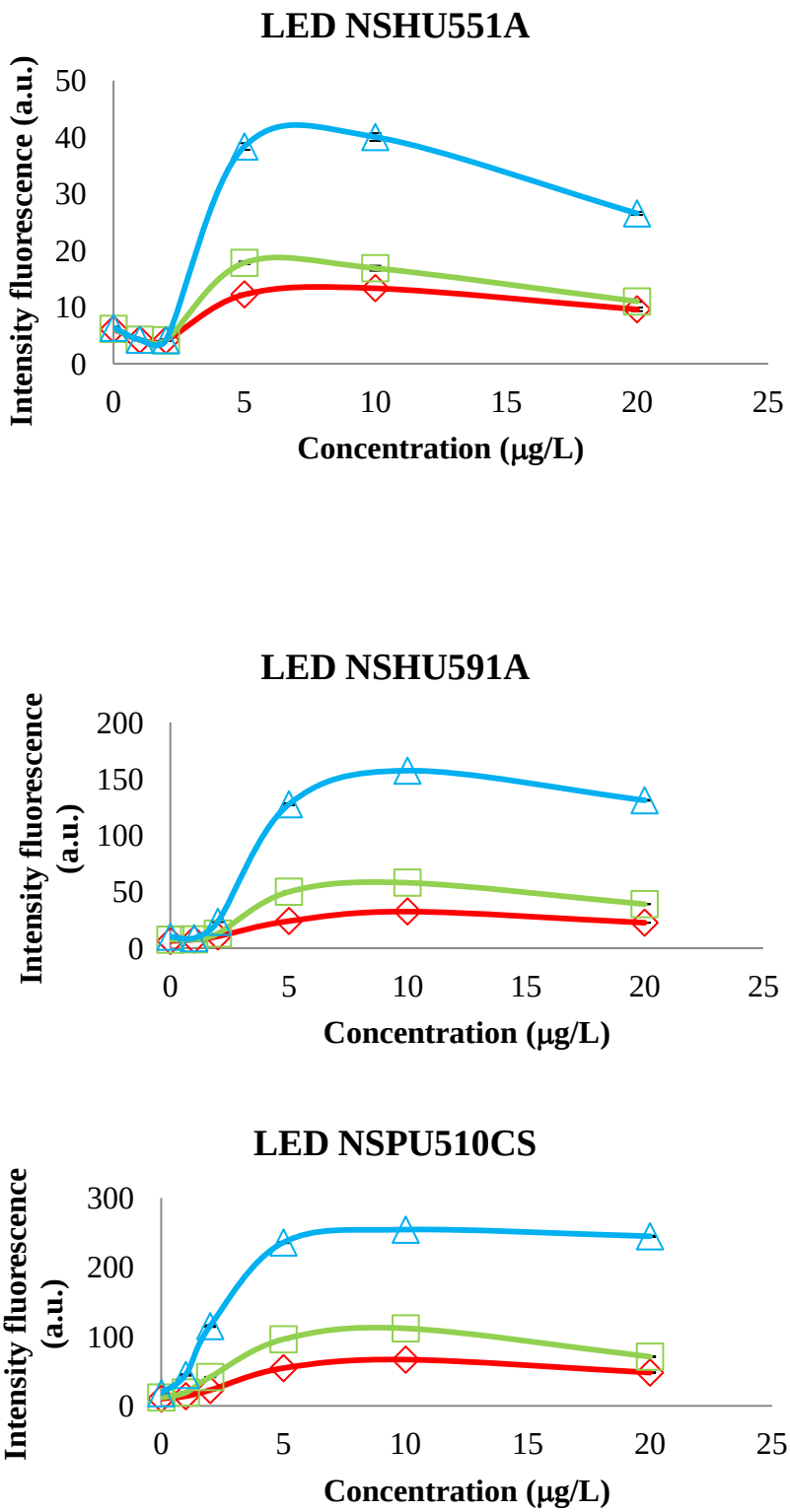

Fig. 63 UV- LEDs charaterized samples of OTA in MeOH at 375 nm. blue Δ refers to the blue component; green □ is related with the green component. Finally, the red compontent was represented as ◊.

The data were normalized for the three components but only for the blue component the results will be presented, ethanol and methanol samples. The normalization of the data consisted of the value provides for each concentration of OTA subtract the value of the sample of Ethanol tested with the fluorescence set-up developed. The figure 64 shows the data normalized and the table 21 presents how affected the normalization to the data.

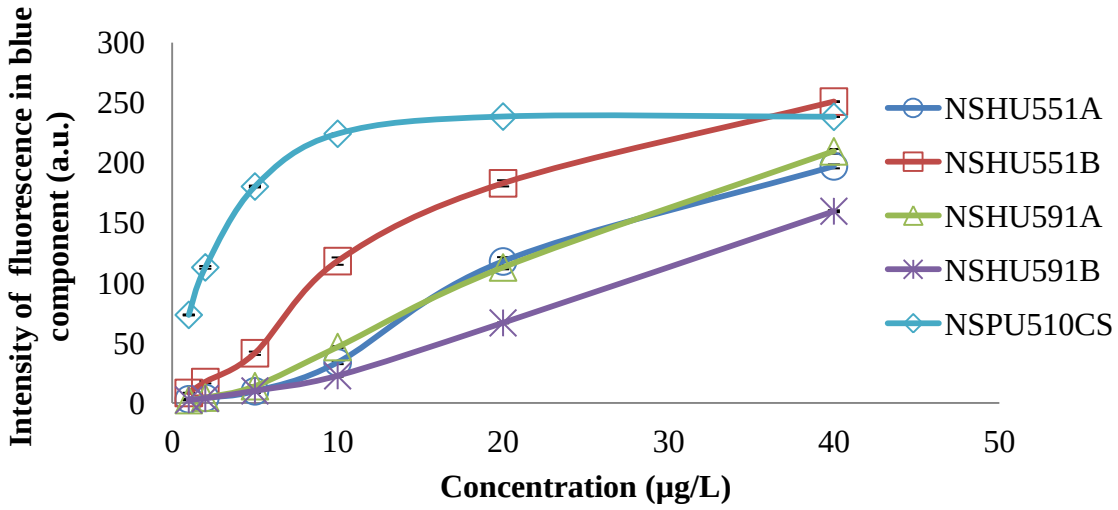

Fig. 64 Response normalized of the UV- LEDs characterized samples of OTA in EtOH.

Table 21 Data normalized for fluorescence provides by the blue component.

LED	Linear range (µg/L)	Linear equation	R^2
NSHU551A	2-40	5.2714X-7.6132	0.9785
NSHU551B	10-40	4.2823x+84.091	0.9694
NSHU591A	2-40	5.4821x-6.2916	0.9950
NSHU591B	2-40	4.1973x-12.1180	0.991
NSPU510CS	1-10	16.006x+75.642	0.9194

In the case of methanol, the results are presented in the figure 65, due to the blank preset values higher that the samples with OTA, to normalized the data this values generated a negative value but it is no possible to appreciate a linear relation, we considered the motive is the continuous use and excitation with UV affected the image sensor.

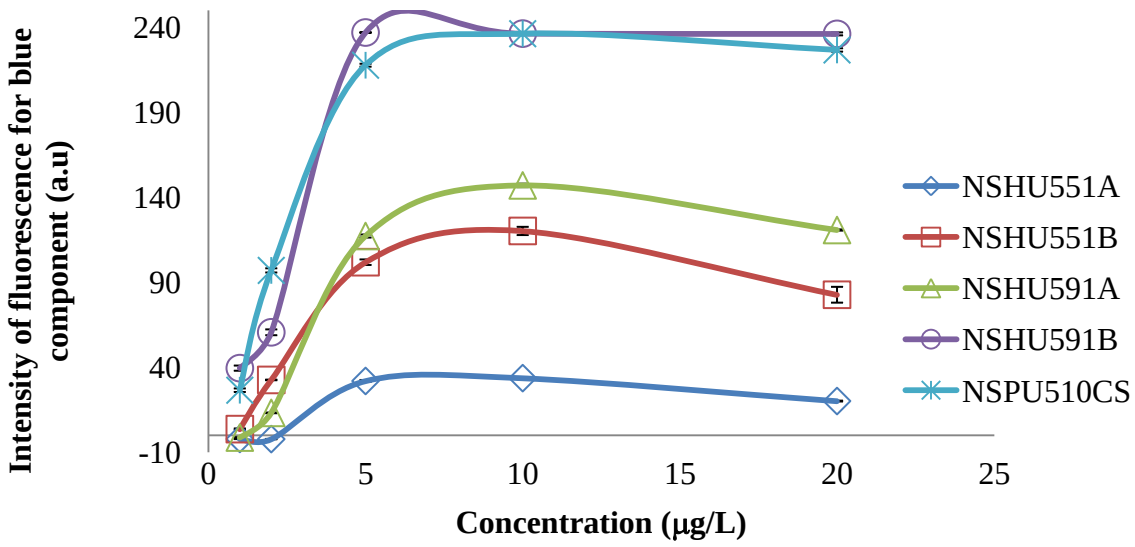

Fig. 65 Response normalized of the UV- LEDs for blue component using MeOH.

Due to the multiples disadvantages of the ArduCAM, the poor quality to identify the low concentrations, other sensing module was tested, this sensing module is communicated by serial port with the computer so the acquisition is fast, easy and automatic because it is no necessary to insert the microSD card and remove to take the new images.

4.4 Detection of OTA using CMOS sensor in serial port camera module

Different concentrations of OTA (1, 2, 5, 10, 20, 30, 40, 50, 80 µg/L) in methanol were prepared and the methanol was considered as blank, 1 mL of OTA or blank sample was poured in the cuvette and it was placed in the chamber of the developed system. The UV-LED was switched on and the serial port camera module covered the cuvette, subsequently the interface was executed. Firstly, the image of blank was taken by clicking the button "*Blank*" in the designed graphical interface and the images of each concentration were captured by pressing the button "*Take Image*".

Once, the images were captured, the button "*Process Image"* was pressed and the folder was selected. The program obtains its RGB values, the image with JPEG format and the mean of the RGB components in a text file, keeping original image name and adding tags to identify the results. The time necessary for this process depends of the quantity of image in the

folder; in this case the time was approximately less than one minute for 120 images to the calibration curve employing a Intel®Core™ i7-2670QM CPU at 2.2GHz and 6Gb in RAM (Random Access Memory). In the real samples, less time was used to capture, analyze the data and to assess the RGB coordinates of the samples, due to less images were captured.

An image of the cuvette at different concentrations of OTA and blank was captured, the area corresponds to the fluorescence of the OTA was selected and relabeled by the interface. The interface obtained the RGB diagram, it should be highlighted that the presence of OTA shows high blue fluorescence intensity and the blank does not show fluorescence, for that reason the blue channel was utilized to establish a relation with the concentrations of OTA how is appreciated in the figure 66. Where the five LED described in the ArduCAM for the calibration curve were used with the serial port camera module, too.

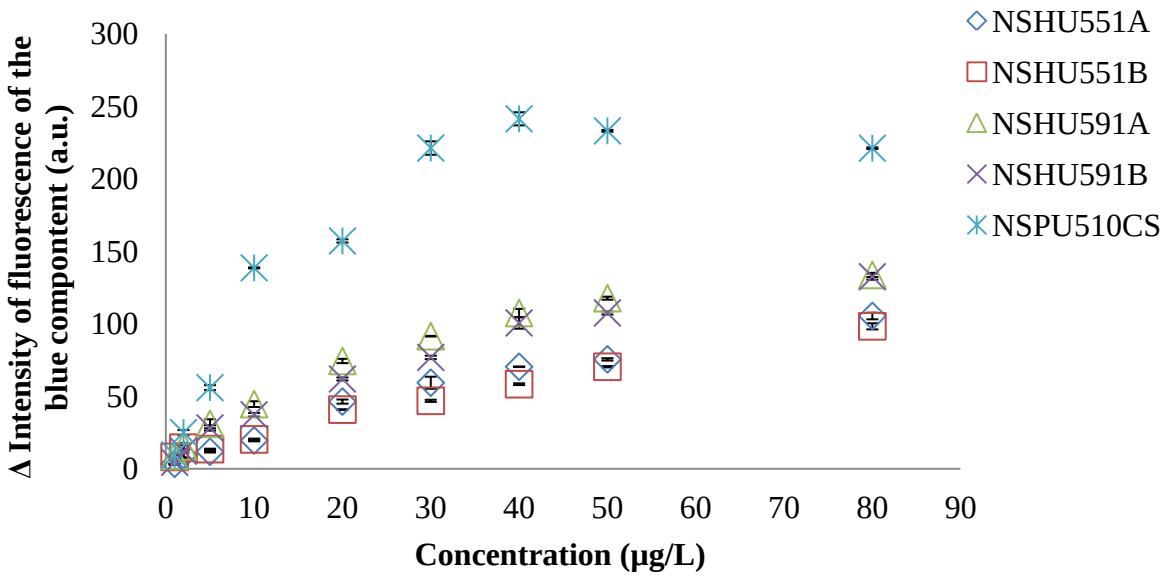

Fig. 66 Calibration curve of the serial port camera module of each UV-LED.

With the UV-LED NSHU551B is no possible to quantify the concentration of 2 and 5 µg/L, the value of the blue component are so close, the value of the blue component together to the standard deviation of this two concentrations correspond to 13.395±0.325 and 14.395±0.565, respectively; the same problem was presented in the NSHU551A, the values obtained were 9.43±0.496 and 11.58±0.585, respectively. In the case of the NSPU510CS

presents very good linear range, the problems is this LED present high intensity that saturated the value of the blue fluorescence for higher concentrations but for low concentrations is a very good option, the problem with this LED is due to the high intensity emitted, it heats easily and the experimental is suspended for a few seconds. The LED NSHU591A has a limit of detection (LOD) of 2 µg/L the same LOD of the NSHU591B. The table 22 indicated the linear range for each LED used in the calibration curves.

Table 22 Linear range of different LED characterized.

Peak wavelength (nm)	LED	Radiant flux (mW)	Linear range (µg/L) / LOD (µg/L)	Linear equation	R^2
375	NSHU591A	9	5-20 / 2	2.9012x+16.001	0.99
	NSHU551A	12	5-30 / 2	1.9958x+1.6509	0.97
	NSPU510CS	15.1	1-10 / 2	14.167x-6.6289	0.99
365	NSHU591B	4	5-40 / 2	2.0492x+17.769	0.99
	NSHU551B	5.4	5-80 / 5	1.1167x+12.143	0.98

The value of the blue component corresponds to analysis the changes in the 256 pixels of the image sensor just for the blue channel, the mean of the intensity of the pixels provided the value for every sample analyzed in the same channel which it is compared with the blank and the different concentrations, to have a relation between the value of the blue component and the presence of OTA.

The intensity mean of the pixels provided the value for every sample analyzed in the same channel, which is compared with the blank and the different concentrations, to establish a relationship between the value of the blue component and the presence of OTA. The fluorescence measurements performed for each concentration of OTA were normalized, by subtracting the fluorescence intensity from the blank (fluorescence intensity of methanol was 30 a.u.).

For the follow experiments, considering the characteristics provides by the UV-LED, the LED with an emission peak at 365 nm, viewing angle is 10 degrees (± 5 °), 4 mW of radiant power was employed. Its calibration curve for the developed system is showed in the figure 67, as a good linearity between the blue component and the concentrations of OTA could be seen. The best linear range was obtained in the range of 5-40 µg/L for OTA detection

is demonstrated in the figure 68. The limit of detection (LOD) of the developed device was found to be 2 µg/L, which is similar to that of HPLC. Each OTA concentration was analyzed by triplicate and the images were taken four times. The value of the average deviation (n=12) for the different concentrations of OTA was ±1.65.

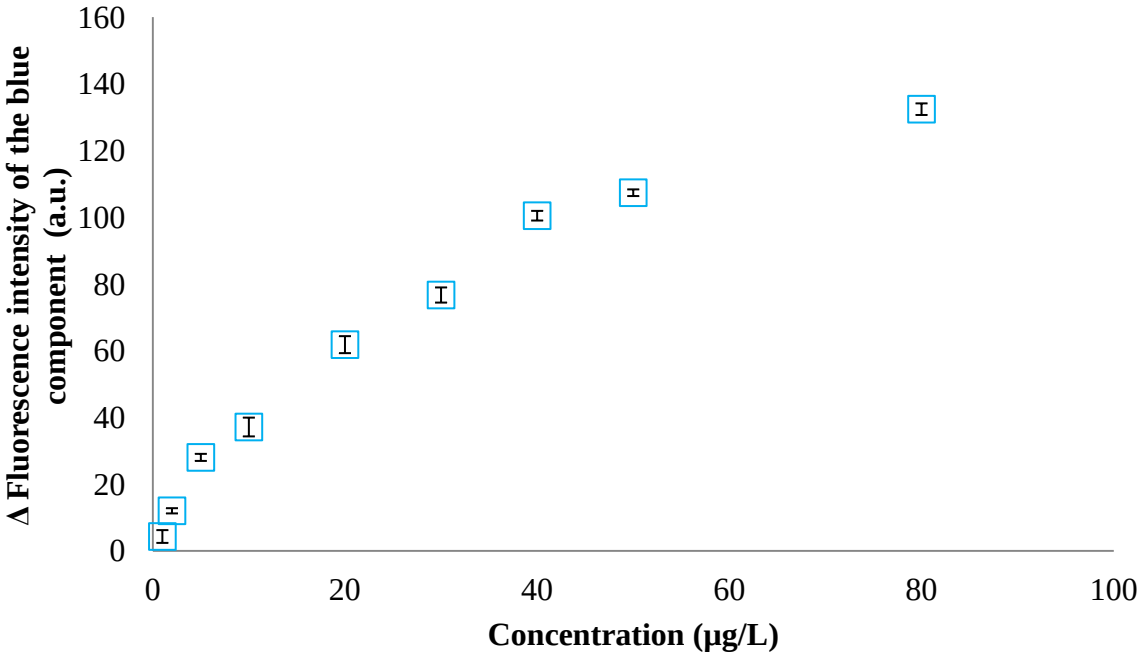

Fig. 67 Calibration curve of OTA concentrations in methanol using developed fluorescence device.

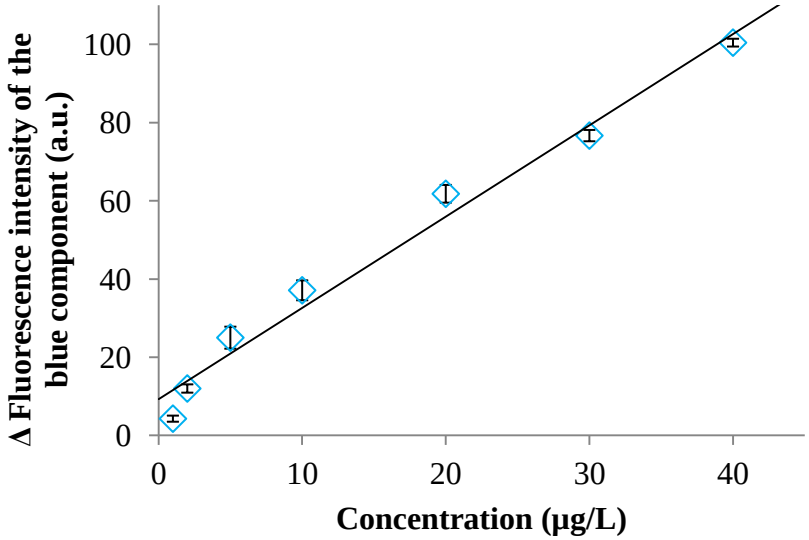

Fig. 68 Linear range of OTA concentrations in methanol using serial port camera module.

4.4.1 Extraction with IAC columns for wine and beer

The known concentrations of OTA prepared in methanol were injected into the HPLC. The analysis time was 8 min and the retention time was 5 min for OTA. In the case of real samples, a mix of 800 µL of wine or beer and 200 µL methanol was injected in HPLC to confirm that the real samples were free of OTA. Subsequently, to avoid the matrix effect, an extraction protocol was used in combination with immune affinity column; the used methodology is described in section 3.9.4.1.

One of the advantages of the immunoaffinity columns is the specific nature of the interaction between the OTA and the antibody. Before to test the elute of real samples using the developed device, these samples were injected in HPLC as described in section 3.8. A linear relationship between the peak area and the concentration of OTA was obtained [194]. The figure 69 shows an example of detection of 10 µg/L OTA using a mobile phase water/acetonitrile/acetic acid (51/48/1) in the HPLC where the software provides the retention time (minutes) in X-axis, the area and high of the peak.

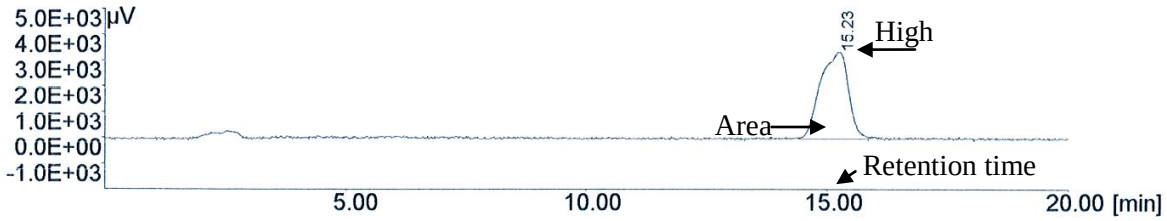

Fig. 69 Detection of OTA in the HPLC.

Table 23 summarizes the mean of the area (n=3) for the standard OTA solutions and the percentage of recovery of OTA using immunoaffinity columns wine and beer samples by HPLC. Besides, the blank exhibited the absence of the peak of OTA. The figure 70 and 71 exhibits the results of detection of OTA using IAC column in the HPLC for wine and beer samples.

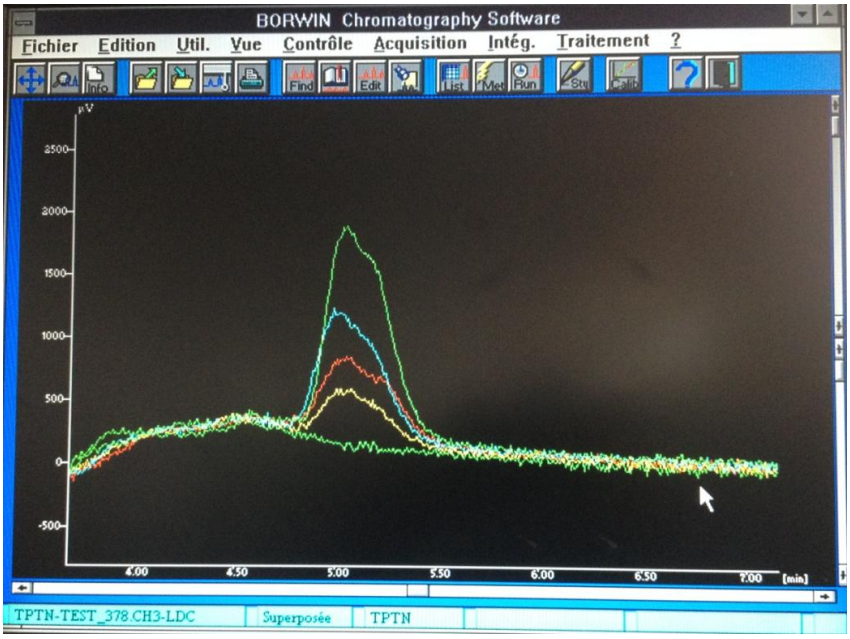

Fig. 70 Elution of wine samples through IAC columns tested in HPLC. Green line corresponds to 10 µg/L OTA. Cyan color is 6 µg/L OTA. For 4 µg/L the color is the red one. In addition, yellow represents 2 µg/L. The blank is exhibit by the green color, is not a peak.

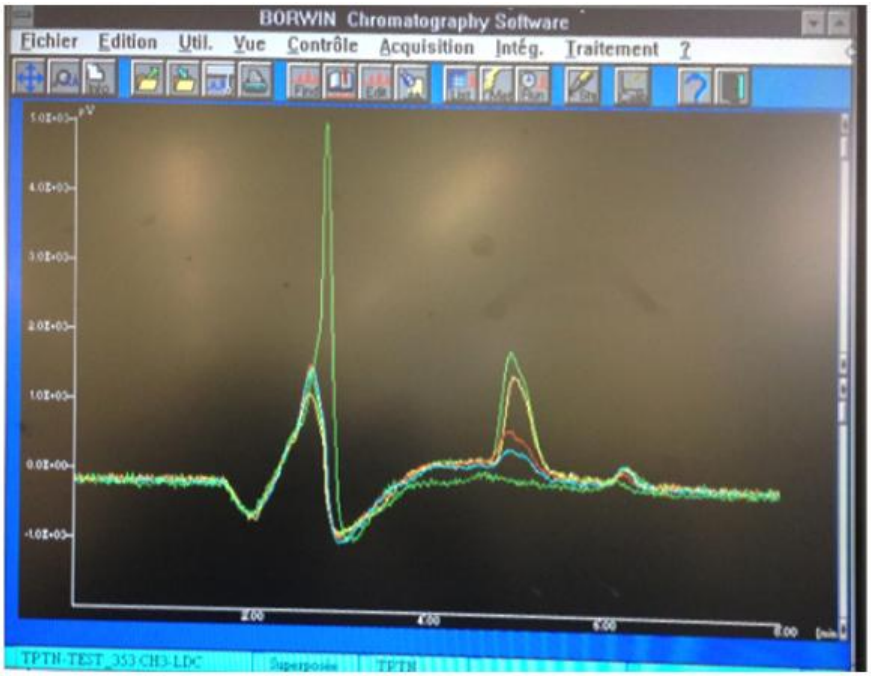

Fig. 71 The recovery through IAC of beer samples through tested in HPLC. Green line corresponds to 10 µg/L OTA. Yellow color is 6 µg/L OTA. Red color is for 4 µg/L OTA. Cyan color represents 2 µg/L OTA. The blank is exhibit by the green color, is not a peak.

Table 23 Recovery of real samples compared with standard solutions of OTA in the HPLC.

Concentration (µg/L)	Peak area of OTA standards (a.u.)	%RSD	Recovery in beer sample (%)	%RSD	Recovery in wine sample (%)	%RSD
2	5825.1	1.39	95.41	0.80	86.97	0.50
4	13375.0	4.97	79.90	3.54	76.47	1.64
6	20062.5	4.89	97.68	3.32	86.59	4.85
10	30492.3	2.12	91.18	2.36	95.98	7.46

In the case of the serial port camera module, the percentage of recovery for OTA using the IAC was calculated dividing the fluorescence intensity of the concentrations of OTA of the real samples by the fluorescence intensity of the concentrations to the calibration curve and the result was multiple by 100 to obtain the percentage. For some concentrations, the value of the peak area and fluorescence intensity was interpolated for the calibration curve.

The results of recovery of using immunoaffinity columns for wine and beer samples are in table 24. The obtained recoveries are better than against those obtained using HPLC. The blank exhibited the absence of the OTA, due to the value of fluorescence of blank is close to the value of fluorescence of methanol.

Table 24 Recovery of real samples compared with the serial port camera module.

Concentrations (µg/L)	Recovery in beer sample (%)	Recovery in wine sample (%)
2	107.76	94.38
4	105.23	91.56
6	98.30	85.72
10	109.68	91.82

In addition, the intensity of fluorescence has a linear relation with the blue component for beer and wine samples spiked with concentrations of OTA; the linear relation is presented in the figure 72a and 72b.

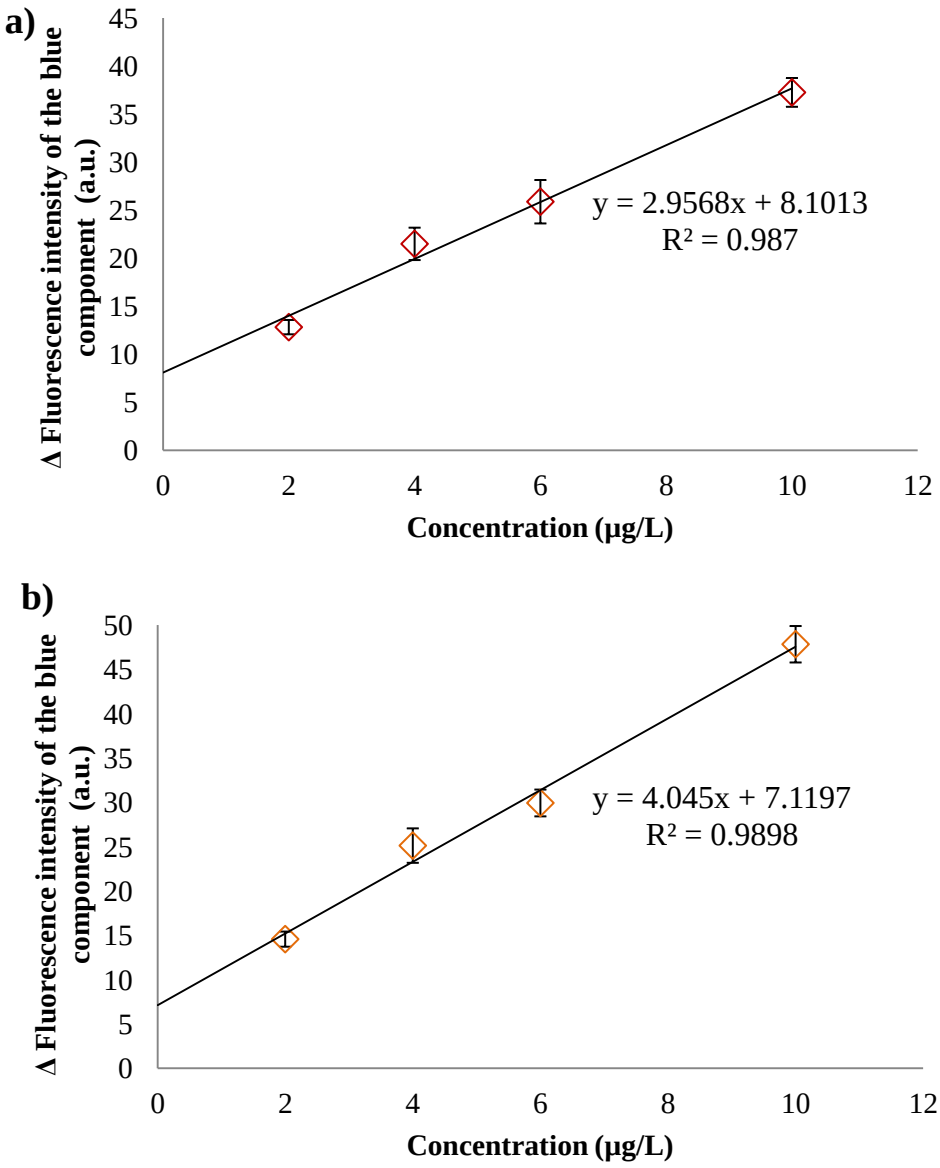

Fig. 72 Behavior of the blue component for OTA spiked samples of wine (a) and beer (b) samples in the serial port camera module.

The average deviation for the intensity of fluorescence for wine samples spiked to determined concentrations of OTA with the developed device was ±1.54 for blank, and 2-10

µg/L of OTA. In the case of beer, the value was ±1.44 for the same concentrations tested in the wine. All the samples were tested in triplicate by both the methods (fluorescence detection device and HPLC).

4.4.2 Extraction with MIP for wine and beer samples

In the case of MIP columns with the serial port camera module, the percentage recovery was calculated in the same way that the IAC column. The recovery results in wine and beer samples are presented as table 25 and 25a for HPLC and developed device, respectively. The obtained recoveries for OTA in beer are more at concentration 2 and 4 µg/L using MIP columns in combination of fluorescence device whereas other two tested concentrations (6 and 10 µg/L) exhibited less recoveries as against HPLC. Similarly, for wine recovery rates, MIP and fluorescence method recorded more recoveries than HPLC in all the tested OTA concentrations.

Table 25 Recovery of real samples with HPLC using MIP columns.

Concentration (µg/L)	Recovery in beer sample (%)	%RSD	Recovery in wine sample (%)	%RSD
2	92.47	2.56	88.35	1.26
4	100.17	1.69	76.01	0.35
6	94.99	0.87	95.33	4.73
10	94.99	3.85	108.05	4.38

Table 25a Recovery of real samples with MIP columns using the developed device.

Concentration (µg/L)	Recovery in beer sample (%)	%RSD	Recovery in wine sample (%)	%RSD
2	111.67	3.25	68.60	4.56

4	114.49	3.67	68.75	4.87
6	82.82	2.85	57.88	5.32
10	93.20	3.09	62.00	6.72

In this case, the intensity of fluorescence does not show a linear relation with the blue component for beer and wine samples spiked with OTA, the results for wine and beer with MIP columns are presented in the figure 73a and 73b.

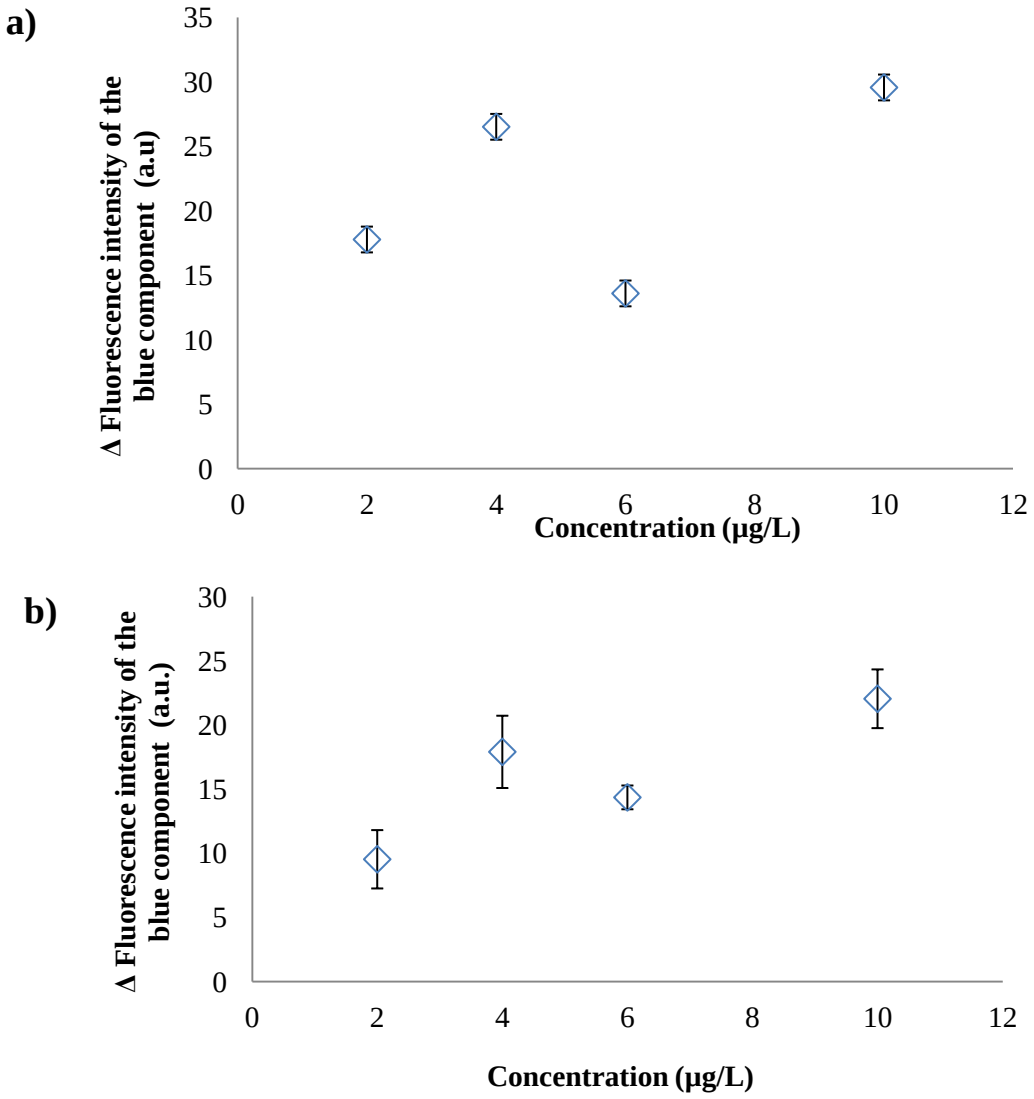

Fig. 73 Samples of beer (a) and wine (b) using MIP columns in the camera module.

The wine samples recovery analysis demonstrated more errors than beer samples and in both cases the sample recoveries are low, this is due to complexity of the wine sample and it may trap into the MIP column and it reduce the recovery percentage. The complexity and impurities can interfere with quantification [195] of OTA using fluorescence instruments.

We considered that the principal problem with the MIP columns was that the package of the MIP columns was previously contaminated. Each step was analyzed in the HPLC as the section 3.9.4.2 described. The first step indicated in yellow color in the figure 74 correspond to the pre-condition of the column with ACN and after with distilled water that is the green color. For the loading step, beer sample without OTA through the MIP column, the samples collected was injected in the HPLC registered in red color. Subsequently, for the washing step represented in cyan color shows the presence of a peak that corresponds to the same retention time of OTA (5 minutes, approximately) with an area peak of 2504.60 and a high of 301. Finally, the elution was carried out and was analyzed in the HPLC, which is presented in green color with a peak at the same retention time of OTA, an area peak of 15553.80 and 660 of high.

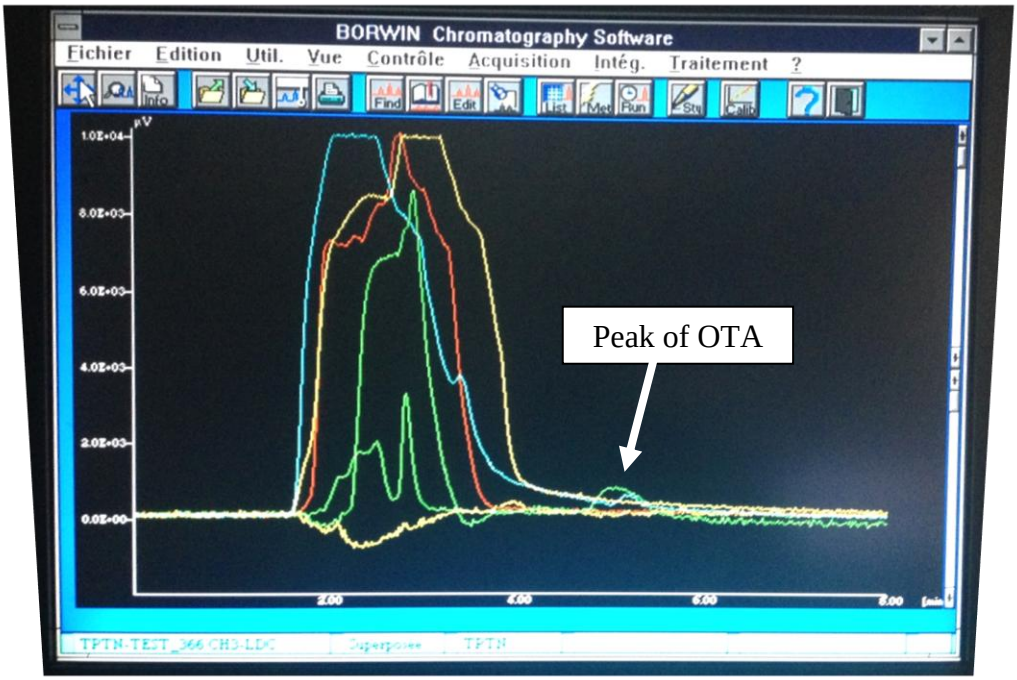

Fig. 74 Samples collected of each step to use MIP columns were analyzed in the HPLC.

The biggest yellow signal corresponds to the beer sample used as blank without OTA. In the sensing module, the same samples collected were tested and the results were comparable with the HPLC, in the pre-conditioned with acetonitrile, the sample of beer without OTA, the washing step and the elution was visible a fluorescence strip, also, see the figure 75. How the columns were contaminated with OTA and it was verified with the HPLC, for that reason the columns were cleaned with 10 mL of 1% of acetic acid in ethyl acetate, it was washed with 20 mL of distilled water. Subsequently, the process to use MIP columns was carried out again with successful, in spite of clean the column, the columns was capable to retain the OTA of the real samples and remove the interferons.

(a) 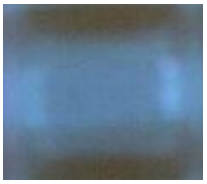 (b) 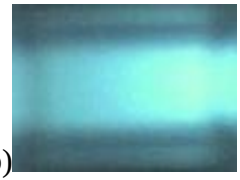 (c) 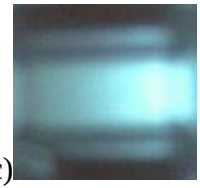 (d) 

Fig. 75 (a) Represents the pre-conditioned step; (b) Corresponds to the real sample; (c) It is the washing step; (d) Elution step with the serial port camera module.

The results were comparable with the Fluoroskan and it shows the same behavior than the serial port camera module. In the same steps that the camera module the Fluoroskan show fluorescence in the samples. This occurs due to the components of the MIP columns reacts to the UV-LED. However, the presence of a contaminant as OTA is also provable with these optic systems besides the HPLC as the table 26 shows.

Table 26 Value of fluorescence provided by the Fluoroskan for the protocol of MIP columns.

Time (minutes)	Acetonitrile	Distilled water	Real sample	Washing step	Elution
0 min	4.1175	0.6365	51.4250	43.15	2.0125
5 min	3.8395	0.6317	50.605	43.005	1.9625

Some MIPs have been already developed for OTA, as promising SPE adsorbents for clean-up and pre-concentration. Nevertheless, the high cost and toxicity of OTA usually involves the use of a synthetic mimic as imprinted template, which greatly limits their affinity

for the analyte [196]. To confirm the results, the samples were tested with the fluorescence instrument, displaying similar results to those obtained with the serial port camera module; the response is showed in the figure 76.

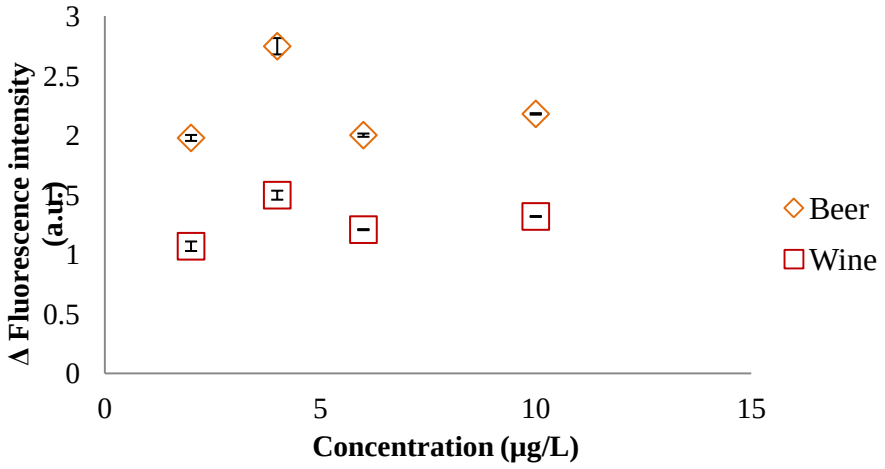

Fig. 76 Fluorescence intensity obtained with the fluorescence equipment.

4.4.3 Extraction of OTA from cocoa using MIP columns

The different OTA concentrations 40, 30, 20, 10, 7.5, 5, 2.5, 1.25 ng/ml were prepared respectively in ethanol and scanned using fluorescence set up to construct a calibration graph presented in the figure 77, besides it was compare with the calibration curve in methanol.

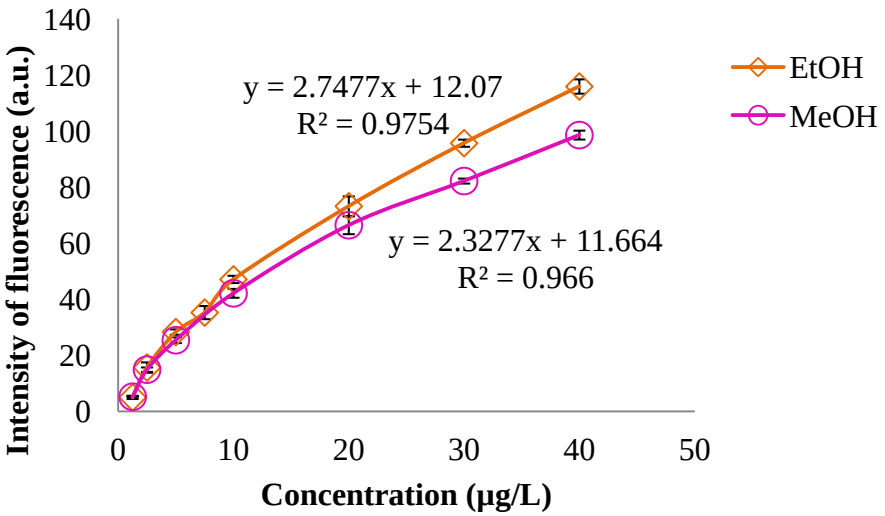

Fig. 77 Calibration curve in EtOH and MeOH using the fluorescence set up.

The fluorescence of the samples is directly proportional to the OTA concentrations; a good linearity was found in the range 1.25-40 µg/L, a correlation factor of 0.97. The developed fluorescence set up was tested to detect OTA in cocoa beans sample by using two different protocols wherein we have used raw cocoa beans and cocoa powder in the two different protocols.

The objective of the comparison of two protocols was to reduce the number of individual steps, eliminate the use of toxic organic solvents, and reduce the time to detect OTA at low level 2µg/Kg within a short time. Under the adopted conditions, OTA eluted within 20 min using the extraction protocol and immediately being tested by developed fluorescence set up.

Five different batches of cocoa beans were tested by developed protocol, but none of them has confirmed the presence of OTA. To evaluate the feasibility of the proposed method for possible applications, experiments were carried out with the artificially contaminated cocoa samples in the concentrations 10, 5 and 2µg/kg in duplicate. Firstly, the raw cocoa samples were extracted using immune-affinity column and further applied for recovery studies. The RSD was calculated to be 4.05% indicating the precision and the reproducibility of the developed system. The accuracy was obtained by comparing the spiked (2, 5 and 10µg/kg) and the average measured values (1.66, 4.23 and 8.75 µg/kg). The obtained recoveries were shown in the table 27**.**

Table 27 Recoveries of OTA using two different protocols of extraction and their evaluation using developed fluorescence set up.

OTA spiked [µg/kg]	**OTA found [µg/kg]**	**% Recovery (1% $NaHCO_3$)**	**%Recovery (Classical)**	**% RSD**
2	1.69	84.5	79.05	3.8
2	1.64	82.0	80.25	3.95
5	4.28	85.6	81.50	4.12
5	4.18	83.6	82.00	3.95

10	8.7	87.0	83.25	4.02
10	8.8	88.0	82.29	4.5

The spiked values were consistent with the obtained concentrations of OTA. The developed system could therefore be applied in a rapid and simple detection of OTA in real cocoa samples at the cocoa origin sites. The recovery was calculated based on calibration curves performed in methanol. The recovery results for the developed system validated the suitability of the method. The difference between the observed and actual value could be due to the interferences from the extract. Further studies are required to improve the sensitivity of the developed system.

The Fluoroskan was used for fluorometric measurement to test the performance of the system using eluted samples of OTA from cocoa beans. The cocoa was provided by our industrial partners M/S Cemoi at Perpignan. Same OTA samples were analyzed using both the systems and dilutions were adjusted to cover a range of fluorescence. The results obtained using developed system shows more fluorescence in terms of image brightness than the commercial equipment.

The prepared OTA samples were also tested for stability check and to see the performance of the developed system in terms of RGB fluctuations of the old samples. It was recorded that the RGB has not changed significantly with stored samples. Similarly, extracted OTA from cocoa beans were also subjected to evaluate the RGB pattern. The extracted samples were also demonstrated the good stability.

The specificity of the method was tested using Ochratoxin B (OTB) solutions, which can be a natural co-contaminant of cocoa samples at origin. The experiments were performed using 5 µg/kg and 10 µg/kg concentrations of OTB by using similar protocol used for OTA. The both eluted samples were diluted to prepare the concentrations 5 and 10 ng/ml and taken in cuvette for fluorescence. After the analysis, lower value of blue coordinate was obtained for OTB as against OTA in the captured image. It is clear from the figure 78 that developed system and the columns were selective for OTA in a manner that is not affected by the presence of other contaminating mycotoxins.

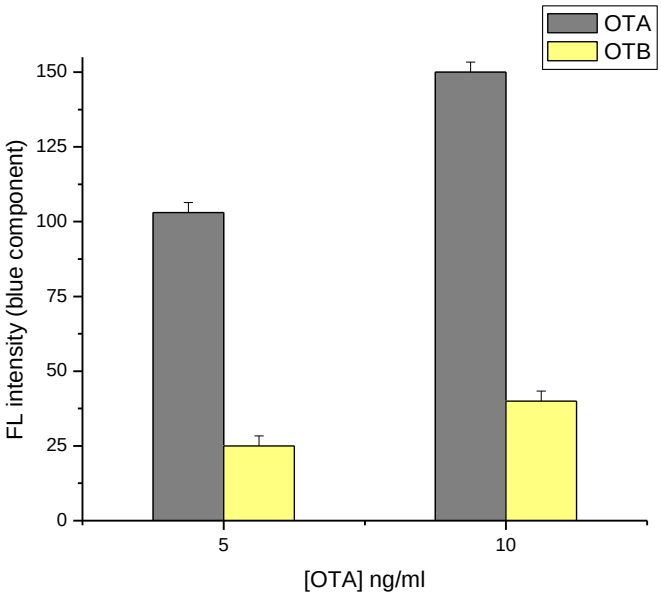

Fig. 78 Specificity of the developed method at a particular wavelength against OTB.

4.5 Smartphone as detector of OTA

To demonstrate the application of the smartphone, the UV LED and the use of the wireless as detector of Ochratoxin A , the beer was chosen due to is an alcoholic beverage produced by starch enzymes derived from malted cereal grains, barley or wheat [197].

The use of the smartphone camera and as a power source allows developing a portable system, different UV-LEDs with a wavelength range of 360-380 nm as an external light source to excite the samples were tested at different radiant flux. The LED is switched on and the captured image is in the personal computer using wireless, to be processed to obtain the RGB values. The sample cuvette was kept in a special black poly methyl methacrylate chamber designed for it to avoid the external lights and to put the electronic circuit that it is supplied by the battery of the smartphone.

Different OTA concentrations were prepared in methanol and scanned using the smartphone camera and the wireless to obtain the calibration curve. The captured fluorescence images at different concentrations based on blue component of the fluorescence intensity provided for each LED at peak wavelength of 365 nm or 375 nm besides the different radiant flux of the transmitters is in the figure 79. It is possible to observe that more fluorescence is presented in high concentrations of OTA otherwise occurs in low OTA concentrations. The fluorescence of the samples is directly proportional to the OTA concentrations.

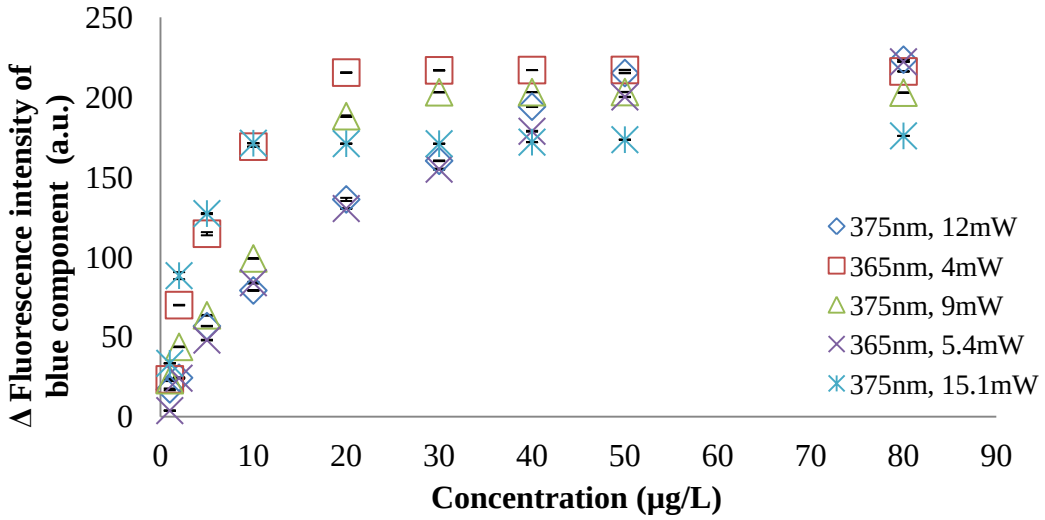

Fig. 79 Calibration curve for OTA based on blue component of the fluorescence intensity.

When the calibration graph was drawn, it was observed that for high concentrations there are no change in the blue component of the fluorescence intensity, hence the linear range was obtained for every LED and these are in the figure 80.

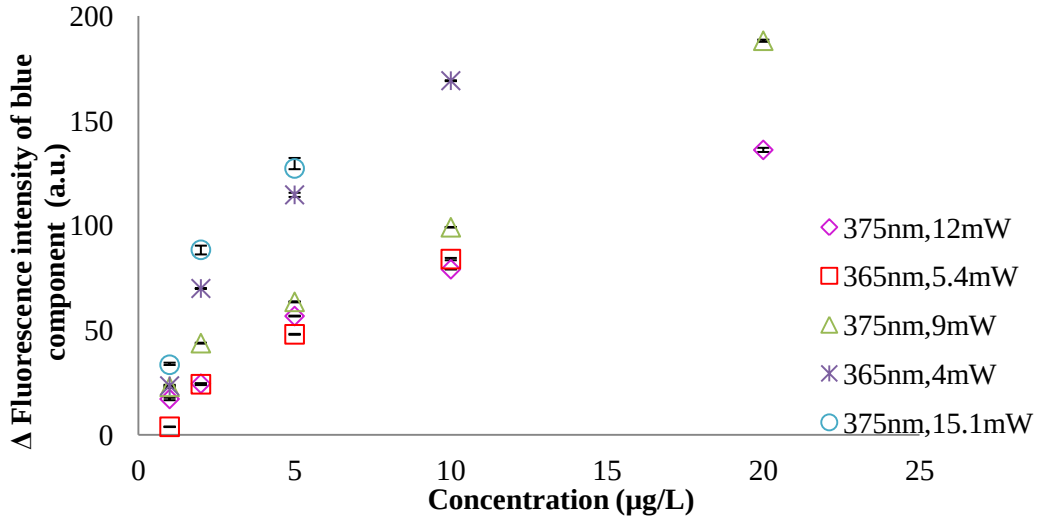

Fig. 80 Linear range for OTA based on blue component of the fluorescence intensity.

The linear range with better linearity was found in the range 1.25-20 µg/L and the results about the correlation factor (R^2), and the linear range based on the peak wavelength and radiant flux are showed in the table 28.

Table 28 Linear range of different LED characterized.

Peak wavelength (nm)	Radiant flux (mW)	Linear range (µg/L)	Linear equation	R^2
375	9	1.25-20	y=8.7746x+13.994	0.98
	12	1.25-20	y=6.4865x+11.123	0.97
	15.1	1.25-5	y=24.867x+12.501	0.90
365	5	1.25-10	y=16.412x+16.297	0.94
	5.4	1.25-10	y=8.5211x+1.285	0.98

The table 29 shows that the best linear range is for the LED at 375 nm with 9 mW, although the LED at 365 nm with 5.4 mW has the same correlation factor, it is possible to detect until 10 µg/L. Therefore, the radiant flux of the LED is an inverse proportional to the OTA concentrations, due to high concentrations the blue component of the fluorescence intensity is saturated and it no possible differentiates OTA concentrations higher than 5 µg/L.

It has been documented the use of NaOH as fluorescence enhancer [16], for that reason in our experiments 1 µL NaOH 3M as fluorescence enhancer was added the next day after the elaboration of the calibration curve. Moreover, the same process with the smartphone camera, UV-LED and wireless was carried out. The results are presented in the figure 81 for this part, the LED at 365 nm and 4 mW was used due to its good linearity and its linear range until 10 µg/L to compare that it is possible to increases the blue component of the fluorescence intensity with an fluorescence enhancer.

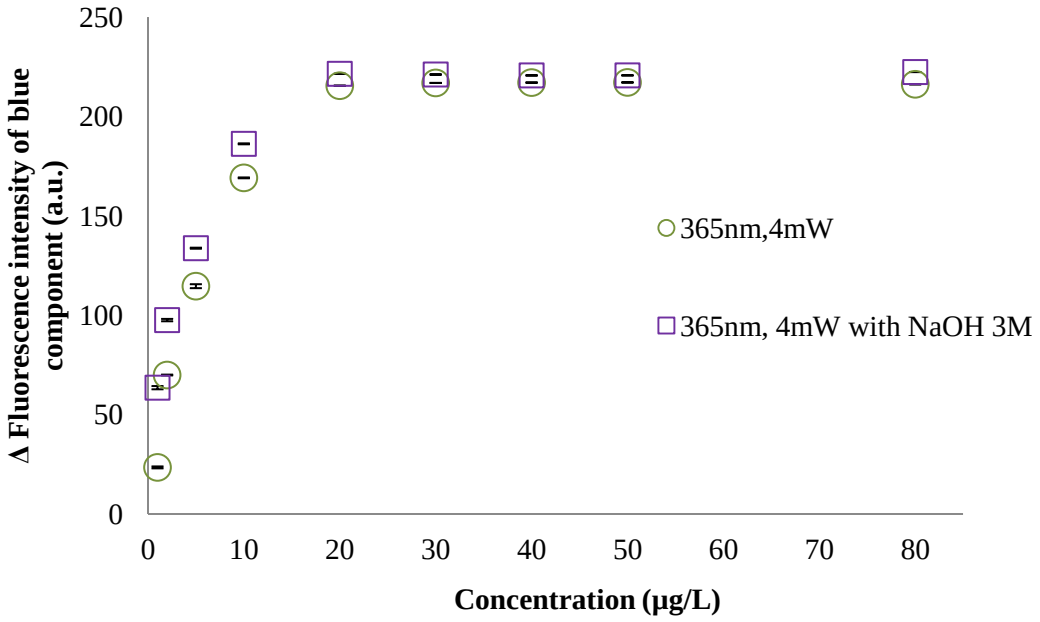

Fig. 81 Increasing the blue component of the fluorescence intensity with a fluorescence enhancer.

With the NaOH as fluorescence enhancer, it was an increasing of the 100 percent for the low concentrations in the blue component of the fluorescence intensity where the greatest increase was presented in the linear range of the UV-LED of 1.25-10 µg/L.

To evaluate the use of the smartphone camera, UV-LED and wireless as detector of mycotoxins, it has tested to detect OTA in beer sample. The accuracy was obtained by comparing the spiked samples and the average measured values. For the LED at 375 nm with 9 mW and 12 mw, the recovery was 90-102 percent with RSD of 4.03%. In case of the LED at 365 nm with 5.4 mW, the recovery was 93-105 percent with RSD of 3.89%. For the four LEDs tested, it was observed that the percent of recovery was reduced at the extreme limits of detection limit. The table 29 shows the recovery for the LED at 365nm with 4 mW.

Table 29 Recovery for the LED at 365 nm.

Concentration (µg/L)	Peak area of OTA standards (a.u.)	%RSD	Recovery in beer sample (%)	%RSD
2	5825.1	3.39	89.65	3.80
4	13375.0	4.97	91.97	3.54

6	20062.5	4.89	96.69	3.89
10	30492.3	3.12	79.20	4.03

The spiked values were consistent with the obtained concentrations of OTA. Due to the narrow linear range of LED at 375 nm with 15 mW, in addition to its rapid saturation at low concentrations and higher margin of error, this LED was discarded of the experiments.

All the results were validated with the HPLC and the Fluoroskan, it was utilized for fluorometric measurement to compare the eluted samples of beer and wine spiked with OTA, with the results provided with the use of the smartphone camera, LED-UV and wireless. In this case, the results obtained with the smartphone camera show more fluorescence intensity in the brightness of the image, the values of the blue component are higher compare with the value of fluorescence provide by the Fluoroskan, but the behavior was the same and the relation in the percent of recovery remained, as the figure 82 demonstrated.

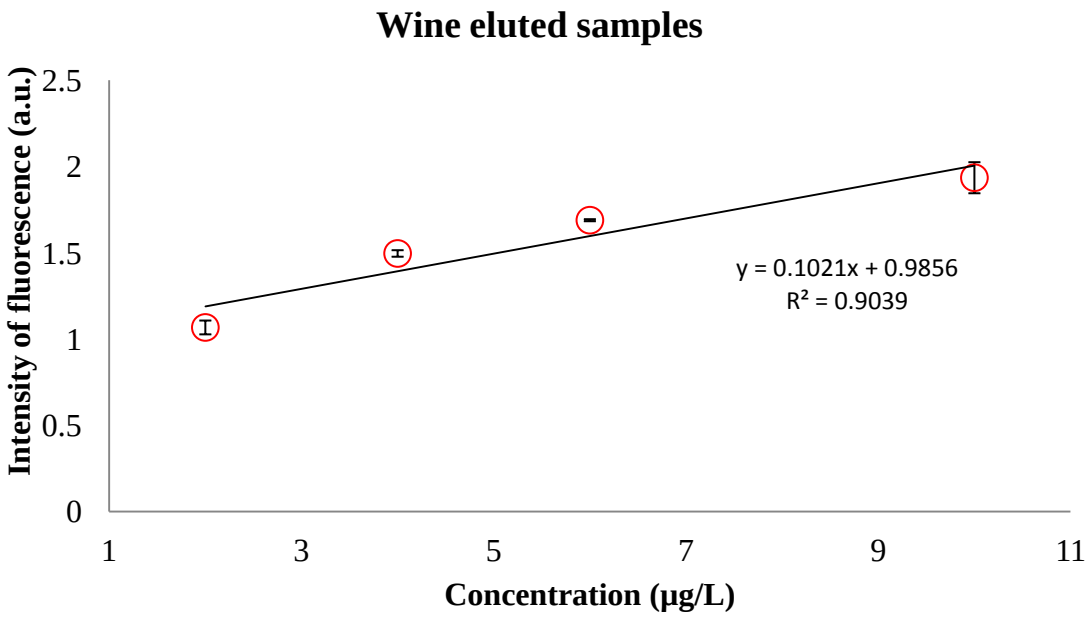

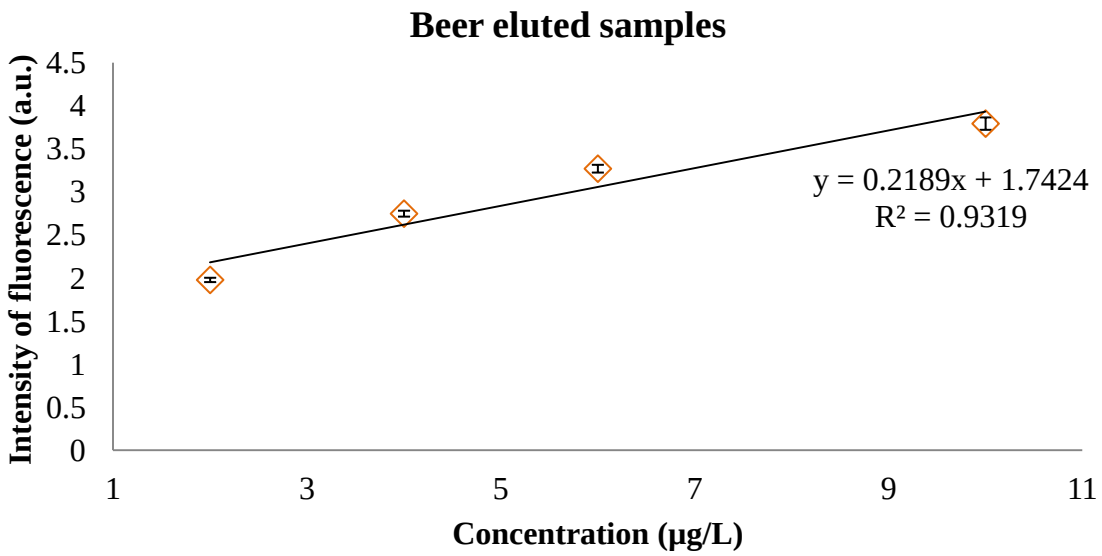

Fig. 82 Fluorescence of wine and beer eluted samples tested with Fluoroskan.

4.6 Flow system

4.6.1 Flow system for Aptamer columns

In the case of the aptamer immunoaffinity column, it was followed the same procedure described by Amina Rhouati et al [163][198] and the solution of percolation, washing and elution were analyzed with the ArduCAM and an automatic flow system. After to prepare the aptamer immunoaffinity column, the samples obtained were excited with ultraviolet light to establish a relation between the blue component and the concentration of OTA in the immunoaffinity columns; in this process we do not have good results. It was possible to detect the presence of OTA in the sample, the figure 83 shows that column does not retain the solution with OTA and was washed easily, it is considered that the problem is the volume used, 1mL is required for the use an optical detection, in this case to employ the ArduCAM as detector. The NSHU591A was the UV-LED and the concentration used in the aptamer column was 10 µg/L of OTA.

Considering the calibration curve, there is a reduction of the intensity of the fluorescence provides us a final concentration of 2 µg/L of OTA. The automatic flow system provides the reduction of time, the automatic process was realized in 40 minutes; decreasing

of the errors due to there is no human intervention. The value of speed was optimized due to a high or slow speed cause that the filter will be dry due to the flow will be no constant.

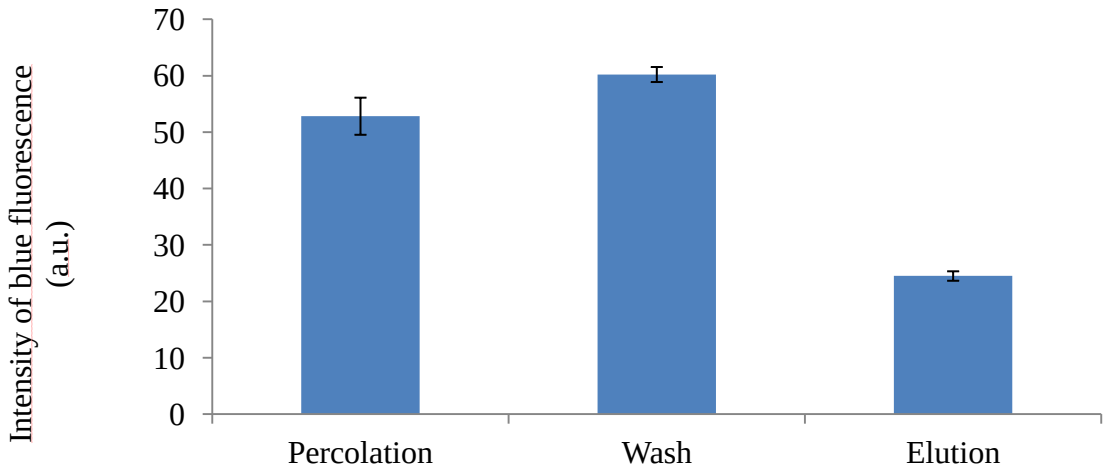

Fig. 83 Comparison of elution profiles of OTA 10 µg/L from the Aptamer Immunoaffinity Column.

4.7 Evaluation of the fluorescence device performance under specific conditions

4.7.1 Effect of solvent of fluorescence intensity of OTA

It has been already reported that the fluorescence behavior (such as the fluorescence maximum) of OTA, strongly dependent on the porogen used. It was observed that the phenolic group of OTA undergoes an excited state proton transfer reaction depending upon the solvent used [108,109]. 20 µg/L of OTA was prepared in different solvents, 1 mL of the solvents were prepared without OTA and these were considered as blank, these were inserted in the cuvette and in the chamber of the developed system.

The buffer solutions (PBS, HEPES) and the alcohols (Methanol, Ethanol) show the best results with high fluorescence intensity of the OTA. As depicted in the figure 87a, the OTA showed less fluorescence in distilled water which is due to the slow decomposition of OTA in water [199]. The significantly higher fluorescence was observed in buffer and methanol in comparison to the acetonitrile [200]. The obtained results further compared with

the fluorescence intensity response recorded using the Fluoroskan microplate reader at 360 nm. It was observed that the developed platform has similar results as depicted in figure 84(a) and 84(b).

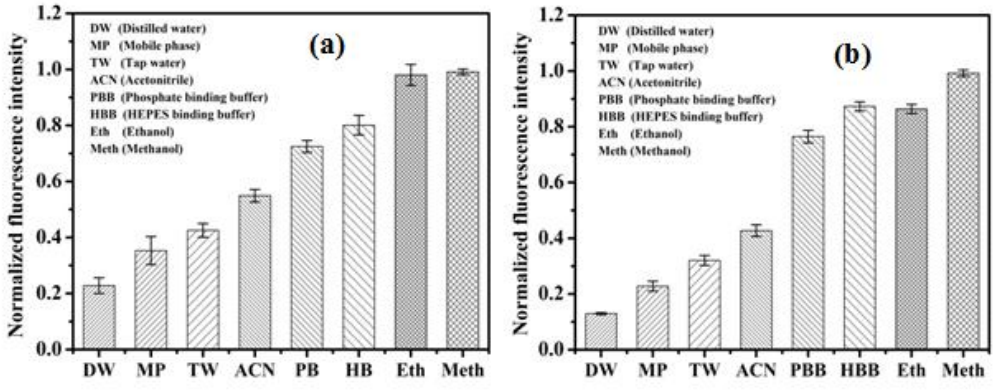

Fig. 84 Fluorescence intensity response 20 µg L^{-1} OTA obtained in different solvent (a) from developed imaging platform (b) from Fluoroskan microplate reader (n=3)

4.7.2 Effect of salt composition of fluorescence intensity of OTA

The effect of salt composition affects the fluorescence emission of fluorophore. To study the phenomenon of fluorescence emission of OTA, the effect of different salt concentration of buffer was tested. As demonstrated in figure 85, the fluorescence emission intensity of OTA increases with increase in concentration of Na^+ salt ranges from 10-120 mM [16][201]. Thus, the results suggested that the salt concentration has significant effect on fluorescence emission of OTA. Further, since, the concentration of optimized salt is optimal for binding interaction of OTA, thus to avoid the effect of excess salt concentration, higher concentrations were not tested [202].

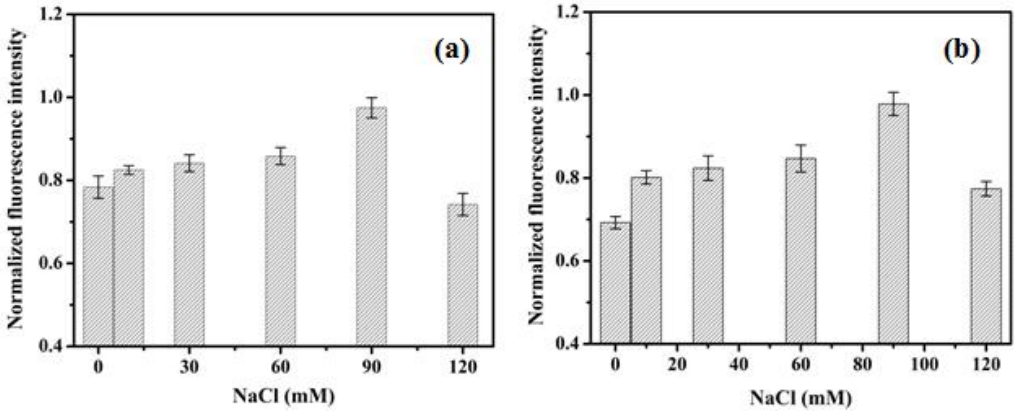

Fig. 85 Fluorescence intensity response 20 µg L^{-1} OTA obtained in HEPES at pH 7.2 with different concentration

of NaCl (a) from developed imaging platform (b) from Fluoroskan microplate reader (n=3)

4.7.3 Effect of pH on fluorescence intensity of OTA

In solution, the OTA shows a pH dependent fluorescence behavior due to the presence of acidic and basic functional entities in its OTA structure, which greatly influence by its protonation state [107]. It was observed in the figure 86 that fluorescence intensity increases with increase pH of HEPES buffer from 6.8 to 7.2. No further increase in fluorescence was observed with further increase in pH of buffer. The increase in pH shift the environment from acidic to alkaline, which results in the hydrolysis of lactone ring causing ring opening [109, 203]. Thus, the obtained result limits the analysis of OTA at high pH that will lead to negative analysis.

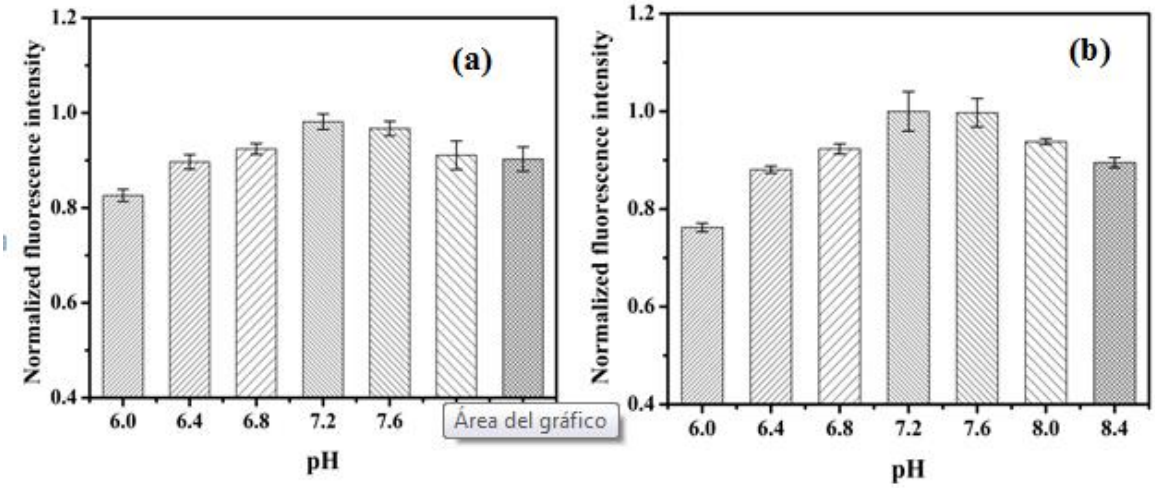

Fig. 86 Fluorescence intensity response 20 μg L^{-1} OTA obtained in HEPES buffer ranging pH from 6-8.4 (a) from developed imaging platform (b) from Fluoroskan microplate reader (n=4)

Follow the methodology previously described, the results were compared with Fluoroskan microplate reader. The developed system showed similar type of results comparing to the microplate reader.

4.8 Employing the APP

The concentrations used in the section 3.2 were evaluated in the APP designed, only to corroborate the function of the APP, this is a first use of the APP, the figure 87 shows as the

APP presents the value RGB of the image capture with the smartphone, the value of RGB does not represent an relation of the intensity of fluorescence for this example.

Fig. 87 Employing APP to capture an image and get its RGB components.

PART C

Image processing

The results for spiked samples of beer and wine with OTA without the use of the extraction columns are presented, the methodology employed as well as the calculation and short explanation of the method used. The first method was to convert the color image in a gray image and finally to get its gray scale histogram; for the calibration curve in the figure 88, for the beer and wine samples spiked with OTA and for wine samples in the figure 89.

In the figure 88 for blank, the spectrum is wider than the range of the OTA concentrations and the higher OTA concentration is a lower spectrum. For the biggest concentration, there is a maximum in the intensity.

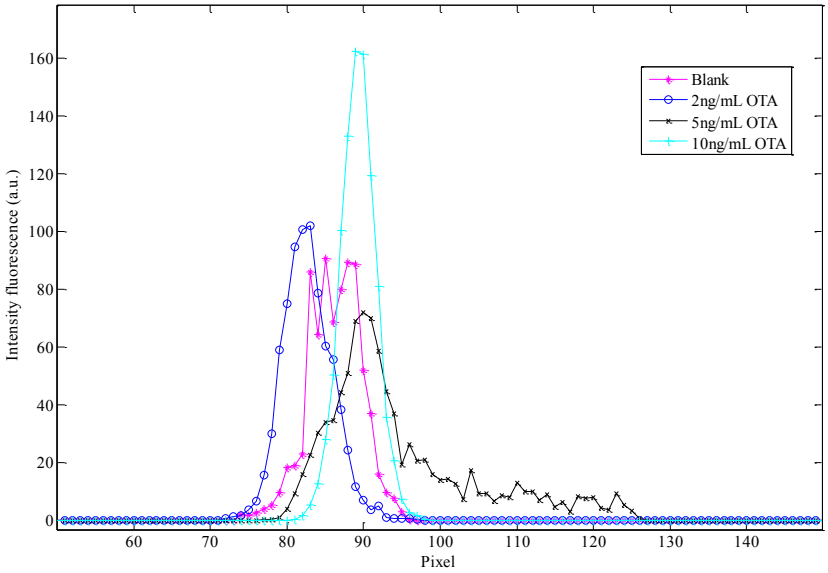

Fig. 88 Histogram in grey scale of calibration curve

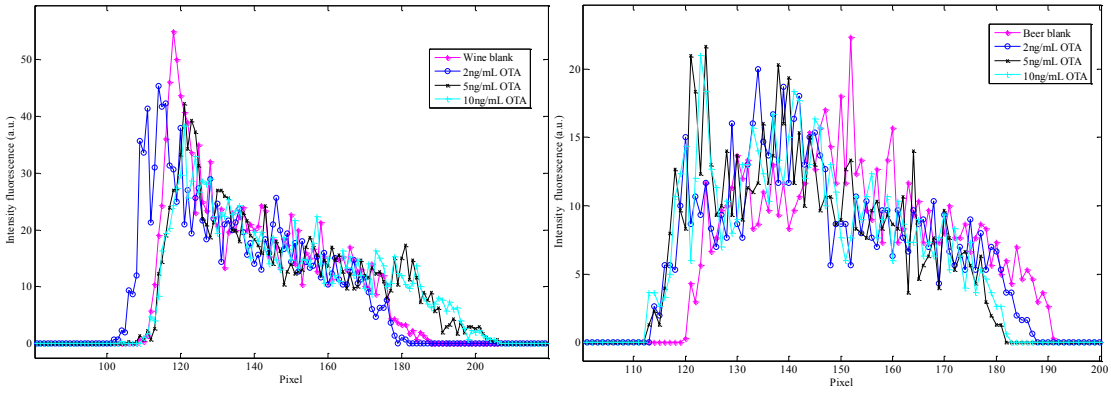

Fig. 89 Histogram in gray scale of wine (left) and beer (right) sample spiked with OTA.

With the gray scale histogram for the wine and beer samples was no possible to identify the concentrations, however was possible to identify these are two different samples, for the beer samples the histogram shows a wide spectrum and in the case of wine samples, the spectrum presents a decreasing slope.

The cumulative histogram is in the figure 90, in this case is possible to see a difference between the concentrations, the concentrations are grouped as follow: 1) Low concentrations (Blank and 2 ng/mL) and 2) High concentrations (5 and 10 ng/mL). In addition, there is a slope but it does not show significate changes between concentrations.

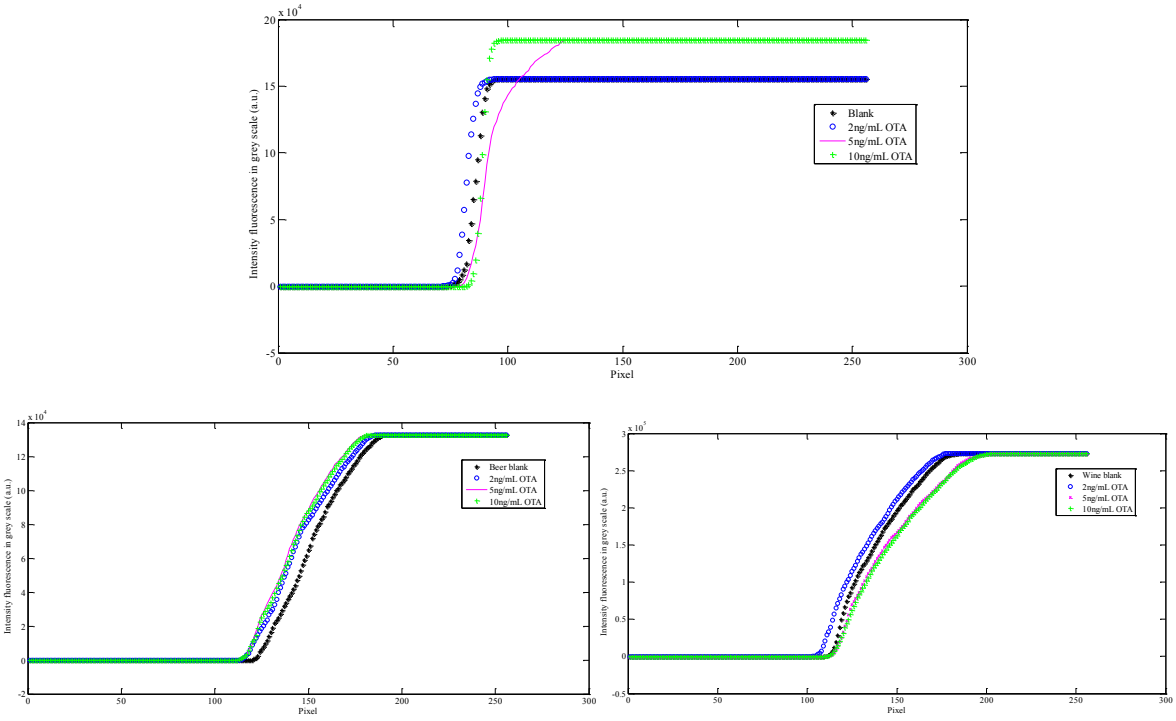

Fig. 90 Cumulative histogram for gray scale for calibration curve (up), beer (left) and wine (right) samples.

In the case of the beer samples spiked with OTA, is possible to separate the blank to samples spiked with OTA, shift leftward, that is to a greater concentration of OTA, the slope shown slightly shifted to the left, although the slope values for each concentration show no significant changes. For the wine samples, the results are group in low or high concentrations as in the case of the calibration curve.

From the calibration curve, the values of the beer samples was subtracted and it is in the figure 94, the graphics represents for blank and 2 ng/mL OTA similar behavior, opposite

in the case of the 5 and 10 ng/Ml, where these are complete identify as the figure 91 (left) represents. Otherwise, the same behavior is repeated with the wine samples (right).

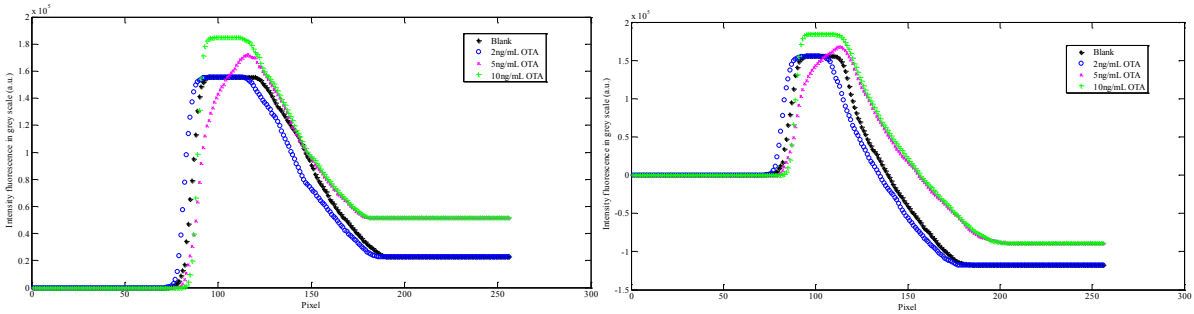

Fig. 91 Cumulative histogram of difference between calibration curve and the real samples spiked: beer (left) and wine (right).

The blue components of the calibration curve and the real samples, the results are in the figure 92, the histogram of blue component for the calibration curve (up) for each concentration is moved to the right, indicating that main light colors, as the intensity of the OTA fluorescence. The histogram of blue component presents the same behavior that the gray scale histogram.

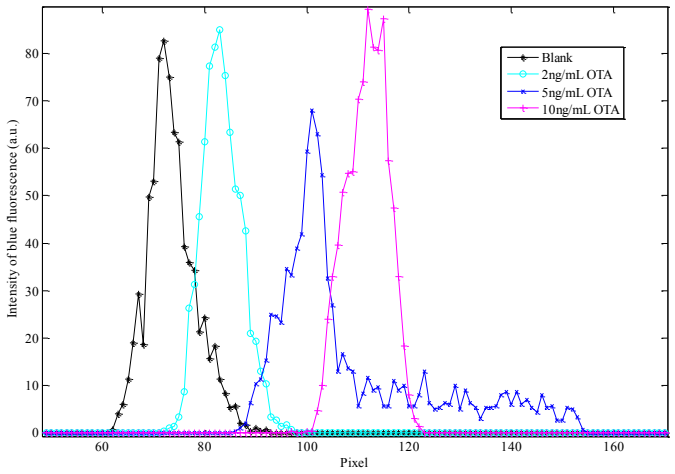

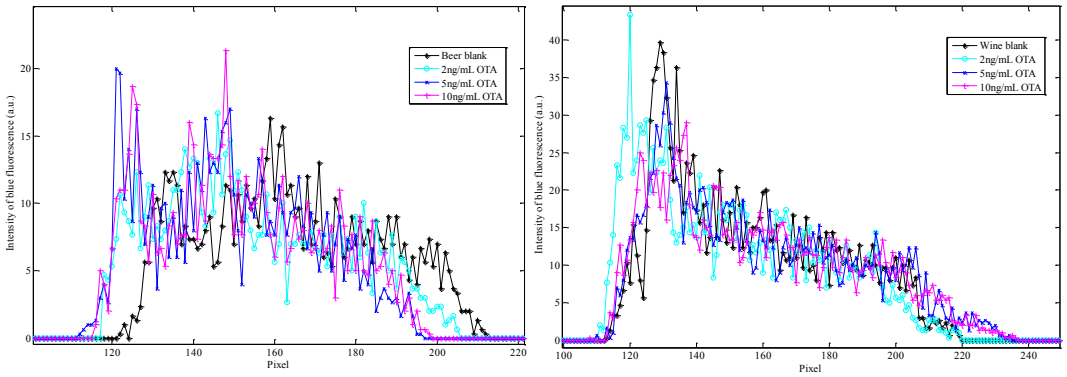

Fig. 92 Histogram of blue component of the calibration curve (up), beer (left) and wine (right) samples.

The table 30 represents the mean of the color models previously mentioned for each concentration employed to build the calibration curve. The figure 93c shows the blue component of the RGB model has a linear relation for the concentrations, except for 10 ng/mL where, It shows that the image sensor is saturated, so it is very approximate value of the previous concentration, as well as the other color models with a linear relation and the saturation of the image sensor for the last concentration.

Table 30 Color model for calibration curve.

		Blank	2ng/mL	5ng/mL	10ng/mL
HSI	**H**	0.1602	0.4461	0.6064	0.6216
	S	0.1173	0.0216	0.1111	0.1433
	I	0.3224	0.3201	0.3801	0.3643
HSV	**H**	0.6742	0.0000	0.6054	0.6190
	S	0.1744	0.0411	0.2056	0.2805
	V	0.3452	0.3837	0.4281	0.4342
Lab	**L**	2.9088	2.8184	3.2277	3.0343
	a	-0.6617	-0.5388	-0.6525	-0.5070
	b	0.3776	0.1251	-0.1919	-0.3332
RGB	**R**	87.6008	80.2075	85.6717	79.5945
	G	86.4510	82.2542	95.9654	88.3748
	B	72.5807	82.3941	109.1670	110.7179
CYY	**C**	167.3992	174.7925	170.9538	175.4055
	M	168.5490	172.7458	161.3792	166.6252
	Y	182.4193	172.6059	148.3449	144.2821

YCC	Y	89.1806	86.1331	97.0433	91.8359
	C	121.7540	128.3479	135.2807	138.9271
	C	129.6457	126.9936	122.4297	122.6169
YIQ	Y	0.3342	0.3202	0.3702	0.3463
	I	0.0202	-0.0050	-0.0407	-0.0487
	Q	-0.0160	-0.0015	0.0076	0.0200

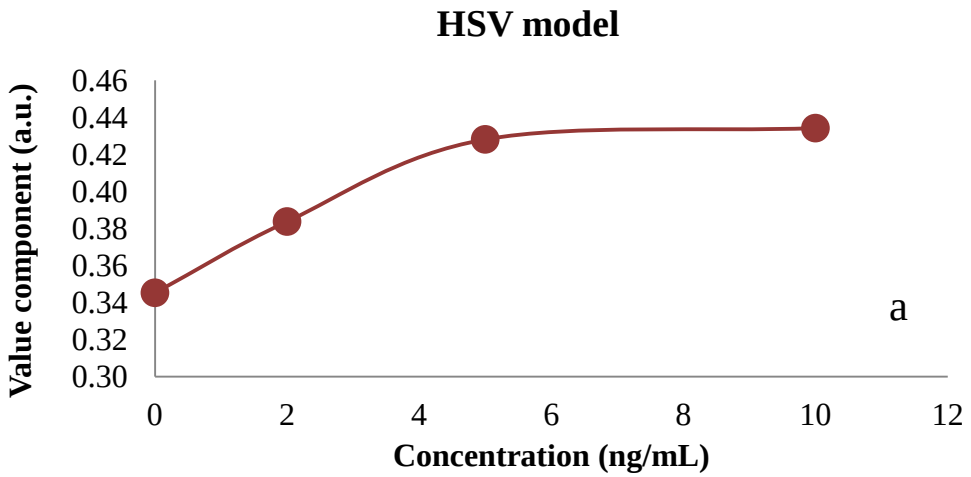

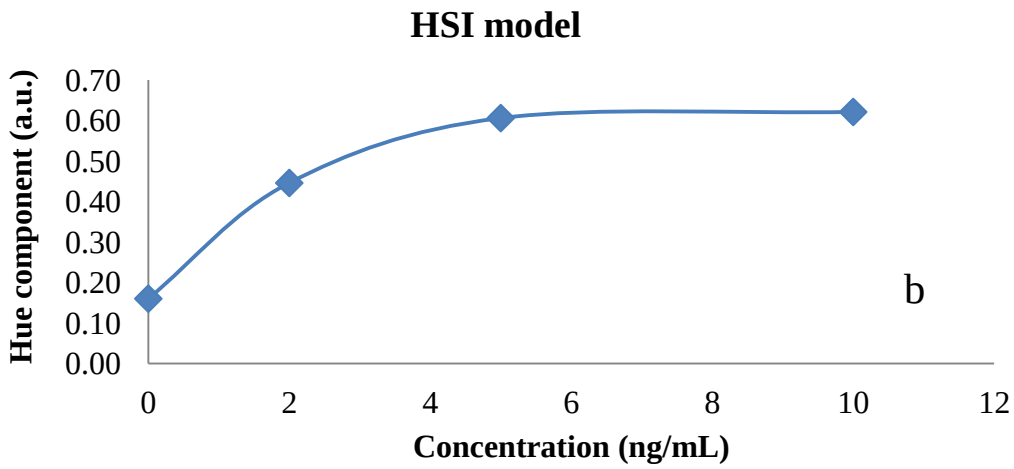

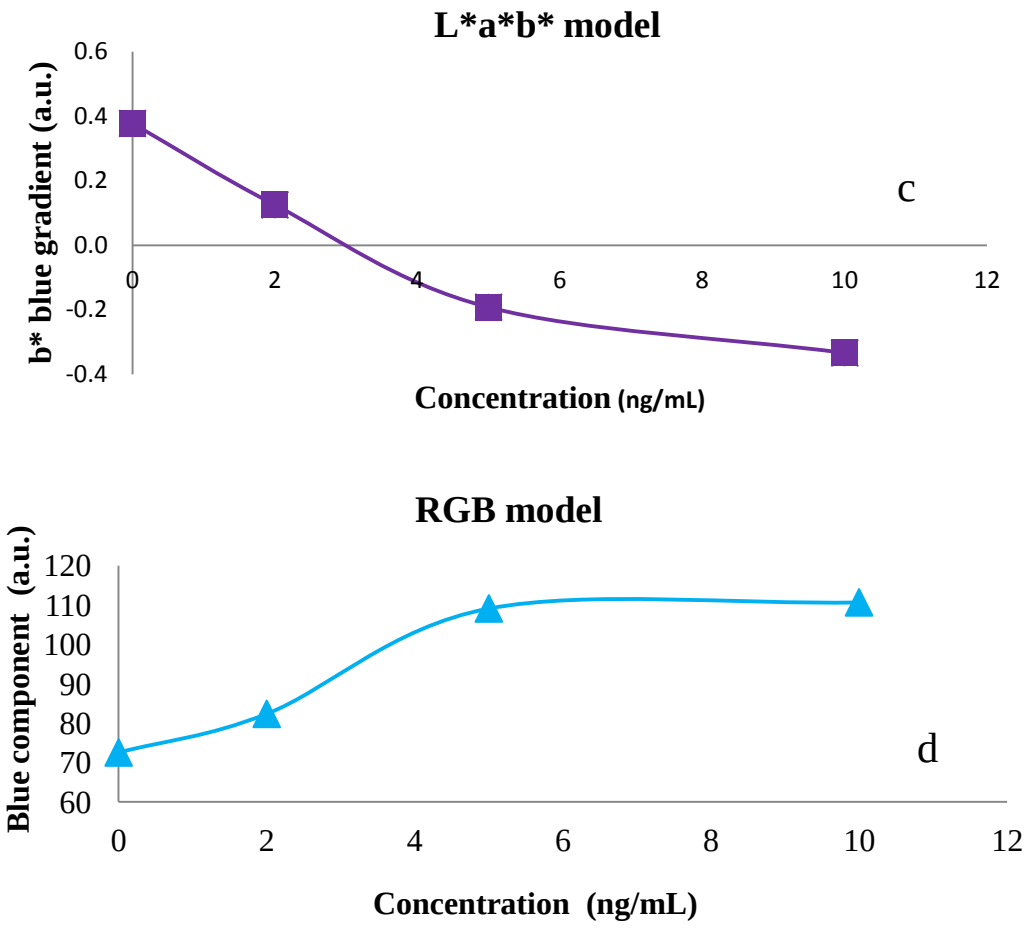

Fig. 93 Color model of calibration curve that presents a linear correlation between the concentrations.

Table 31 Beer samples spiked with OTA

		Blank	2ng/mL	5ng/mL	10ng/mL
HSI	**H**	0.4849	0.4784	0.4742	0.4740
	S	0.2181	0.1950	0.1838	0.1920
	I	0.5823	0.5580	0.5449	0.5483
HSV	**H**	0.4933	0.4806	0.4716	0.4712
	S	0.3059	0.2807	0.2687	0.2774
	V	0.6565	0.6254	0.6090	0.6140
Lab	**L**	5.1720	4.9538	4.8370	4.8375
	a	-1.6932	-1.5951	-1.5425	-1.5571
	b	-0.1835	-0.1205	-0.0877	-0.1052

RGB	**R**	115.7367	114.0567	112.9867	79.5767
	G	167.2433	159.4667	155.3033	156.5533
	B	162.4400	153.3400	148.5233	148.5036
CMY	**C**	139.2627	140.9454	142.0120	142.4231
	M	87.7549	95.5338	99.6962	98.4466
	Y	92.5584	101.6566	106.4797	104.6501
YCC	**Y**	145.9599	140.6992	137.8622	138.5479
	C	133.4952	131.9739	131.2191	131.7138
	C	105.7098	108.4872	109.9113	109.0998
YIQ	**Y**	0.5933	0.5694	0.5564	0.5596
	I	-0.1143	-0.0984	-0.0903	-0.0950
	Q	-0.0486	-0.0451	-0.0434	-0.0441

For the beer samples spiked with OTA, presented in the table 31, the same result for the last concentration as the calibration curve, in spite of different components provide a linear relationship for each concentration as the figure 94 represents.

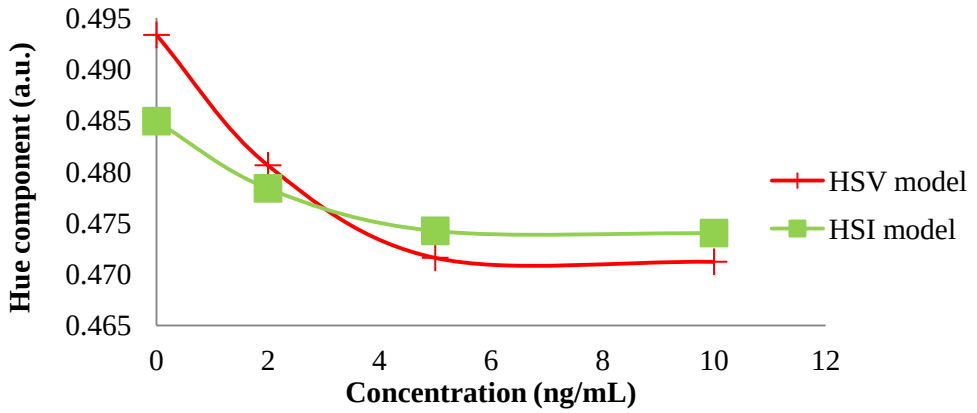

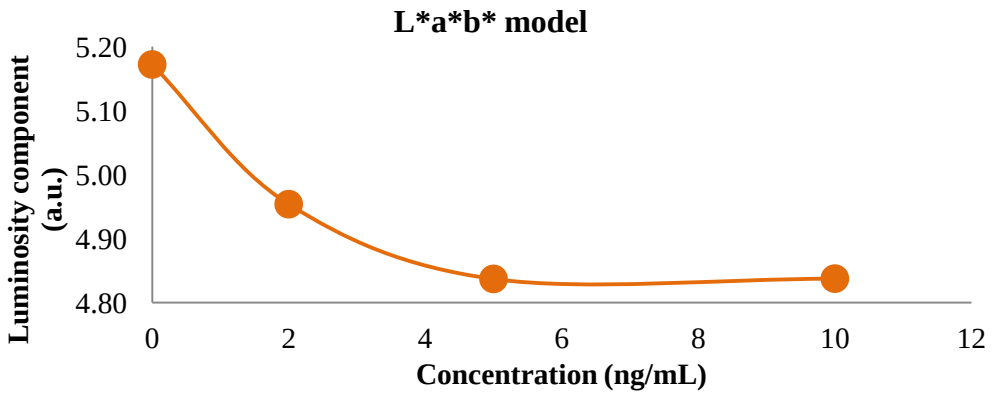

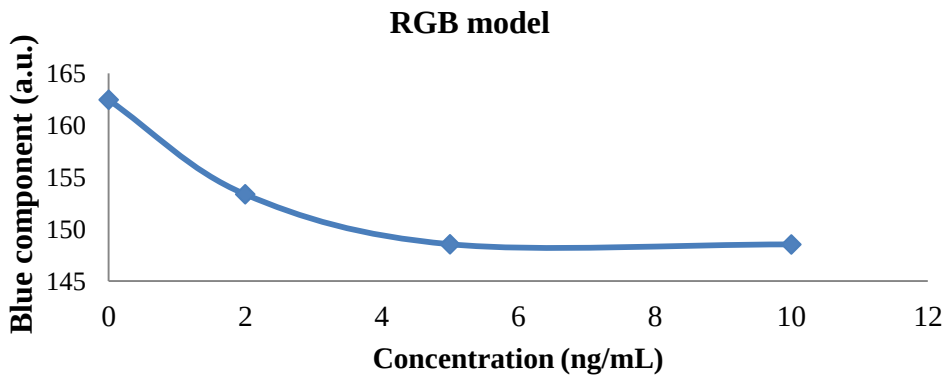

Fig. 94 Color model of beer samples spiked with OTA that presents a linear correlation between the concentrations.

Table 32 Color models of wine samples spiked with OTA.

		Blank	2ng/mL	5ng/mL	10ng/mL
HSI	**H**	0.5176	0.5197	0.4957	0.4894
	S	0.1956	0.1898	0.2066	0.2043
	I	0.5019	0.5220	0.5608	0.5631
HSV	**H**	0.5208	0.5226	0.5027	0.5015
	S	0.2805	0.2736	0.2859	0.2859
	V	0.5689	0.5860	0.6252	0.6293
Lab	**L**	3.3598	4.5206	4.9374	4.9740
	a	-1.3657	-1.3097	-1.5539	-1.5833
	b	-0.2887	-0.2834	-0.2229	-0.1923
RGB	**R**	110.1233	107.0967	112.6433	113.4567
	G	148.5033	142.9267	158.4767	159.9333
	B	147.2698	149.3367	157.8900	157.8915
CYY	**C**	144.8752	147.9013	142.3575	141.5453
	M	106.4976	112.0714	96.5263	95.0646
	Y	100.5051	105.6637	97.1099	97.5938
YCC	**Y**	134.2763	130.1840	140.2895	141.1679
	C	136.2398	136.0407	134.4983	133.6966
	C	110.7673	111.8285	107.8862	107.7507
YIQ	**Y**	0.5401	0.5214	0.5675	0.5716
	I	-0.0972	-0.0918	-0.1064	-0.1054
	Q	-0.0245	-0.0219	-0.0387	-0.0416

The table 32 summarized the value of the different models employed with wine samples to detect the concentration of OTA without use an extracting column, the color models that presents a direct or indirect linear relation with the concentration evaluated are in the figure 95.

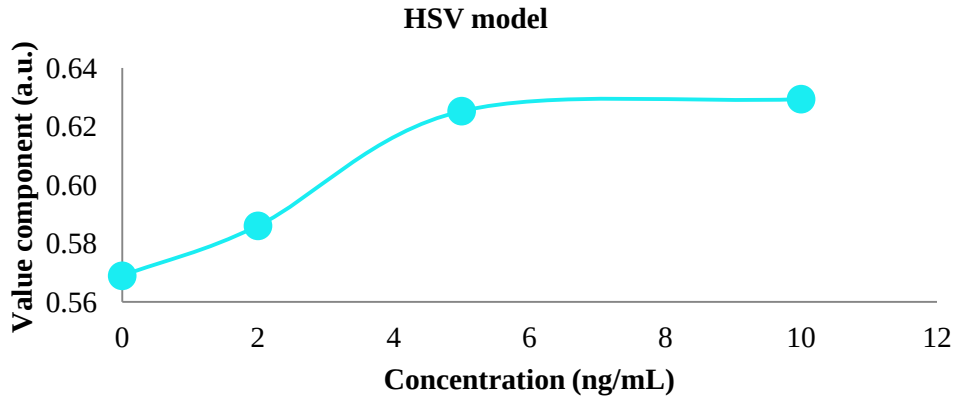

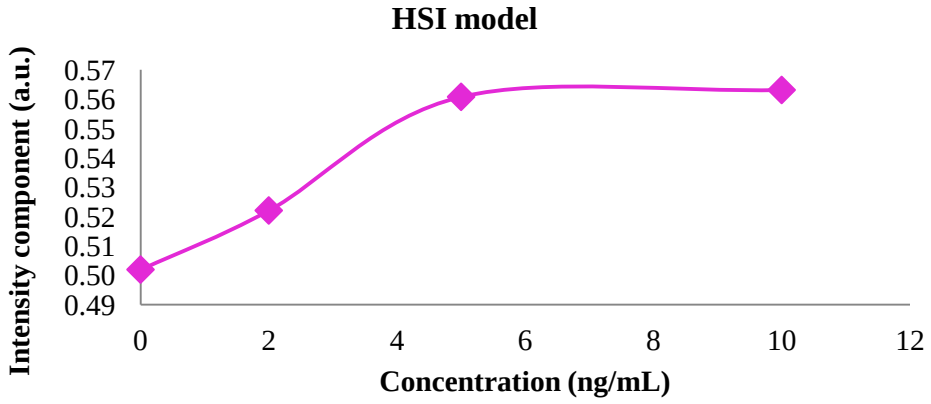

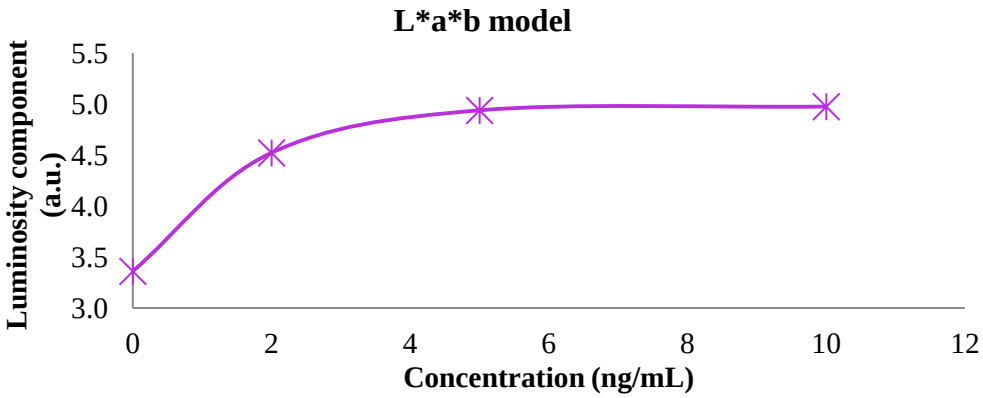

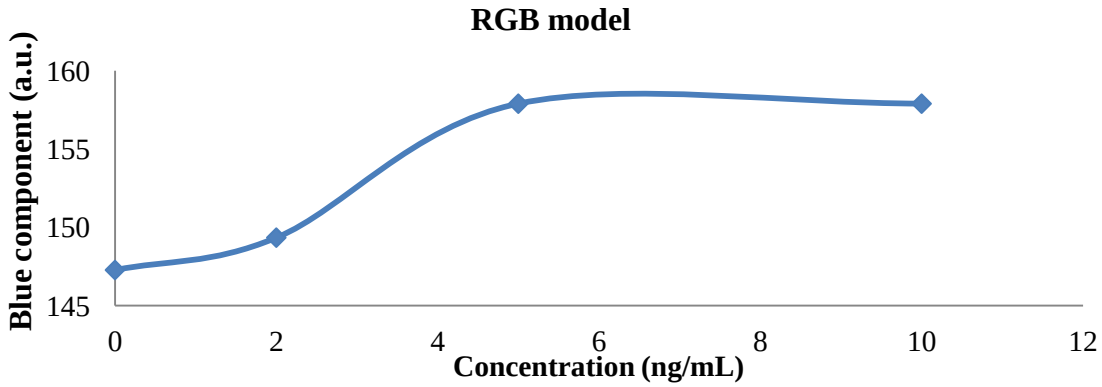

Fig. 95 Color models of wine samples that present relation between the concentrations.

The color model of the beer and wine samples were subtract from the color models of the calibration curve to normalize the data and find components to different among the concentrations tested, the results are presented in the figure 96 for the beer samples.

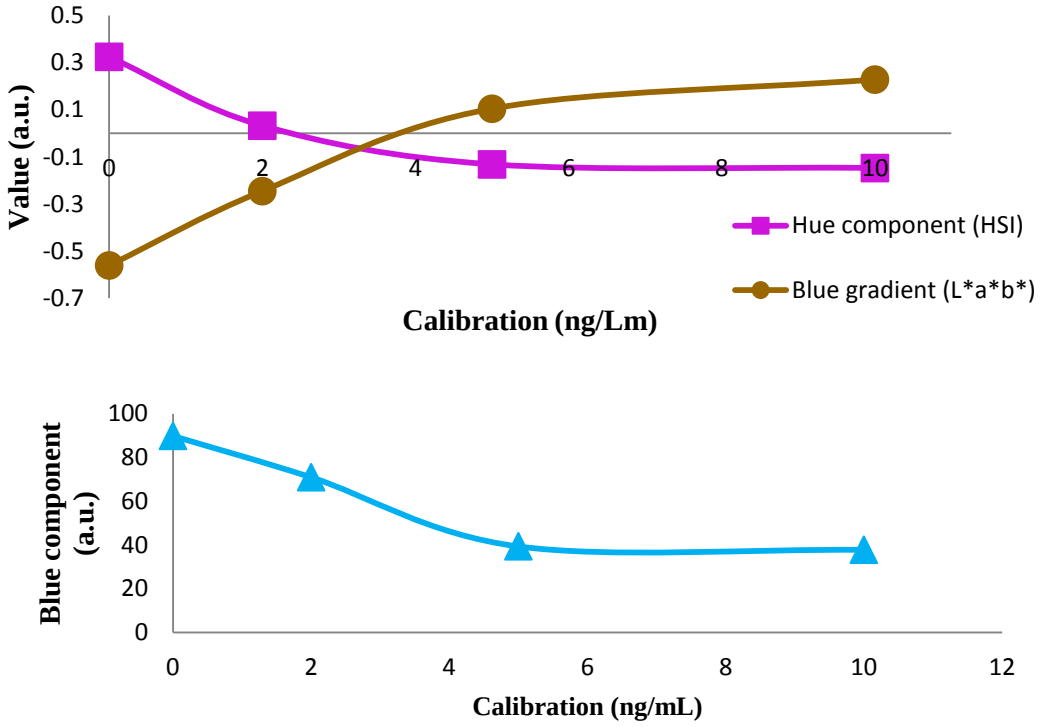

Fig. 96 Color model with a relation for beer samples, Hue component from HSI and Blue gradient from L*a*b* (up) and RGB is expressed as blue component.

In the case of wine, the comparative components are in the figure 97. The blue component from RGB model used again. This component presented good results a direct relation from the fluorescence of OTA in the case of extraction columns and without extraction columns. These confirm that there is a direct relation of the blue component and the fluorescence intensity provide by each concentration of OTA.

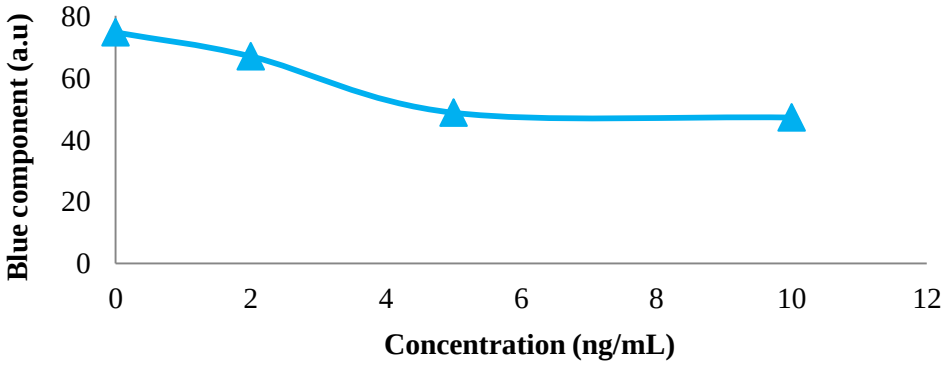

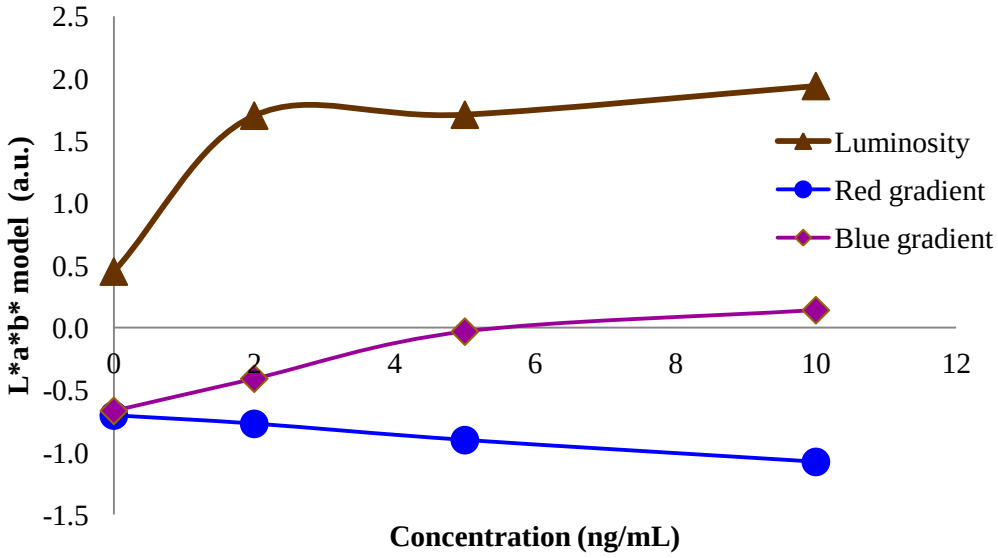

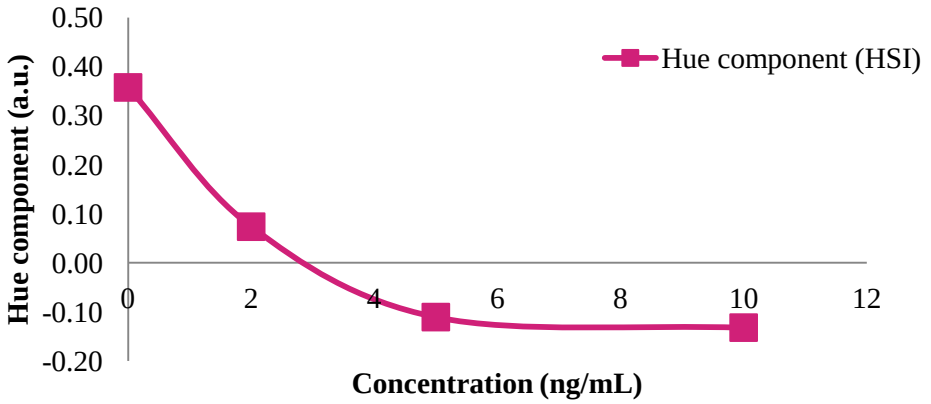

Fig. 97 Color model with a relation for beer samples, RGB, L*a*b* and HIS, respectively.

The color model such as CMY, YCC and YIQ does not present a significant difference or a relation among the concentrations. One more color model employed was to get the CIE XYZ diagram for each concentration, the images of the diagrams presented in the figure 98 (see figure 40, equation 21), where there is no difference among the concentrations; however, the values obtained demonstrated that the excitation spectrum was located at 450-460 nm depends of the solution. This wavelength is consistent in all samples evaluated, except for the blank of the calibration curve that corresponds to methanol, the wavelength is superior to the others.

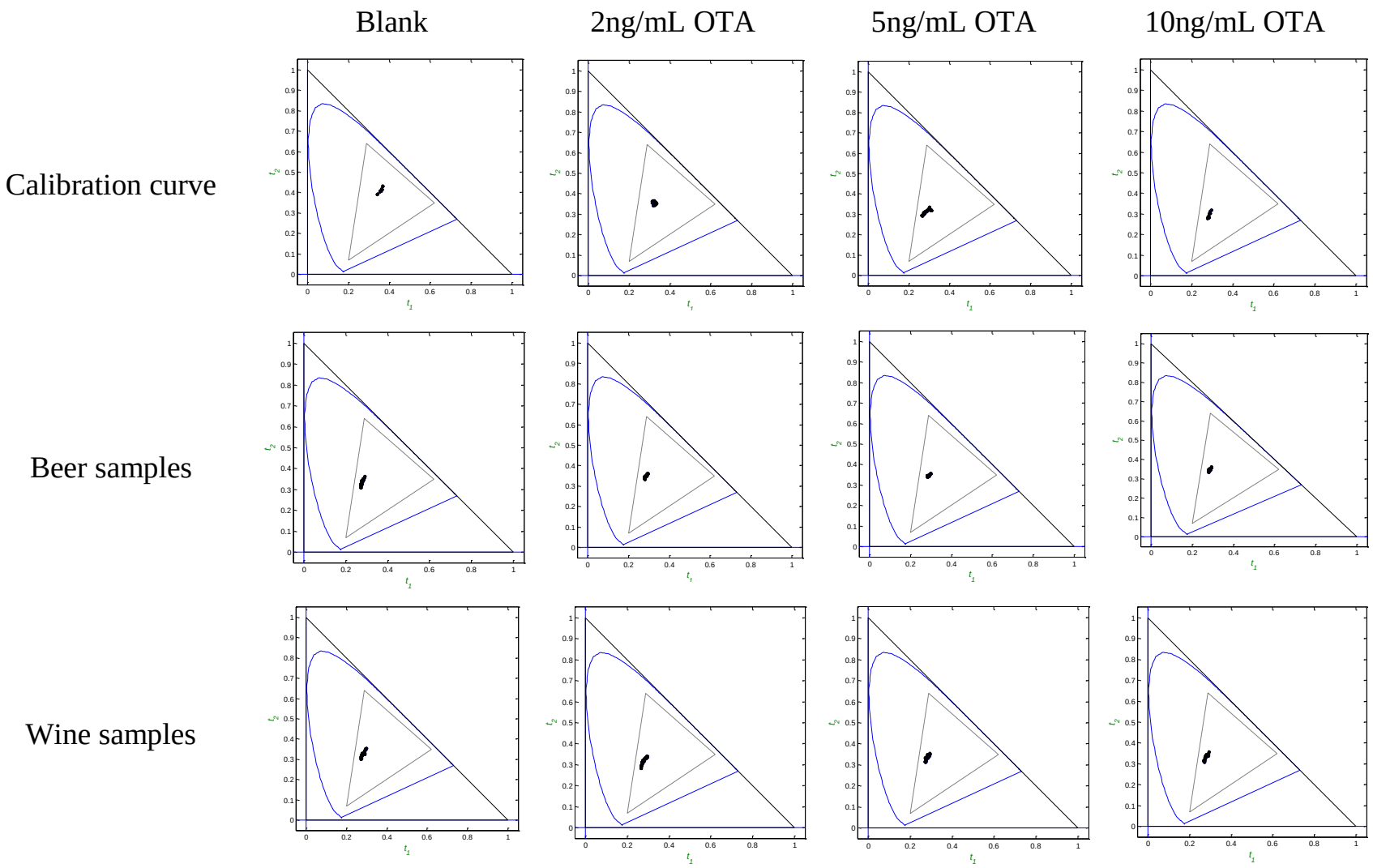

Fig. 98 Diagram CIE XYZ from the samples tested.

Employing the command of MATLAB, graycoprops to calculate the contrast, correlation, energy and homogeneity (see table 13). The contrast, correlation and homogeneity not provide significant changes among concentrations of the components of RGB model. The energy provides differences and a direct relation for the samples used in the calibration curve and the wine samples as the figure 99 shows. In the case of beer samples, there is not a relation between the energy calculated and the concentrations tested.

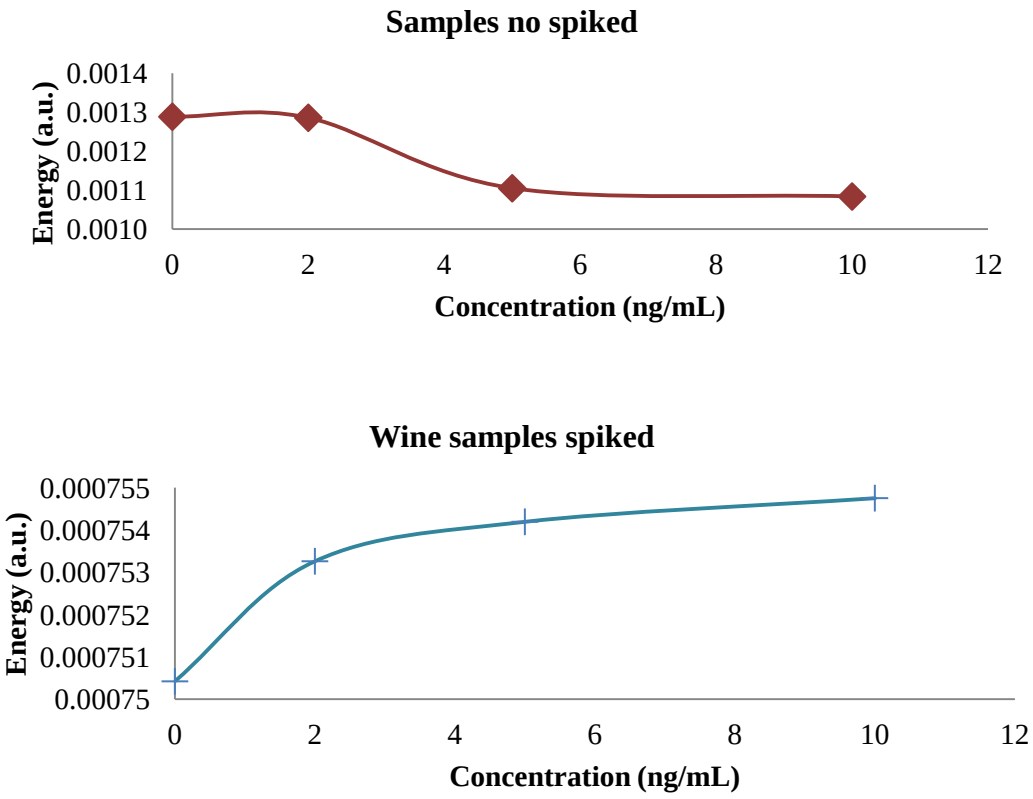

Fig. 99 Energy calculated based on the command graycoprops of MATLAB.

The correlation between the images is to know the relation that the image keep between them, the table 33 presents the relation of the concentrations used to build the calibration curve, the best correlation correspond to the concentration tested with its correspondent images. Some case, there is a small correlation with concentrations close to the tested concentration. The correlation was obtained for the blue component and for the gray-scale component.

Table 33 Correlation between the concentrations of the calibration curve.

	Blue component				Gray-scale component			
	Blank	**2ng/mL OTA**	**5ng/mL OTA**	**10ng/mL OTA**	**Blank**	**2ng/mL OTA**	**5ng/mL OTA**	**10ng/mL OTA**
Blank	**0.90444**	0.18317	0.00000	0.00000	**0.65753**	0.55437	0.00000	0.00000
2ng/mL OTA	0.18317	**0.89565**	0.00000	0.00000	0.55437	**0.90261**	0.00000	0.00000
5ng/mL OTA	0.00000	0.00000	**0.64827**	0.15684	0.00000	0.00000	**0.74592**	0.66997
10ng/mL OTA	0.00000	0.00000	0.15684	**0.91119**	0.00000	0.00000	0.66997	**0.79744**

Table 34 Correlation between the beer samples spiked with OTA.

	Blue component				Gray-scale component			
	Blank	**2ng/mL OTA**	**5ng/mL OTA**	**10ng/mL OTA**	**Blank**	**2ng/mL OTA**	**5ng/mL OTA**	**10ng/mL OTA**
Blank	**0.82734**	0.65834	0.56620	0.60349	**0.8377**	0.71425	0.67351	0.68837
2ng/mL OTA	0.65834	**0.79584**	0.71550	0.73835	0.71425	**0.87127**	0.76846	0.81317
5ng/mL OTA	0.57225	0.71550	**0.81404**	0.75472	0.67351	0.76846	**0.83353**	0.78295
10ng/mL OTA	0.60349	0.73835	0.75472	**0.82157**	0.68837	0.81317	0.78295	**0.86574**

Table 35 Correlation between the wine samples spiked with OTA.

	Blue component				Gray-scale component			
	Blank	**2ng/mL OTA**	**5ng/mL OTA**	**10ng/mL OTA**	**Blank**	**2ng/mL OTA**	**5ng/mL OTA**	**10ng/mL OTA**
Blank	**0.83278**	0.67031	0.78164	0.77067	**0.89061**	0.73302	0.80895	0.82205
2ng/mL OTA	0.67031	**0.86840**	0.72736	0.75043	0.73302	**0.89702**	0.66841	0.68630
5ng/mL OTA	0.78164	0.72736	**0.83947**	0.79422	0.80895	0.66841	**0.90275**	0.88356
10ng/mL OTA	0.77067	0.75043	0.79422	**0.88894**	0.82205	0.68630	0.88356	**0.93539**

The tables 34 and 35 present the correlation for beer and wine samples, respectively. For example in the case of blue component employed in this method of beer samples, the lower values correspond to the blank spiked, so one can conclude, that this method for beer can be separated the blank to the OTA samples. The wine is a very complex samples, it was no possible to find a correlation that allow identifying or separating the concentrations.

The mean in X-axis of the image in gray scale was obtained and the results show a behavior associated to theory of lenses due to the diffraction patterns of lenses. It is presented in the images; the maximum peak is the same and the minimum peak and it can be associated with the radiation pattern of the emitter, in this case the UV-LED as the figure 100 shows. Details of the distribution of light over the diffraction pattern depend on the distances of both the source and the screen from the diffracting aperture.

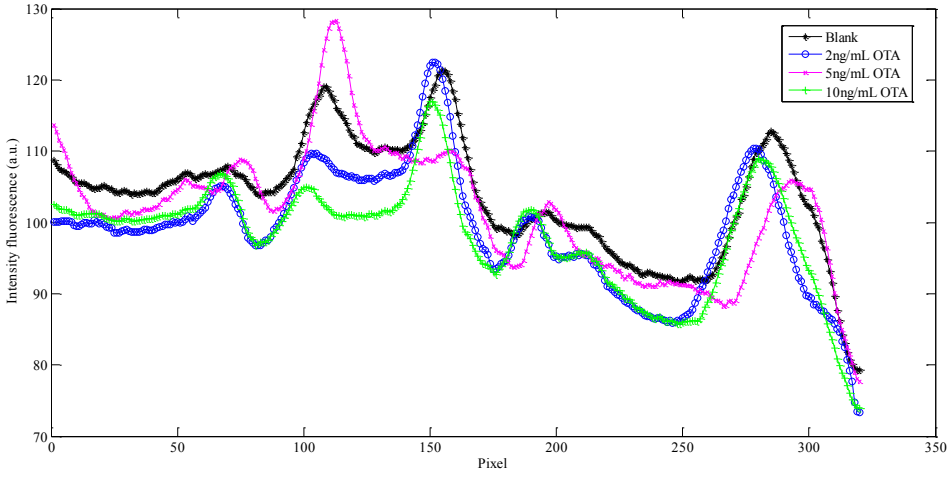

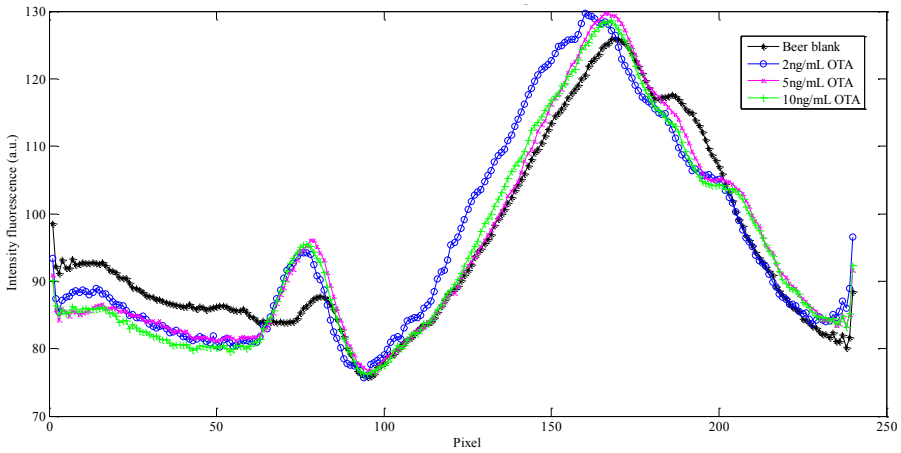

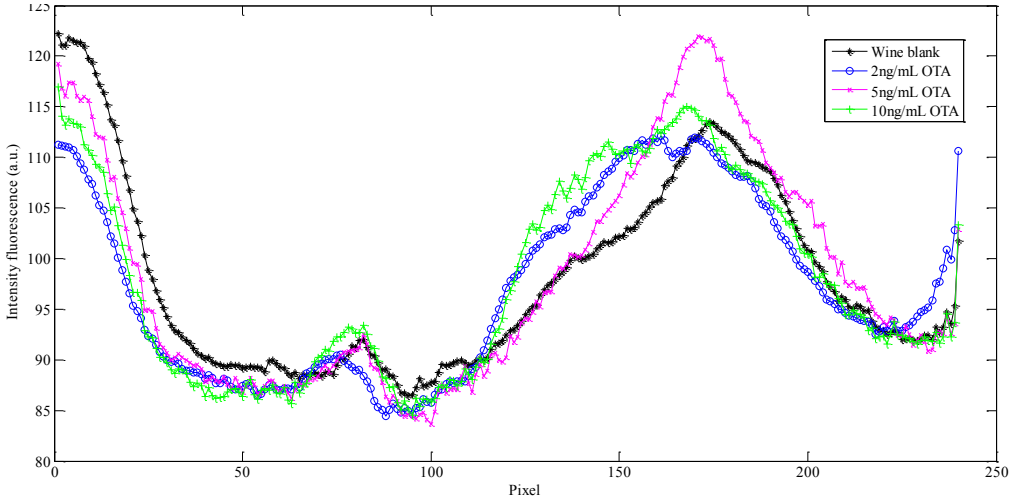

Fig. 100 Mean of the calibration curve, beer samples and wine samples, respectively.

This pattern may be associated to the concentration of OTA, changes in the maximum, minimum, focus and width or height of the peaks. Finally, the FFT was used to know how the behavior of the components, these are presented in the figure 101 (see equation 25-27). The samples used as calibration curve shows a specific peak, except the concentration of 5 ng/mL. The real samples spiked shows frequencies in X-axis.

.

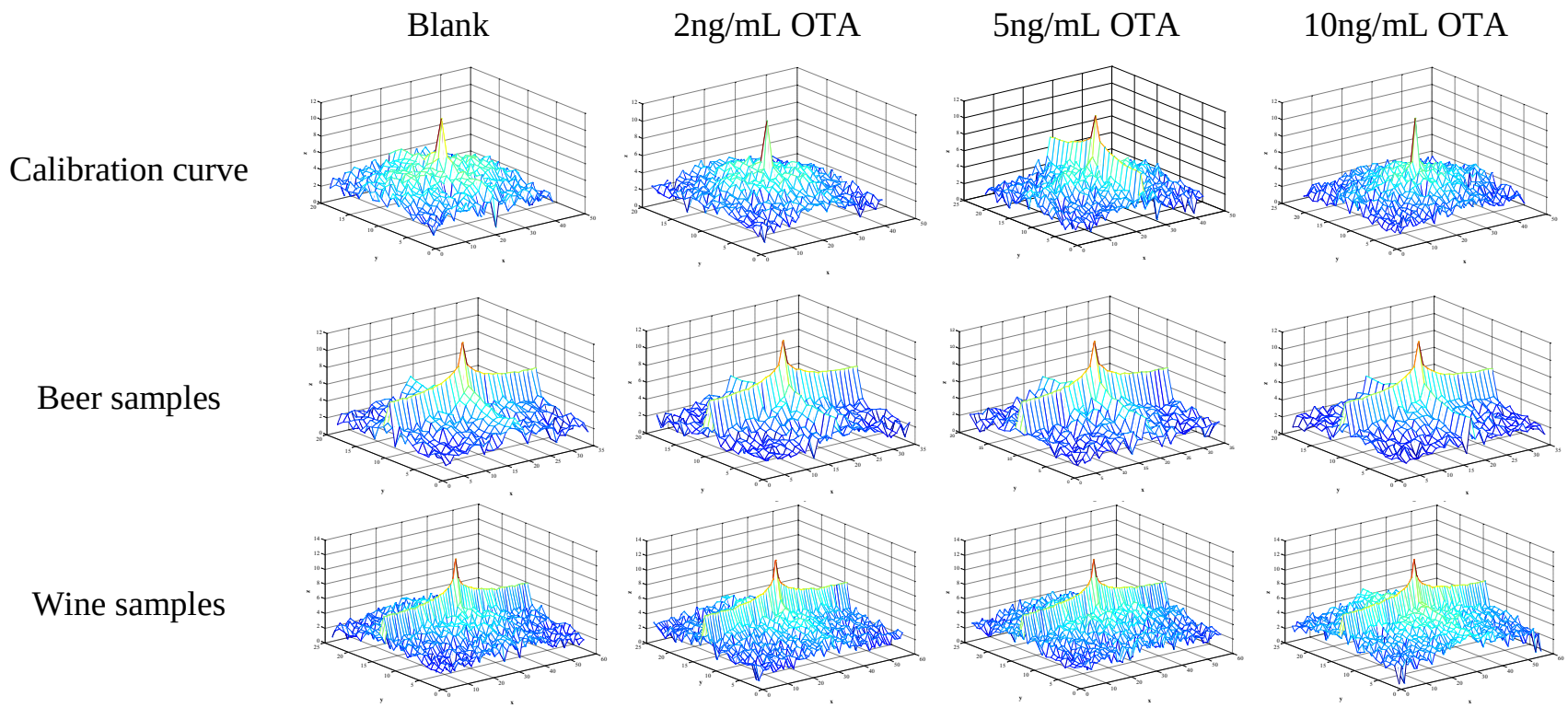

Fig. 101 FFT for the samples of OTA in 3D.

CHAPTER V

CONCLUSIONS AND FUTURE WORK

Automated flow-based electrochemical aptasensor

The applicability of the developed flow-based aptasensor was validated by detecting OTA in beer samples; the incorporation of the aptamer into flow device increased the sensitivity of the system to detect low concentration of OTA; this improvement was achieved by automating the procedures, from the fabrication of the aptasensor to the detection step. Besides a reduction in the analysis time and a decrease of the complexity of the method was achieved. The simplicity of the automated flow based system and it does not require trained personal allow to extended to other bio-molecules. For the indirect assay, the obtained LOD and IC50 were lower than that obtained in the direct competitive assay resulting in a high sensitive flow-based indirect competitive aptasensor.

Detection of pesticides with the use of LEDs as emitter

The LOD of optical system is three times lower than the spectrophotometer system. As expected from the inhibition rate constants values, the inhibitory effect of carbofuran on the genetically modified D. melanogaster was weaker than the electric eel and wild D. melanogaster. Moreover, we observed a high sensitivity of B394-AChE toward the two organophosphate pesticides. Entire system requires inexpensive equipment, is an innovative, efficient and easy-to-use optical system, with low-cost development process that makes it possible for the in situ detection of pesticides. Besides, it permits the acquisition of the data and save it with a computer. A miniature spectrophotometer for 412 nm was produced with LEDs and photo detectors.

Detection of OTA with UV-LEDs

The best linear range was obtained with a UV-LED at 365 nm, 4mW but the best distribution of the intensity of fluorescence respect to the concentrations was presented by UV-LED at 375nm, 15.1 mW that provides a higher value in voltage for each concentration than the other UV-LEDs. In spite is a system easy to use, allows portability and acquisition

data with a computer. It is no possible to detect concentration of OTA less than 250 ng/mL, it is a high concentration if it is compared with the limit permissible that is 2 µg/L for some foods.

ArduCAM as fluorescence set-up

The use of CMOS sensor as detector of fluorescence solutions was possible, to measure the concentration of these solutions, the concept of RGB components was employed, considering the natural fluorescence of OTA. The image capture was decomposed in each component RGB allowing find that exist a relation of blue component directly proportional with the fluorescent intensity of the concentrations of OTA.

However, the use of ArduCAM is no good in the absence of light, the image is pixilated and poor quality even though a sensor of 5 MP was used, the image is dark and the cuvette is not defined completely, producing confusion to select the fluorescence strip. Besides, it is no possible to identify the low concentrations in spite of the good coefficient of linear correlation employing UV-LEDs. The UV-LED at 375nm to 9mW present the best results to detect the low concentration with a linear range of 2-40 µg/L of OTA, this wavelength for us experimental shows the best results to detect low concentration of OTA using the ArduCAM fluorescence set-up. For the NSPU510CS, the intensity of the UV-LED is so high that the intensity saturated the image sensor of the ArduCAM in the highest concentrations, the value do not present changes for concentrations greater than 10 µg/L in the blue component. However, the green component shows a lineal correlation that corresponds when OTA in acid medium due to OTA shows green fluorescence. This is because the intensity of the LED is so high that the color emitted by LED (green color) produces an acid medium in the OTA solution.

The best results were with the samples prepared in EtOH because with the samples in MeOH presented a reduction of the fluorescence, it is attributed to a probably damage in the CMOS sensor to the continuous exposition to the UV-light.

CMOS sensor in serial port camera module for detect OTA

A developed device using a CMOS sensor to detect OTA was designed and its graphical user interface . Both are easy to use, allowing the portability by its small dimensions,

the device is powered by USB port. It demonstrated a good stability and reproducibility in real samples such as wine, beer and cocoa. The relation of blue component is directly proportional with the fluorescent intensity of the concentrations of OTA, which was corroborated with this CMOS sensor. In the case of wine and beer, the LOD was 2µg/L comparable with the LOD of OTA in the HPLC. The coefficient of the correlation $r \geq 0.9$, showing a good linear correlation. An important factor is the efficiency of mycotoxins recovery, in both cases, an expected the recovery for IAC ranged between 70-110% for the HPLC and the CMOS sensor. For the use of MIP columns, these do not show an acceptable recovery using the CMOS sensors, ether a linear correlation between the concentration of OTA and the blue fluorescence intensity. More responses of interferons were observed in the chromatogram of samples spiked with OTA after clean up with MIP. Using cocoa extracted OTA, the proposed methodology provides a LOD at 2 µg/L with good reproducibility. It is a very low cost relative to the HPLC and the results between both devices are comparable.

Smartphone as detector of OTA

A portable system with the use of smartphone camera, LED-UV and wireless was designed and successfully tested to detect OTA in beer samples. The measurements were compared with commercial equipment and the system designed provides a LOD at 2 µg/L with good reproducibility and stability. The graphical user interface developed is easy to use, allowing the portability by its small dimensions and the electronic circuit is powered by USB port using the smartphone as a source of energy. It was found that the fluorescence of the samples is directly proportional to the OTA concentrations but the radiant flux of the LED is an inverse proportional to the OTA concentrations. The best emitter to detect OTA is at 375 nm with a radian flux of 9 mW and it is capable to detect 1.25-20 µg/L. It is possible to use a fluorescence enhancer to increase the blue component fluorescence intensify to had better resolution. The use of new technologies allows employ equipment of the laboratory in the field in a simple, economical and portable mode.

Flow systems

Due to the automatization of the methodologies was possible controlled the speed, volume and time, the reduction of reactive, a trained personal was not required and decreased

the complexity of the method. The reduction in the analysis time was no achieved. The use of HyperTerminal allows portability and it can be used with a portable computer with minimum requirements.

Evaluation of the fluorescence device performance under specific conditions

The influence of solvent, pH and ionic strength on fluorescence emission of OTA allows seeing, that there is maximum fluorescence intensity in buffer and alcoholic solvent, the pH studies suggested the structure dependent fluorescence emission pattern and the buffer with highest salt concentration reveals a high fluorescence.

APP designed

It is possible to use the new technologies together the analytical methods, the new technologies provides fast test as scanning methods, the optic devices do not affect, destroy or alter the sample for that reason an APP designed and installed in the smartphone was developed. It is necessary to do more experiments to evaluate the practicability of the application and it is a first approximation of its functionality. For the moment, the APP work to capture the image and to show the RGB values, directly. To save the information and to send it by email for future analysis.

Image processing

More analysis and other methods are required to quantify the OTA concentration without the use of extraction columns. Exist a relation of blue component directly proportional with the fluorescent intensity of the concentrations of OTA, it was demonstrated also with this methodology. More than one color model can use to identify samples spiked with OTA, however the same cannot prove good results for the sample, so it is possible to use more than one method at the same time to identify the OTA concentrations. The wine samples are more complex that the beer samples, the color of the wine causes more false positive or negative or not to find any relationship between the spiked samples at different concentrations.

Future work

For future work, I proposed to design other electronic circuit to reduce the LOD, to search the photodiode or phototransistor capable to work when is excited with UV light. Improve the LOD of the fluorescence detection systems using an LED at 330 nm. Besides to characterize other CMOS sensors with higher resolution. In the case of flow system, it must be optimize and implemented using pumps with higher volumes. Improve the design and testing of the application of the APP in field, transfer it to other portable devices.

Make a greater number of experiments of real samples spiked to employ with neural networks to quantify the concentration of the mycotoxin without using extraction columns, may be this analysis provides best results. The use of extraction grids to ensure that the excitation spectrum corresponds to the OTA, also it can provide other analysis or results. Finally, build a portable and low cost system with a commercial design, so it can be used in laboratory, low-income schools. Try different real samples or samples naturally contaminated.

References

[1] L. Abrunhosa, R. R. M. Paterson, and A. Venâncio, "Biodegradation of ochratoxin a for food and feed decontamination," *Toxins (Basel).*, vol. 2, pp. 1078–1099, 2010.

[2] T. Kuiper-Goodman, "Risk assessment to humans of mycotoxins in animal-derived food products," *Vet. Hum. Toxicol.*, vol. 32, pp. 6–13, 1990.

[3] D. Bueno, G. Istamboulie, R. Muñoz, and J. L. Marty, "Determination of Mycotoxins in Food: A Review of Bioanalytical to Analytical Methods," *Appl. Spectrosc. Rev.*, vol. 50, no. 9, pp. 728–774, 2015.

[4] A. Rhouati, A. Hayat, D. B. Hernandez, Z. Meraihi, R. Munoz, and J. Marty, "Development of an automated flow-based electrochemical aptasensor for on-line detection of Ochratoxin A," *Sensors Actuators B. Chem.*, vol. 176, pp. 1160–1166, 2013.

[5] J. Huffman, R. Gerber, and L. Du, "Recent advancements in the biosynthetic mechanisms for polyketide-derived mycotoxins," *Biopolymers*, vol. 93, no. 9, pp. 764–776, 2010.

[6] S. De Saeger, *Determining mycotoxins and mycotoxigenic fundi in food ans feed*, 1st. ed., vol. 1. Philadeplphia, USA: Woodhead Publishing Limited, 2011.

[7] M. M. Abouzied, A. D. Horvath, P. M. Podlesny, N. P. Regina, V. D. Metodiev, R. M. Kamenova-Tozeva, N. D. Niagolova, A. D. Stein, E. A. Petropoulos, and V. S. Ganev, "Ochratoxin A concentrations in food and feed from a region with Balkan Endemic Nephropathy.," *Food Addit. Contam.*, vol. 19, no. 8, pp. 755–64, 2002.

[8] A. Pfohl-Leszkowicz and R. A. Manderville, "Ochratoxin A: An overview on toxicity and carcinogenicity in animals and humans," *Mol. Nutr. Food Res.*, vol. 51, no. 1, pp. 61–99, 2007.

[9] R. Fuchs and M. Peraica, "Ochratoxin A in human kidney diseases," *Food Addit. Contam.*, vol. 22, no. Suppl 1, pp. 53–57, 2005.

[10] A. el Khoury and A. Atoui, "Ochratoxin A: General overview and actual molecular status," *Toxins (Basel).*, vol. 2, no. 4, pp. 461–493, 2010.

[11] M. Weidenbörner, *Encyclopedia of food mycotoxins*, 1st. ed. GieBen Germany: Springer- Verlag Berlin Heidelberg GmbH, 2001.

[12] S. Budavari, *The Merck Index*, 11th ed. USA: Merck&Co, 1989.

[13] R. Mateo, Á. Medina, E. M. Mateo, F. Mateo, and M. Jiménez, "An overview of ochratoxin A in beer and wine," *Int. J. Food Microbiol.*, vol. 119, no. 1–2, pp. 79–83, 2007.

[14] T. Mariana, "Evaluation du risque de contamination alimentaire en mycotoxines néphrotoxiques et cancérogènes (notamment l'ochratoxine A): Validation de biomarqueurs d'exposition et d'effet," Institut National Polytechnique de Toulouse, 2008.

[15] T. Vo-Dinh, *Biomedical photonics handbook*. Boca Raton ,Florida, USA: CRC Press LLC, 2003.

[16] J. Hashemi and N. Alizadeh, "Investigation of solvent effect and cyclodextrins on fluorescence properties of ochratoxin A," *Spectrochim. Acta - Part A Mol. Biomol. Spectrosc.*, vol. 73, pp. 121–126, 2009.

[17] J. E. Dickens, M. S. Vaughn, M. Taylor, and M. Ponstingl, "An LED array-based light induced fluorescence sensor for real-time process and field monitoring," *Sensors*

Actuators, B Chem., vol. 158, pp. 35–42, 2011.
[18] C. Cucci, a. G. Mignani, C. Dall'Asta, R. Pela, and a. Dossena, "A portable fluorometer for the rapid screening of M1 aflatoxin," *Sensors Actuators B Chem.*, vol. 126, no. 2, pp. 467–472, 2007.
[19] G. Chen, "Versatile portable fluorometer for time-resolved luminescence analysis," *Rev. Sci. Instrum.*, vol. 76, p. 063107, 2005.
[20] A. K. Roy Choudhury, *Principles of colour appearance and measurement. Volume 1: Object appearance, colour perception and instrumental measurement*, 1st ed. Oxford, UK: Woodhead Publishing Limited, 2014.
[21] D. Bueno, G. Alonso, R. Muñoz, and J. L. Marty, "Low-cost and portable absorbance measuring system to carbamate and organophosphate pesticides," *Sensors Actuators, B Chem.*, vol. 203, pp. 81–88, 2014.
[22] G. L. Ellman, K. D. Courtney, V. Andres, and R. M. Featherstone, "A new and rapid colorimetric determination of acetylcholinesterase activity," *Biochem. Pharmacol.*, vol. 7, no. 2, pp. 88–95, 1961.
[23] W. Brügel, *An Introduction to Infrared Spectroscopy*, 1st. ed. New York, USA: John Wiley & Sons Inc., 1962.
[24] G. S. Nunes, T. Montesinos, P. B. . Marques, D. Fournier, and J. L. Marty, "Acetylcholine enzyme sensor for determining methamidophos insecticide. Evaluation of some genetically modified acetylcholinesterases from Drosophila melanogaster," *Anal. Chim. Acta*, vol. 434, pp. 1–8, 2001.
[25] I. . Segel, *Enzyme Kinects: Behavior and analysis of rapid equilibrium and steady-state enzyme systems*, 1st. ed. New York, USA: Wiley, 1993.
[26] P. S. Steyn, "Mycotoxins, general view, chemistry and structure," *Toxicol. Lett.*, vol. 82/83, pp. 843–851, 1995.
[27] D. P. H. Hsieh, "Health risks posed by mycotoxins in food," *Korean J. Toxicol.*, vol. 6, no. 2, pp. 159–166, 1990.
[28] M. Pal, F. Gizaw, F. Abera, P. K. Shukla, and R. A. Hazarika, "Mycotoxins : A growing concern to human and animal health," *Beverage Food world*, vol. 42, no. 5, pp. 42–50, 2015.
[29] B. Radic, R. Fuchs, M. Peraica, and A. Lucic, "Ochratoxin A in human sera in the area with endemic nephropathy in Croatia," *Toxicol. Lett.*, vol. 91, pp. 105–109, 1997.
[30] S. de Salud, "NORMA Oficial Mexicana NOM-188-SSA1-2002, Productos y Servicios. Control de aflatoxinas en cereales para consumo humano y animal. Especificaciones sanitarias," 2002. [Online]. Available: http://www.salud.gob.mx/unidades/cdi/nom/188ssa12.html. [Accessed: 27-Dec-2015].
[31] S. de Salud, "NORMA Oficial Mexicana NOM-187-SSA1/SCFI-2002, Productos y servicios. Masa, tortillas, tostadas y harinas preparadas para su elaboración y establecimientos donde se procesan. Especificaciones sanitarias. Información comercial. Métodos de prueba," 2003. [Online]. Available: http://www.salud.gob.mx/unidades/cdi/nom/187ssa1scfi02.html. [Accessed: 27-Dec-2015].
[32] S. de Salud, "NORMA Oficial Mexicana NOM-184-SSA1-2002, Productos y servicios. Leche, fórmula láctea y producto lácteo combinado. Especificaciones sanitarias," 2002. [Online]. Available: http://www.salud.gob.mx/unidades/cdi/nom/184ssa12.html. [Accessed: 27-Dec-2015].

[33] M. Rouvier, “L’ochratoxine A : nature, origine et toxicité,” Ecole National Veterinaire Toulouse, 2002.
[34] “PubChem Compound Database,” *Center, National for Biotechnology Information*, 2001. [Online]. Available: http://pubchem.ncbi.nlm.nih.gov/compound/ochratoxi. [Accessed: 25-Dec-2015].
[35] M. Castegnaro, J. Barek, J.-M. Frémy, M. Lafontaine, M. Miraglia, E. B. Sansone, and G. M. Telling, “Laboratory decontamination and destruction of carcinogens in laboratory wastes : Some mycotoxins,” *IARC Sci. Publ. Lyon, Int. Agency Res. Cancer*, vol. 113, p. 63, 1991.
[36] IARC, “Some naturally occurring substances: Food items and constituents, heterocyclic aromatic amines and mycotoxins,” *IARC Monogr. Eval. Eval. Carcinog. risks to humans*, vol. 56, pp. 489–521, 1993.
[37] L. Reddy and K. Bhoola, “Ochratoxins-food contaminants: Impact on human health,” *Toxins (Basel).*, vol. 2, no. 4, pp. 771–779, 2010.
[38] M. Rai and A. Varma, Eds., *Mycotoxins in food, feed and bioweapons*, vol. 1. Springer-Verlag Berlin Heidelberg, 2010.
[39] Council for Agricultural Science and Technology, “Mycotoxins_Risk in plant, animal and human systems,” Iowa,USA, 2003.
[40] G. J. Soleas, J. Yan, and D. M. Goldberg, “Assay of ochratoxin A in wine and beer by high-pressure liquid chromatography photodiode array and gas chromatography mass selective detection,” *J. Agric. Food Chem*, vol. 49, pp. 2733–2740, 2001.
[41] K. Mayura, R. Vijayapal Reddy, A. Wallace Hayes, and W. O. Berndt, “Embryocidal, fetotoxic and teratogenic effects of ochratoxin A in rats,” *Toxicology*, vol. 25, pp. 175–185, 1982.
[42] K. Mayura, A. F. Stein, W. O. Berndt, and T. D. Phillips, “Teratogenic effects of ochratoxin A in rats with impaired renal function,” *Toxicology*, vol. 32, no. 4, pp. 277–285, 1984.
[43] K. Mayura, R. Parker, W. O. Berndt, and T. D. Phillips, “Ochratoxin A-induced teratogenesis in rats: partial protection by phenylalanine.,” *Appl. Environ. Microbiol.*, vol. 48, no. 6, pp. 1186–1188, 1984.
[44] R. D. Hood, M. J. Naughton, and A. W. Hayes, “Prenatal effects of ochratoxin A in hamsters,” *Teratology*, vol. 13, pp. 11–14, 1976.
[45] S. H. Gilani, J. Bancroft, and M. Reily, “Teratogenicity of ochratoxin A in chick embryos,” *Toxicol. Appl. Pharmacol*, vol. 46, pp. 543–546, 1987.
[46] E. Petzinger and A. Weidenbach, “Mycotoxins in the food chain: the role of ochratoxins,” *Livest. Prod. Sci.*, vol. 76, pp. 245–250, 2002.
[47] G. Müller, P. Kielstein, A. Berndt, H. Köhler, H. Rosner, and M. Heller, “Studies of the influence of ochratoxin A on immune and defence reactions in weaners.,” *Mycoses*, vol. 42, no. 7–8, pp. 495–505, 1999.
[48] “Opinion of the scientific panel on contaminants in the food chain on a request from the commission related to Ochratoxin A in food,” *EFSA J.*, vol. 365, pp. 1–56, 2006.
[49] V. Ostry, F. Malir, and J. Ruprich, “Producers and important dietary sources of ochratoxin A and citrinin,” *Toxins (Basel).*, vol. 5, no. 9, pp. 1574–1586, 2013.
[50] M. Weidenbörner, *Mycotoxins in Foodstuffs*, 2nd ed. Bonn, Germany: Springer, 2013.
[51] H. Otteneder and P. Majerus, “Occurrence of ochratoxin A (OTA) in wines: influence of the type of wine and its geographical origin.,” *Food Addit. Contam.*, vol. 17, no. 9,

pp. 793–8, 2000.
[52] E. H. Soufleros, C. Tricard, and E. C. Bouloumpasi, “Occurrence of ochratoxin A in Greek wines,” *J. Sci. Food Agric.*, vol. 83, no. 3, pp. 173–179, 2003.
[53] J. Varga and Z. Kozakiewicz, “Ochratoxin A in grapes and grape-derived products,” *Trends Food Sci. Technol.*, vol. 17, no. 2, pp. 72–81, 2006.
[54] M. Weidenbörner, *Mycotoxins in feedstuffs*, vol. 1. Bonn, Germany: Springer.
[55] W. H. Organization, “IARC-International Agency for Research on Cancer,” 2012. [Online]. Available: http://www.iarc.fr/index.php. [Accessed: 29-Dec-2015].
[56] N. W. Turner, S. Subrahmanyam, and S. A. Piletsky, “Analytical methods for determination of mycotoxins: A review,” *Anal. Chim. Acta*, vol. 632, no. 2, pp. 168–180, 2009.
[57] European Mycotoxin Awareness Network, “Mycotoxins Legislation Worldwide,” 2000. [Online]. Available: http://services.leatherheadfood.com/eman/FactSheet.aspx?IDD79. [Accessed: 29-Dec-2015].
[58] D. Bueno, R. Muñoz, and J. L. Marty, “Common Methods to Detect Mycotoxins : A Review with Particular Emphasis on Electrochemical Detection,” in *Sensing in Electroanalysis*, vol. 8, 2014, pp. 85–114.
[59] L. Monaci and F. Palmisano, “Determination of ochratoxin A in foods : state-of-the-art and analytical challenges,” *Anal. Bioanal. Chem.*, vol. 378, pp. 96–103, 2004.
[60] WHO, “Evaluation of certain food additives and contaminants. Thirty-seventh report of the joint FAO/WHO Expert Committee on Food Additives,” Geneva, Switzerland, 1991.
[61] Joint FAO/WHO Expert Committee on Food Additives, “Report on meeting of experts committeed and study groups,” Geneve, 2002.
[62] EC European Community., “Opinion on of the Scientific Committee on Food (SCF) on Ochratoxin A,” 1998. [Online]. Available: http://ec.europa.eu/food/fs/sc/scf/out14_en.html. [Accessed: 29-Dec-2015].
[63] G. A. A. Silverio, “La détection des composés organophosphorés utilisant enzymes génétiquement modifiées et Intelligence Artificielle et systèmes automatiques,” CINVESTAV/UPVD, 2012.
[64] N. W. Turner, H. Bramhmbhatt, M. Szabo-vezse, A. Poma, R. Coker, and S. A. Piletsky, “Analytical methods for determination of mycotoxins : An update (2009 e 2014),” *Anal. Chim. Acta*, vol. 901, pp. 12–33, 2015.
[65] J. M. Soriano del Castillo, *Micotoximas en Alimentos*, 1st ed. España: Díaz de Santos, 2007.
[66] B. Zimmerli and R. Dick, “Determination of ochratoxin A at the ppt level in human blood, serum, milk and some foodstuffs by high-performance liquid chromatography with enhanced fluorescence detection and immunoaffinity column cleanup: methodology and Swiss data,” *J Chromatogr B Biomed Appl*, vol. 666, no. 1, pp. 85–99, 1995.
[67] M. Z. Zheng, J. L. Richard, and J. Binder, “A review of rapid methods for the analysis of mycotoxins,” *Mycopathologia*, vol. 161, no. 5, pp. 261–273, 2006.
[68] D. Barug, D. Bhatnagar, H. P. Van Egmond, J. W. Van Der Kamp, W. A. Van Osenbruggen, and A. Visconti, *The mycotoxin factbook*, 1st ed. The Netherlands: Wageningen Academic Publishers, 2006.
[69] A. Visconti, M. Pascale, and G. Centonze, “Determination of ochratoxin A in wine by

means of immunoaffinity column clean-up and high-performance liquid chromatography," *J. Chromatogr. A*, vol. 864, pp. 89–101, 1999.
[70] E. a Santos and E. a Vargas, "Immunoaffinity column clean-up and thin layer chromatography for determination of ochratoxin A in green coffee.," *Food Addit. Contam.*, vol. 19, no. 5, pp. 447–458, 2002.
[71] E. Chiavaro, A. Lepiani, F. Colla, P. Bettoni, E. Pari, and E. Spotti, "Ochratoxin A determination in ham by immunoaffinity clean-up and a quick fluorometric method," *Food Addit. Contam.*, vol. 19, no. 6, pp. 575–581, 2002.
[72] A. Pittet, "Modern methods and trends in mycotoxin analysis," *Mitt. Leb. Hyg*, vol. 96, no. September, pp. 424–444, 2005.
[73] J. Cao, S. Zhou, W. Kong, M. Yang, L. Wan, and Y. Shihai, "Molecularly imprinted polymer-based solid phase clean-up for analysis of ochratoxin A in ginger and LC-MS/MS confirmation," *Food Control*, vol. 33, pp. 337–343, 2013.
[74] J. Jodlbauer, N. M. Maier, and W. Lindner, "Towards ochratoxin A selective molecularly imprinted polymers for solid-phase extraction," *J. Chromatogr. A*, vol. 945, pp. 45–63, 2002.
[75] J. C. C. Yu and E. P. C. Lai, "Molecularly imprinted polymers for Ochratoxin A extraction and analysis," *Toxins (Basel).*, vol. 2, pp. 1536–1553, 2010.
[76] T. P. Lee, B. Saad, W. S. Khayoon, and B. Salleh, "Molecularly imprinted polymer as sorbent in micro-solid phase extraction of ochratoxin A in coffee, grape juice and urine," *Talanta*, vol. 88, pp. 129–135, 2012.
[77] N. M. Maier, G. Buttinger, S. Welhartizki, E. Gavioli, and W. Lindner, "Molecularly imprinted polymer-assisted sample clean-up of ochratoxin A from red wine : merits and limitations," *J. Chromatogr. B*, vol. 804, pp. 103–111, 2004.
[78] K. Haupt, Ed., *Molecular Imprinting*. German: Springer- Verlag Berlin Heidelberg, 2012.
[79] I. Kralj and H. Prosen, "An overview of conventional and emerging analytical methods for the determination of mycotoxins," *Int. J. Mol. Sci.*, vol. 10, pp. 62–115, 2009.
[80] B. Prieto-Simón, T. Noguer, and M. Campàs, "Emerging biotools for assessment of mycotoxins in the past decade," *Trends Anal. Chem.*, vol. 26, no. 7, pp. 689–702, 2007.
[81] A. Logrieco, D. W. M. Arrigan, K. Brengel-Pesce, P. Siciliano, and I. Tothill, "DNA arrays, electronic noses and tongues, biosensors and receptors for rapid detection of toxigenic fungi and mycotoxins: a review," *Food Addit. Contam.*, vol. 22, no. 4, pp. 335–344, 2005.
[82] D. Bueno Hernandez, "Sistema de Caracterización para Biosensores," Centro de Investigación y de Estudios Avanzados del Instituto Politécnico Nacional, 2011.
[83] A. P. F. Turner, I. Karuve, and S. Wilson, George, Eds., *Biosensors fundamentals and applications*, 1st ed., no. 1. New York, USA: Oxford University Press, 1987.
[84] D. R. Thévenot, K. Toth, R. a. Durst, and G. S. Wilson, "Electrochemical biosensors: Recommended definitions and classification," 2001.
[85] M. S. Thakur and K. V. Ragavan, "Biosensors in food processing," *J. Food Sci. Technol.*, vol. 50, no. 4, pp. 625–641, 2013.
[86] D. R. Thévenot, K. Toth, R. A. Durst, and G. S. Wilson, "International Union of Pure and Applied Chemistry: Physical chemistry division, steering committee on biophysical chemistry, analytical chemistry division, commission V.5 (Electroanalytical chemistry) Electrochemical Biosensors: Proposed, definition and c," *Food Chem.*, vol. 55, no. 2, p.

201, 1996.
[87] D. Grieshaber, R. MacKenzie, J. Vörös, and E. Reimhult, “Electrochemical biosensors - Sensor principles and architectures,” *Sensors*, vol. 8, pp. 1400–1458, 2008.
[88] F. Long, A. Zhu, and H. Shi, “Recent advances in optical biosensors for environmental monitoring and early warning,” *Sensors*, vol. 13, pp. 13928–13948, 2013.
[89] C. Perez Conde, *Sensores ópticos*, 1st ed. Universität de València, 1996.
[90] C. M. Maragos, “Emerging Technologies for Mycotoxin Detection,” *J. Toxicol. Toxin Rev.*, vol. 23, no. 2&3, pp. 317–344, 2004.
[91] J. Yuan, D. Deng, D. R. Lauren, M.-I. Aguilar, and Y. Wu, “Surface plasmon resonance biosensor for the detection of ochratoxin A in cereals and beverages,” *Anal. Chim. Acta*, vol. 656, no. 1–2, pp. 63–71, 2009.
[92] M. M. Ngundi, L. C. Shriver-Lake, M. H. Moore, M. E. Lassman, F. S. Ligler, and C. R. Taitt, “Array biosensor for detection of ochratoxin A in cereals and beverages,” *Anal Chem*, vol. 77, pp. 148–154, 2005.
[93] N. Adányi, I. a. Levkovets, S. Rodriguez-Gil, A. Ronald, M. Váradi, and I. Szendro, “Development of immunosensor based on OWLS technique for determining Aflatoxin B1 and Ochratoxin A,” *Biosens. Bioelectron.*, vol. 22, pp. 797–802, 2007.
[94] K. E. Sapsford, M. M. Ngundi, M. H. Moore, M. E. Lassman, L. C. Shriver-Lake, C. R. Taitt, and F. S. Ligler, “Rapid detection of foodborne contaminants using an array biosensor,” *Sensors Actuators, B Chem.*, vol. 113, pp. 599–607, 2006.
[95] F. Yu, T. Chi, B. Liu, and C. Su, “Development of a sensitive enzyme-linked immunosorbent assay for the determination of ochratoxin A,” *J. Agric. Food Chem.*, vol. 53, pp. 6947–6953, 2005.
[96] E. Schneider, E. Usleber, and E. Märtlbauer, “Rapid detection of fumonisin B1 in corn-based food by competitive direct dipstick enzyme immunoassay/enzyme-linked immunofiltration assay with integrated negative control reaction,” *J. Agric. Food Chem.*, vol. 43, pp. 2548–2552, 1995.
[97] S. De Saeger, L. Sibanda, A. Desmet, and C. Van Peteghem, “A collaborative study to validate novel field immunoassay kits for rapid mycotoxin detection,” *Int. J. Food Microbiol.*, vol. 75, pp. 135–142, 2002.
[98] A. Leung, P. M. Shankar, and R. Mutharasan, “A review of fiber-optic biosensors,” *Sensors Actuators B Chem.*, vol. 125, pp. 688–703, 2007.
[99] M. Espinosa Bosch, A. J. Ruiz Sánchez, F. Sánchez Rojas, and C. Bosch Ojeda, “Recent development in optical fiber biosensors,” *Sensors*, vol. 7, pp. 797–859, 2007.
[100] R. Wang, Y. Xiang, X. Zhou, L. Liu, and H. Shi, “A reusable aptamer-based evanescent wave all-fiber biosensor for highly sensitive detection of Ochratoxin A,” *Biosens. Bioelectron.*, vol. 66, pp. 11–18, 2015.
[101] W. Wang, M. Zhang, J. Fang, L. Zhang, X. Zou, and X. Wang, “Improved Detection of Ochratoxin A by Marine Bioluminescent bacteria V. harveyi BA,” *Czech J. Food Sci.*, vol. 31, no. 1, pp. 88–93, 2013.
[102] L. Su, W. Jia, C. Hou, and Y. Lei, “Microbial biosensors: A review,” *Biosens. Bioelectron.*, vol. 26, pp. 1788–1799, 2011.
[103] B. Valeur and M. N. Berberan-Santos, “A brief history of fluorescence and phosphorescence before the emergence of quantum theory,” *J. Chem. Educ.*, vol. 88, pp. 731–738, 2011.
[104] J. B. Birks, “Fluorescence quantum yield measurements,” *J. Res. Natl. Bur. Stand. Sect.*

A Phys. Chem., vol. 80A, no. 3, pp. 389–399, 1976.
[105] J. R. Lakowicz, *Principles of fluorescence spectroscopy*, 3rd ed. New York, USA: Springer Science+Business Media LLC, 2006.
[106] A. P. Demchenko, "Fluorescence detection techniques," in *Introduction to fluorescence sensing*, 1st ed., Springer Science+Business Media, 2009, pp. 65–118.
[107] Y. V. Il'ichev, J. L. Perry, R. A. Manderville, C. F. Chignell, and J. D. Simon, "The pH dependent primary photoreactions of Ochratoxin A," *J. Phys. Chem. B*, vol. 105, pp. 11369–11376, 2001.
[108] C. Frenette, R. J. Paugh, M. Tozlovanu, M. Juzio, A. Pfohl-Leszkowicz, and R. A. Manderville, "Structure-activity relationships for the fluorescence of ochratoxin A: insight for detection of ochratoxin A metabolites.," *Anal. Chim. Acta*, vol. 617, pp. 153–161, 2008.
[109] D. Steinbrück, C. Rasch, and M. U. Kumke, "Photophysics of Ochratoxin A in Aqueous Solution," *Zeitschrift für Naturforsch.*, vol. 63, no. b, pp. 1321–1326, 2008.
[110] J. C. Lindon, G. E. Tranter, and J. L. Holmes, Eds., *Encyclopedia of spectroscopy and spectrometry*, 1st ed. Academic Press, 2000.
[111] A. Pittet and D. Royer, "Rapid, low cost thin-layer chromatographic screening method for the detection of ochratoxin A in green coffee at a control level of 10 ug/kg," *J. Agric. Food Chem.*, vol. 50, pp. 243–247, 2002.
[112] A. Rahmani, S. Jinap, and F. Soleimany, "Qualitative and quantitative analysis of mycotoxins," *Compr. Rev. Food Sci. Food Saf.*, vol. 8, pp. 202–251, 2009.
[113] A. C. Entwistle, W. A.C., M. P.J., S. P.T., and G. J., "Liquid chromatographic method with immunoaffinity column clean up for determination of ochratoxin A in barley: Collaborative study," *J. Assoc. Anal. Comm*, vol. 83, pp. 1377–1383, 2000.
[114] A. C. Entwistle, A. C. Williams, P. J. Mann, J. Russell, P. T. Stack, and J. Gilbert, "Combined phenyl silane and immunoaffinity column clean up with liquid chromatography for determination of ochratoxin A in roasted coffee: Collaborative study," *J. Assoc. Anal. Comm*, vol. 84, pp. 440–450, 2001.
[115] S. Corneli and C. M. Maragos, "Capillary electrophoresis with laser induced fluorescence: Method for the mycotoxin Ochratoxin A," *J. Agric. Food Chem*, vol. 46, pp. 3162–3165, 1998.
[116] G. Köller, G. Wichmann, U. Rolle-Kampczyk, P. Popp, and O. Herbarth, "Comparison of ELISA and capillary electrophoresis with laser induced fluorescence detection in the analysis of Ochratoxin A in low volumes of human blood serum," *J. Chromatogr. B*, vol. 840, pp. 94–98, 2006.
[117] N. Duan, S.-J. Wu, and Z.-P. Wang, "An aptamer based fluorescence assay for Ochratoxin A," *Chinese J. Anal. Chem.*, vol. 39, no. 3, pp. 300–304, 2011.
[118] Z. Lv, A. Chen, J. Liu, Z. Guan, Y. Zhou, S. Xu, S. Yang, and C. Li, "A simple and sensitive approach for ochratoxin A detection using a label free fluorescent aptasensor," *PLoS One*, vol. 9, no. 1, p. e85968, 2014.
[119] Y. Kostov and G. Rao, "Low-cost optical instrumentation for biomedical measurements," *Rev. Sci. Instrum.*, vol. 71, no. 12, pp. 4361–4374, 2000.
[120] P. C. Hauser and D. W. Chiang, "A photometric detector based on a blue light emitting diode," *Talanta*, vol. 40, no. 8, pp. 1193–1200, 1993.
[121] G. Veras, E. Cirino Silva, W. Silva Lyra, S. F. Carreiro Soares, T. Brito Guerreiro, and S. R. Bezerra Santos, "A portable, inexpensive and microcontrolled spectrophotometer

based on white LED as light source and CD media as diffraction grid," *Talanta*, vol. 77, pp. 1155–1159, 2009.
[122] D. Anh Bui and P. C. Hauser, "Absorbance measurements with light emitting diodes as sources: Silicon photodiodes or light-emitting diodes as detectors?," *Talanta*, vol. 116, pp. 1073–1078, 2013.
[123] M. O'Toole and D. Diamond, "Absorbance based light emitting diode optical sensors and sensing devices," *Sensors*, vol. 8, pp. 2453–2479, 2008.
[124] Ł. Tymecki, L. Brodacka, B. Rozum, and R. Koncki, "UV-PEDD photometry dedicated for bioanalytical uses.," *Analyst*, vol. 134, pp. 1333–1337, 2009.
[125] G. Gauglitz, "Direct optical sensors: Principles and selected applications," *Anal. Bioanal. Chem.*, vol. 381, pp. 141–155, 2005.
[126] P. K. Dasgupta, H. Huang, G. Zhang, and G. P. Cobb, "Photometric measurement of trace As (III) and As (V) in drinking water," *Talanta*, vol. 58, pp. 153–164, 2002.
[127] K. M. Gomes de Lima, "A portable photometer based on LED for the determination of aromatic hydrocarbons in water," *Microchem. J.*, vol. 103, pp. 62–67, 2012.
[128] Q. Li, K. J. Morris, P. K. Dasgupta, I. M. Raimundo, and H. Temkin, "Portable flow-injection analyzer with liquid-core waveguide based fluorescence, luminescence, and long path length absorbance detector," *Anal. Chim. Acta*, vol. 479, pp. 151–165, 2003.
[129] Y. Kostov and G. Rao, "Low-cost device for ratiometric fluorescence measurements," *Rev. Sci. Instrum.*, vol. 70, pp. 4466–4470, 1999.
[130] Ł. Tymecki, M. Rejnis, M. Pokrzywnicka, K. Strzelak, and R. Koncki, "Fluorimetric detector and sensor for flow analysis made of light emitting diodes," *Anal. Chim. Acta*, vol. 721, pp. 92–96, 2012.
[131] M. Belz, F. A. Klein, H. S. Eckhardt, K.-F. Klein, D. Dinges, and K. Grattan, "Optical detection techniques and light delivery with UV LEDs and optical fibres," *J. Phys. Conf. Ser.*, vol. 85, p. 012034, 2007.
[132] W. J. O'Hagan, M. McKenna, D. C. Sherrington, O. J. Rolinski, and D. J. S. Birch, "MHz LED source for nanosecond fluorescence sensing," *Meas. Sci. Technol.*, vol. 13, pp. 84–91, 2002.
[133] S. Schmid, M. Macka, and P. C. Hauser, "UV-absorbance detector for HPLC based on a light-emitting diode," *Analyst*, vol. 133, pp. 465–469, 2008.
[134] D. Caputo, G. de Cesare, C. Fanelli, A. Nascetti, A. Ricelli, and R. Scipinotti, "Amorphous silicon photosensors for detection of Ochratoxin A in wine," *IEEE Sens. J.*, vol. 12, no. 8, pp. 2674–2679, 2012.
[135] P. Novo, G. Moulas, D. M. França Prazeres, V. Chu, and J. P. Conde, "Detection of ochratoxin A in wine and beer by chemiluminescence-based ELISA in microfluidics with integrated photodiodes," *Sensors Actuators, B Chem.*, vol. 176, pp. 232–240, 2013.
[136] D. Harvey, "Spectroscopic methods of analysis," in *Modern analytical chemistry*, 1st ed., USA: McGraw-Hill Higher Education, 2000.
[137] J. Ohta, *Smart CMOS Image Sensors and Applications*, 2nd ed. Boca Raton ,Florida, USA, 2008.
[138] I. S. McLean, *Electronic imaging in astronomy Detectors and instrumentation*, 2nd ed. Germany: Springer- Verlag Berlin Heidelberg New York, 2008.
[139] E. Cuevas, D. Zaldivar, and M. Pérez, *Procesamiento digital de imagenes con MATLAB y Simulink*, 1st ed. Madrid, España: Alfaomega RA-MA, 2010.
[140] X. Luo, P. Liu, C. Hou, D. Huo, J. Dong, H. Fa, and M. Yang, "A novel chemical

detector using colorimetric sensor array and pattern recognition methods for the concentration analysis of NH3.," *Rev. Sci. Instrum.*, vol. 81, pp. 105113–6, 2010.
[141] L. Liu and H. Lin, "Paper based colorimetric array test strip for selective and semiquantitative multi-ion analysis: Simultaneous detection of Hg2+ , Ag+ , and Cu2+," *Anal. Chem.*, vol. 86, pp. 8829–8834, 2014.
[142] A. Lapresta-Fernández and L. F. Capitán-Vallvey, "Multi-ion detection by one-shot optical sensors using a colour digital photographic camera.," *Analyst*, vol. 136, no. 19, pp. 3917–3926, 2011.
[143] K. S. Suslick, N. A. Rakow, and A. Sen, "Colorimetric sensor arrays for molecular recognition," *Tetrahedron*, vol. 60, no. 49, pp. 11133–11138, 2004.
[144] K. S. Suslick, N. A. Rakow, M. E. Kosal, and W. B. M. Iii, "Chemsensing : A Colorimetric Array Detector," *Proc. Int. Soc. Olfaction Electron. Noses*, pp. 46–52, 2003.
[145] C. Zhang and K. S. Suslick, "A colorimetric sensor array for organics in water," *J. Am. Chem. Soc.*, vol. 127, no. 33, pp. 11548–11549, 2005.
[146] A. Sen, J. D. Albarella, J. R. Carey, P. Kim, and W. B. McNamara III, "Low-cost colorimetric sensor for the quantitative detection of gaseous hydrogen sulfide," *Sensors Actuators B Chem.*, vol. 134, no. 1, pp. 234–237, 2008.
[147] A. Choodum and N. Nic Daeid, "Rapid and semi-quantitative presumptive tests for opiate drugs," *Talanta*, vol. 86, no. 1, pp. 284–292, 2011.
[148] D. S. Lee, M. Y. Jung, B. G. Jeon, and M. J. Sohn, "Novel optical absorbance-based multi-analytes detection module using a tri-chromatic LED, PDs and plastic optical fibers and its application to a palm-sized urine test strip reader," *Proc. IEEE Sensors*, pp. 1411–1414, 2010.
[149] P. Montes-Navajas, L. A.Baumes, A. Corma, and H. Garcia, "Dual-response colorimetric sensor array for the identification of amines in water based on supramolecular host–guest complexation," *Tetrahedron Lett.*, vol. 50, no. 20, pp. 2301–2304, 2009.
[150] C. J. Musto, S. H. Lim, and K. S. Suslick, "Colorimetric detection and identification of natural and artificial sweeteners.," *Anal. Chem.*, vol. 81, no. 15, pp. 6526–6533, 2009.
[151] S. H. Lim, C. J. Musto, E. Park, W. Zhong, and K. S. Suslick, "A Colorimetric Sensor Array for Detection and Identification of Sugars," *Org. Lett.*, vol. 10, no. 20, pp. 4405–4408, 2008.
[152] L. Feng, C. J. Musto, J. W. Kemling, S. H. Lim, W. Zhong, and K. S. Suslick, "Colorimetric sensor array for determination and identification of toxic industrial chemicals," *Anal. Chem.*, vol. 82, no. 22, pp. 9433–9440, 2010.
[153] L. Feng, C. J. Musto, J. W. Kemling, S. H. Lim, and K. S. Suslick, "A colorimetric sensor array for identification of toxic gases below permissible exposure limits," *Chem. Commun.*, vol. 46, no. 12, pp. 2037–2039, 2010.
[154] E. Y. Basova, I. Y. Goryacheva, D. a. Mikhirev, T. Y. Rusanova, N. a. Burmistrova, B. Kerkaert, T. Cucu, S. De Saeger, and B. De Meulenaer, "Rapid method for qualitative detection of 2,4,6-trinitrotoluene in environmental water samples," *Anal. Methods*, vol. 1, no. 3, pp. 170–176, 2009.
[155] A. Choodum, P. Kanatharana, W. Wongniramaikul, and N. NicDaeid, "Rapid quantitative colourimetric tests for trinitrotoluene (TNT) in soil," *Forensic Sci. Int.*, vol. 222, no. 1–3, pp. 340–345, 2012.

[156] K. León, D. Mery, F. Pedreschi, and J. León, “Color measurement in L∗a∗b∗ units from RGB digital images,” *Food Res. Int.*, vol. 39, pp. 1084–1091, 2006.
[157] J. R. Askim, M. Mahmoudi, and K. S. Suslick, “Optical sensor arrays for chemical sensing: the optoelectronic nose,” *Chem. Soc. Rev.*, vol. 42, no. 22, pp. 8649–8682, 2013.
[158] K. Yabe, Y. Ando, M. Ito, and N. Terakado, “Simple method for screening aflatoxin producing molds by UV photography,” *Appl. Environ. Microbiol.*, vol. 53, no. 2, pp. 230–234, 1987.
[159] Z. Cvetni and S. Pepeljnjak, “UV photography to identify aflatoxin-producing strains of Aspergillus flavus and A . parasiticus,” *Z Leb. Unters Forsch*, vol. 201, pp. 399–401, 1995.
[160] S. Hara, D. I. Fennell, and C. W. Hesseltine, “Aflatoxin-producing strains of Aspergillus flavus detected by fluorescence of agar medium under ultraviolet light,” *Appl. Microbiol.*, vol. 27, no. 6, pp. 1118–1123, 1974.
[161] M. Schmidt-Heydt, H. Bode, F. Raupp, and R. Geisen, “Influence of light on ochratoxin biosynthesis by Penicillium,” *Mycotoxin Res.*, vol. 26, pp. 1–8, 2010.
[162] A. Mustafic, E. E. Roberts, M. D. Toews, and M. A. Haidekker, “LED Induced fluorescence and image analysis to detect stink bug damage in cotton bolls,” *J. Biol. Eng.*, vol. 7, no. 5, pp. 1–9, 2013.
[163] A. Rhouati, “Développement de méthodes bioanalytiques à base d’aptamères pour la détermination de l'Ochratoxine A,” Université Constantine 1- Université de Perpignan Via Domitia, 2013.
[164] D. G. Buerk, *Biosensors theory and applications*, 1st ed. Lancaster,Pennsylvania,USA: Technomic Publishing AG, 1993.
[165] M. Pokrzywnicka, R. Koncki, and ??ukasz Tymecki, “A concept of dual optical detection using three light emitting diodes,” *Talanta*, vol. 82, no. 1, pp. 422–425, 2010.
[166] Y. Bingcheng, T. Hongzhe, X. Jing, and G. Yafeng, “An integrated light emitting diode-induced fluorescence detector for capillary electrophoresis,” *Talanta*, vol. 69, no. 4, pp. 996–1000, 2006.
[167] M. M. Hoehl, P. J. Lu, P. A. Sims, and A. H. Slocum, “Rapid and robust detection methods for poison and microbial contamination,” *J. Agric. Food Chem.*, vol. 60, no. 25, pp. 6349–6358, 2012.
[168] K. Tong Lau, S. Baldwin, R. L. Shepherd, P. H. Dietz, W. S. Yerzunis, and D. Diamond, “Novel fused- LEDs devices as optical sensors for colorimetric analysis,” *Talanta*, vol. 63, pp. 167–176, 2004.
[169] W. Hernandez, “Input-output Transfer Function Analysis of a Photometer Circuit Based on an Operational Amplifier,” *Sensors*, vol. 8, no. 1, pp. 35–50, 2008.
[170] G. Istamboulie, S. Andreescu, J. L. Marty, and T. Noguer, “Highly sensitive detection of organophosphorus insecticides using magnetic microbeads and genetically engineered acetylcholinesterase,” *Biosens. Bioelectron.*, vol. 23, no. 4, pp. 506–512, 2007.
[171] A. . Marangoni, *Enzyme Kinetics: A modern approach*, vol. 182. New Jersey, USA: John Wiley & Sons Inc., 2003.
[172] H. Bisswanger, *Enzyme Kinetics: Principles and methods*, 2nd ed. Weinheim, Germany: Wiley-VCH, 2008.
[173] C. Joseph, M. Boukadoum, J. Charlson, D. Starikov, and A. Bensaoula, “High-speed

front end for LED-Photodiode based fluorescence lifetime measurement system," in *Circuits and Systems, 2007. ISCAS 2007. IEEE International Symposium on*, 2007, pp. 3578 – 3581.
[174] M. Boukadoum, A. Trabelsi, and C. Fayomi, "FPGA-based multispectral fluorometer using CDMA and embedded neural network," in *Proceedings of the International Conference on Microelectronics, ICM*, 2009, pp. 199–202.
[175] N. Pires, T. Dong, U. Hanke, and N. Hoivik, "Recent Developments in Optical Detection Technologies in Lab-on-a-Chip Devices for Biosensing Applications," *Sensors*, vol. 14, no. 8, pp. 15458–15479, 2014.
[176] G. G. Guilbault, *Practical Fluorescence*, 2nd ed. New York: CRC Press, 1990.
[177] V. Karumanchi, M. K. Taylor, K. J. Ely, and W. C. Stagner, "Monitoring powder blend homogeneity using light-induced fluorescence.," *AAPS PharmSciTech*, vol. 12, no. 4, pp. 1031–1037, 2011.
[178] K. D. Mielenz, *Optical radiation measurements Volume 3 Measurements of photoluminescence*, 1st ed. New York, USA, 1982.
[179] C. Rasch, M. Kumke, and H. G. Löhmannsröben, "Sensing of Mycotoxin Producing Fungi in the Processing of Grains," *Food Bioprocess Technol.*, vol. 3, no. 6, pp. 908–916, 2010.
[180] A. Economou, P. D. Tzanavaras, and D. G. Themelis, "Sequential Injection Analysis: Principles, instrument construction and demonstration by a simple experiment," *J. Chem. Educ.*, vol. 82, no. 12, pp. 1820–1822, 2005.
[181] N. W. Barnett, C. E. Lenehan, and S. W. Lewis, "Sequential injection analysis : an alternative approach to process analytical chemistry," *Trends Anal. Chem.*, vol. 18, no. 5, pp. 346–353, 1999.
[182] A. Roda, E. Michelini, M. Zangheri, M. Di Fusco, D. Calabria, and P. Simoni, "Smartphone-based biosensors: A critical review and perspectives," *TrAC Trends Anal. Chem.*, 2015.
[183] H. Parastar and H. Shaye, "MVC app: A smartphone application for performing chemometric methods," *Chemom. Intell. Lab. Syst.*, vol. 147, pp. 105–110, 2015.
[184] D. Zhang and Q. Liu, "Biosensors and bioelectronics on smartphone for portable biochemical detection," *Biosens. Bioelectron.*, vol. 75, pp. 273–284, 2016.
[185] F. Lamonaca, G. Polimeni, K. Barbé, and D. Grimaldi, "Health parameters monitoring by smartphone for quality of life improvement," *Measurement*, vol. 73, pp. 82–94, 2015.
[186] M. H. Mobasheri, M. Johnston, U. M. Syed, D. King, and A. Darzi, "The uses of smartphones and tablet devices in surgery: A systematic review of the literature," *Surgery*, vol. 158, no. 5, pp. 1352–1371, 2015.
[187] C. on R. C. through A. C. Imaging, B. on C. S. and Technology, and D. on E. and L. Studies, *Visualizing Chemistry The progress and promise of advanced chemical imaging*. Washington,DC, USA: National Academies Press, 2006.
[188] S. N. Jha, *Nondestructive evaluation of food quality*, 1st ed. Heildelberg, Germany: Springer Berlin Heidelberg, 2010.
[189] C. Fernandez Maloigne, *Advanced color image processing and analysis*, 1st ed. New York, USA: Springer Science+Business Media, 2013.
[190] C. Solomon and T. Breckon, *Fundamentals of digital image processing*, 1st. ed. West Sussex, UK: Wiley-Blackwell, 2011.

[191] K. N. Plataniotis and A. N. Venetsanopoulos, *Color image processing and applications*. New York, USA: Springer- Verlag Berlin Heidelberg, 2000.
[192] I. The MathWorks, "R2015b Documentation." [Online]. Available: http://www.mathworks.com/help/images/ref/graycoprops.html. [Accessed: 13-Feb-2016].
[193] M. Cortina, M. Del Valle, and J. L. Marty, "Electronic tongue using an enzyme inhibition biosensor array for the resolution of pesticide mixtures," *Electroanalysis*, vol. 20, no. 1, pp. 54–60, 2008.
[194] J. Cao, W. Kong, S. Zhou, L. Yin, L. Wan, and M. Yang, "Molecularly imprinted polymer-based solid phase clean-up for analysis of ochratoxin A in beer, red wine, and grape juice," *J. Sep. Sci.*, vol. 36, no. 7, pp. 1291–1297, 2013.
[195] C. He, Y. Long, J. Pan, K. Li, and F. Liu, "Application of molecularly imprinted polymers to solid-phase extraction of analytes from real samples," *J. Biochem. Biophys. Methods*, vol. 70, no. 2, pp. 133–150, 2007.
[196] M. T. Giardi, G. Rea, and B. Berra, Eds., *Bio-farms for nutraceuticals. Functional food and safety control by biosensors. Preface.*, vol. 698. New York: Springer Science+Business Media LLC, 2010.
[197] R. Barth, *The chemsitry of beer*, 1st ed. Hoboken, New Jersey, USA, 2013.
[198] A. Rhouati, N. Paniel, Z. Meraihi, and J. L. Marty, "Development of an oligosorbent for detection of ochratoxin A," *Food Control*, vol. 22, pp. 1790–1796, 2011.
[199] M. Brow, D. J, M. Wright, I. Gillman, and R. Manderville, "Photochemically catalyzed reaction of ochratoxin A with D- and L-cysteine," *Photochem. Photobiol.*, vol. 76, no. 6, pp. 649–656, 2002.
[200] N. Turner, E. Piletska, K. Karim, M. Whitcombe, M. Malecha, N. Magan, C. Baggiani, and S. Piletsky, "Effect of the solvent on recognition properties of molecularly imprinted polymer specific for ochratoxin A," *Biosens. Bioelectron.*, vol. 20, no. 6, pp. 1060–1067, 2004.
[201] W.-T. Liu, J.-H. Wu, E.-Y. Li, and E. Selamat, "Emission Characteristics of Fluorescent Labels with Respect to Temperature Changes and Subsequent Effects on DNA Microchip Studies," *Appl. Environ. Microbiol.*, vol. 71, no. 10, pp. 6453–6457, 2005.
[202] J. Cruz-Aguado and G. Penner, "Determination of Ochratoxin A with a DNA Aptamer," *J. Agric. Food Chem.*, vol. 56, no. 22, pp. 10456–10461, 2008.
[203] I. Bazin, V. Faucet-Marquis, M.-C. Monje, M. El Khoury, J.-L. Marty, and A. Pfohl-Leszkowicz, "Impact of pH on the Stability and the Cross-Reactivity of Ochratoxin A and Citrinin," *Toxins (Basel).*, vol. 5, no. 12, pp. 2324–2346, 2013.

Highlights

- Applications of LED in kinetic enzymatic reaction.
- UV-LEDs as excitation of fluorescence solutions.
- Application of the concept of RGB model, to extract these components from an image and tie in with the natural fluorescence of OTA.
- Cleaning of the columns with 10 mL of 1% of Acetic acid in ethyl acetate, it was washed with 20 mL of distilled water does not affected the retention of OTA for experiments posterior.
- The design or creation of pieces. Some important pieces employed were:

  Cell

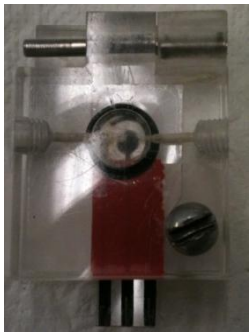

  The bracket designed to allocate the different CMOS sensors

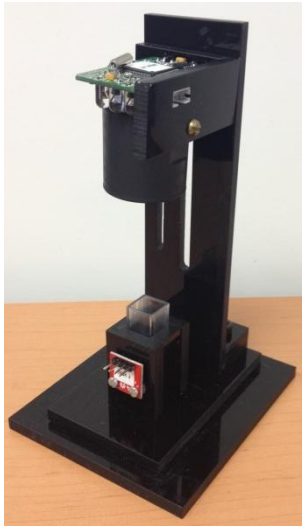

Base to insert the cuvettes 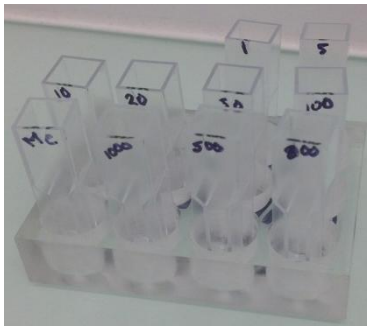

Base to put on the columns 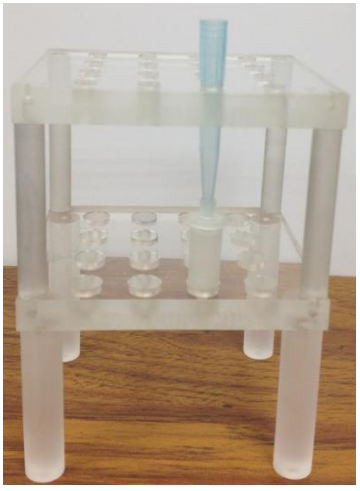 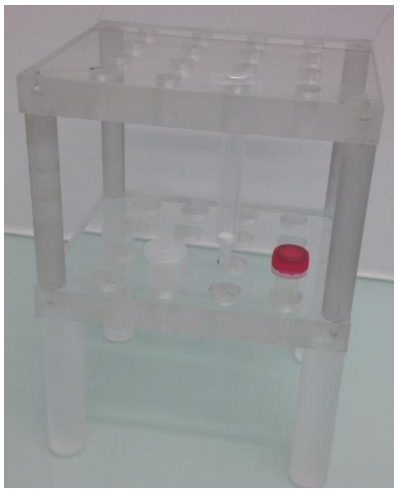

- Low cost systems, portables, reduction time in the samples, the samples are no destroyed, so can be compared with analytical methods.
- Automatized system controlled by the computer (optical devices and flow system)
- Implementation of the new technologies such as smartphone as detector and source, Wi-Fi communication, APP, image processing.
- The methodologies and the system developed were tested with real samples.
- Results comparable with commercial equipment.

PUBLICATIONS

PUBLISHED ARTICLE

Diana Bueno, Roberto Munoz, Jean Louis Marty. Fluorescence analyzer based on smartphone camera and wireless for detection of Ochratoxin A. Sensors and Actuators B 232 (2016) 462–468.

Diana Bueno, George Istamboulie, Roberto Muñoz, Jean Louis Marty. Determination of Mycotoxins in Food: A Review From Bioanalytical to Analytical Methods. Applied Spectroscopy Reviews. DOI:10.1080/05704928.2015.1072092. July 2015.

Diana Bueno, Gustavo Alonso, Roberto Muñoz , Jean Louis Marty. Low cost and portable absorbance measuring system to carbamate and organophosphate pesticides. Sensors & Actuators: B. Chemical, 81-88, 2014.

Amina Rhouati, Akhtar Hayat, **Diana Bueno**, Zahia Meraihi, Roberto Munoz, Marty Jean Louis. Development of an automated flow-based electrochemical aptasensor for on-line detection of OTA. Sensors and Actuators B 176, 1160– 1166, 2013.

CHAPTER OF BOOK

Diana Bueno, Roberto Muñoz and Jean Louis Marty. Common Methods to Detect Mycotoxins: A Review with Particular Emphasis on Electrochemical Detection. Sensing in Electroanalysis 8, 85-114, 2013/2014.

PARTICIPATION AND ATTENDANCE CONFERENCES

Diana Bueno, Roberto Muñoz, Jean Louis Marty. "Low cost and optical detection from fluorescence of Ochratoxin A", GMEPE/PAHCE 2016, 4-9 April, Madrid, Spain (Poster session)

Diana Bueno, Roberto Muñoz, Jean Louis Marty. "Optical methods to detect fluorescence of Ochratoxin A". IC-ANMBES, June 13-15th, 2014, Brasov, Romania. (Oral session)

Diana Bueno, Rupesh K. Mishra, Roberto Muñoz, Jean Louis Marty. "Detection methods for Ochratoxin A in wine samples". Journées d'Electrochimie, July 6-10, 2015, Rome, Italy. (Poster session)

Rupesh K. Mishra, **Diana Bueno**, Jean Louis Marty. "Detection methods for Ocharatoxin A in cocoa beans by innovative approaches". 19th Transfrontier Meeting of Sensors and Biosensors, September 25-26th, 2014, Bellaterra, Barcelona, Spain. (Poster session)

Diana Bueno, Gustavo Alonso, Roberto Muñoz, Jean Louis Marty. "Development of an enzymatic optosensor for detection of carbamate and organophosphate pesticides". Journées d'Electrochimie, September 8-12, 2013, Paris, France. (Poster session)

D. Bueno, G.A. Alonso, R. Muñoz, J.L. Marty. "Development of an enzymatic optosensor for detection of carbamate and organophosphate pesticides". XVII Trobada Transfronterera on Sensors and Biosensors. September 2012, Tarragona, Catalonia, Spain. (Poster session)

Development of a fully automated flow aptasensor for Ochratoxin A detection in foodstuffs». A. Rhouati, **D.B. Hernandez**, A. Hayat, R. Munoz, Z. Meraihi and J.L. Marty. 8ème workshop Franco-Chinois "Surface electrochemistry molecules of biological interest and biosensor applications", Lacanau-Océan-France. September 2012. (Oral session)

A novel rapid and simple electrochemical aptasensor coupled to an automated flow system for Ochratoxin A detection». A.Rhouati, A.Hayat, **D.B. Hernandez**, Z. Meraihi, R. Munoz and J.L. Marty. International conference on analytical and nanoanalytical methods for biomedical and environmental sciences, Brasov-Romania. May 2012. (Oral session)

SUBMITTED ARTICLES

Akhtar Hayat, Amina Rhouati, Rupesh K Mishra; **Diana Bueno**; Roberto Munoz; Jean louis Marty. Ligand assisted stabilization of fluorescence nanoparticles; an insight on the fluorescence characteristics, dispersion stability and DNA loading efficiency of nanoparticles. (Submitted in Journal of Fluorescence).

Jean Louis MARTY, **Diana Bueno**, Rupesh K Mishra, Akhtar Hayat, Gaëlle Catanante, Vinay Sharma, Roberto Muñoz. Portable and low cost fluorescence set-up for in-situ screening of Ochratoxin A based on RGB components (Submitted in Journal of Luminescence).

Diana Bueno, Rupesh K. Mishra, Roberto Muñoz, Jean Louis Marty. Low cost, optical device for detection of fluorescence from Ochratoxin A using a CMOS sensor (Submitted in Journal Food Control).

Diana Bueno, Atul Sharma, Roberto Muñoz, Sunil Bhand and Jean Louis Marty. Impact of pH, solvent and salt composition on the fluorescence emission behavior of Ochratoxin A (Submitted in Spectroscopy Letters).

Résumé

Un appareil de mesure de la fluorescence, à faible coût et portable a été développé pour quantifier les concentrations d'Ochratoxine A (OTA) dans des échantillons réels. Le système est basé sur l'excitation par une UV-LED à 365 nm et un photo détecteur contrôlé par une interface dans LabVIEW. Aussi, une image capteur, CMOS, contrôlée par une interface conçue dans MATLAB. L'OTA est une molécule naturellement fluorescente. Après excitation par une UV-, l'image de la fluorescence émise est captée par une caméra et traitée en vue de la mesure de la concentration de l'OTA. Le système d'analyse a été basé sur les 3 composants rouge, vert et bleu (RGB, selon l'acronyme anglais). La gamme est linéaire entre de 2-40 µg/L. L'extraction de l'OTA est réalisée par des colonnes d'immuno affinité (IAC, selon l'acronyme anglais) et les colonnes à empreinte moléculaire (MIP, selon l'acronyme anglais) pour les échantillons de cacao, de la bière et du vin. Les résultats obtenus ont été validés par la méthode chromatographique (HPLC). L'appareil conçu est facile à utiliser, économique et portable. En outre, l'utilisation des nouvelles technologies a été inclus tels que l'emploi du smartphone pour détecter l'OTA et la création d'un APP. Des données d'image de fluorescence provenant de la caméra du smartphone et sont analysées par un ordinateur personnel et présentés dans les composantes RGB, où l'image est envoyée à l'ordinateur par WIFI et le téléphone intelligent est utilisé comme source d'énergie trop. Enfin, une APP pour le système Android a été créé pour capturer l'image et fournit les valeurs RGB. Enfin l'utilisation du traitement de l'image a été utilisée pour quantifier l'OTA dans les échantillons réels sans colonnes IAC ou MIP, employée pour extraire la mycotoxine. L'analyse a été réalisée par des techniques colorimétriques et d'analyse de la couleur.

Abstract

A portable and low cost fluorescence set-up to quantify the concentrations of Ochratoxin A (OTA) in real samples was developed. The detection through the device consist of an ultraviolet light at 365 nm and an photo detector or a CMOS sensor controlled by an executable interface designed in LabVIEW or MATLAB. It has been reported that OTA is naturally fluorescent, so it allows the user to get a UV LED to excite the sample, get a value in voltage when a photodetector is employed or a photograph of the OTA under excitation conditions, and process that image in order to predict the concentrations of the sample. To capture and process the image, in an automatically manner, the system was completely based on the Red, Green and Blue (RGB) components. The linearity for OTA obtained in the range of concentrations corresponds to 2-40 µg/L. Immunoaffinity columns (IAC) and molecular imprinted polymer columns (MIP) were used with cocoa, beer and wine samples. The obtained results were cross-validated using chromatographic method such as HPLC and the Fluoroskan equipment. The developed setup is easy to use, economical and portable. Besides, the use of new tendencies was included such as employ the smartphone to detect OTA and the creation of an APP. Fluorescence image data from the smartphone camera are analyzed by a personal computer and presented in RGB components, where the image is sent to the computer by WIFI and the smartphone is used as a power source too. Finally, an APP for android system was created to capture the image and provides the RGB values. At the end, the use of image processing to quantify the OTA in real samples without incorporated IAC or MIP columns to extract the mycotoxin from a complex solution, employing colorimetric techniques and color analysis.